ISSN 2303-4521

Periodicals of

Engineering and Natural Sciences

VOL. 5 NO. 1
(2017)

Published by International University of Sarajevo

Periodicals of Engineering and Natural Sciences (PEN)

Periodicals of Engineering and Natural Sciences (ISSN: 2303-4521) is an international open access single-blind review journal published online.

Publication frequency: Semiyearly (1. January - June; 2. July - December).

Publication Fees: No fee required (no article submission charges or processing charges).

Digital Object Identifier DOI: 10.21533/pen

Editorial Office

Mailing Address

Hrasnicka cesta 15
71000 Sarajevo
Bosnia

Principal Contact

Benjamin Durakovic
Managing Editor
International University of Sarajevo
Hrasnicka cesta 15
71000 Sarajevo
Bosnia
Phone: +387 33 957 229
Email: pen@ius.edu.ba

Available online at:

http://pen.ius.edu.ba

Editorial Team

DOI: 10.21533/pen

Publication Frequency

Expected frequency of publication is twice per year:
1. January - June;
2. July - December.

Journal items can be published collectively, as part of an issue with its own Table of Contents. Alternatively, individual items can be published as soon as they are ready, by adding them to the "current" volume's Table of Contents.

Open Access Policy

This journal provides immediate open access to its content on the principle that making research freely available to the public supports a greater global exchange of knowledge.

Journal Ethics and Malpractice Statement

PEN Journal is committed to ensure and uphold standards of ethical behavior at all stages of the publication process, whereby such values also rely on editors, reviewers, contributors and authors who are expected to behave ethically. The standards are based on Committee on Publication Ethics' (COPE) code of conduct, and provide guidelines for best practices in order to meet these requirements. The following ethical guidelines are only intended to give a summary of our key expectations of editors, peer-reviewers, and authors but if you have any questions or concerns please also feel free to contact the Editor of the Journal.

1. Ethical Expectations

Editors' responsibilities

- To carry out their duties in a fair, objective and consistent manner, without discrimination on grounds of gender, sexual orientation, religious or political beliefs, ethnic or geographical origin of the authors.
- To take care that each article undergoes the proper peer-review process.
- To promote consistent ethical policies of PEN journal, and to ensure the confidentiality of the reviewing process.
- To uphold integrity in their work as editors of the journal, doing away with any personal interest, so that articles are considered and accepted solely on their academic merit and without commercial influence.
- To work with authors, reviewers, and the Editorial Board members to ensure the implementation of journals' ethics and publishing policies.
- To adopt and follow reasonable procedures in the event of complaints of an ethical or conflict nature, in accordance with the policies and procedures. To handle process of complaints and giving authors an opportunity to respond any complaints. All complaints should be investigated and the documentation associated with any such complaints should be retained.

Reviewers' responsibilities

- To act objectively, fairly and in a timely manner in reviewing submitted manuscript with the aim of improving its quality such as pointing out relevant published work, which is not cited, etc.
- To alert PEN in case of any competing interest that could affect the impartiality of their reviewing, or any potential conflict of interest that includes any relationship between reviewer and author, or any content that is substantially similar to that under review.
- To conduct themselves fairly and impartially.
- To keep the confidentiality of the review process and to not retain or copy the manuscript.

DOI: 10.21533/pen

Authors' responsibilities

- To ensure that their work submitted to the journal is original and authored by them and has not been previously published nor under consideration or accepted for publication elsewhere.
- To ensure that original ideas, data, findings and materials taken from other sources (including their own published writing) are properly documented and cited. Any content reproduced from other sources author should have permission.
- To ensure that their data is their won, true and not manipulated. Thus, authors are responsible to maintain accurate records and to provide access to their data associated with their manuscript.
- To ensure their work does not violate any rights of others, including privacy rights and intellectual property rights. In addition, authors should ensure that any studies involving human or animal subject are in accordance with local lows and requirements.
- To declare any real or apparent conflicting or competing interest at any stage during the publication process that could be considered or viewed as exerting an undue influence on his/her duties.
- To alert PEN in case if a significant error in their publication is identified and correct any errors prior or subsequent to publication of their work.
- To adhere to all research ethics guidelines of their discipline, and to ensure that authorship and/or co-authorship of the paper was accurately represented.

PEN responsibilities

- The journal and the publisher shall ensure that good practice is maintained to the standards outlined above.
- To deal with research misconduct allegations appropriately when it is occurred. The journal and the publisher shall undertake reasonable actions to identify and prevent the publication of papers where research misconduct has occurred.
- To maintain the editorial independence of journal editors.
- To support journal editors in ethical and academic matters.
- To ensure critical and objective assessment of all articles by reviewers and referees. To keep an accurate and transparent record, including publishing corrections and retractions when necessary.
- The following commonly recognized procedure for dealing with unethical behavior is adopted.

2. Procedures for Dealing With Unethical Behavior

Identification of unethical behavior

- Misconduct and unethical behavior may be identified and brought to the attention of the editor and publisher at any time, by anyone.
- Misconduct and unethical behavior may include, but need not be limited to, examples as outlined above.
- For an investigation sufficient information and evidence should be provided. All allegations should be taken seriously and treated in the same way, until a successful decision or conclusion is reached.

Investigation

- An initial decision should be taken by the editor, who should consult with or seek advice from the publisher, if appropriate.
- Evidence should be gathered, while avoiding spreading any allegations beyond those who need to know.

Minor breaches

- Minor misconduct might be dealt with without the need to consult more widely. In any event, the author should be given the opportunity to respond to any allegations.

DOI: 10.21533/pen

Serious breaches

- Serious misconduct might require that the employers of the accused be notified. The editor, in consultation with the publisher should make the decision whether or not to involve the employers, either by examining the available evidence themselves or by further consultation with a limited number of experts.

Outcomes (in increasing order of severity; may be applied separately or in conjunction)

- Informing or educating the author or reviewer where there appears to be a misunderstanding or misapplication of acceptable standards.
- A more strongly worded letter to the author or reviewer covering the misconduct and as a warning to future behavior.
- Publication of a formal notice detailing the misconduct.
- Publication of an editorial detailing the misconduct.
- A formal letter to the head of the author's or reviewer's department or funding agency.
- Formal retraction or withdrawal of a publication from the journal, in conjunction with informing the head of the author or reviewer's department, Abstracting & Indexing services and the readership of the publication.
- Imposition of a formal embargo on contributions from an individual for a defined period.
- Reporting the case and outcome to a professional organization or higher authority for further investigation and action.

Originality and Plagiarism Policy

Authors by submitting their manuscript to PEN declare that their work is original and authored by them, their work submitted to PEN has not been previously published, original ideas, data, findings and materials taken from other sources (including their own published writing) are properly documented and cited, their work does not violate any rights of others, including privacy rights and intellectual property rights, their data is their won, true and not manipulated. Plagiarism in whole or in part without proper citation is not tolerated by the Journal. Manuscripts submitted to the journal will be checked for originality using anti-plagiarism software.

DOI: 10.21533/pen

ISSN 2303-4521
PERIODICALS OF ENGINEERING AND NATURAL SCIENCES
Vol. 5 No. 1 (2017) – Special Issue (Recent Topics in Environmental Science)
Available online at: http://pen.ius.edu.ba

The Potential of Solar Energy for Sustainable Water Resource Development and Averting National Social Burden in Rural Areas of Zambia

Mabvuto MWANZA
Solar Energy Institute, Ege University, Izmir Turkey

Mwansa KAOMA
School of Engineering, Unıversıty of Zambia, Lusaka, Zambia

Chilala K.BOWA
Faculty of Engineering And BuiltEnvironment University of Johannesburg, South Africa

Numan S.ÇETIN
Solar Energy Institute, Ege University, Izmir Turkey

Koray ÜLGEN
Solar Energy Institute, Ege University, Izmir Turkey

Abstract
About 50% of the Zambia's population in the rural areas do not have access to an improved source of water supply, thus relies on untreated water from shallow wells, streams and rivers for drinking and other activities. The lack of access to clean water is associated with water related illnesses and other negative social impacts. This paper aimed to propose use of solar energy in water pumping systems for water supply in rural areas of Zambia. The information used is from secondary sources.Use of the solar energy in water pumping system is not only an important part of providing household with clean drinking water alternative, but also important for access to an improved source of water supply for rural households and sustainable water resource development in Zambia. The paper further investigates the potential of using solar energy in water pumping system to avert the nation's disease burden and its sustainability using number of employment created as indicator. The analyzed results indicate that the use of solar energy in water pumping systems have the potential of reducing the Zambia's social cost burden by 30% which translate to about US$61million saving per year and can create employment of about 24,000 in Zambia.
country.

Keywords: PV water pumping system; solar energy; Photovoltaic; Water; Sustainable water development**,**

1. Introduction

Zambia is located in the heart of Southern Africa between latitudes 8 and 18 degrees south of the equator. Over 98.77% of Zambia's surface is taken up by land leaving only 1.23% covered by surface water such as rivers, streams, lakes and other inland water (Source). It has no access to the sea or ocean. The country is surrounded by eight neighboring countries namely; Tanzania and Democratic Republic of Congo (DR Congo) to the North, Angola to the West and Namibia to the South West; Botswana and Zimbabwe to the South; and Mozambique and Malawi to the east as shown in fig.1 [1,2]. It has a population of approximately 15.5million people (2015 estimates) of which 58% live in rural areas and 42% in urban areas [1,3,4]. According to UNICEF data, the level of access to improved source of water supply in Zambia for the whole population is about 64% and 50% for access to adequate sanitation [5]. However, only 55,3% of the rural populations have access to improved source of water supply and adequate sanitation [6]. The country has favorable climate with average sunshine of about 6-8hours per day throughout the country with monthly average of daily solar irradiation of 5.5kWh/m2/day throughout the year. Such irradiation is adequate for using solar energy technologies such as Photovoltaic water pumping systems [7]. The supply of clean and reliable water and reduction in distance to water supply source in rural areas is vital for the life of the community, livestock and agriculture. The use of solar energy in water pumping system is one of the best alternative solutions for rural areas that are located far from the electric grid since the solar energy resource is readily available in the communities.

The aim of the study is to assess the potential of solar energy in averting the water borne disease burden in the rural areas of Zambia, through improved access to safe clean water supply sources by using solar energy in water pumping systems. This desktop study involved collecting data from various literatures.

DOI: 10.21533/pen.v5i1.64

2. Water Situation in Zambia

2.1. Water Resources

The country has adequate water resources as compared to other countries in the region with water surface area of about 9,220km^2. It is rich in lakes such as Lake Mweru, Bangweulu, and Tanganyika and manmade lakes of Kariba and Itezhi-Tezhi, and rivers like Zambezi, Kafue, Luapula, Chambeshi, and Luangwa as shown in figure 1[2]. Table 1 shows statistics on the river catchment areas of some rivers and lakes in Zambia [2]. However, despite rich in water resources the availability of water in the country, the surface water is not evenly distributed as shown in fig.1, and the access to safe clean water by the rural population is low. The country has average annual rainfall ranging between 600 mm in the south and 1, 500 mm in the north [2,6].

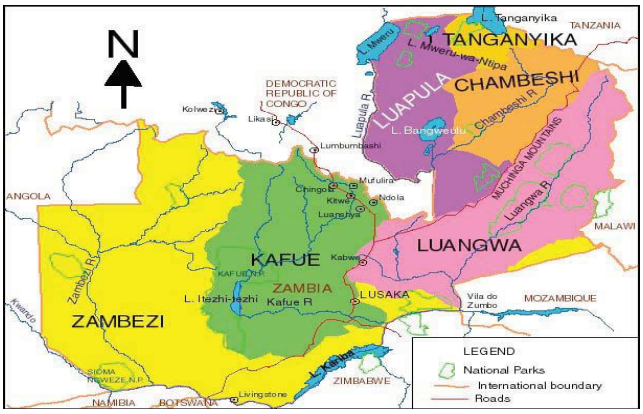

Fig. 1: River Basins of Zambia [2]

Table 1: Percentage Contribution of Rivers and Lakes to Water Resource [2]

River/Lake	Total Area(km^2)	Contribution to Surface water Potential (%)	Annual Run-Off (km^3)
Zambezi	803,267	36,36	41,75
Luapula	268,235	26,25	30,14
Luangwa	144,358	19,44	22,32
Chambeshi	44,427	7,62	8,75
Kafue River	156,995	8,40	9,88
Tanganyika	15,856	1,73	1,99
Total for Zambia	803,267	99,8	114,830

(Source: Ministry of Energy and Water Development)

2.2. Water Quality

The water quality in Zambia is generally good, however due to increase in population since independence this have resulted in increasing pressure on the water resource. As the results of human activities and ever increasing population in the country the water quality has generally reduced [2,6]. According to the World Health Organization 2013 report, water pollution of drinking water in most developing countries like Zambia are due to poor sewerage disposal, such as use of pit latrines for toilets in many rural and sub-urban areas and lack of access to clean water [8]. When pit latrines are used for toilets, the wastes are kept in the toilets holes because there is no sewerage system for disposing off the wastes far from the residential areas, thus during rain seasons, the polluted water from the toilets are gradually washed into the nearby groundwater or surface waters. This leads to affecting the environments and leads to water related diseases such as dysentery, cholera, diarrhea, and many other kinds of illnesses related to drinking untreated water from shallow wells in many rural areas.

2.3. Access to Safe Water

Zambia's total annual water consumption is just under 40 km^3 per year with hydropower generation taking the largest amount of water followed by agriculture, industry, drinking water and domestic water supply as shown in figure 3[2,6]. The government is facing with the challenge of satisfying 4,8 million people without access to safe water and 6,6 million people without access to adequate sanitation facilities [2,5]. This has been due to lack of investment in the water and sanitation infrastructure by the government and also because of the settlement patterns in the country [2,9]. As the result, there is low rate of access to water supply and sanitation especially in rural areas where the majority of the population lives as shown in table 2 section 3 below. Therefore, most people in these areas use untreated shallow water wells for their household water needs. However, the uses of these untreated water resources are mostly related to water borne related illness. Table 3 below in section 3 show the national outpatient and admission cases due to water borne related diseases due to lack of access to safe clean water and sanitation.

The government of Zambia stated a standard for access to domestic water supply which was set at 500 m and each water point is supposed to serve about 200 people [2,9]. These set standards can easily be achieved by use of solar energy technologies in water pumping systems in rural communities far from the grid.

3. PV Water Pumping System

A photovoltaic water pumping system is a water pumping system that uses solar energy as the primary energy source for pumping water. In these systems, the photovoltaic cells are used to convert solar energy into electrical energy, which is then used by the motor-pump unit for pumping water. This system offers best alternative solution for rural areas far from electric grid for pumping and supplying clean and improved water to the communities. In these systems water is usually pumped during the day and kept in water tanks for treatment and use during day time, night or under cloud cover [12].

Access to water supply in rural areas in many developing countries such as Zambia (for household, livestock and irrigation use) is very difficult and time consuming [13]. This is because people have to walk for long distances to draw water from rivers, streams, shallow wells, or boreholes that are usually located far from the communities [14]. Thus, water pumping systems that use solar energy are the best alternative solutions for rural areas for improved access to clean water supply source [14,15]. Typical Stand-alone solar water pumping systems generally consist of PV array, power conditioning unit, motor-pump unit, and water tank. The use of PV water pumping system in rural areas can greatly contribute to the development of the rural areas as it has potential for not only pumping and supplying water to the communities but also creating employment and reducing the use of untreated shallow water sources, thus, reducing the water borne related diseases such as mentioned in table 3.

4. Materials and Methods

This section shows the summary of the data considered for the investigation, the results and brief discussion of the results. In the study, polycrystalline PV module has been considered with the following specifications; PV power 250WP, Voltage VMPP 30.3V, operating current IMPP 8.25 and PV module area of 1.64m2 [24]. The monthly averages of daily solar irradiation for the study area have been extract from the NASA Surface Meteorology and Solar Energy. Table 4 contains the input parameters used for sizing a PV water pumping system for each serving point using the above equations above. In this study, only the direct employment at each serving point has been considered. Furthermore, in calculation of saving on social burden cost, the assumption was access to safe clean water reduces the water related diseases by 30% which was according to the study carried out by Esrey, S.A. The data used to estimate the cost of social burden was according to the study carried out in Zambia by Lumbwe Chola as shown in Table 5.

In order to investigate the potential of using solar energy in water pumping system to avert the nation's disease burden and its sustainability, the number of employment created has been used as indicator at 100% access to safe and clean water. According to the Zambian standards the average family size is 5 [1] and the average amount of water required per person per day in this study has been assumed to be 40 liters per day. According to the government of Zambia, the standard access point to domestic water supply is set at 500 meters from the furthest house and each water point is suppose to serve about 200 people [2,9]. Furthermore, according to [26] the cost of water on average is \$0.25/m^3 (0-6m^3) and the annual average of daily solar energy is 6,37kWh/m^2-day [7,25].
The components efficiency and factors considered in this study have been extracted from various literatures: Inverter MPPT set efficiency of 98% [24], Motor-Pump set efficiency of 42% [18, 23], cable losses 2% and PV other losses 10% [23].

Table 2: Summary of Access to Safe Water Supply and Sanitation in Zambia (Source: 2013,2014, NWASCO reports[4,5,9,11])

	2012			2013			2014		
	Population	Coverage (%)		Population	Coverage (%)		Population	Coverage (%)	
		SW	S		SW	S		SWS	S
Zambia	13,817,480	68,5	41,9	14,222,230	72,3	47,8	14,638,510	67,2	54,9
Urban	5,760,541	81,8	57,3	5,965,575	83,9	58,7	6,122,284	83,8	60,7
Rural	8,056,939	59,0	31,0	8,256,655	64,0	40,0	8,516,226	55,3	50,8

*SW-Safe Water Supply, S-Sanitation (Source: 2013,2014, NWASCO reports[4,5,9,11])

Table 3: Water Borne Related Disease Cases

Disease Description	Year					
	2010		2011		2012	
	Outpatient	Admission	Outpatient	Admission	Outpatient	Admission
Typhoid Cases	977	37	2,657	101	2,433	93
Severe Diarrheal (with Dehydration) Cases	1,546	59	25,742	982	29,948	1,143
Cholera Cases	8,893	339	796	30	483	18
Dysentery Cases	60,327	2,302	64,525	2,463	56,902	2,172
Diarrheal Non-Blood Cases	1,038,596	39,640	1,127,520	43,033	1,148,832	43,847
Total Cases	1,110,338	42,378	1,221,239	46,610	1,238,598	47,273
Total Population	13,460,310		13,881,340		13,817,480	
Percentage (%)	8,25	0,31	8,80	0,34	8,96	0,34

(Source: Ministry of Health, Planning and Policy Department [9,10])

Table 4: PV Water Pumping System Sizing Parameters

Parameter	Quantity
Average water required per person per day	0.04m3/day
Average Borehole Depth	30m

Tank Height from ground level	10m
Annual Monthly solar radiation	Maximum Radiation: 7.23 (kWh/m2/day)
	Average Radiation: 6.37(kWh/m2 /day)
	Minimum Radiation: 5.19 (kWh/m2/day)
Location	15057'40'' S, 26022'1''E
Optimal Inclination Angle	210
Number of people at each serve point	200 (40 house, 5 people per house on average)
Specific Pumping time (average sunshine time)	6hrs
Autonomy period	3Days

Table 5: Cost of Treatment for Water Borne Related Diseases [9,10]

Cost Description		**Amount ($/visit)**	**Amount ($/bed/day)**	**Number of visits (days)**	**Amount ($/a)**
Outpatient Costs					
Treatment Cost	Treatment	26	26	4	104
	Outpatient	3	3	4	12
Transport Cost	Transport and incidentals	10	10	1	10
Productivity Cost	Productivity Losses	25	25	1	25
Total Cost for Outpatient					151
Admitted Patient Costs					
Treatment Cost	Admission cost	78	78	4	312
	Treatment	26	26	4	104
Transport Cost	Transport and incidentals	10	10	5	50
Productivity Cost	Productivity Losses	25	25	4	100
Total Cost for Admitted Patient Costs					566
Water Treatment Cost		$0.7/person/a	a-annual		
Maintenance Cost (Well, Boreholes, Taps, Pumps)		$2/person/a			
Cost of Installing PV Water Pump System (assumed)		$10/W			

5. Theory/Calculation

5.1. Amount of Water Required

The amount of water required V_t to be supplied at each serving point per day, has been determined in terms of water required per person per day V_p and the number of people at the serving point N_p. Therefore, the volume of water V (m^3) in a tank that is required to supply each serving point for any number of autonomy days has been determined by [14,17].

$$V_t = N_P \cdot V_P T_D \quad (1)$$

Where Vt is total amount of water required to be pumped per day (m^3), Np is total number of people at serving point, Vp is total amount of water per person per day (m^3), and T_D is number of autonomy days (3 days in this case study).

The pumping rate which is also called water flow rate has been estimated using the average number of peak sunlight hours and the total amount of water required to be pumped per day using the equation given below [14,18].

$$Q = v.A = \frac{V_t}{t_T} \quad (2)$$

Where Q is pumping rate (m3 /s) or (m3/hr), t_T is number of sunlight hours or the total pumping time (hr), v is velocity of water (m/s), A is cross-section area of the pipe (m^2), and Vt is total amount of water required per day per serving point (m^3).

5.2. Pumping Head

The total dynamic head TDH is the sum of suction head H_{SH}, discharge head H_{DH} and total frictional head losses H_{HL} [18]. Assuming only 5% friction head losses should be allowed in the system the total dynamic head has been determined using eq. 3 [18,19]

$$H_{TDH} = 1{,}05(H_{SH} + H_{DH}) \quad (3)$$

Where H_{TDH} is total dynamic head (m), H_{SH} is suction head (m), and H_{DH} is discharge head (m).

5.3. Pump Hydraulic Power

The energy required by the motor-pump set depends on the efficiency of both the motor and the pump. However, the efficiency of subsystem depends on the efficiencies of motor-pump set, cables, other electronic components and inverter-MPPT system, these efficiencies translate into the total subsystem efficiency used to determine the total energy required per day. The power delivered by the pump to the fluid called hydraulic power which is required per day to supply volume of water Vt (m^3) at total dynamic head H_{TDH} has been determined using eq. 4 [12,18,20].

$$P_{hyd} = \frac{\rho g Q H_{TDH.}}{1000.} \quad (4)$$

Where P_{hyd} is Hydraulic power delivered by the pump to water (kW), ρ is water density (1000 kg/m3), g is acceleration due to gravity (9.81 m/s^2), H_{TDH} is total dynamic head (m), and Q is water flow rate (m^3/ s). The subsystem efficiency is given as:

$$\eta_{subsyst} = \eta_{mp}\,\eta_c\,\eta_{pcu} \quad (5)$$

Where $\eta_{subsystem}$ is efficiency of the subsystem, η_{pcu} is efficiency of power condition Units and other electronics, η_c is efficiency of Cables, and η_{mp} is efficiency of Motor-Pump set.

The total energy E_T (kWh) that has to be supplied to the subsystem for the specific period of time t_T called specific pumping time has been determined using eq.6.

$$E_T = \frac{P_{hyd}\, t_{T.}}{\eta_{subsyst}} \quad (6)$$

5.4. PV Generator Sizing

In order to determine the size of the PV generator and the number of PV panels required for the system. Firstly, it is important to determine the required PV area A_{PV} (m^2) from the worst case minimum monthly average of daily solar radiation, H (kWh/m^2-day), the PV module laboratory efficiency $\eta_{PV,u}$ and the operating efficiency of the PV module, and has been estimated using the eqs.7,8,9,10 and 11 given below [14, 22, 23]. PV module laboratory efficiency $\eta_{PV,u}$ has been determined using eq. 7.

$$\eta_{PV\ddot{o}u} = \frac{V_{MPP}\, I_{MPP}}{1000\ A_{PV\ddot{o}u}} \quad (7)$$

Where V_{MPP} is PV module Voltage (V), I_{MPP} is PV module current (A), and $A_{PV,u}$ is PV module area (m^2). The PV module operating efficiency has been calculated using eq.8.

$$\eta_{PV} = \eta_{PV,u} \cdot \eta_o \quad (8)$$

Where $\eta_{PV,U}$ is array efficiency at 1000 (W/m2) and 25 ^{0}C and η_O is array efficiency due to other losses in PV (shading, dirty, Temperature, etc, 10% losses due to other losses has been considered in this study.) The total active area that is required for the PV generator A_{PV} has been calculated using eq. 9 given as:

$$A_{PV} = \frac{E_{subsyst}}{H\ \eta_{PV}} \quad (9)$$

The Total PV generator Power PV_{MPP} and the number of panels N_{PV} that is required to supply the energy to the pumping subsystem has been determined using eq. 10 and 11 given below.

$$PV_{MPP} = 1000. \frac{\rho g Q H_{TDH}\, \eta_{PV,u}}{\eta_{PV}\, \eta_{subsyst} H_{OPT}} \quad (10a)$$

$$PV_{MPP} = 1000.\, \eta_{PV,u}\, A_{PV} \quad (10b)$$

$$N_{PV} = \frac{PV_{MPP}}{P_{MPP}} = \frac{PV_{MPP}}{V_{MPP}\, I_{MPP}} \quad (11)$$

6. Results and Discussion

Assuming that lack of access to clean safe water is the main cause of all the water borne related diseases in Zambia, the estimation of the average total social burden cost of the diarrheal illnesses to the country's economy is summarized in table 6. Fig.2 illustrates the projection of the diarrheal illnesses and the social burden cost per year expected to be in the future. It is worth noting that both the social burden cost and diarrheal illnesses are expected to continue increasing yearly if a anything is not done to combat the situation.

Table 6: Estimation of Social Burden Cost of Diarrheal illness

Cost Description	Year		
	2010	2011	2012
Outpatient Cases	1,110,338	1,221,239	1,238,598
Outpatient Cost ($/Patient)	151	151	151
Total Outpatient Cost ($/a)	167,661,038	184,407,089	187,028,298
Patient Admission Cases	42,378	46,610	47,273
Admitted Patient Cost ($/Patient)	566	566	566
Total Admitted Patient Cost($/a)	23,985,948	26,381,260	26,756,518
Total Burden Cost ($/year)	191,646,986	210,788,349	213,784,816
Average Total Burden Cost($/yr)	205,406,717		

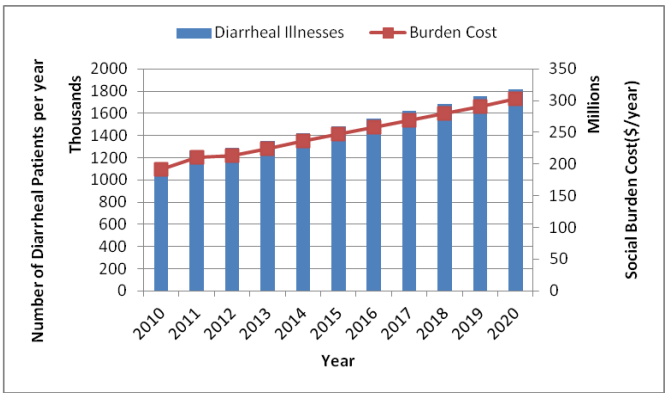

Fig. 2: Projected Social Burden Cost and Diarrheal illness cases

There is a link between lack of access to adequate safe water supply source and diarrheal diseases. When communities do not have access to safe water sources they tend to use unclean and untreated water sources. However, with the use of solar energy technologies in water pumping system in the rural areas means access to safe clean water supply source and reduction in time spend to collect water, since the use of solar energy in water pumping system can be used to pump the water into the storage tanks for treatment and supply to the consumers. Table 7 summarizes the findings of the study and shows the social burden cost saving and potential of solar energy in water pumping technology to provide clean and reliable water source for rural communities in Zambia. According to [28] the improvements in water supply system in most cases would reduce the water borne related diseases by 30%. Considering the 30% reduction in diarrheal case due to use of solar energy in water pumping systems for improved safe clean water supply to communities means saving 30% of the social burden cost. Therefore, by implementation of the solar energy technologies in water pumping systems in Zambia, the government would save approximately $61,6 million per year from the social burden cost and be able to create direct employment of about 24,000 by employing kiosk attendants. Furthermore, it can be noticed from the analyzed results, that if these systems are used in the country a huge number of people will have access to clean safe water sources, and also both direct and indirect employment will be created which will result into boosting the economy of the communities. On the other hand, the system has short payback period of about 7years.

Table 7: Calculation of PV Water Pumping System Costs and Saving on Social Burden Cost of Diarrheal illness

Description	2014
Population to be Serviced	4.8million
No. of Water Serve Points	24,000
No. of PV Water Pump Systems	24,000
Total Water to be Pumped(m3/a)	264.09million
Total Water Sell Cost ($/a)	66million
Total Power to be Installed (MW)	36.0
Total Installation Cost ($)	360Million
Total Water Treatment Cost ($/a)	3,36Million
Total Maintenance Cost($/a)	9,6Million
Average Total Burden Cost($/a)	205.41Million
Saving on Social Burden Cost($/a)	61.62million
Payback Period (years)	7
Saving on Social Burden Cost ($) (7yrs Period)	431,354,105.7
Employment Created	24,000

Conclusion

In this paper the water situation and diseases related to water situation in Zambia were outlined. At the same time, the potential of solar energy to contribute to improving access to safe and clean water supply source and avert the nation's water borne related disease burden has been assessed. There is a saying that's goes like ''Prevention is better than cure''. It is vital to prevent water borne related disease transmission than to cure them. This can be achieved through increasing access to safe clean water supply sources and reduction in use of untreated water from shallow wells. The analyzed results show that through improved access to safe clean water supply, the government will be able to create employment of about 24,000 people and also reduce on the social burden cost related to water borne disease by 30% which is translated to about US$61million savings per year. This money can be used in other development activities such as rural electrification. Therefore, the use of solar energy for water pumping systems in Zambia can greatly benefit the nation in averting the social burden costs related to water borne disease and create employment for rural communities. Furthermore, through the use of solar energy in water systems gives the government the ability to achieve four (4) of the SDGs (Sustainable Development Goals) of access to safe clean water supply source, creation of employment, and better health for the population of Zambia.

Acknowledgements

The authors are grateful to University of Zambia and Turkish Government for financial support.

References

[1] Likonge Makai, Marta Molinas (2013). Biogas-An Alternative Household Cooking Technique for Zambia", IEEE Conference, 2013.

[2] Prof. Dr. Imasiku A. Nyambe, Miriam Feilberg, '' Zambia- National Water Resources Report for WWDR3; Theme-Water in a Changing World'', Repubulic of Zambia, Ministry of Energy and Water Development. Pp 6-50

[3] Index Mundi, www.indexmundi.com

[4] NWASCO, 2014,'Urban and Peri-Urban Water Supply and Sanitation Sector Report 2014'', pp 2

[5] http://www.unicef.org/Zambia

[6] Chola Kasoma Mbilima, 2012, ''Water Supply and Sanitation in Zambia'',

[7] Ministry of Mines, Energy and Water Development of Zambia[MEWD] (2008). National Energy Policy. http://www.mewd.gov.zm/

[8] Chric Woodford, 2015, ''Water Pollution: An introduction'', June 29, 2015. www.explainthatstuff.com/waterpollution

[9] Zambia NGO water, Sanitation and Hygiene Forum, 2012, "Financing water supply and sanitation in Zambia: 2007-2012: Study to Establish Levels and Trends of Sector Financing", report 12/10/2012, pp 9-52.

[10] Lumbwe Chola and Bjarne Robberstad: Estimating average inpatient and outpatient costs and childhood pneumonia and diarrhoea treatment costs in an urban health centre in Zambia. *Cost Effectiveness and Resource Allocation* 2009, **7**:16.

[11] NWASCO, 2013,'Urban and Peri-Urban Water Supply and Sanitation Sector Report 2013'', pp 2

[12] S.S. Chandel, M. Nagaraju Naik, R. Chandel, 2015,'Review of solar photovoltaic water pumping system technology for irrigation and community drinking water supplies', Renewable and Sustainable Energy Reviews 49 (2015) 1084-1099, ScienceDirect

[13] M. Benghanem, A. Hadj Arab, 2007, ' Photovoltaic Water Pumping Systems for Algeria', Desalination 209 (2007) 50-57. ScienceDirect.

[14] K.G. Mansaray, 2014,'Optimum Design of Solar Photovoltaic Pumping Systems by Computer Simulation', International Journal of Emerging Technology and Advanced Engineering, www.ijetae.com (ISSN 2250-2459, ISO 9001: 2008 Certified Journal, Volume 4, Issue 9, September 2014)

[15] R. Posadillo, R. Lopez Luque, 2008, ' A sizing method for Stand-alone PV installations with variable Demand', Renewable Energy 33 (2008) 1049-1055, ScienceDirect.

[16] Yahia Bakelli, Amar Hadj Arab, Boubekeur Azoui, 2011, 'Optimal sizing of photovoltaic pumping system with water tank storage using LPSP concept', Solar Energy 85 (2011) 288-294, ScienceDirect.

[17] Tamer Khatib, 2010, 'Design of Photovoltaic Water Pumping Systems at Minimum Cost for Palestine: A Review', Journal of Applied Sciences 10 (22): 2773-2784, 2010 ISSN 1812-5654.

[18] Paul Mac Berthouex, Linfield C. Brown , 2015, 'Pollution Prevention and Control: Part II Material and Energy Balances'. pp 257-265, www.bookboon.com

[19] Abdelmalek Molceddem, Abdelhamid Midoun, D.Kadri, Said Hiadsi, Iftikhar A. Raja, 2011, ' Performance of a Directly-Coupled PV water Pumping System', Energy Conversion and Management 52 (2011) 3089-3095, ScienceDirect.

[20] A.Hamidat, B.Benyouced, 2009, 'Systematic Procedures for Sizing Photovoltaic Pumping System, Using Water Tank Storage', Energy Policy 37 (2009) 1489-1501, ScienceDirect.

[21] Tuma Nocchi Pentair Water, Electric Pumps Catalogue

[22] Ceyda Olcan, 2015, 'Multi-objective analytical model for optimal sizing of stand-alone photovoltaic water pumping systems', Energy Conversions and Management 100 (2015) 358-369, ScienceDirect.

[23] Mete Cubukcu, 2015, 'Reliability of Photovoltaic Power System Lecture Notes', Solar Energy Institute, Ege University.

[24] http://www.alibaba.com/product-detail/High-efficiency-good-price-pv solar_1824340428.html?spm=a2700.7724838.30.26.KvgWT1&s=p

[25] http://re.jrc.ec.europa.eu/pvgis/

[26] NWASCO, 2014,'' Water Supply And Sewerage Tariffs- 2014'' report

[27] http://www.alibaba.com/product-detail/solar-water-pump-inverter-mppt_60097638956.html?spm=a2700.7724838.29.81.SLIVyu

[28] Esrey, S.A., J.B:potash, L.Roberts and C.Shiff, 1991, Effects on Improved Water Supply and Sanitation on Ascariasis, Diarrhea, Dracunculiasis, Hookworm Infection, Schistosomiasis, and Trachoma Bulletin of the World Health Organization 695609-12.21

[29] Ahmad Agus Setiawan, Didik Hari Purwanto, Didit Setyo Pamuji, Nurul Huda, 2014, ' Development of a Solar Water Pumping System in Karsts Rural Area Tepus, Gunungkidul through Student Community Services', Energy Procedia 47 (2014) 7-14. ScienceDirect.

ISSN 2303-4521
PERIODICALS OF ENGINEERING AND NATURAL SCIENCES
Vol. 5 No. 1 (2017) – Special Issue (Recent Topics in Environmental Science)
Available online at: http://pen.ius.edu.ba

THE EFFECT OF SEALING SYSTEM ON ZERO FUGITIVE EMISSIONS AND GLOBAL WARMING

Adem CALISKAN, Adem ONAT

*Sakarya University, Vocational School of Sakarya, 54188 SAKARYA – TURKEY

Abstract

Nowadays keeping the air clean is one of the most important aims in environmental protection. The fugitive emissions especially Volatile Organic Compounds (VOC's) and the ozone-precursors nitrogen oxides (NO_X) have a great impact on the quality of the atmospheric air. Worldwide fugitive emissions from leaking valves, pumps and flanges amount to over a million metric tonnes per year. Elimination or reduction of fugitive emissions could save industry many millions of dollars and prolong scarce resources.

Sealing system is the major contributing factor will be through the lowering of fugitive emissions. In this study, various kind of fibre reinforced Nitrile Butadiene Rubber (NBR) sheet sealing materials and new developed expanded graphite sheets were investigated. Experimental results shown that, the sealing performance has been improved by the development in material technologies. Fibre base materials have higher permeability than expanded graphite for both liquid and gas environments. They have adequate sealing performance to need for all over applications. Expanded graphite shows better sealing performance than fibre base materials but it has lower recovery.

As a result, for every specific application, careful selection, correct installation and operation according to the performance envelope, regular inspection and maintenance must be considered for low or zero emission requirements.

Keywords: Fugitive Emission; Global Warming; Volatile Organic Compound; Sealing Materials; Characterization; Sealing Performance

1. Introduction

It is recognised that industry must reduce its impact on the environment if we are to continue global development for future generations. A major contributory factor will be through the lowering of industrial emissions, which has been catalysed by a combination of public pressure, environmental legislation and the internal requirement to minimise the loss of valuable feed-stocks. Large proportions of the emissions to atmosphere are represented by the by-products of combustion (notably the oxides of carbon, nitrogen and sulphur), along with known losses of Volatile Organic Compounds (VOC's) and steam. In general, these are all emissions anticipated from the industrial process, under the control of the plant operator [1-3].

The fugitive emission is often defined as; *any chemical, or mixture of chemicals, in any physical form, which represents an unanticipated or spurious leak, from anywhere on an industrial site* [1-3]. It also covers all losses of materials (usually volatile) from a process plant, through evaporation, flaring, spills and unanticipated or spurious leaks [1].

The fugitive emissions especially VOC's are of significant environmental concern because some have the potential for Photochemical Ozone Creation Potential (POCP), Ozone Depletion Potential (ODP), Global Warming Potential (GWP), toxicity, carcinogenicity and local nuisance from odour. These properties mean that VOC's are a major contributor to the formation of "Summer Smog". The prevention of VOC emissions is therefore one of the most important issues facing the operation of many industrial processes [1, 4, 5].

VOC is the generic term applied to those organic carbon compounds which evaporate at ambient temperature, and is defined usually as "*a substance having a vapour pressure of greater than 0.3kPa at 20°C".* The term covers a

DOI: 10.21533/pen.v5i1.65

diverse group of substances and includes all organic compounds released to air in the gas phase, whether hydrocarbons or substituted hydrocarbons. Their properties, and hence need for control, vary greatly and so systems have been developed to categorise VOC's according to their harmfulness. The three classes are [1]:

- ***Extremely hazardous to health*** (such as benzene and vinyl chloride)
- ***Class A compounds***, which may cause significant harm to the environment (e.g., acetaldehyde, aniline and benzyl chloride)
- ***Class B compounds***, which have lower environmental impact

Some VOC's may also be highly odorous, for example aldehydes, amines, mercaptans and other sulphur-containing compounds. This may necessitate additional stringency in the prevention measures (e.g. high integrity equipment to reduce fugitives) and the abatement of losses.

To put the scale of the challenge into perspective, fugitive emissions in the USA have been estimated to be in excess of 300,000 tonnes per year, accounting for about one third of the total organic emissions from chemical plants, and inevitably mirrored in Europe. Irrespective of any environmental impact which it may cause, this is a tremendous financial burden on industry because it represents a huge loss of potentially valuable materials, and cause of plant inefficiency [4]. Yet in most instances, the true costs are not appreciated, since many of the costs associated with fugitive emissions are invisible (Figure 1) [1-4]. The values of fugitive emissions will depend upon [1, 2]:

- Equipment design
- Age and quality of the equipment
- Standard of installation
- Vapour pressure of the process fluid
- Process temperature and pressure
- Number and type of sources
- Method of determination
- Inspection and maintenance routine
- Rate of production

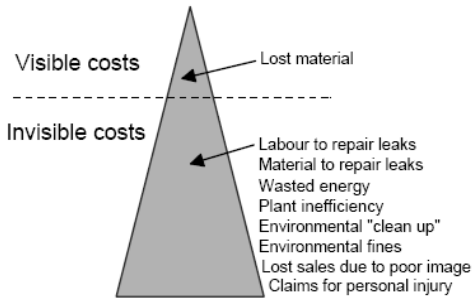

Figure 1. The sources and costs of fugitive emissions [1-4]

A significant proportion of fugitive emissions can be losses from unsealed sources, including storage of liquid and gas tanks, open-ended (non-blanked) lines, pressure-relief valves, vents, flares, blow-down systems, spills and evaporation from water treatment facilities. These are part of the industrial process, usually anticipated by the process operator. In other cases, these losses may be caused by leaks in the sealing elements of particular items of equipment, such as [1]:

- Agitators / Mixers
- Compressors
- Flanges
- Pumps
- Tank Lids
- Valves

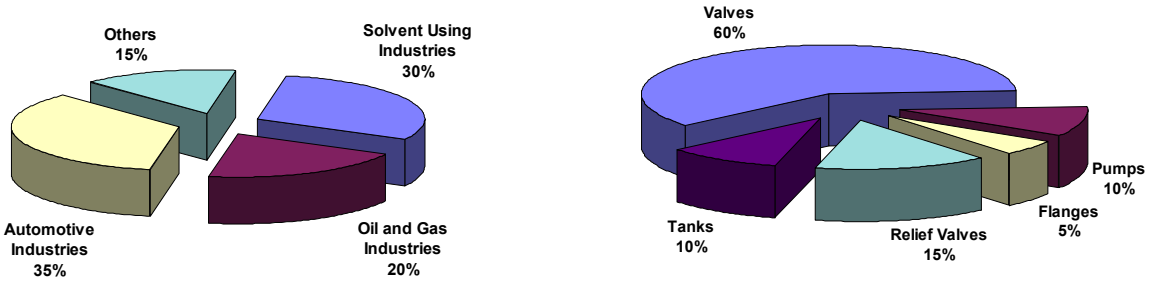

Figure 2. Fugitive emissions by source type [3]

As can be seen Figure 2, valves are considered to account for approximately 50-60% of fugitive emissions. Furthermore, the major proportion of fugitive emissions comes from only a small fraction of the sources [1-4]. Leaking losses are often hard to determine since there are many potential sources and they are very dependent on how well the installation is operated, maintained and inspected. Some important causes of leaking losses are [1]:

- Ill-fitting sealing elements
- Installation faults
- Construction faults
- Wear and tear
- Ageing
- Equipment failure
- Contamination of the sealing element
- Excursions out of normal process conditions
- Poor maintenance procedures

Sealing systems play a vital role in the environmental performance of industrial installations. After careful selection appropriate for the specific application, correct installation, and operation according to the performance envelope, regular inspection and maintenance must be considered for low or zero emission requirements.

A seal is a basically a device closing (sealing) a gap or making a joint-tight the fluid in this case being either a gas or liquid [6, 7]. The primary purpose of a seal is to contain a fluid and so protect the immediate environment from contamination and vice versa [8]. This may vary in significance from innocuous fluid loss such as steam and water up to nauseous, toxic or hazardous fluid loss. In the former case, the loss of such innocuous fluid will lead primarily to lack of plant efficiency for the operator, although such leakages may still present hazards such as leakages of high pressure water or steam. Clearly, in the latter case it is not only financially inefficient but also environmentally dangerous; for employees, members of the public and for nature at large! Consequently, the correct selection and use of the appropriate sealing technology for the application is just part of the environmental responsibility of the plant operator.

Sealing takes place between surfaces which do not move relative to one another in static seals or gaskets whereas a dynamic seal where sealing takes place between surfaces which have relative movement [6, 9].

It is possible to say that a static seal or gasket is one of the most important mechanical construction parts of each kind of machines and transport systems used in automotive and aerospace industry, piping systems and petrochemical industry [10-12].

2. Experimental Studies

In this study, parameters affecting system performances to elimination of fugitive emissions were determined and effects of variations on these parameters on sealing performance and mechanical properties are characterised according to tests given by ASTM, DIN, BSI standards. For this aim the widespread used soft gasket materials, have 0.80 mm thickness, were investigated in experimental studies. For this aim, fibre based static sealing materials widespread using in sealing applications were determined then procured. Also new developed expanded graphite sheet materials were used for characterisation.

Experimental equipment's were designated and manufactured according to international standards. Also test samples were prepared in steel cutting moulds to achieve close tolerance. Before every test five samples were conditioned as specified for particular type of material and tests according to relevant standards.

3. Results and Discussions

The important sealing materials properties affecting system performance and fugitive emissions are discussed below:

a) ***Density*** is the one of the most important properties affecting sealing performance. It is given by calculation of the grams of material in a cubic centimetre (g/cm^3). The sealing ability depends on the porosity amount of materials. Generally, the higher the density gives the better the performance. But sealing elements must be compressible enough to fill surface irregularities of flanges. Average densities of sealing materials used in experimental studies are given in Figure 3.

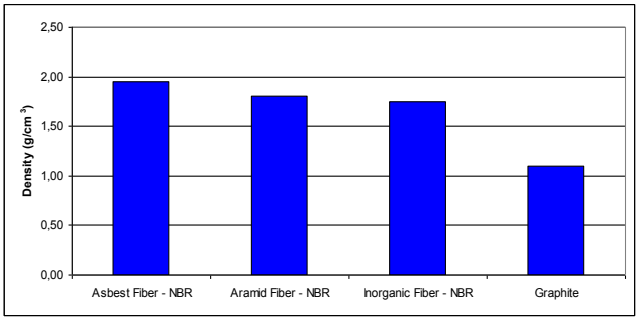

Figure 3. Density of selected gasket material types

As can be seen the above figure new developed graphite base materials have lover density from the other commercial materials. Also it is clear that as the sealing materials technology develops, density decreases. On the other hand, in the international sealing literatures sealing materials can be classified into three groups according to their density:

1. Low density (lower than 0.88 g/cm^3): Offer high degree of conformability for used or scratched flanges that are often encountered in the aftermarket or service industries. Generally, lower density materials don't seal as well as high density material, and don't have sufficient torque retention for the more demanding applications of global OEM manufacturers**.** In this investigation all of samples have low density.

2. Medium density (between 0.88 g/cm^3 and 1.36 g/cm^3): Offers a balance or compromise between low and high density. These materials are acceptable for OEM use and offer the necessary sealability and torque retention capability. Used in joints that does not require mechanical integrity or outstanding sealability. In this study, only graphite base material is in this group.

3. High density (greater than 1.36 g/cm^3): These materials are less compressible and suited for applications with uniform flange pressures, since these materials will not conform well to flanges that bend or distort. High density materials have excellent sealability, crush resistance and torque retention. Suitable for most OEM applications**.** The asbestos and aramid fibre base sealing materials in this investigation are suitable for this criteria widespread used material in the world.

b) ***Sealability*** is probably the most important of all gasket properties, because it measures the primary function of a gasket's ability to seal. It is a measure of how much fluid escapes from a controlled flange surface and measured as a leakage rate, generally in ml/h.

Standard ASTM testing used ASTM Fuel A or Nitrogen as the fluid, with the flange being a very smoothly finished steel surface (thus evaluating leakage through the material only and takes flange surface condition out as a variable).

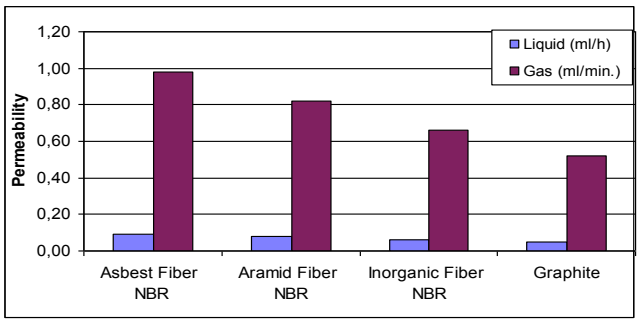

Figure 4. Leakage rates of selected gasket material types

c) ***Compressibility*** *is e*xpressed in percentage; it is a measure of how much the thickness of a material changes under a given load, compared to its original thickness. Compressibility properties of gasket materials vary depending upon the type of material and the applications for which they are intended.

In order to function effectively, a gasket material must be somewhat compressible. This is necessary for two reasons. First, the gasket material must be able to conform to surface irregularities of flanges. Second, in the case of fibrous sheets, the gasket material must be sufficiently compressible to close the pores and render the material

impermeable for sealing purposes. In addition, however, the gasket material must not be so soft as to easily crush or creep [13].

d) ***Recovery*** is *e*xpressed in percentage; it is a measure of the resiliency of the material. The number indicates the percentage of "spring back" of the material after it has been compressed under a given load. For example, a material with 20% recovery means it regains 20% of the thickness it lost after being compressed under a given load.

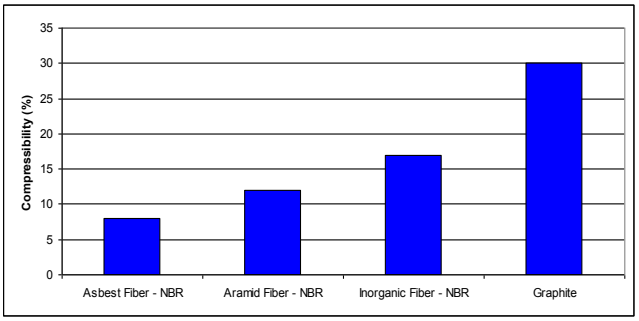

Figure 5. Compressibility of selected gasket material types

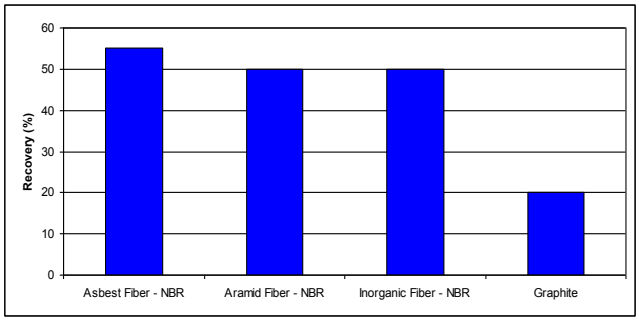

Figure 6. Recovery of selected gasket material types

Once compressed, most gasket materials do not act like perfect springs. If the compressive load on gasket materials is removed immediately after application, the material will usually not totally re expand to its full initial thickness (~100% recovery). Rather, the gasket material takes a partial compression set and recovers only partially. The amount of recovery and the residual compressive strength of a gasket can be crucially important in applications involving thermal cycling or vibration that can cause flanges to move with respect to each other.

On seating, a gasket must be capable of overcoming minor alignment and flange imperfections, such as:

- Non-parallel flanges
- Distortion troughs / grooves
- Surface waviness
- Surface scorings
- Other surface imperfections

So, the primary function of a gasket is to create and maintain a seal between flanges, under conditions which may vary markedly from one joint to another, dependent upon the nature and type of application. To meet these varying conditions, a number of flange / fastener / gasket systems have been developed.

Importantly, for all of these systems, the performance of the seal depends upon the interaction of the various elements of the flange joint system [9, 14]. Only when all the components of the system working together in harmony, the seal can be expected to provide a good performance over a reasonable lifetime. The integrity of a safe seal depends upon:

- Selection of correct components appropriate for the application
- Careful preparation, cleaning, installation and assembly
- Correct bolt tightening and loading
- Regular inspection

The behaviour of a flanged joint in service depends on whether or not the tension created in the fasteners will clamp the joint components together with a force great enough to resist failure of the seal, but small enough to avoid damage to the fasteners, joint components, gasket etc. The clamping load on the joint is created on assembly, as the nuts on the fasteners are tightened. This creates tension in the fastener (i.e. *preload*). Although there may be some plastic deformation in the threads when a fastener is tightened normally, especially on the first tightening, most of the joint components respond elastically as the nuts are tightened. Effectively, the entire system operates as a spring, with the fasteners being stretched and the other joint components being compressed.

e*) Working Temperature and Pressure:* Temperature will have a significant effect on the sealing performance since hot and cold conditions will degrade the physical properties of the jointing materials and deform them. Sealing material has to withstand maximum and minimum working temperature. Variations in thermal conditions cause the flanges to expand and contract, giving rise to a complex array of lateral forces on the sealing materials. The sealing material must either be able to withstand these lateral forces or the forces must be reduced to an

acceptable level. Application of the anti-friction coating can also help reduce flanges distortion. The application ranges of sealing materials are given in Figure 7 and Figure 8.

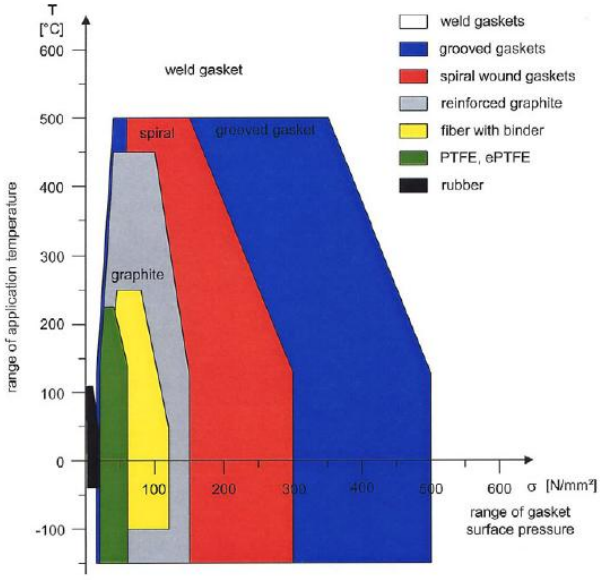

Figure 7. The range of gasket surface pressure limits in relation to the range of temperature for typical gasket types [2]

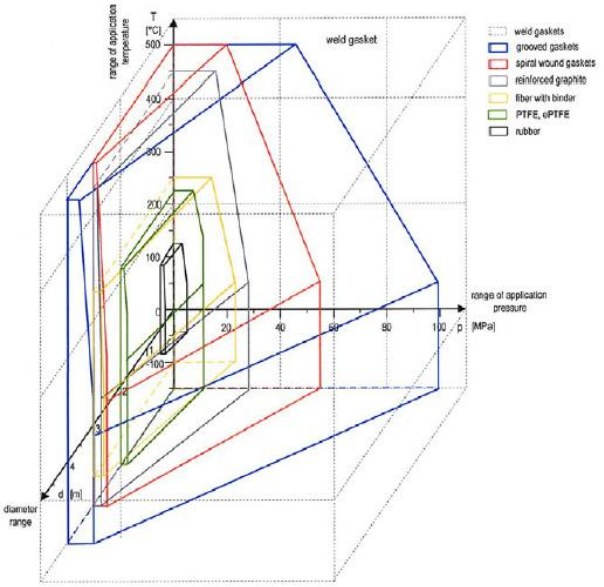

Figure 8. Pressure-temperature range and gasket diameter (p – T – d) for the gasket type or material may be used safely [2]

In maintaining a seal, temperature can never be treated as a completely independent factor. For example, temperature has effect on torque loss. Beyond that, temperature ties in with relative motion of flanges as well as with the chemical considerations in maintaining the initial seal.

As temperature rises from the ambient condition under which a joint assembly is initially tightened, the seal usually improves by a perceptible degree. This can be attributed to a softening effect in the gasket produced by heat. The gasket flows into flange surface imperfections, thereby improving the initial conformation between the gasket and flange.

Prolonged exposure to higher than ambient temperature will cause many non-metallic materials to harden abnormally high temperatures can cause complete breakdown in the initial seal. These are the temperatures which produce burning or charring in non-metallic gaskets. If such conditions exist, preference should be given to high performance fibre-rubber gaskets. [10].

f) ***Cost:*** Probably the most important factor considered in any sealing design is cost. However, the cost of the sealing materials, in terms of actual piece price and tooling, should be considered with the cost of other components in the system, that is influenced by seals. In most cases, the cost of the actual sealing technology is infinitesimally small when compared with the investment made in the plant as a whole (Figure 9). Indeed, for many sealing technologies, the cost per unit may be in the region of a few cents, completely insignificant when the total plant costs are considered.

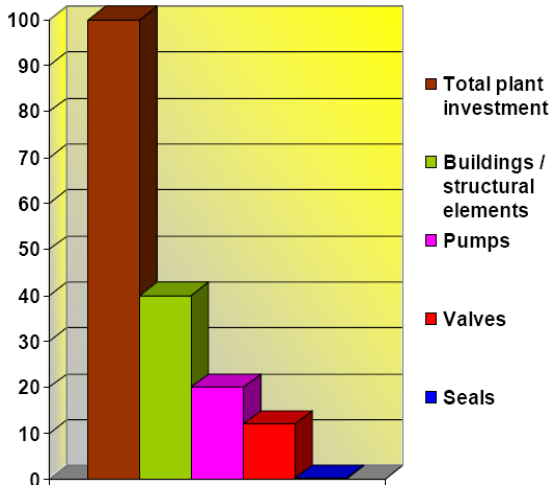

Figure 9. The cost of the sealing technology [2]

Importantly, the unit cost of the sealing technology is overwhelmed completely by the labour costs required to fit the seal, let alone the downtime of the plant. Consequently, the actual cost of the sealing device is immaterial in terms of economic considerations for best available techniques (BAT). However, for the sake of completeness, the following diagram provides an overview of the relative cost of the gasket and the environmental impact of the sealing system (Figure 10).

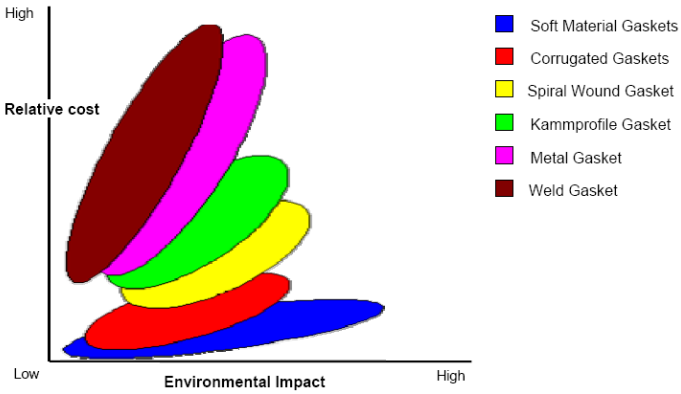

Figure 10. Relative cost of gasket versus environmental impact [2]

Alongside the introduction of asbestos-free gasket materials, there have been many developments for alternative gasket technologies. The following diagrams represent the sealing requirements of the vast majority of process applications.

4. Conclusions

It is recognized that industry must reduce its impact on the environment for sustained global development for future generations. A major contributing factor will be through the lowering of industrial emissions, which has been catalysed by a combination of public pressure, environmental legislation and the internal requirement to minimize the loss of valuable feed-stocks. Sealing systems play a vital role in the environmental performance of industrial installations. After careful selection appropriate for the specific application, correct installation, and operation according to the performance envelope, regular inspection and maintenance must be considered for low or zero emission requirements.

As a result, with increasing requirements to reduce industrial emissions, with new sealing technologies, and with new sealing materials requiring more careful selection, handling and installation. Overall, these new materials can outperform their asbestos equivalent, but are usually less forgiving; users must exercise more care in selecting the right material for the job and assembling the seal.

References

[1]. Sealing Technology-BAT Guidance Notes, European Sealing Association e.V. ESA Publication No: 014/04-draft 4, January 2004

[2]. Guidelines for Safe Seal Usage -Flanges and Gaskets- ESA/FSA Publication No: 009/98 September 1998.

[3]. B. S. ELLIS, "Emission Legislation-Development and Progress", International Seal Forum at Achema '97, Frankfurt, Germany, 9-13 June 1997.

[4]. R. SZWEDA, "Fugitive Emissions: The Matter of Imperfect Seals", Sealing Technology, No: 83, 9-11

[5]. A. C. ALKIDAS, "Combustion-Chamber Crevices: The Major Source of Engine-out Hydrocarbon Emissions under Fully Warmed Conditions", Progress in Energy and Combustion Science, 25 (1999), 253-273.

[6]. I. BROVNICAR, P. PEVEC, Static Industrial Sealing, Donit Tesniti, 1995.

[7]. Non - Metallic Gasketing Handbook, Fluid Sealing Association (FSA), USA.

[8]. A Primer on Cylinder Head Gaskets: Society of Automotive Engineers (SAE) Vol: 88, No: 8, August 1980.

[9]. R. H. WARRING, Seals and Sealing Handbook, Section 2A- Gaskets, Trade&Technical Press Limited, 1981.

[10]. Gasket Engineering Manual, Armstrong Industry Products Division, USA, 1987.

[11]. R. H. SWICK, "Designing The Leakproof", Machine Design, January 1976, 100-103

[12]. I. BROVNICAR, F. BERNARD, "New Concepts-New Technologies to Meet New Standards and Customer Requirements", International Seal Forum at Achema '97, Frankfurt, Germany, 9-13 June 1997.

[13]. A. ONAT, "Manufacturing and Characterisation of Composite Static Sealing Materials", PhD Thesis, The Graduate School of Natural and Applied Sciences of Sakarya University (SAU), Metallurgy Engineering & Materials Science Department, 2000.

[14]. "The Search for a Replacement for Asbestos Gaskets", Sealing Technology, No: 72, 7-9

ISSN 2303-4521
PERIODICALS OF ENGINEERING AND NATURAL SCIENCES
Vol. 5 No. 1 (2017) – Special Issue (Recent Topics in Environmental Science)
Available online at: http://pen.ius.edu.ba

A Comparison of Perturb & Observe and Fuzzy-Logic Based MPPT Methods for Uniform Environment Conditions

Ekrem Kandemir
Solar Energy Institute, Ege University, Izmir, Turkey
ekremkdemir@gmail.com

Numan S. Cetin
Solar Energy Institute, Ege University, Izmir, Turkey

Selim Borekci
Faculty of Engineering, Electrical - Electronic Engineering, Akdeniz University, Antalya, Turkey

Abstract
The power generation from photovoltaic (PV) system is not constant and it varies based on solar irradiance and temperature. For any environmental condition, to convert maximum available solar energy, PV systems must be operated at maximum power point. To accomplish that two different maximum power point tracking (MPPT) methods have been presented in this study. The first method can determine MPP point by measuring the derivative of PV cell power (dP) and PV cell voltage (dV) which is called Perturb & Observe (P&O) method. The second method uses fuzzy-logic-control (FLC) based MPPT method to determine MPP point for actual environment conditions. In this paper, 3kW PV system model is studied in MATLAB. According to the simulated results, FLC based MPPT method has better performance than P&O method. Compared to the P&O method, FLC-based MPPT can increase tracking accuracy and efficiency performance 0.13% under standard test conditions (STC).

Keywords: PV model, PV characteristic curves, Maximum Power Point Tracking (MPPT), Perturb & Observe (P&O) Method, Fuzzy Logic Control (FLC)

1. Introduction

Demand for energy is increasing every day. Due to fossil fuel exhaustion and the environmental problems caused by the conventional power generation such as gasoline, coal, etc…, renewable energy sources such as photovoltaic panels and wind – generators are now widely used [1]. They are popular and environmental friendly energy sources [2, 3]. When enough solar irradiance reaches PV panel, PV panel generates electrical power without any harmful effect to environment.

Recently, due to its development and cost reduction, PV systems become an efficient solution to the environment problem [4]. However, the development for improving the efficiency of the PV system is still a challenging field of research [5]. Efficiency of the PV panel system depends on load and environment condition.

Generated power from PV panels varies depending on electrical loads at the same environment condition. Because of that, generation of maximum available power is not guaranteed at all electrical loads [6]. Hence, Maximum available power can be generated at a specific point which is called Maximum Power Point (MPP). It is a single operating point given by a localized voltage and current for each environmental condition. The position of MPP point varies depending on solar irradiance, temperature and electrical load [7]. This problem requires a controller algorithm to find and track the MPP point for all atmospheric changes. In the literature, there are various maximum power point tracking methods used to operate PV systems at MPP.

Because of being simple and easy to implement, Perturb & Observe (P&O) method is one of the most used ones in the literature. However, this method presents some drawbacks. P&O method shows convergence and oscillation problems around MPP region. Also, depending on small derivation parameters, it has slow response rate to reach MPP. To enhance the performance and remove these drawbacks of the P&O method, this study presents Fuzzy Logic Control (FLC) based MPPT method. The simulation and a general comparison between P&O and FLC based MPPTs are discussed in this paper.

DOI: 10.21533/pen.v5i1.67

2. Equivalent Circuit Model of PV Panels

PV cells are p – n junction semi – conductors that when exposed to light releases electrons around a closed electrical circuit [8]. In the literature, there are various types of PV cell equivalent circuit model. Commonly, single diode equivalent circuit model is used to express typical electrical characteristic of PV arrays [6].

A PV panel is built from connecting several PV cells in series or parallel. Figure 1 shows a PV cell equivalent circuit and a PV panel with 9 cells.

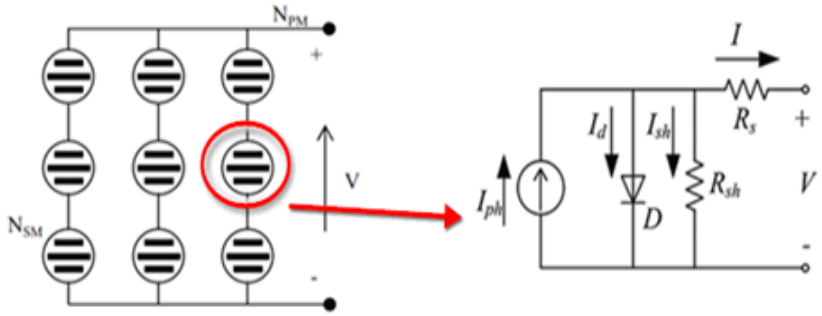

Figure 1. A PV panel and Equivalent circuit model of a PV cell

Electrons from the cell are excited to higher energy levels when a collision with a photon occurs. These electrons are free to move across the junction and create a current. This current is modelled by the light generated current source (I_{ph}). The intrinsic p – n junction characteristic of the PV cell is represented as a diode in the equivalent circuit model [9].

The PV load current show in Fig. 1 is defined as

$$I = I_{ph} - I_o\left(e^{\frac{q(V+R_sI)}{AkT}} - 1\right) - \frac{V+R_sI}{R_{sh}} \quad (1)$$

where I and V represent PV cell output current and voltage. R_s and R_{sh} are the PV cell series and shunt resistance respectively. I_{ph} is the PV cell photo current, I_o is the diode saturation current, A is the diode quality factor (≅1.2), K is Boltzmann's constant (1.38×10^{-23} J/K) and T is the PV cell temperature in kelvins.

By using Eq. (1), the 3 kW PV panel system is modelled in MATLAB. As known by researches about PV cells and panels, solar irradiance and temperature affect PV panel operating point and electrical characteristics. In this context, the voltage – current and voltage – power characteristic curves are plotted for different solar irradiance and temperature values to show electrical changes.

Variation of solar irradiance affects PV panel power directly that PV power increases if solar irradiance increases. Figure 2 shows PV electrical characteristics curves for different solar irradiance levels (0-250-500-750-1000 W/m^2) at a constant temperature (25°C). The maximum power occurs at around 80% of the open circuit voltage of PV panel.

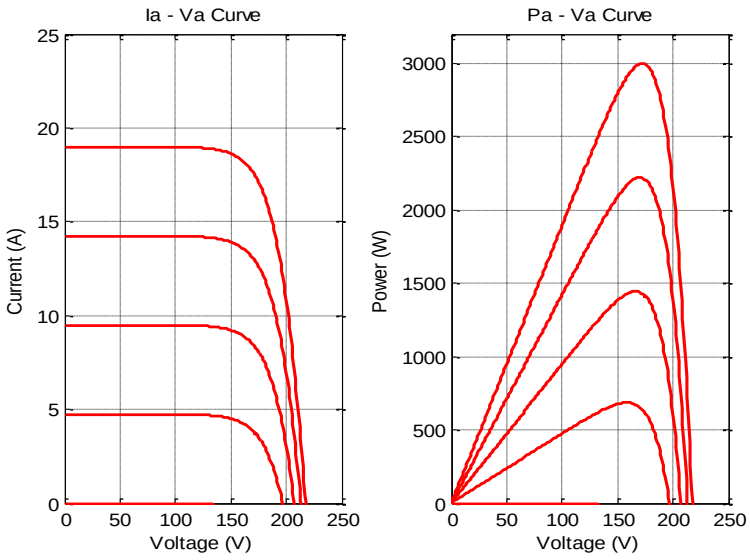

Figure 2. Current, voltage and power curves of PV panel under constant temperature and different solar irradiance

Variation of ambient temperature also affects PV panel power inversely that PV power increases if ambient temperature decreases. Figure 3 shows PV electrical characteristics curves for different ambient temperature levels (0°C, 25°C, 50°C, 75°C and 100°C) at a constant solar irradiance (1000 W/m^2). Unlike previous case, the maximum available power of the PV panel can be at different voltage level in different temperature.

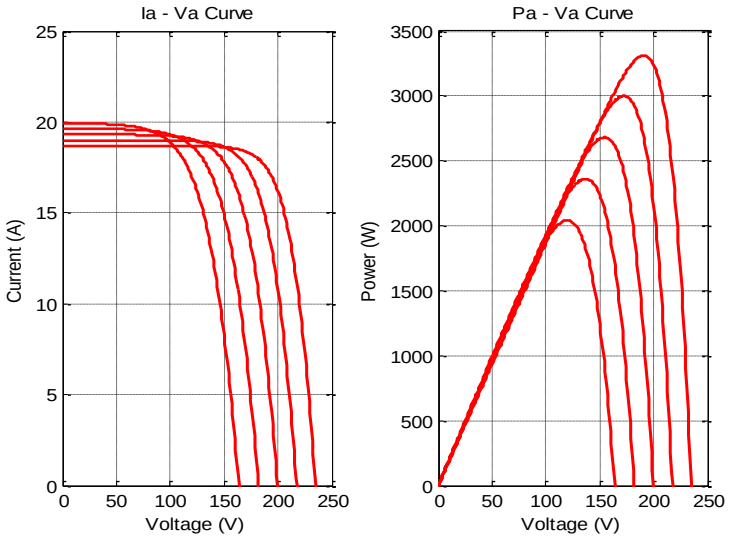

Figure 3. Current, voltage and power curves of PV panel under constant solar irradiance and different temperature

3. Maximum Power Point Tracking Methods for PV Panels

PV cells and panels generate different power depended on different environment condition and electrical load. Because of that, generation of maximum power is not guaranteed at all electrical loads [6]. Figure 4 illustrates maximum power point where PV panels operates maximum efficiency for a specific solar irradiance and temperature values. As shown in Figure 4, there is only one electrical load point which corresponds to the MPP for uniform environment condition. To utilize the PV panels on MPP, there are many MPPT algorithms have been developed and implemented by the researchers in the literature [10-11].

$$G = 1kW/m^2, T = 25°C$$

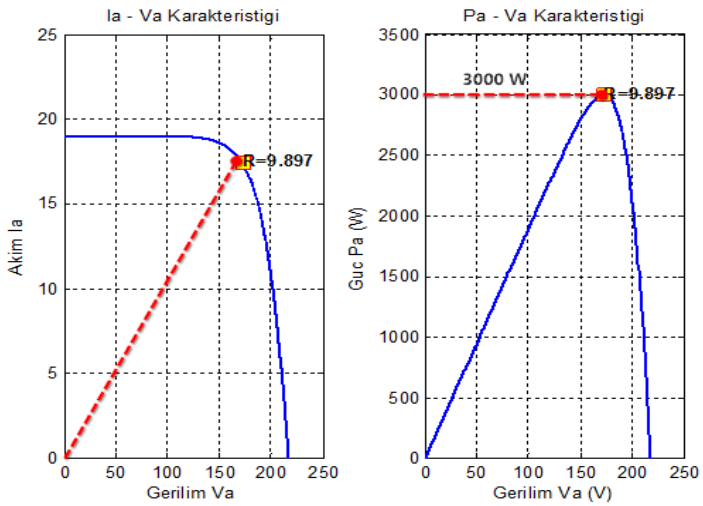

Figure 4. V – I and P – V curves for electrical load value of maximum power

To accomplish MPPT for 3kW PV system, two different MPPT methods are presented and compared in this study. The first method is P&O method which operates by periodically incrementing and decrementing the output voltage of the PV panel and compares output power of PV panel. The second method is fuzzy logic control (FLC) based MPPT method to determine MPP point.

3.1. Perturb & Observe (P&O) MPPT Method

One of the most and popular techniques of MPPT is the P&O technique. The main concept of this method is to push the system to operate at the direction which the output power obtained from the PV system increases [5]. Basically, this method measures the derivative of PV panel power (dP) and derivative of PV panel voltage (dV) and uses PV power-voltage curve to determine the movement of the operating point. If the sign of (dP/dV) is positive, the actual point is in the left side of the MPP; else (dP/dV) is negative, the actual point is in the right side of the MPP. And this process continues until (dP/dV) equals to zero. The implementation of the P&O algorithm is shown in Figure 5.

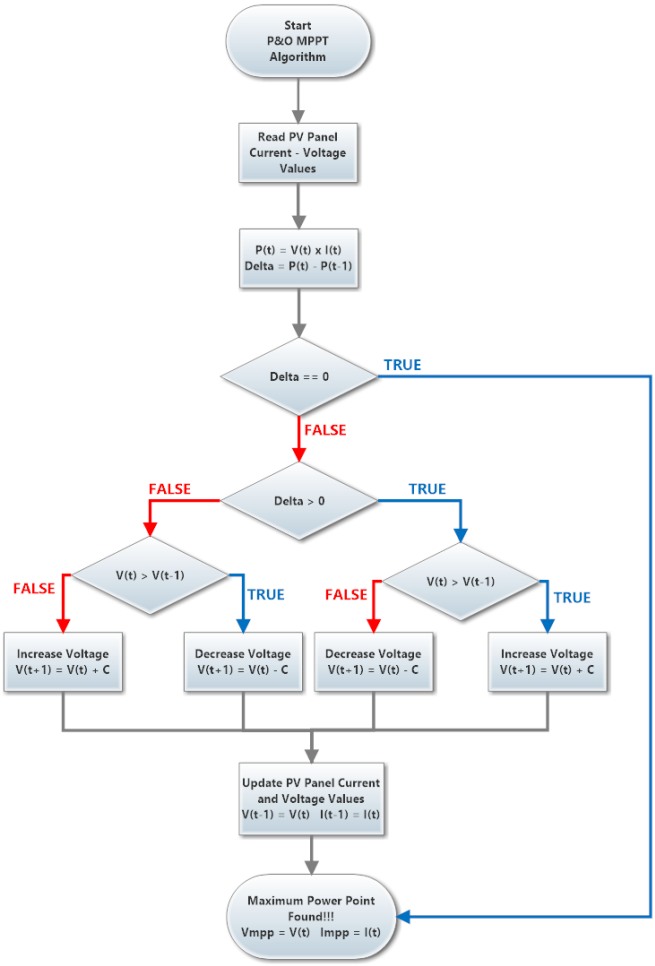

Figure 5. P&O maximum power point algorithm

This method works well in the steady state condition (solar irradiance and temperature changes slowly). However, the P&O method fails to track MPP when the environment condition is rapidly changed [5].

3.2. Fuzzy Logic Control (FLC) MPPT Method

Fuzzy logic control (FLC) based MPPT is one of the most used method to perform MPPT for any PV system in any environment condition. FLCs gain several advantages of better performance, robust and simple design. In addition, this method does not require the knowledge of the exact model of system [5]. The main parts of FLCs are examined in four parts, which are fuzzification, fuzzy rule-base, fuzzy inference engine and defuzzification. A general FLC control scheme is shown in Figure 6.

In the proposed FLC system, the input of FLC is sum of angle conductance ($\theta_1 = \tan^{-1}(dI_{pv}/dV_{pv})$) and angle of increment of conductance ($\theta_2 = \tan^{-1}(I_{pv}/V_{pv})$). The input variables are described in Eq. (2) and the MPPT determination condition was illustrated in Figure 7.

$$\theta_1 + \theta_2 = \tan^{-1}\left(\frac{dI_{pv}}{dV_{pv}}\right) + \tan^{-1}\left(\frac{I_{pv}}{V_{pv}}\right) = 0° \quad (2)$$

As seen in Figure 7, sum of the angles of PV panel conductance and increment of conductance equals to zero around MPPT point. Therefore, the membership function of the input and the rule base set of the FLC MPPT must

be identified according to that condition for fuzzy inference system. In this context, the input variable of sum of angles ($\theta_1 + \theta_2$) is assigned to several linguistic variables which are denoted by NB (Negative Big), NS (Negative Small), ZE (Zero), PS (Positive Small) and PB (Positive Big). The membership functions for the input and output are illustrated in Figure 8 and the corresponding fuzzy rule set is shown in Figure 9.

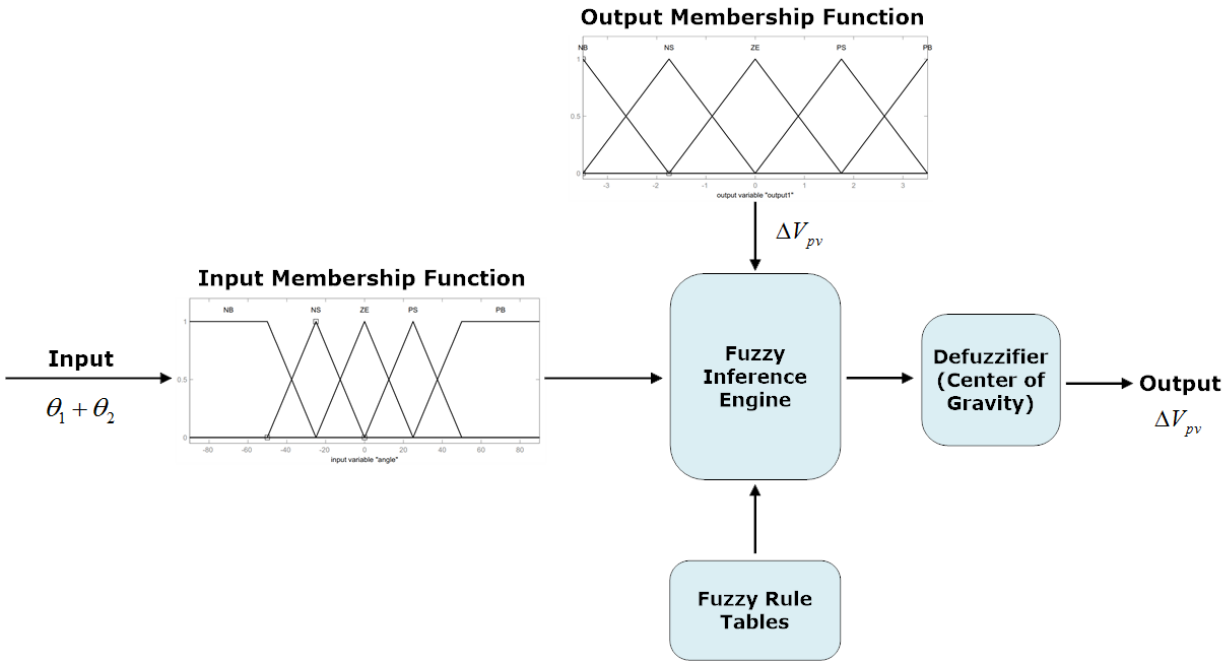

Figure 6. Block diagram of the proposed FLC-based MPPT system

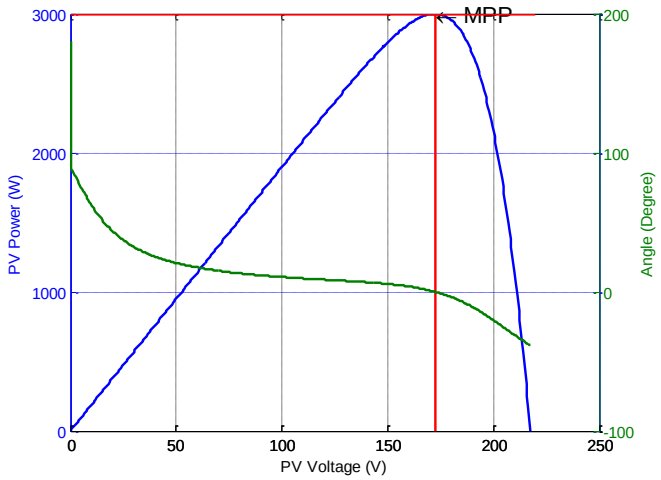

Figure 7. PV power – voltage and angle MPPT diagram for the proposed FLC-based MPPT system

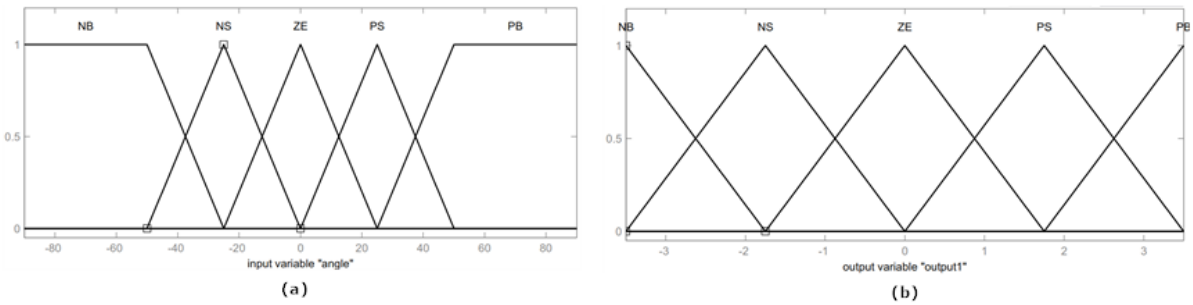

Figure 8. Membership functions for the FLC based MPPT (a) Membership function for input ($\theta_1 + \theta_2$) (b) Membership function for output (ΔV_{pv})

$\theta_1 + \theta_2$	NB	NS	ZE	PS	PB
ΔV_{pv}	NB	NS	ZE	PS	PB
Region Area	Region 1		Region 2	Region 3	

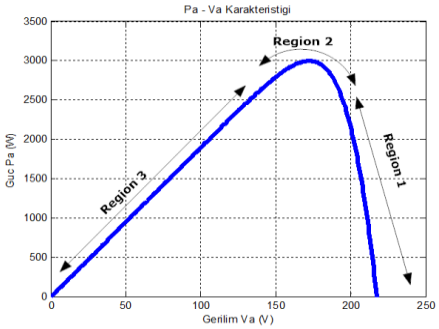

Figure 9. Fuzzy rules and PV power – voltage and angle MPPT diagram for the proposed FLC-based MPPT system

The defuzzification method used in this study is center of gravity method, which is one of the commonly used method in the literature shown in Eq. (3):

$$\boldsymbol{Y_{COG}} = \frac{\sum_{i=1}^{n} \boldsymbol{Y_i}(\boldsymbol{X_i}) \times \boldsymbol{X_i}}{\sum_{i=1}^{n} \boldsymbol{Y_i}(\boldsymbol{X_i})} \quad (3)$$

where $\boldsymbol{Y_i}$ is the inference result of rule $\boldsymbol{i}$; $\boldsymbol{X_i}$ is the corresponding output value of rule $\boldsymbol{i}$; and $\boldsymbol{Y_{COG}}$ is the output value of defuzzification process.

4. Simulation Results of MPPTs and Discussion

This study compares tracking performance and accuracy between P&O method and FLC method using MATLAB. The performances of P&O method for 0.5V and 3.5V derivation parameters and FLC control method are shown in Figure 10. The simulations have been investigated under standard test conditions (1000 W/m^2 - 25°C).

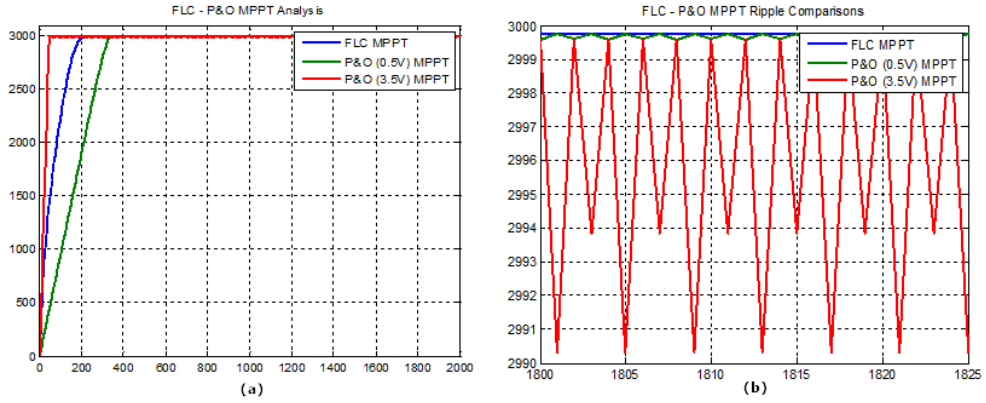

Figure 10. PV power curves under standard test condition (a) P&O and FLC MPPT method response (b) P&O and FLC MPPT oscillations

As shown in Figure 10, P&O (3.5V) MPPT has the best response iteration rate but the worst accuracy performance because of more oscillations. The P&O (3.5V) method is 6.88 times iteration faster than 0.5V P&O and 5.4 iteration times faster than FLC method. Nevertheless, its accuracy performance is almost 99.86% and worse than P&O (0.5V) and FLC MPPT method. The overall simulation results for response iteration rate, tracking accuracy performance are presented in Table 1.

Table 1. Comparison results for P&O and FLC MPPT

MPPT	Iteration Number	MPP Power (W)	Tracking Accuracy
P&O (3.5V)	50	2995.85	%99.86
P&O (0.5V)	344	2999.65	%99.98
FLC	270	2999.7	%99.99

To highlight the FLC MPPT method performance, the following simulation results are shown in Figure 11 for different solar irradiance values (1000 – 800 – 600 – 400 W/m^2) at fixed temperature of 25°C. The P&O (0.5V) algorithm has better MPPT accuracy than P&O (3.5V) MPPT but slower response rate than FLC and P&O (3.5V) MPPT methods. Also, oscillations remain around MPP. The FLC method has better response time than P&O (0.5V), and best MPPT accuracy performance (99.99%). In addition, oscillations do not occur around MPP. Hence,

the FLC MPPT method has increased 0.13% the tracking accuracy – performance compared to P&O MPPT method.

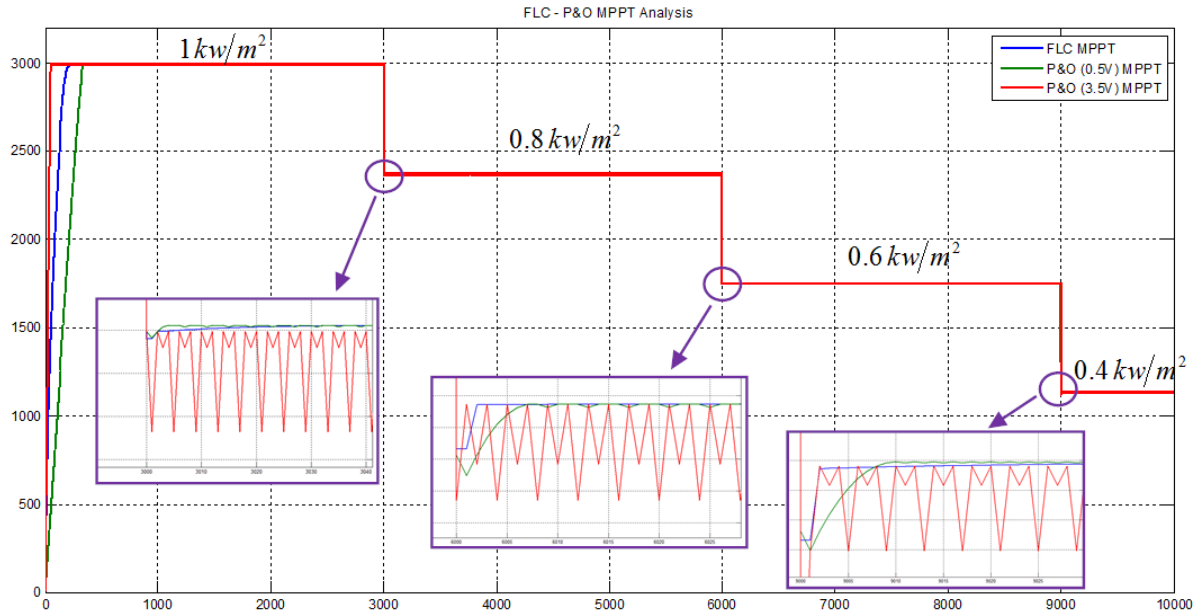

Figure 11. PV power curves under standard test condition (a) P&O and FLC MPPT method response (b) P&O and FLC MPPT oscillations

For practical application, the FLC method must be selected for its higher performance and acceptable response rate compared to P&O method. The FLC method has better tracking efficiency and less oscillation at each step.

5. Conclusions

Photovoltaic power is one of the cleanest and abundant energy type in environment. It is practically free and inexhaustible in the world. According to the researches and applications, it is likely to be an alternative main source of power in the future. The power generation from PV systems depends on atmospheric changes like solar irradiance and temperature. Because of that fact, MPPT methods play important role to operate PV system at maximum efficiency for all environment condition. This paper presents electrical characteristics of 3kW PV system and general comparison of FLC based and P&O MPPT methods. Both MPPT methods are investigated and realized in MATLAB environment. The tracking accuracy and performance efficiency are compared in detail by simulation results in MATLAB. Based on the simulation results, it can be concluded that with both MPPT methods PV system can generate maximum power for actual environment condition. However, the tracking accuracy and performance of FLC MPPT is better and more convenient than P&O MPPTs for PV system. FLC MPPT has no oscillations around MPP region and more stable output power than conventional MPPTs.

References

[1] Koutroulis E, Kalaitzakis K, Voulgaris NC. Development of a Microcontroller-Based Photovoltaic Maximum Power Point Tracking Control System. IEEE Transactions on Power Electronics 2001;16/1.

[2] Yadav APK, Thirumaliah S, Haritha G. Comparison of MPPT Algorithms for DC – DC Converters Based PV Systems. International Journal of Advanced Research in Electrical, Electronics and Instrumentation Engineering 2012:18-23.

[3] Hernanz JAR, Martin JJM, Belver IZ, Lesaka JL, Guerrero EZ, Perez EP. Modelling of Photovoltaic Module. International Conference on Renewable Energies and Power Quality 2010

[4] Subiyanto, Mohamed A, Hannan MA. Maximum Power Point Tracking in Grid Connected PV System Using A Novel Fuzzy Logic Controller. IEEE Student Conference on Research and Development 2009.

[5] Takun P, Kaitwanidvilai S, Jettanasen C. Maximum Power Point Tracking using Fuzzy Logic Control for Photovoltaic Systems. Proceedings of the International MultiConference of Engineers and Computer Scientists 2011; 2.

[6] Borekci S, Kandemir E, Kircay A. A Simpler Single-Phase Single-Stage Grid-Connected PV System

with Maximum Power Point Tracking Controller. Elektronika ir Elektrotechnika 2015;21/4:44-49.

[7] Chekired F, Larbes C, Rekioua D, Haddad F. Implementation of a MPPT fuzzy controller for photovoltaic systems on FPGA circuit. Energy Procedia 2011; 6: 541-549.

[8] Bounechba H, Bouzid A, Napti K, Benalla H. Comparison of perturb & observe and fuzzy logic in maximum power point tracker for PV systems. Energy Procedia 2014;50:677–684.

[9] Jiyong L, Honghua W. Maximum Power Point Tracking of Photovoltaic Generation Based on the Fuzzy Control Method. IEEE SUPERGEN'09 2009: 1-6.

[10] Yeong-Chau K, Tsorng-Juu L, Jiann-Fuh C. Novel Maximum Power Point Tracking Controller for Photovoltaic Energy Conversion System. IEEE Transactions on Industrial Electronics 2001; 48/3.

[11] Yinqing Z, Youling Y, Yu Z, Jicheng L. MPPT Control for PV Generation System Based on an Improved Inccond Algorithm. Procedia Engineering 2012; 29: 105-109.

ISSN 2303-4521
PERIODICALS OF ENGINEERING AND NATURAL SCIENCES
Vol. 5 No. 1 (2017) – Special Issue (Recent Topics in Environmental Science)
Available online at: http://pen.ius.edu.ba

Optimum Air Feed Locations on Medical Waste Incineration Rotary Kiln by Computational Fluid Dynamics (CFD)

S. Levent KUZU
Yildiz Technical University, Davutpasa Campus,
Civil Engineering Faculty, 34220
Esenler/Istanbul, Turkey
skuzu@yildiz.edu.tr

Murat AKSEL
Istanbul Kultur University, Ataköy Campus,
Civil Engineering Department, 34156
Bakırköy/Istanbul, Turkey

Arslan SARAL
Yildiz Technical University, Davutpasa Campus,
Civil Engineering Faculty, 34220
Esenler/Istanbul, Turkey

Abstract
Twenty-four tons of medical waste is combusted every day in Istanbul. The plant is operated by ISTAÇ AŞ and combustor type is rotary kiln. The air was being fed manually along with the waste being introduced to the kiln. This case caused some problems regarding the combustion efficiency. The administration staff decided to open holes to supply air to the combustor. In this study, CFD was utilized in order to determine the optimum places for air inlets. Flow geometry of the air was prepared and then meshed for calculations. k-ε turbulence model was utilized in the calculations. Four air inlet pipes were placed on the edges of the circular inlet area. Different locations were tested. When the air was fed from the top, waste could not completely contact with the air. Additionally, different inlet angles were tested from zero degrees to thirty degrees. The degree of the inlet did not distinguishably change the combustion characteristics inside the kiln. Piping holes were burrowed from the bottom at zero degree angle.

Keywords: Incineration; rotary kiln; CFD; medical waste

1. Introduction

Medical waste is produced firstly from medical treatment and secondly from medical research [1]. The generated medical waste amount was reported as 50 600 kg per day in Istanbul in 2010 [2]. The amount of waste per bed in one day is 2.35 kg. Infectious waste is a large portion of the medical wastes and handling of this waste type should be very sensitive due to its pathogenic ingredient [3].

There are several methods in order to dispose medical waste. Incineration and sterilization are the most preferred methods worldwide. The first plant installed was the incineration process in Istanbul, which has 24 tons per day waste capacity [4]. The plant was started accepted taking wastes in 1995. Later, sterilization plant was constructed in addition to incineration system. Sterilization plant has an operating capacity of 110 tons per day [5]. It is expected that this system is going to be able to accept medical wastes of Istanbul in a 30 year time.

Incineration is the ultimate point of the elimination of the pathologic wastes. The kiln is operated at 900°C for 2 hours. This serves a volume reduction of 75 to 95 percent of the total waste volume [3].

Heat distribution is a critical part of the incineration operation. There are several studies on the evaluation of the heat distribution in a furnace [6-8]. This study was conducted in order to i) investigate the current state of a medical waste rotary kiln that is being operated, ii) investigate the effect of auxiliary air supply on waste combustion, and iii) place the auxiliary air pipes to the kiln.

2. Materials and Method

Ansys Fluent v15 was used in this study for the computation of the fluid dynamic [9]. Calculations of this study were executed in five steps. At first, the geometry of the flow volume was regenerated in AutoCad and converted to "iges" file which can further be applied in the DesignModeller of Ansys. In the second step, the generated volume was meshed. The calculations were executed at each generated mesh. In the third step, model parameters were defined. The defined parameters are given in Table 1.

DOI: 10.21533/pen.v5i1.68

Table 1. Fluent model configurations

Parameter	Value
Mesh Quality	
Mesh Elements	206830
Mesh Size Method	Proximity and Curvature
Minimum Mesh Size	1.25600 e-03 m
Minimum Orthogonal Quality	2.01889 e-01
Maximum Aspect Ratio	2.33404 e+02
Turbulent Model	
Reynold Stress	Linear Pressure-Strain
Near-Wal Treatment	Standart Wall Fuctions
Operating Conditions	
Operating Temperature	1000 °C
Operating Pressure	101325 Pa
Solution Methods	
Formulation	Implicit
Flux Type	Reo-FDS
Spetial Discretization Method	
Grandient	Least Squares Cell Based
Flow	Second Order Upwind
Boundary Conditions	
Rotationary Wall Speed	0.3 rad/sec
Roughness Height	0.001 m
Mass Flow Inlet Flow Rate	2 kg/sec

In the fourth and fifth step, solution results were acquired and their results were shown on figures.

2.1. Geometry Design

Inner section of the rotary kiln, where air flow is occurred, is generated as a 3D plot in AutoCad. The flow field is given in Figure 1.

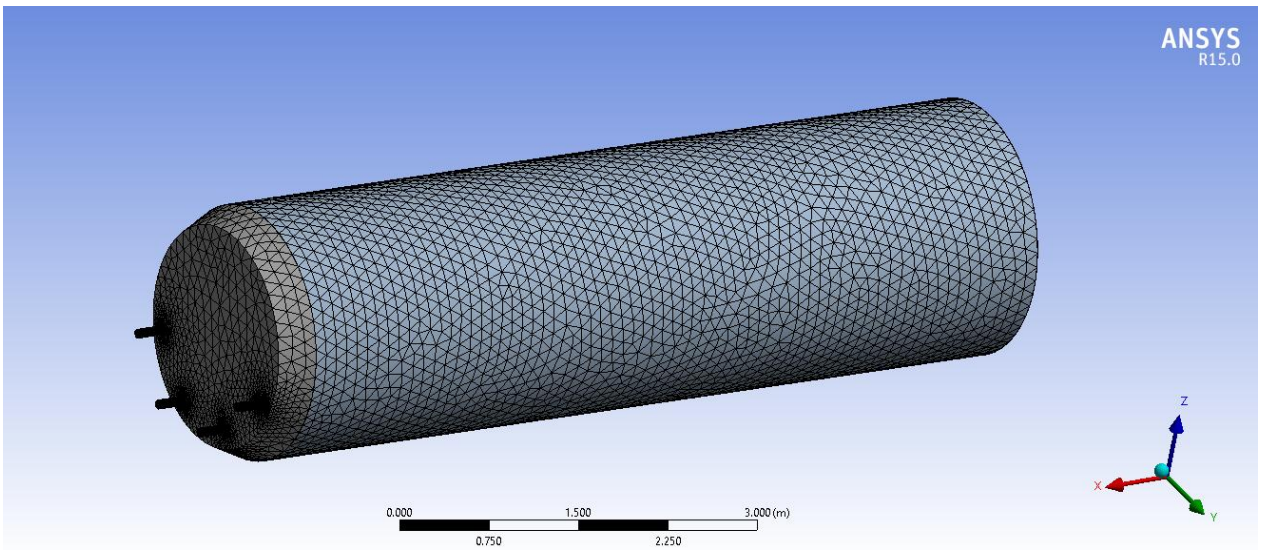

Figure 1. Modelling volume

Figure 1 was drawn by the actual kiln parameters. The length of the kiln is 7.5 m. Inner diameter, between the

refractory material, is 2.70 m. The thickness of the refractory material is 20 cm. The rotary kiln has an incline of 3°. In the previous design of the kiln, there was no inlet for auxiliary air feed. The air introduced along with the waste being fed to the kiln. When the feeding door is closed, contact with the air from the upstream of the kiln was stopped. This causes some inefficiencies such as high unburned content of the waste in the ash and high CO amount in the flue gas. For that reason, it was decided to include four pipes to the inlet wall of the kiln. The diameter of these pipes was 75 mm. The position of those pipes was approximately decided by the result of the CFD model. The actual system now being operated in the plant is the one shown in Figure 1.

2.2. Theory/calculation

Some assumptions are present in order to solve the numerical problem. These are the conservation of mass and momentum. These two equations were taken from Yaghmaelian et al. [10]. The mass conservation is given in Eq 1.

$$\frac{\partial(\rho u)_i}{\partial x_i} = 0 \tag{1}$$

The conservation of momentum is given in eq 2.

$$\frac{\partial \rho u_i u_j}{\partial x_j} = \frac{\partial P}{\partial x_i} + \frac{\partial}{\partial x_j}\mu_{eff}\left(\frac{\partial u_i}{\partial x_j} + \frac{\partial u_j}{\partial x_i}\right) - \frac{2}{3}\mu_{eff}\frac{\partial u_k}{\partial x_k} + \rho g_i \tag{2}$$

The effective viscosity is calculated as follows (3):

$$\mu_{eff} = \mu_l + \mu_t \tag{3}$$

where, μ_l is the absolute viscosity of the laminar flow, whereas μ_t is the absolute viscosity of the turbulent flow. μ_t is calculated according to Eq(4).

$$\mu_t = \rho C_\mu \frac{k^2}{\varepsilon} \tag{4}$$

The solution was executed by Reynolds stress turbulent model. For this turbulent model, C_μ is 0.09. The Reynolds stress from k and ε can then calculated as follows (5):

$$-\rho\overline{u_i' u_j'} = \mu_t\left(\frac{\partial u_i}{\partial x_j} + \frac{\partial u_j}{\partial x_i}\right) - \frac{2}{3}\rho k\delta_{ij} = 2\mu_t E_{ij} - \frac{2}{3}\rho k\delta_{ij} \tag{5}$$

$$\delta_{ij} = 1 \; if \; i = j \; and \; \delta_{ij} = 0 \; if \; i \neq j$$

Above equations from 1 to 5, were given in one dimension. In the actual processing of the model these were executed in three-dimensions.

3. Results

The study was conducted in two steps. In the first one, the positioning of the inlet pipes was determined. In the second one, inlet pipes were placed at different angles. Effect of different inlet angles was investigated.

3.1. Positioning of the inlet pipe holes

In this section, optimum height of the inlet air that is introducing to the kiln is decided. Four holes were located at the top first and at the bottom next. The model was executed for both of these different geometries. Results of these two studies are shown in Figure 2.

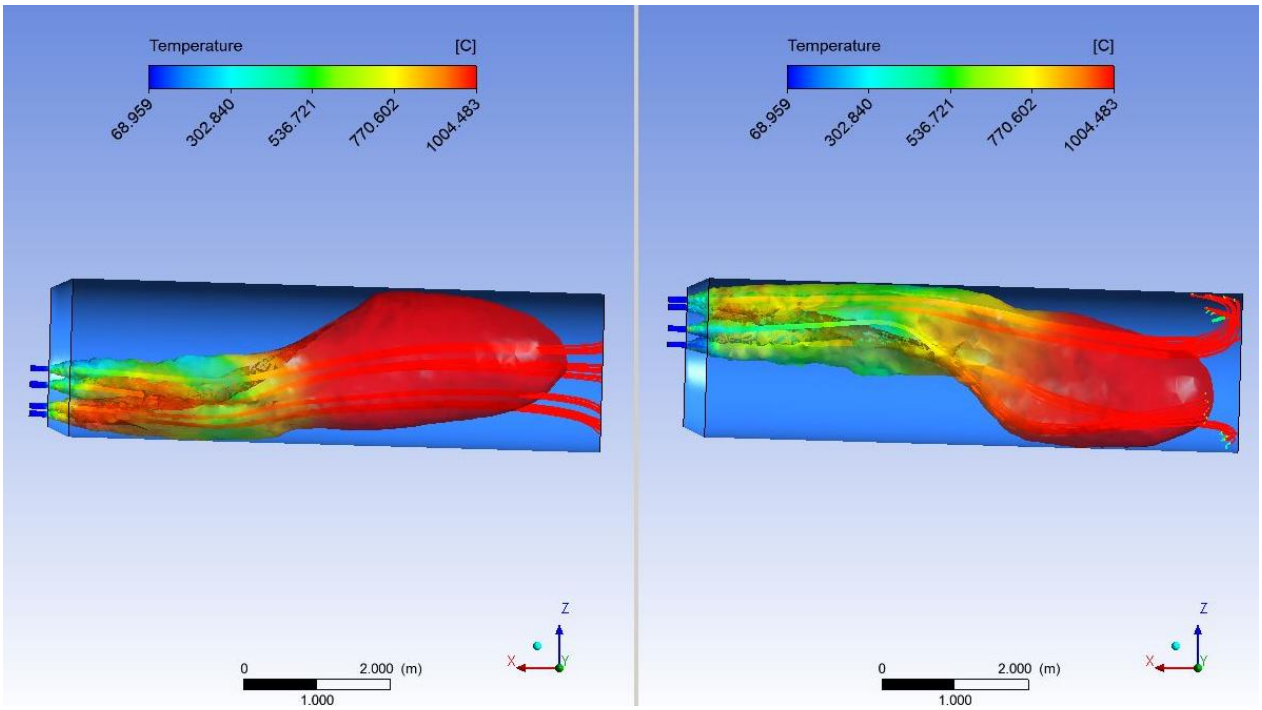

(a) (b)

Figure 2. (a) Auxiliary air inlet from below (b) Auxiliary air inlet from top

These results suggest that, if the air is fed from the top of the kiln, air would not contact with the waste homogenously. It is obvious that due to temperature different of the waste and the air being fed leads to a temperature layering. Air is being mixed after traveling some distance within the kiln. This may cause to oxygen-lean burn in some parts of the furnace. Thus, elevated carbon fraction in the ash and CO in the flue gas can be measured. In the previous configuration of the kiln, the air was being fed from between the center and top of the kiln. In this case, revision is mandatory for this system, in order to increase the combustion efficiency and to lower pollutant emissions.

When air is fed from the bottom, it is can contact with the waste, where it did not have possibility in the other configuration. Additionally, air is gradually being heated with the waste as can be seen from Figure 2. So that, layering does not occur. Further calculations at different angles were studied from the bottom-feeding configuration.

3.2. Effect of inlet angle

Different angles from 0^o to 30^o were studies at five different stages, which were 0^o, 5^o, 10^o, 15^o, and 30^o, respectively. The aim of this was to determine whether the inlet angle has a significant effect on the temperature distribution or not. Volume rendering results are shown in Figure 3.

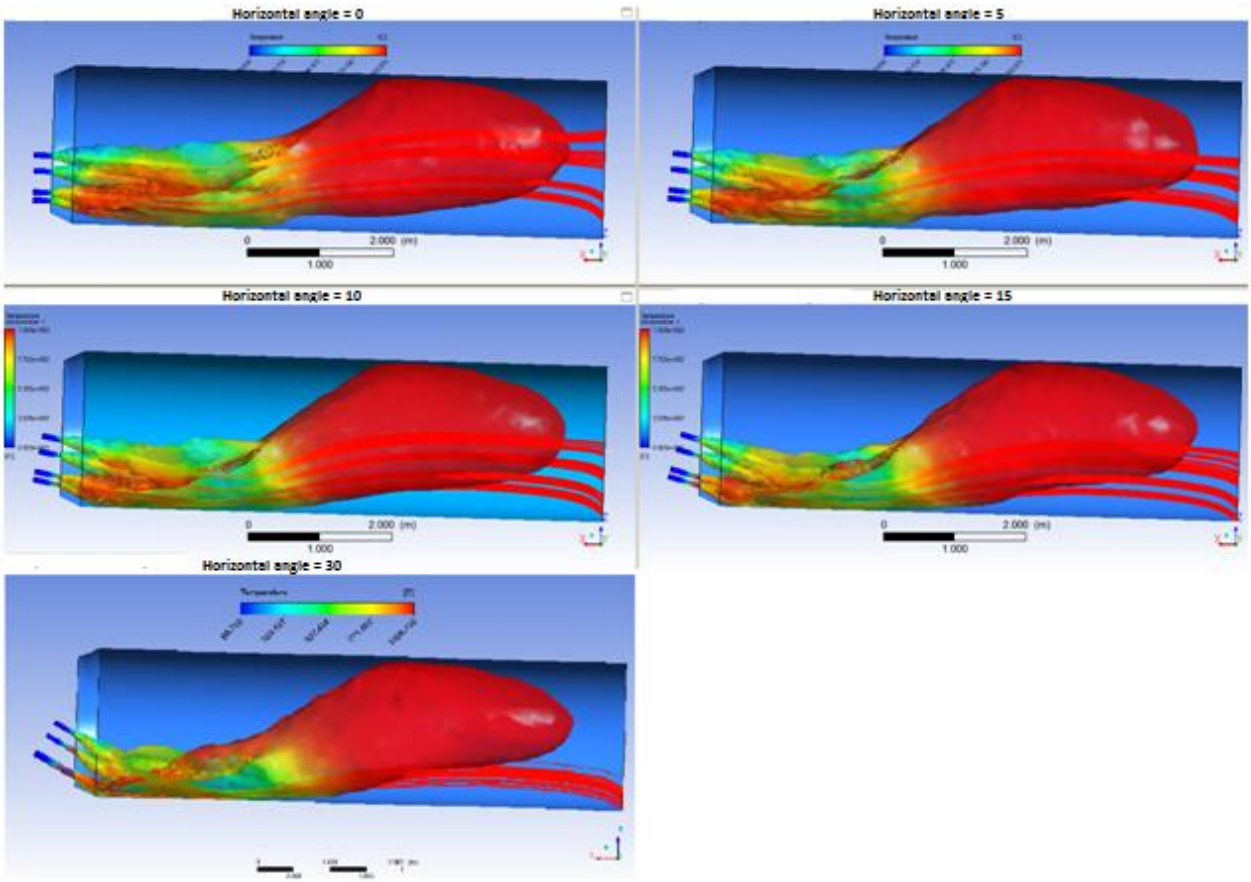

Figure 3. Temperature distribution at different inlet angles

According to the plots in Figure 3, any significant visual variation was not achieved. Apart from 0^o angle, the inlet with 15^o and 30^o seems to have a better temperature distribution. However, in the inlet with 30^o contact with the waste is lesser in the downstream of the kiln. Inlet with 15^o is somewhat more preferable than inlet with 30^o. Inlet with 0^o and 15^o were compared in Figure 4.

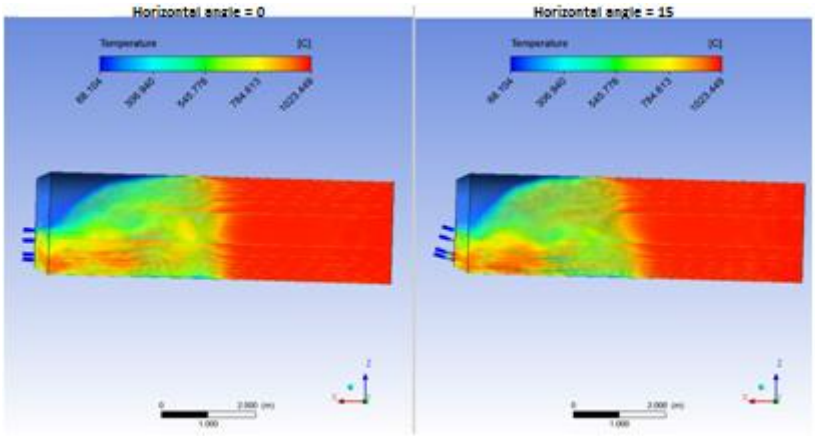

Figure 4. Comparison of inlet angles of 0^o and 15^o

Figure 4 shows the temperature distribution on a planar surface which is vertically placed in the kiln. The temperature difference at the waste contact level is not significant. Thus, considering this insignificancy and ease of engineering application for hole opening, 0^o angle was selected for the inlet angle. That means auxiliary air pipes are parallel to the surface of the kiln.

4. Discussion

In the previous configuration of the kiln, there was no auxiliary air feed channel. This study helped us to find the accurate places for more efficient combustion. It is decided to open holes for auxiliary air pipes at the bottom of the

kiln. Thus, the air had opportunity to contact with the waste at any part of the kiln.

Secondly, different geometries with varying inlet hole angles were prepared. It was decided that there was not a significant difference between different configurations. So the inlet pipes were placed parallel to the kiln.

The plant is now being operated with the proposed configuration suggested in this study.

5. Conclusions

Air feed from the middle or the top of the kiln is not appropriate for the operational purpose. Temperature layering occurs between the air and the waste. This prevents the complete combustion in the upstream of the kiln. The best place for air feed was the bottom of the inlet wall, which is perpendicular to the kiln. Furthermore, the variations in the inlet angles didn't make significant changes. Pipes were placed parallel to the kiln.

Acknowledgements

The authors would like to acknowledge ISTAC AS for sharing the rotary kiln geometry and operation details in order to make this study.

References

[1] Marinkovic N, Vitale K, Holcer NJ, Dzakula A, Pavic t. Management of hazardous medical waste in Croatia. Waste Management 2007; 28:1049-56.

[2] Eker HH, Bilgili MS, Sekman E, Top S. Evaluation of the regulation changes in medical waste management in Turkey. Waste Management and Research 2010; 28, 1034-8.

[3] Birpınar ME, Bilgili MS, Erdoğan T. Medical waste management in Turkey: A case study of Istanbul. Waste Management 2009; 29, 445-8.

[4] Güneş G, Saral A, Yıldız Ş, Kuzu SL. Determination of optimum dose of adsorbent for PCDD/F removal in the flue gas of a medical waste incineration plant. Chemical Engineering Research and Design 2015; 104, 695-702.

[5] http://www.istac.istanbul/tr/hizmetlerimiz/istanbul-tibbi-atik-yonetimi#, accessed on 31.05.2016

[6] Yaghmaeian K, Jaafarzadeh N, Nabizadeh R, Dastforoushan G, Jaafari J. CFD modeling of incinerator to increase PCBs removal from outlet gas. J Environ Health Sci&Eng, 2015; 13, 60-5.

[7] Goh Y, Lim C, Zakaria R, Chan K, Reynolds G, Yang Y. Mixing modelling and measurements of incinerator bed combustion. Process Saf Environ Prot. 2000; 78, 21–32.

[8] Khiari B, Marias F, Zagrouba F, Vaxelaire J. Transient mathematical modelling of a fluidized bed incinerator for sewage sludge. J Clean rod. 2008;16, 178–91.

[9] Anonymous. Ansys Fluent User's Guide Book. Canonsburg, PA, USA, 2011.

[10] Kaya O. Kare Kesitli Helisel Kanalda Türbülanslı Akışta Basınç Düşüşünün Deneysel ve Nümerik Analizi. Pamukkale Univ. Eng. Col. J. Eng. Sci. 2004; 10, 283-9.

ISSN 2303-4521
PERIODICALS OF ENGINEERING AND NATURAL SCIENCES
Vol. 5 No. 1 (2017) – Special Issue (Recent Topics in Environmental Science)
Available online at: http://pen.ius.edu.ba

Land Use Suitability Classification for the Actual Agricultural Areas within the Bartın Stream Watershed of Turkey

Melih Öztürk
Bartın University, Faculty of Forestry, Department of Landscape Architecture, Bartın, Turkey
melihozturk@bartin.edu.tr

İlyas Bolat
Bartın University, Faculty of Forestry, Department of Forest Engineering, Bartın, Turkey
ilyasbolat@bartin.edu.tr

Ercan Gökyer
Bartın University, Faculty of Forestry, Department of Landscape Architecture, Bartın, Turkey
egokyer@bartin.edu.tr

Ömer Kara
Karadeniz Technical University, Faculty of Forestry, Department of Forest Engineering, Trabzon, Turkey
okara@ktu.edu.tr

Abstract
Suitability classification of the land uses particularly involves the lands' qualification based on their ecological characteristics. Hence, ecological land use serves the sustainable planning objectives which ultimately constitute the fundamentals of environmental landscape planning. Among the diverse land uses, suitable agricultural areas occupy a significant interest not only because of their scarcity but also because of their environmental vulnerability. For this purpose, in this study, the land use suitability classification was performed for the actual agricultural areas within the Bartın stream watershed. The mesoscale watershed that covers approximately 1943 km^2 is located at the Western Black Sea Region of Turkey. The watershed is mountainous with the average slope of 15° and with the altitudes ranging between 20 m and 1735 m asl. The actual agricultural areas cover almost 37% of the watershed and particularly located within the lower altitudinal gradients of the watershed. Based on the slope degree and soil depth parameters, land use suitability classification was conducted for the agricultural areas. Between the slope degrees of 0° and 25°, five categories of slope degree ranges each of which was 5°, were determined. On the other hand, the soil depth parameter was divided into two categories; "moderate deep and deep (50> cm)" and "too shallow and shallow (50< cm)". Merging the digital map values of these two parameters using the GIS (Geographical Information Systems), yielded the 10 classes of land suitability for the agricultural areas. These 10 classes of land suitability for agricultural areas were displayed on the ultimate digitized map. According to the results of this study, only 25% of the agricultural areas were within the first three land suitability classes. However, almost 32% of the agricultural areas were within the last three land suitability classes. Furthermore, these problematic agricultural areas are particularly located at the higher altitudinal gradients within the watershed. These results indicated the significant misuse of the agricultural areas within the watershed. Consequently, re-arrangement of the land use plans and programs should be proposed in order to achieve the sustainable use of the agricultural areas within the watershed. This re-arrangement and re-handling will serve the objectives of landscape planning compatible with the environmental ethics and morality.

Keywords: Environmental land use; suitability classification; agricultural areas; landscape ecology and planning; Bartın stream watershed.

1. Introduction

The use of lands deals with many aspects of natural science including particularly the ecological, hydrological and environmental issues [1]. Hence, the land use is associated with various earth and atmosphere processes involving water [2, 3] and biogeochemical cycles [4], nutrient dynamics [5], soil erosion [6] and land degradation [7], biodiversity [8] and habitat fragmentation [9]. Because of their significant roles on the environment, the land uses must be in accordance with their natural and ecological characteristics [1]. Otherwise, the misuse of lands incompatible with their creation will gradually lead to the degradation of these lands [10]. Frequently, agricultural areas constitute the major land uses together with the forests and settlements [11]. Therefore, they play fundamental role on the environmental processes and dynamics, influencing and being influenced by the overall landscape ecology [12]. In particular, during the recent decades, agricultural areas not only face abandonment but also be exposed to the urbanization and urban sprawl threats. The situation is

DOI: 10.21533/pen.v5i1.70

also valid for the Western Black Sea Region (such as other regions) of Turkey which loses its' farmer population of the villages to the city centers and metropolitans [13]. Furthermore, the region suffers the conversion of agricultural lands to the forests due to the land abandonment [3] and experiences the transformation of agricultural lands to the poplar cultivation [14] and settlements due to the agricultural labor loss. Accordingly, the remaining dwellers of the villages are forced to practice cultivation at some places unsuitable for the agriculture [15].

In order to achieve and sustain comprehensive land use planning, land use suitability classification should especially be applied for the sensitive and vulnerable areas including such as the agricultural lands [16, 17]. Thus, ecological health of the agricultural land will be maintained and a control mechanism for the environment will be supplied. Bartın stream watershed at the Western Black Sea Region of Turkey have encountered the forest spread into the agricultural areas due to the land abandonment at the last few decades in the region [3]. Besides, some of the villagers have converted their agricultural areas close to the town and city centers to the settlements due to finding real estate more lucrative and due to the agricultural labor deficiency. Moreover, agriculture was performed compulsorily in some relatively steep and shallow areas due to the lack of suitable areas around some villages. Consequently, in this study, land use suitability classification was conducted for the actual agricultural areas of the Bartın stream watershed based particularly on the topography and soil physical characteristics. Thereby, the consistencies and inconsistencies within the usage of the actual agricultural lands were tried to be revealed.

2. Material and Method

2.1. Study area

The mesoscale watershed covers approximately 1943 km^2 at the Western Black Sea Region of Turkey [18] (Fig. 1). The watershed is located within the 41°17' and 41°45' northern latitudes and 32°13' and 32°60' eastern longitudes (Fig. 1). The altitude of the watershed ranges between 20 and 1735 m asl. [19] whereas the mean altitude is 517 m asl. (Figure 1). Almost 2/3 of the watershed is within the first 600 m asl. altitudinal gradients. About 71% of the rest of the watershed has the altitudinal gradients between 600 m asl. and 900 m asl. The average slope of the watershed is 15°. Almost 10% of the watershed constitutes relatively the plain areas with the average slope of 5°. These plain areas are particularly concentrated at the lowest altitudes of the watershed. There is no definite dominant aspect within the watershed. In other words, the exposure of the watershed is directed evenly towards all aspects.

The major land uses are the forests, agricultural areas and the settlements respectively. Forests cover almost 58% of the watershed [20]. Approximately 14% of these forests are handicapped [20]. On the other hand, agricultural areas constitute about 37% of the watershed [21, 20].

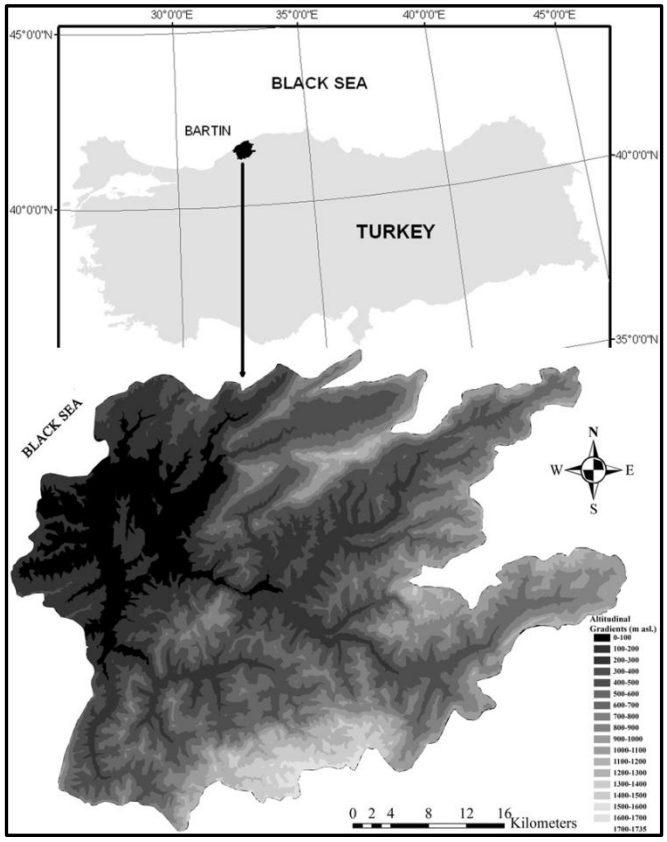

Figure 1. Altitudinal gradients of Bartın stream watershed at Western Black Sea Region of Turkey.

Urban settlements spread especially at the lower altitudes covering about 2% of the watershed. However, rural settlements exist at the 2% of the watershed in the form of scattered villages. The arable lands that belong to the land capability classes of I, II, and III intensively occur at the lower parts of the watershed and at the riparian zones of the stream and tributary channels [21]. These areas that belong to the first three land capability classes cover only 10% of the watershed. However, the rest of the lands that belong to the capability classes up to VIII, and that are able to be used for forest, pasture and recreation are particularly located at the higher and mountainous parts of the watershed. Furthermore, more than half of the watershed belong to the land capability class of VII. Brown forest soils and grey-brown podsolic soils [21] have formed on sandstone-mudstone formation in particular [22]. These two soil groups cover approximately 80% of the watershed [21]. The remaining lands are covered by red-yellow podsolic soils, alluvial and colluvial soils respectively [21]. More than half of the watershed has the shallow soils

with the depth ranging between 20 cm and 50 cm. Limestones and vulcanite-sedimentary rocks are the second and third major geological formations after the sandstone-mudstone formation within the watershed [22].

According to the 30 years (between 1982 and 2011) of meteorological data based on the measurements of meteorological station in the city center of Bartın Province, the average annual total precipitation is 1033 mm whereas the average annual temperature is 12.6°C [23]. The region drops into the humid mesothermal climate regime [24]. Nominately, October is the wettest month with the 123 mm mean monthly total precipitation. May is the driest month with the 49 mm mean monthly total precipitation [23]. The warmest month is July with the mean monthly temperature of 22.2°C. On the other hand, the coldest month is January with the mean monthly temperature of 4.1°C [23]. Dependent upon the blowing durations, the dominant winds are from western-northwestern and north-northeastern directions where Black Sea is located [23].

2.2. Method

The slope degree and soil depth parameters were referred for the land use suitability analysis of the actual agricultural areas in Bartın stream watershed (Table 1). Although the slope degree extends up to values higher than 30° within the watershed, the areas steeper than 25° were not included into the land use suitability classification. Because, the agricultural areas do not exist at these steeper areas. Initially, the slope degrees between 0° and 25° were categorized into 5° ranges (Fig. 2). The areas with 0° to 5° slope were assumed as relatively plane (Table 1). In some places particularly close to the stream and tributary channels, the depth of the soil reaches down to the levels lower than -90 cm (Fig. 3). The soil depth was grouped under "impervious (0 cm)", "too shallow (0-20 cm)", "shallow (20-50 cm)", "moderate deep (50-90 cm)" and deep (90+ cm)" (Fig. 3). In order to simply incorporate this soil depth parameter into the suitability classification, the "shallow" and "too shallow" soils were categorized together as soils below 50 cm depth whereas "moderate deep" and "deep" soils were categorized together as soils above 50 cm (Table 1).

Table 1. Based on slope degree ranges and soil depth, land use suitability classification for actual agricultural areas.

Slope Ranges	Soil Depth Categories		Suitb. Class
0-5°	50> cm	Moderate and Deep	1
0-5°	50< cm	Shallow and Too Shallow	2
5-10°	50> cm	Moderate and Deep	3
5-10°	50< cm	Shallow and Too Shallow	4
10-15°	50> cm	Moderate and Deep	5
10-15°	50< cm	Shallow and Too Shallow	6
15-20°	50> cm	Moderate and Deep	7
15-20°	50< cm	Shallow and Too Shallow	8
20-25°	50> cm	Moderate and Deep	9
20-25°	50< cm	Shallow and Too Shallow	10

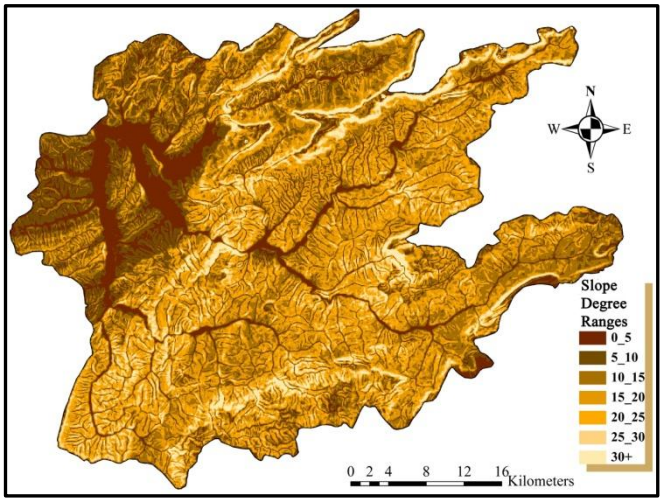

Figure 2. Slope degree ranges within Bartın stream watershed.

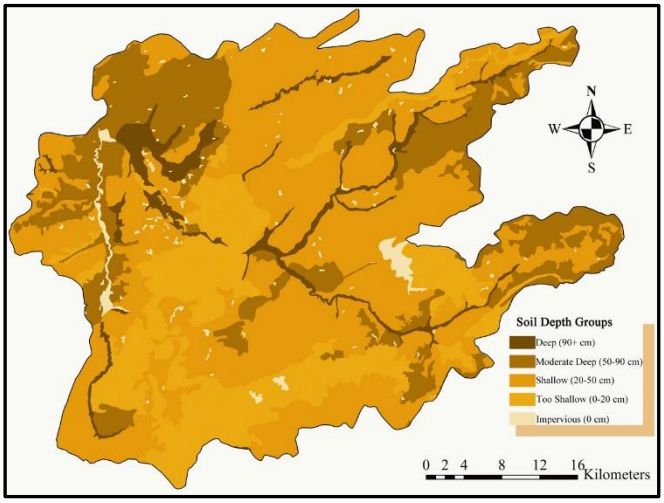

Figure 3. Soil depth groups within Bartın stream watershed.

Accordingly, the first two suitability classes represent the relatively plane (0-5° slope) actual agricultural areas with soils above and below 50 cm depths respectively (Table 1). The third and fourth classes represent areas of 5-10° slope and with soils above and below 50 cm respectively (Table 1). The fifth and sixth classes represent areas of 10-15° slope and with soils above and below 50 cm respectively (Table 1). The seventh and eighth classes represent areas of 15-20° slope and with soils above and below 50 cm respectively (Table 1). The ninth and tenth classes represent areas of 20-25° slope and with soils above and below 50 cm respectively (Table 1). Ultimately, the distribution of the ten land use suitability classes for the actual agricultural areas were

plotted on the Bartın stream watershed map (Fig. 4) which was generated by merging these definite slope degree ranges and soil depth categories via GIS.

Table 2. According to altitudinal gradients, distribution of land use suitability classes for actual agricultural areas.

Altitudinal Gradient (m asl.)	Land Use Suitability Classes for Actual Agricultural Areas (%)									
	1	***2***	***3***	***4***	***5***	***6***	***7***	***8***	***9***	***10***
20-100	**8.14**	**2.74**	**3.88**	**3.17**		0.86	0.15	0.17	0.04	0.05
100-200	0.78	0.88	**2.27**	**2.80**	**1.27**	**2.73**	0.40	**1.27**	0.12	0.47
200-300	0.82	0.53	**1.06**	**1.53**	**1.07**	**2.54**	0.51	**2.48**	0.14	**1.28**
300-400	0.47	0.38	0.61	**1.24**	0.92	**2.67**	0.70	**3.21**	0.21	**1.88**
400-500	0.33	0.28	0.41	**1.18**	0.82	**2.95**	**1.06**	**3.61**	0.33	**2.08**
500-600	0.14	0.19	0.27	0.88	0.64	**2.77**	0.84	**3.23**	0.28	**2.19**
600-700	0.02	0.18	0.06	0.56	0.38	**2.07**	0.52	**1.97**	0.18	**1.79**
700-800	0.01	0.08	0.06	0.31	0.31	**1.22**	0.32	**1.19**	0.15	**1.34**
800-900	0.01	0.17	0.03	0.44	0.16	0.92	0.19	0.63	0.08	0.75
900-1000	0.02	0.10	0.09	0.23	0.16	0.41	0.08	0.30	0.04	0.43
1000-1100	0.02	0.04	0.06	0.09	0.04	0.07	0.03	0.07	0.01	0.34
1100-1200		0.001	0.001	0.006		0.008		0.016		0.19
1200-1300		0.001		0.007		0.009		0.011		0.06
1300-1400				0.002				0.002		0.01
Total	**10.8**	**5.6**	**8.8**	**12.4**	**5.8**	**19.2**	**4.8**	**18.2**	**1.6**	**12.9**

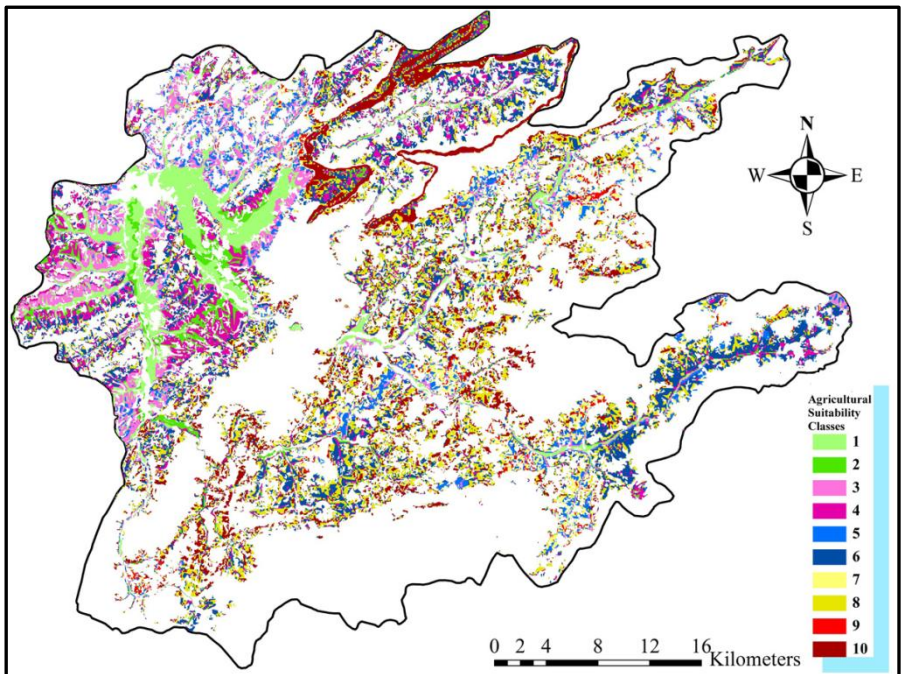

Figure 4. Land use suitability classes for actual agricultural areas within Bartın stream watershed.

3. Results

After delineating the map of land use suitability classes for the actual agricultural areas, the distribution of these classes based on altitudinal gradients was calculated. Almost 11% of the watershed belong to the suitability class of "1". (Table 2). The cultivated areas are about half of the "1" class for the "2" class agricultural areas which have the similar slope and soil characteristics except the shallower soil depth (Table 2). These "1 and 2" classes of agricultural areas are concentrated intensively on the plains at the lower altitudes of the watershed (Fig. 4). These plains have productive and deep alluvium soils. The "3" class agricultural areas where the average slopes are 5° higher than that of the former two classes, constitute almost only 9% of the total actual agricultural areas. These "3" class agricultural areas especially extend to 300 m asl. (Fig. 4). The shallower "4" class agricultural areas constitute eighth of

the total actual agricultural areas and reach to 500 m asl. in the watershed (Table 2 and Fig. 4).

The "5" class agricultural areas where the average slopes are about 12.5°, constitute almost only 6% of the total actual agricultural areas. The shallower "6" class agricultural areas cover the highest portion of the total actual agricultural areas with about 19% (Table 2). Hence, they reach up to 800 m asl. (Fig. 4). The "7" class agricultural areas where the average slopes are about 17.5°, constitute almost only 5% of the total actual agricultural areas. The shallower "8" class agricultural areas cover the second highest portion of the total actual agricultural areas with about 18% (Table 2). Together with "6 and 10" class agricultural areas, they climb up to 800 m asl. (Fig. 4). The "9" class agricultural areas where the average slopes are about 22.5°, constitute the lowest portion of the total actual agricultural areas with almost only 2%. The shallower "10" class agricultural areas cover the third highest portion of the total actual agricultural areas with almost 13% (Table 2).

4. Discussion

According to the results of the land use classification for the actual agricultural areas in the Bartın stream watershed, the lands with slope degrees lower than 10° cover almost only 38% (Table 2 and Fig. 4). Yet these lands belong to the first four suitability classes which are relatively more suitable for agriculture compared to the subsequent six classes. The lands of the subsequent six classes that have slope degrees higher than 10°, constitute about 62% of the total actual agricultural areas (Table 2 and Fig. 4). The soils of these relatively steep lands; particularly the shallower ones are susceptible to erosion and degradation. Also taming these soils are more difficult compared to the ones at the plains. Bakker et al. [25] emphasized that the increasing slope degree had triggered soil erosion which then had led to decrease in soil depth and consequently to land abandonment.

Moreover, these last six classes of agricultural lands that belong to the suitability classes from "5 to 10" are mostly widespread at the higher altitudes compared to the previous four classes. Such that they intensely occur at the altitudes up to 900 m asl. (Table 2 and Fig. 4). Agricultural cultivation is practiced particularly at the lowlands with the lower slope degrees rather than upland. In their study, Gautam et al. [26] indicated that the agricultural areas at the lowland had been more susceptible to settlement expansion whereas upland agriculture had been susceptible to forest vegetation invasion. The agricultural areas that belong to the last two land suitability classes (9 and 10) have steep slopes higher than 20° which severely threaten the stability of the soil. These lands constitute considerable portion of the total actual agricultural areas with 14% most of which has "shallow" and "too shallow" soils.

Despite agriculture was practiced at the problematic lands at the higher altitudinal gradients with high slope degrees and shallow depths, the lands at the lower altitudinal gradients with relatively plain, productive and deep soils are sealed by settlements. Furthermore, these soils sealed by buildings pertain to the first three land capability classes. According to Öztürk et al. [27], about 37% of all the housing in the watershed have been settled on these productive and deep soils pertaining to I., II., and III. land capability classes.

5. Conclusion

Even though the referred slope degree and soil depth parameters significantly serve the construction of land use suitability classification for the actual agricultural areas, more advanced classification supported by multiple other components will be essential for the watershed. These components should involve geological, topographical, hydrological, ecological, meteorological, environmental and management parameters [28]. In consequence of the integrated analysis of these parameters, a comprehensive land use suitability classification will build up fundamentals in order to achieve sustainable landscape planning.

Due to the settlements constructed on the productive and deep alluvial soils particularly at the lower altitudinal gradients of the watershed, the agricultural areas lost a potential to expand on. Beyond that, current development and sprawl of the town and city centers over the actual productive soils, pose considerable threat and handicap for the sustainable agriculture. Besides, such that urban sprawl may trigger possible silent climate change which directly or indirectly would threaten agricultural biodiversity. Alteration in the agricultural crop ranges may lead to leave the existing cultivated area which ultimately put pressure on other natural and reserved areas [29].

Because of the more frequent human intervene, agricultural areas are very sensitive and vulnerable landscapes prone to the anthropogenic disturbances rather than forests and natural reserves. Therefore, they require exclusive attention and protection against external constraints. For this purpose, an environmental land use model that is established on ecological basis and that inquire spatial and temporal dynamics can project and serve for the respond to the unplanned urbanization, flood disaster and climate change impacts on the agricultural areas of the Bartın stream watershed.

Acknowledgements

The authors of this study would like to appreciate The Scientific Researches Project Unit of Bartın University for the project (BAP-2011-028-Land Use Situation and

Suitability Classification in Bartın Stream Watershed) which the data of this study are based on. They also gratefully acknowledge The Turkish General Directorate of Forestry (TGDF) and Turkish State Meteorological Service (TSMS) for the data support.

References

[1] Randolph J. Environmental Land Use Planning and Management. Washington, USA: Island Press; 2004.

[2] Ward RC, Robinson M. Principles of Hydrology. London, UK: McGraw-Hill Publications; 2000.

[3] Öztürk M, Copty NK, Saysel AK. Modeling the impact of land use change on the hydrology of a rural watershed. Journal of Hydrology. 2013; 497: 97-109.

[4] Tarbuck, EJ, Lutgens, FK, Tasa D. Earth Science, 12th ed. New Jersey, USA: Pearson International Edition. Prentice Hall; 2009.

[5] Schaetzl R, Anderson S Soils, Genesis and Geomorphology. Cambridge, UK: Cambridge University Press; 2010.

[6] Nearing MA. Soil Erosion and Conservation. In: Wainwright J, Mulligan M, editors. Environmental Modelling; Finding Simplicity in Complexity, West Sussex, England: John Wiley & Sons Ltd.; 2004, p. 277-290.

[7] Lambin EC. Modelling Land-Use Change. In: Wainwright J, Mulligan M, editors. Environmental Modelling; Finding Simplicity in Complexity, West Sussex, England: John Wiley & Sons Ltd.; 2004, p. 245-254.

[8] Forman RTT, Godron M. Landscape Ecology. USA: John Wiley & Sons Ltd.; 1986.

[9] Odum EP, Barrett GW. Ekoloji'nin Temel İlkeleri (Beşinci Baskıdan Çeviri). Çeviri Editörü: Prof. Dr. Kani Işık. Ankara, Türkiye: Palme Yayıncılık; 2008.

[10] Marsh WM. Landscape Planning; Environmental Applications. 5th ed. New Jersey, USA: John Wiley & Sons Inc.; 2010.

[11] Ürgenç Sİ. Kırsal Peyzaj; Koruma-Onarım-Düzenleme. İstanbul, Türkiye: Yıldız Teknik Üniversitesi, Mimarlık Fakültesi Yayınları; 2000.

[12] Dirik H. Kırsal Peyzaj (Planlama ve Uygulama İlkeleri). İstanbul, Türkiye: İstanbul Üniversitesi, Orman Fakültesi Yayınları; 2005.

[13] Kırdar MG, Saracoğlu DŞ. Migration and regional convergence: An empirical investigation for Turkey. Papers in Regional Science. 2008; 87(4): 545-566.

[14] Yılmaz B, Daşdemir İ, Atmiş E, Lise W. Factors affecting rural development in Turkey: Bartın case study. Forest Policy and Economics. 2010; 12: 239-249.

[15] Göl C, Özden S, Yılmaz H. Interactions between rural migration and land use change in the forest villages in the Gökçay Watershed. Turkish Journal of Agriculture and Forestry. 2011; 35: 247-257.

[16] Kılıç Ş, Evrendilek F, Şenol F, Çelik İ. Developing a suitability index for land uses and agricultural land covers: a case study in Turkey. Environmental Monitoring and Assessment. 2005; 102: 323-335.

[17] Doygun H, Alphan H, Gürün DK. Analysing urban expansion and land use suitability for the city of Kahramanmaraş, Turkey, and its surrounding region. Environmental Monitoring and Assessment. 2008; 145: 387-395.

[18] Öztürk M, Bolat İlyas, Gökyer E, Kara Ö. Altitudinal Variation of Leaf Area Index for Mixed Stands of Fagus orientalis Lipsky within Mountainous Landscape of Bartın Watershed, Turkey. International Conference on Natural Science and Engineering (ICNASE'16), 1413-1424., March, 19-20, 2016, Kilis, Turkey. 2016.

[19] Turoğlu H, Özdemir H. Bartin'da Sel ve Taşkınlar; Sebepler, Etkiler, Önleme ve Zarar Azaltma Önerileri. İstanbul, Türkiye: Çantay Yayınevi; 2005.

[20] TGDF (Turkish General Directorate of Forestry). Forest Management Plans of Bartın Forest Administration. Ankara, Turkey: 2011.

[21] TMFAL (Turkish Ministry of Food, Agriculture and Livestock). Digital Soil Maps of Bartın Stream Watershed. Ankara, Turkey: 2005.

[22] TGDMRE (Turkish General Directorate of Mineral Research and Exploration). Digital Geological Maps of Zonguldak F-29 Section. Ankara, Turkey: 2007.

[23] TSMS (Turkish State Meteorological Service), Daily Meteorological Data. Ankara, Turkey: 2013.

[24] Atalay İ. Türkiye İklim Atlası. İstanbul, Türkiye: İnkılâp Kitabevi Yayınları; 2011.

[25] Bakker MM, Govers G, Kosmas C, Vanacker V, van Oost K, Rounsevell M. Soil erosion as a driver of land-use change. Agriculture, Ecosystems and Environment. 2005; 105: 467-481.

[27] Öztürk M., Bolat İ, Kara Ö. Bartın Çayı Havzasında Mevcut Yerleşim Alanları için Arazi Kullanım Uygunluk Sınıflandırması (Land Use Suitability Classification for the Actual Settlement Areas within the Bartın Stream Watershed of Turkey). Ekoloji Sempozyumu (Ecology Symposium), 123-123., May, 6-9, 2015, Sinop, Turkey. 2015.

[26] Gautam AP, Webb EL, Shivakoti GP, Zoebisch MA. Land use dynamics and landscape change pattern in a mountain watershed in Nepal. Agriculture, Ecosystems and Environment. 2003; 99: 83-96.

[28] Berberoğlu S. Sustainable Management for the Eastern Mediterranean Coast of Turkey. Environmental Management. 2003; 31(3): 442-451.

[29] Da Fonseca GAB, Sechrest W, Oglethorpe J. Managing the Matrix. In: Lovejoy TE, Hannah L, editors. Climate Change and Biodiversity, Michigan, USA: Yale University Press; 2005. p. 346–358.

ISSN 2303-4521
PERIODICALS OF ENGINEERING AND NATURAL SCIENCES
Vol. 5 No. 1 (2017) – Special Issue (Recent Topics in Environmental Science)
Available online at: http://pen.ius.edu.ba

Determination of the Dam Axis Permeability for the Design and the Optimization of Grout Curtain: An Example from Orhanlar Dam (Kütahya-Pazarlar)

Mustafa Can CANOĞLU
Sinop University, Faculty of Engineering and Architecture, Environmental Engineering Department Sinop/TURKEY

Bedri KURTULUŞ
Muğla Sıtkı Koçman University, Engineering Faculty, Geological Engineering Department, Muğla/TURKEY

Abstract
Rural projects become an important issue considering the rapid increase of population in Turkey. Alongside the contribution to the national economy, dams serve as an environmental structure, which are utilized in flood prevention, sustainable energy, fighting with forest fire and recreation. However, dam construction must be well planned and projected to minimize the unexpected events such as water leakage. This study comprise the geotechnical studies and the design of the planned grout curtain in Orhanlar Dam (Kütahya/Pazarlar). In this context, field and laboratory studies was realized in Orhanlar Dam axis and reservoir area. Within the scope of field studies, engineering geology map was generated, a suitable axis location was specified for the dam and drilling and in-situ testing was realized. Within the field studies, the joint conditions of the geological units under the dam axis and its effect on permeability was observed. For the geotechnical purposes drilling works performed during the planning stage, 5 boreholes total 166 m was realized on dam axis, 1 borehole total 10 m was realized on cofferdam, 1 borehole total 10 m was realized on diversion tunnel and 1 borehole total 10 m was realized on spillway. To determine the permeability profile on dam axis and design the grout curtain, Lugeon tests in Dağardı ophioloitic melange units observed in dam axis, falling head permeability tests in alluviums observed in thalveg and slope debris observed in right abutment were performed. As a result of these studies geotechnical information about the permeability of Orhanlar Dam was collected and the grout curtain hole was designed.

Keywords: Orhanlar Dam; Lugeon Tests; Falling head permeability tests; Design and optimization of grout curtain hole

1. Introduction

In the last decade, dams achieved important economic benefit to the national economy in context of agricultural irrigation, recreation, potable water supply and many more. Additionally, environmental benefits of dams such as recreation, fighting with forest fire, sustainable energy, flood protection and swamp draining are not negligible. Due to the difficulty of finding a suitable dam axis location, residential areas in upstream are submerged in order to provide irrigation or water supply of the residential areas, which are located in downstream. Additionally, in some cases, dam construction cause destruction of common areas belong to the village legal entity such as pastures. These areas must be protected due to its environmental importance. To overcome this injustice, finding an optimum axis location that aggrieve nobody is the soil remedy. However, in Orhanlar Dam, this location is unsuitable to construct a dam body due to the permeable ground conditions. Permeable grounds can be remediated with the use of cement grouting technique. To achieve this problem engineering solutions become prominent.

Construction of a grout curtain under the dam body is a technique, which is used in several dams all around the world including huge dams such as Atatürk Dam (Turkey), Keban Dam (Turkey), Al Wehdah Dam (Jordan), Douera Dam (Algeria), Berke Dam (Turkey) etc. Many researchers studied on dams and reservoirs considering many different points of views such as liquefaction, earthquake impact, landsliding etc. (Lombardi, 1985; Nonveiller, 1989; Karagüzel and Kılıç, 2000; Aksoy and Ercanoğlu, 2006; Aksoy and Ercanoğlu, 2007; Ulusay et al., 2007; Gurocak and Alemdağ, 2012; Tunar et al., 2013; Eryılmaz and Korkmaz, 2015; Aldemir et al., 2015).

Study area is located in Eagean Region in which the climate has a semi-arid continental climate with hot, dry summers and cold, snowy winters. Water supply to 590 ha of agricultural area, fire fighting in case of a forest fire and recreation are the construction benefit of Orhanlar Dam. The dam and reservoir area is identified in 1/25000 scaled Kütahya K22-a1 topographic map prepared by National Mapping Agency of Turkey. Transport to the dam axis from Kütahya city is accessed by 131.5 km of asphalt and 3.5 km of dusty road (fig.1). In case of excessive rainfall transport to the dam axis location can be failed. For this reason a new access road

DOI: 10.21533/pen.v5i1.72

to the dam axis must be projected for the construction stage.

862.95 and maximum water elevation is 876.80 m. Spillway is designed in left abutment.

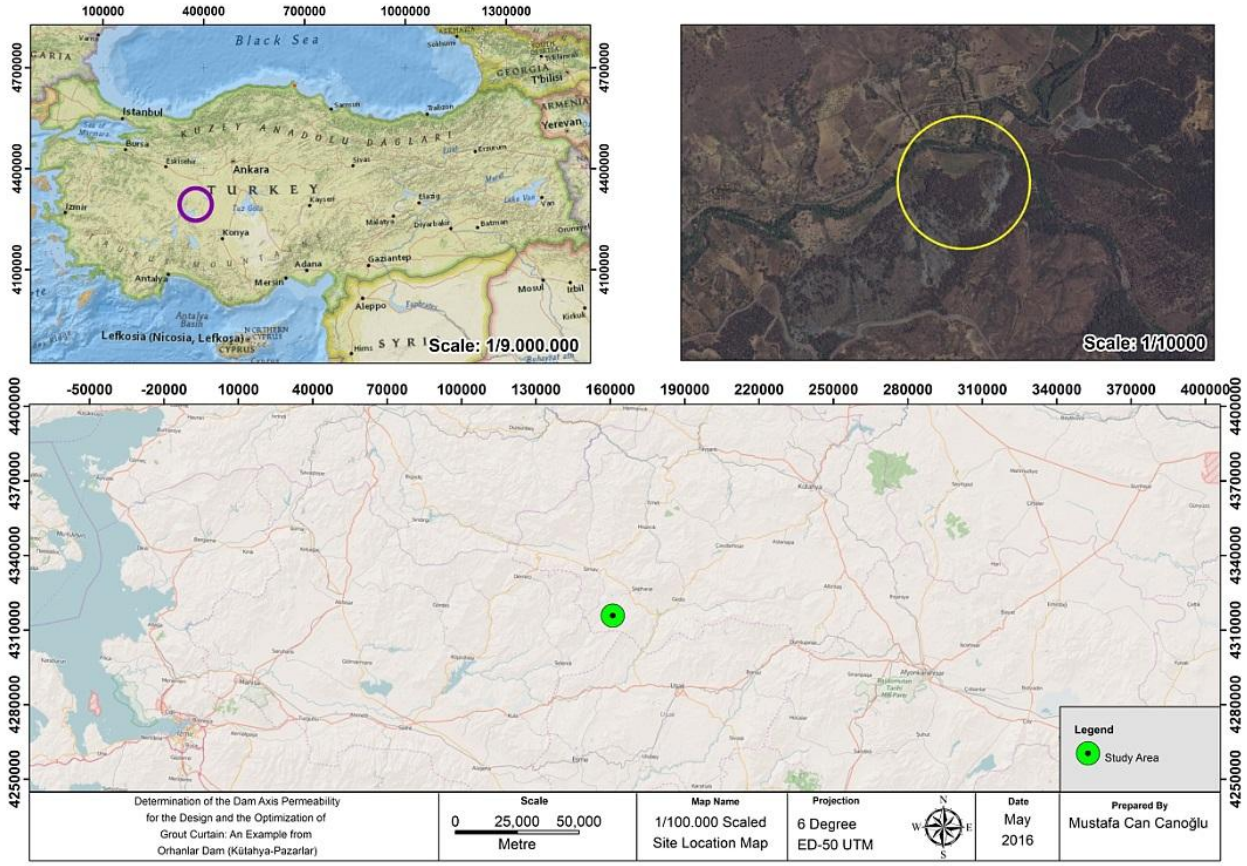

Figure 1. Location map of study area

The aim of this study is briefly, determination of the hydraulic conductivity characteristics of Orhanlar Dam axis location and designing grout curtain hole. In this context, optimization of grout curtain hole depths and water income to the excavation pits are specified. Grout curtain hole depth is calculated considering the empirical formula proposed by Şekercioğlu (2007). However the ultimate grout curtain hole depth is designed based on the engineering judgement by taking into consideration the hydraulic head on the rock medium.

Within this framework, desk studies, field studies and laboratory studies have been performed. Within the desk studies, literature survey is reviewed. Geological mapping, drilling and in situ testing is realized under field studies. Laboratory studies are realized on the samples obtained from drilling operation. 1/1000 scaled engineering geology map of axis location is shown on figure 2.

2. Engineering Geology of Study Area

Orhanlar dam body is planned as clay cored rock-fill dam. Height from thalweg of dam is 29.70 m and height from foundation is 33.20 m. Crest length of dam is 244 m. Minimum water elevation of reservoir area is

5 borehole (total 200 m of depth) is drilled along the dam axis in context of field works. Lugeon (1933) tests were performed in these boreholes in order to determine hydraulic conductivity characteristics of geological units under different hydraulic heads. Hydraulic conductivity of soils is identified by the falling head permeability tests. During the construction stage soils of the dam foundation will be stripped, for this reason calculation of groundwater income into the excavation pit is important.

Geological units in the study area and its surroundings pertain to Mesozoic and Cenozoic Eras. The rocks observed are in the range of Cretaceous and Quaternary (Fig. 2). Nethermost Cretaceous aged Dağardı Melange (Kdm) is covered up with lower-middle Miocene aged flysch units (Mç). Quaternary units such as Alluvium (Qal) and Slope Debris (Qym) draw nigh discordantly the older units. Geological map of the study area and its surroundings is shown on figure 2.

2.1. Dağardı Melange (Cretaceous)

The geological unit defined as Dağardı melange spread on large areas in Aegean Region. This unit is aged as Cretaceous by many researchers. In the study area

peridotite type rocks which pertain to Dağardı Melange are observed. According to Bacak and Uz (2003) Neogene units overly Dağardı Melange discordantly. An important leakage problem is not expected regarding the discontinuity orientations and dam axis location based on the field observations. Infilling material of the discontinuities is generally clay and the mean discontinuity spacing is 3 m. The relation between Cretaceous aged Dağardı Melange and Quaternary aged alluviums and slope debris is represented by the cross section (fig. 3).

2.2 Alluvium (Quaternary)

Quaternary aged alluviums are located along Koyulduk riverbed (figure 2). This unit is formed as a result of erosion transportation and deposition processes. It contains gravel, sand, silt and clay sized material. Mean granulometric percentage of the alluvium sampled from the borehole SK-3 is specified as %42 gravel, %62 sand and %6 fine material (clay and silt) based on the laboratory test results. The data obtained from the drilling works shows that the thickness of the alluvium is changed between 4.50 - 5.00 m.

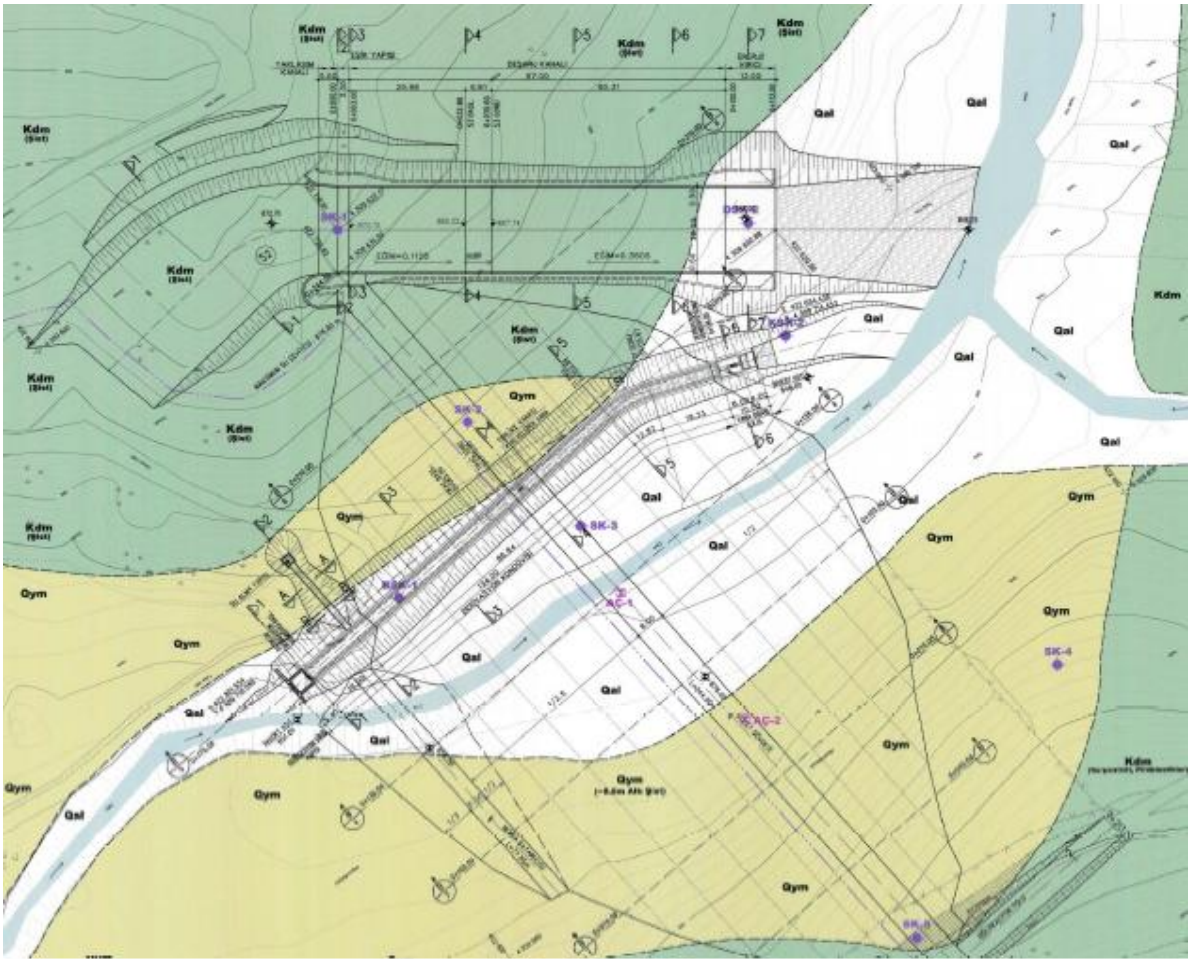

Figure 2. Engineering geology map of Orhanlar Dam

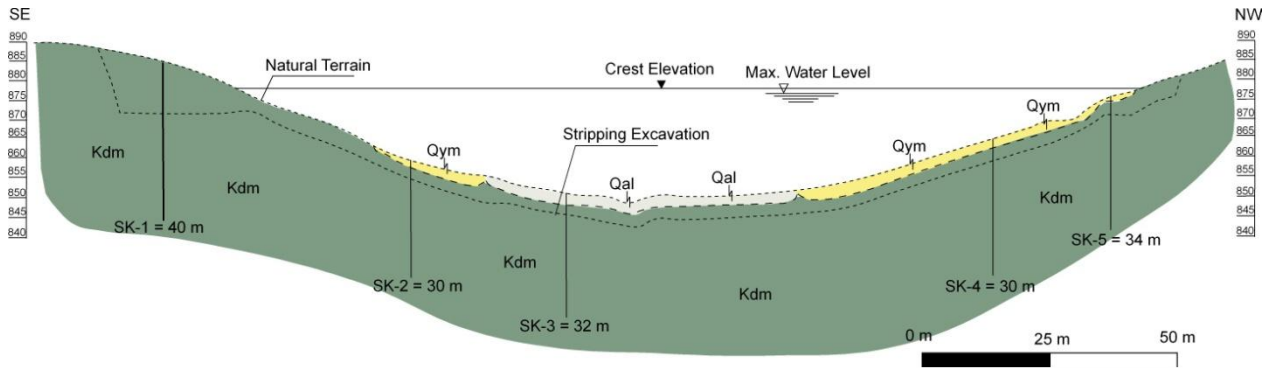

Figure 3.Cross section of Orhanlar Dam body axis location

2.3 Slope Debris (Quaternary)

Quaternary aged slope debris is formed as a result of transportation process of the weathered bedrock to piedmont (figure 2). It contains as well as gravel, sand, silt and clay sized material. Mean granulometric percentage of the slope debris sampled from the boreholes SK-4 and SK-2 is determined as %15 block, %15 gravel, %20 sand and %50 fine material (clay and silt) based on the laboratory test results. Maximum thickness of the slope debris is obtained by the drilling operations as 3.50 m depth.

3. Methodology

3.1. Lugeon tests

Lugeon test is an in-situ test applied in a borehole with the purpose of hydraulic conductivity determination of rock masses under different hydraulic heads (Canoğlu and Kurtuluş, 2017). This test is applied generally to test levels varying between 2 – 5 m (Canoğlu and Kurtuluş, 2017). Test level length is designate based upon the physical and structural properties of rock mass. In a uniform and impermeable rock mass test level can be applied with 5 – 10 m test zone and in a permeable rock mass which has variable physical properties, this test zone can be reduced until 1 m (Akyüz, 2010). Test method proposed by Lugeon (1933), 1 Lugeon is defined as the water amount pumped to the 1 meter length of test zone under 10 atm hydraulic pressure in 1 minute. The pressure applying to the test zone is also specified by engineering judgement depending on the physical properties of rock but general application in Turkey is using 2, 4, 6, 8, 10 kg/cm^2 of test pressures (Canoğlu and Kurtuluş, 2017). Each pressure stage applied to the rock during 10 minutes and the water leakages are recorded each 5 minutes. Then, 9, 7, 5, 3, 1 kg/cm^2 of test pressures are applied and water leakages are recorded (Canoğlu and Kurtuluş, 2017). Lugeon value is calculated by equation 1.

$$LU = (Q \times 10) / (P \times L) \qquad \text{(equation 1)}$$

In this expression, LU is Lugeon value (lt/min/m), Q is water amount given to the rock formation (lt/min), P is hydraulic head applied to the test zone (kg/cm^2) and L is test length (m). The permeability class corresponding to the Lugeon values is presented in table 1.

Table 1. Permeability classification based on the Lugeon values of rock masses

Lugeon Values	Permeability Class
<1 Lugeon	Impermeable
1 - 5 Lugeon	Low Permeable
5 - 25 Lugeon	Permeable
>25 Lugeon	Highly Permeable

Lugeon test gives important information in dam projects for the prediction of grout amount injected into the rock mass. For this reason, Lugeon tests have been realized in the boreholes drilled on the Orhanlar Dam axis. Minimum, maximum and mean Lugeon values obtained from each boreholes are presented in table 2.

Table 2. Minimum, maximum and mean Lugeon values of each borehole

	Lugeon Values (LU)				
	SK-1	**SK-2**	**SK-3**	**SK-4**	**SK-5**
Minimum	0.18	0.25	0.50	0.30	0.18
Mean	1.90	1.21	2.41	2.35	1.30
Maximum	31.90	6.05	11.94	4.29	3.87

3.2 Design and optimization of grout curtain

A number of method is proposed by many researchers for the calculation of grout curtain depth design (Bureau of Indian Standard, 1993; Pettersson and Molin, 1999; Evert, 2003; Şekercioğlu, 2007; Schleiss and Pougatsch, 2011). Results of these calculations are generally close but, in Turkey the method of Şekercioğlu (2007) get in favour as utilized in this study. The calculation of the method proposed by Şekercioğlu (2007) is as follow;

$$h' = \left(\frac{1}{2}\right)h + 15 \qquad \text{(equation 2)}$$

In this equation, h' represents grout curtain depth, h is height of water on the rock formation. In order to be in safe side, the same grout curtain depth is applied to the abutments considering the engineering judgement. In addition, the grout curtain is extended through the reservoir area for avoiding the potential leakages. The grout curtain design and the permeability profile of Orhanlar Dam axis is presented in figure 4.

It is planned to prevent the potential leakages with the grout curtain shown in figure 4. The grout curtain depth in left abutment is changing between 28 - 30 m. Augmentation of hydraulic head trigger the leakages with the increase of the hydrostatic pressure in rock medium. As the maximum hydrostatic pressure will be on thalweg, grout curtain depth is augmented (approximately 35 m) approaching to thalweg. For the right abutment, grout curtain depth changes between 25-30 m as well as left abutment.

3.3 Calculation of water income to the excavation pit

Koyulduk River flows during spring season but during summers and autumns river is dry and groundwater flows through quaternary aged alluvium. The groundwater level surveys shows that the phreatic water is changing between 3 m and 4 m. After cut-off excavation on dam axis location, water flux will be

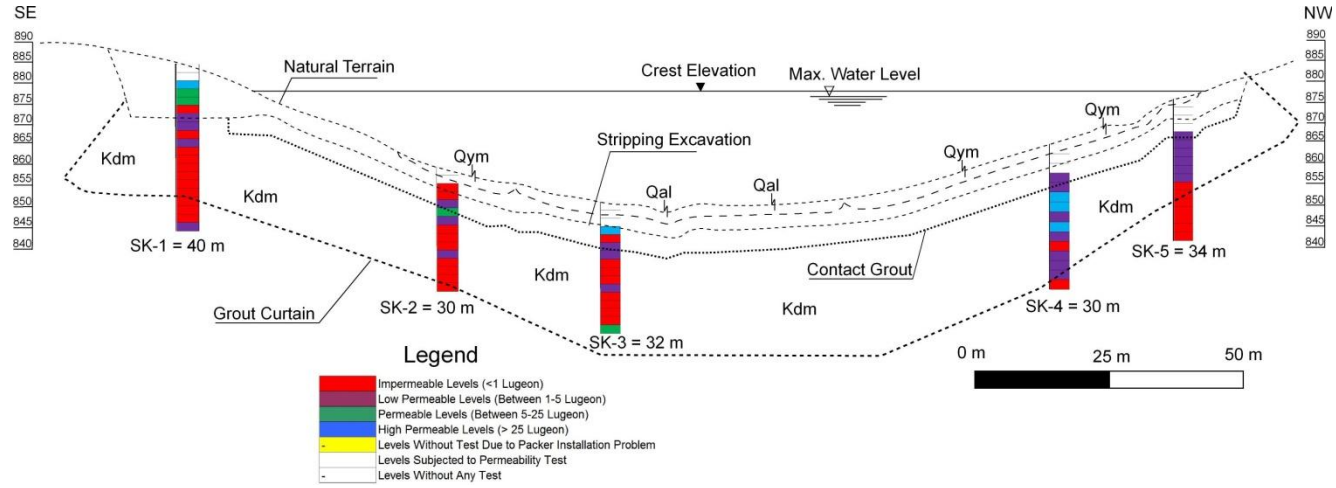

Figure 4. Orhanlar Dam permeability profile and grout curtain borderline

oriented through the excavation pit. According to Darcy Law the flow rate will depend on the new hydraulic gradient and the hydraulic conductivity of the alluviums. The permeability tests (falling head) performed in the alluviums (borehole SK-3) indicates that mean hydraulic conductivity is approximately $K=10^{-4}$cm/s. The water income to the excavation pit can be estimated by Darcy Law considering the alluviums are homogenous and isotropic (eq. 2). Figure 5 represents a dam body cross section.

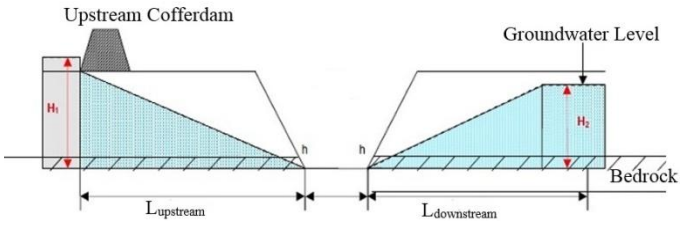

Figure 5. Orhanlar Dam permeability profile and grout curtain borderline

Darcy Formula is

$$Q = A \times K \times i \qquad \text{(equation 2)}$$

In this formula, "Q" is flow rate of water income to the excavation pit, "K" is hydraulic conductivity of alluvium, "A" is section area of the alluvium perpendicular to the flow, "i" is hydraulic gradient, "H" is water height accumulated behind the upstream cofferdam, "h" is water height in the excavation pit and "L" is the horizontal distance between "H" and "h".

Calculation of water income to the excavation pit is realized based on the following assumptions:

1. Mean alluvium thickness is (based on the geological cross section) = 5.0 m.
2. Mean static level is = 4.0 m.
3. Mean width of the alluvium is = 50.0 m.
4. Hydraulic pressure behind the upstream cofferdam (H_2) is assumed as free static groundwater level

H_2 = (Alluvium thickness + Formation) – static groundwater level

$H_2 = 7.0 – 4.0 = 3.0$ m

5. Water amount incoming from rock formation is neglected.
6. Water amount incoming from the upstream excavation wall and downstream excavation wall are assumed as equal.
7. Alluvium is fully saturated under static level.

Considering all these assumptions, water income to the excavation pit is calculated as follow:

H_1 = Alluvium thickness (5 m) + Formation (2 m) = 7 m

Water income from the upstream excavation wall is;

$i_{upstream} = (7.0 – 0.0) / 50 = 0.14$

$Q = (A \times K \times i_{upstream}) \times 2$

$Q = 800m2 \times 10^{-4}$ cm/sn x 0.14 x 2

$Q \approx 0.224$ lt/sn

Water amount incoming from the upstream excavation wall is calculated as 6.72 lt/min. In this circumstance, the total amount of water flowage to the excavation pit is calculated as approximately 13.44 lt/min. This water must be drained with suitable pumps.

4. Results and Conclusion

By favour of this study, destruction of arable lands and environmentally important areas is avoided by finding a new dam axis location and using grouting techniques for soil remediation. In addition, injustice between the villages located in the upstream of the planned dam axis is averted. In this context, optimization of grout curtain hole depths and water income to the excavation pits are specified considering the universal consent techniques using with engineering judgement. The following results and conclusions can be drawn from the present study.

a) The Lugeon test results of the boreholes drilled along dam axis are evaluated for right abutment, left abutment and thalweg separately based on the permeability classification table (table 1).

b) Lugeon tests of the left abutment performed in the boreholes SK-1 and SK-2 drilled for indicates some permeable layers in first ten meter but going to deeper low permeable layers are observed. As for thalweg, the borehole SK-3 shows the same permeability character.

c) The permeability profile of right abutment is low permeable for first 15 meter and impermeable after 15 meter as obtained from the boreholes SK-4 and SK-5. But there are some permeable layers for the first 15m fo SK-4.

d) The bedrock of dam axis location belongs to Cretaceous aged Dağardı Melange constituted of peridotites. In addition, core samples obtained from the drilling operations show that 4.5 – 5 m thick of alluvium and 3.5 m thick of slope debris exist in dam axis location. This alluvium and slope debris must be stripped before the construction stage.

e) Water income to the stripping excavation pit is calculated based upon Darcy Law. According this calculation total amount of water income to the excavation pit will be approximately 13.44 lt/min. This water must be discharged out of the excavation pit with suitable pumps.

f) As a result of this study a huge leakage potential is no encountered in dam axis. Small quantity of water leakages from upstream to downstream are planned to restrained by the construction of grout curtain.

g) Considering the strength parameters of bedrock, any stability problem in dam axis is not awaited.

Acknowledgements

This study is realized under the project of "Sakarya: Pamukova-Çilekli, Kemaliye (Deveboynu) and Turgutlu, Central -Beşevler, Kütahya: Pazarlar-Orhanlar, Tavşanlı-Kışlademirli, Bilecik: Söğüt-Savcıbey Dams Planning Engineering Services" realized for Republic Of Turkey Ministry Of Forestry and Water Affairs, General Directorate of State Hydraulic Works, Eskişehir 3. Regional Directorate with the contributions of SUYAPI Engineering Consulting Co.

Author thanks to DSİ 3. Regional Directorate engineer staff and SUYAPI for funding and their experience share.

References

Aksoy, H. and Ercanoğlu, M., 2006. Determination of the rockfall source in an urban settlement area by using a rule-based fuzzy evaluation. Natural Hazards and Earth System Science, 6, 941-954.

Aksoy, H. and Ercanoğlu, M., 2007. Fuzzified kinematic analysis of discontinuity-controlled rock slope instabilities. Engineering Geology, 89, 206-219.

Akyüz, S., 2010. Kargı baraj yeri (Çorum) litolojik birimlerin geçirgenlik özellikleri yönünden incelenmesi. Çukurova Üniversitesi, Fen Bilimleri Enstitüsü, Jeoloji Mühendisliği Anabilim Dalı, Yüsek Lisans Tezi, 134s.

Aldemir, A., Yılmaztürk, S.M., Yücel, A.R., Binici, B., Arıcı, Y., Akman, A., 2015. Beton barajların deprem davranışlarının incelenmesinde kullanılan analiz metotları. İMO Teknik Dergi, 6943-6968.

Bacak, G., and Uz, B., 2003. Dağardı Güneyi (Tavşanlı-Kütahya) ofiyolitinin jeolojisi ve jeokimyasal özellikleri, İTÜ Dergisi D. Serisi, 86 – 99.

Bureau of Indian Standard, 1993. "Guidelines for the Design of Grout Curtain: Part 2: Masonry and Concrete Gravity Dams".

Eryılmaz Türkkan, G., Korkmaz, S., 2015. Kuyu ve akifer testlerinde uygulanan analitik ve sayısal yöntemlerle hidrolik iletkenliğin belirlenmesi. İMO Teknik Dergi, 6969-6991.

Ewert, F.K., 2003. Discussion of Rock Type Related Criteria for Curtain Grouting". Proceedings of the Third International Conference on Grouting in Rock and Ground Improvement, ASCE Special Publication, No. 120.

Gürocak, Z. ve Alemdağ, S., 2012. Assessment of permeability and injection depth at the Atasu dam site (Turkey) based on experimental and numerical analyses. Bulletin of Engineering Geology and the Environment, 71, 221-229.

Karagüzel, R. ve Kılıç, R., 2000. The effect of the alteration degree of ophiolitic melange on permeability and grouting. Engineering Geology, 57, 1-12.

Lombardi, G., 1985. The Role of Cohesion in Cement Grouting of Rock, 15. ICOLD-Congress, Lausanne, 3, 235–261.

Lugeon, M. (1933). Barrage et Géologie. Dunod. Paris

Nonveiller, E., 1989. Grouting Theory in Practice. Elsevier, Tokyo.

Pettersson, S.A. and Molin, H., 1999. "Grouting & Drilling for Grouting: Purpose, Application, Methods with Emphasis on Dam and Tunnel Projects". Atlas Copco. 6991 1019 01

Schleiss, A. J. - Pougatsch, H., 2011. "Les Barrages: Du projet à la mise en service. Presses Polytechniques Universitaires Romandes, 17, 714p.

Suyapı, 2013. Savcıbey Göleti, mühendislik jeolojisi planlama raporu rev.1. DSİ 3. Bölge Müdürlüğü, Eskişehir.

Şekercioğlu, E., 2007. Yapıların projelendirilmesinde mühendislik jeolojisi. JMO yayınları, 28, 4. Baskı, s.117.

Tunar, N.Ö., Ulusay, R., and Işık, N.S., 2013. A study on geotechnical characterization and stability of downstream slope of a tailings dam to improve its storage capacity (Turkey). Environmental Earth Sciences, 69, 1871-1890.

Ulusay, R., Tuncay, E., and Hasançebi, N., 2007. Liquefaction assessments by filed-based methodologies for the foundation soils at a dam site in northeast Turkey. Bulletin of Engineering Geology and the Environment, 66 (3), 361-375.

ISSN 2303-4521

PERIODICALS OF ENGINEERING AND NATURAL SCIENCES
Vol. 5 No. 1 (2017) – Special Issue (Recent Topics in Environmental Science)
Available online at: http://pen.ius.edu.ba

Forecasting Foreign Trade of Bosnia and Herzegovina for Wood and Articles of Wood, Wood Charcoal by Seasonal ARIMA Model

Nadir ERSEN

Vocational School, Department of Management and Organization Artvin Çoruh University, Turkey,

İlker AKYÜZ

Faculty of Forestry, Department of Forestry Industry Engineering Karadeniz Technical University, Turkey

iakyuz@ktu.edu.tr

Abstract

In this study, it is aimed that the analysis of export and import values of Bosnia and Herzegovina for wood and articles of wood, wood charcoal with seasonal ARIMA model and forecasting of export and import values for next term by the best appropriate seasonal ARIMA model. The data used in this study were obtained from Trade statistics for international business development (TRADEMAP) and monthly data covering the period of January 2007 and December 2015. Augmented Dickey-Fuller test was used for the stationarity test. Temporary model that have smallest values of forecasting accuracy measurement was determined. The appropriateness of the model (whether plot of autocorrelation has white noise) was determined by using the Box-Ljung test. As a result, ARIMA $(3,1,0)(0,1,2)_{12}$ model was found as the best forecasting model for both export and import series. It was estimated that export value of Bosnia and Herzegovina for wood and articles of wood, wood charcoal is approximately 531 million$, while import value is 160 million$ in 2020.

Keywords: Seasonal ARIMA model; wood and articles of wood; wood charcoal; export; import; forecasting

1. Introduction

Export provides to remain in the balance of foreign trade by supply the amount of foreign currency going abroad. In addition, companies are becoming more powerful in global competition by expanding the market network with export and as well negative trend of exports in the future. Export / import that are in a close relationship with GDP, interest rates, inflation, etc. may affect the country's economy. Therefore, the forecasting of accurately value of export/import is very important.

There are many forecasting techniques that including qualitative and quantitative for predicting the future. Quantitative methods are contained in the method of time series analysis [1]. There are many methods for analyzing time series. Box-Jenkins method is one of the most used methods. This method is called as ARIMA (autoregressive integrated moving average) analysis. ARIMA model is divided into two. These are non-seasonal and seasonal ARIMA models. ARIMA model combine differencing with autoregression (AR) and a moving average (MA) models. This model can be expressed as $w_t=c+\phi_1 w_{t-1}+\ldots\ldots+\phi_p w_{t-p}+\theta_1\varepsilon_{t-1}+\ldots+\theta_q\varepsilon_{t-q}+\varepsilon_t$. Here, w_t is the differenced series, p is order of the autoregressive part and q is order of moving average part. Also, we said this an ARIMA (p,d,q), where, d is a degree of difference [2]. General process of ARIMA model is as follows [2];

1. Plot the data. Identify unusual obversations.
2. If necesarry, transform the data to stabilize the variance.
3. If the data are non-stationary, take first difference the data until the data are stationary.
4. Plot the autocorrelation function (ACF)/partial autocorrelation function (PACF) of the differenced data and try to determine possible candidate models.
5. Try your chosen model(s) and use the akaike information criterion (AIC) to search for better model.
6. Check the residuals from your chosen model by plotting the ACF of the residuals and doing a Ljung-Box test of the residuals. If model has not white noise, determine model again.
7. If model has white noise, calculate forecasts.

ARIMA model was applied many studies [3, 4, 5, 6, 7, 8, 9, 10, 11, 12, 13, 14, 15, 16, 17, 18, 19]. In this study, it is aimed that the analysis export and import values of Bosnia and Herzegovina for wood and articles of wood with SARIMA model. In addition, the best appropriate SARIMA model estimated export and import values.

DOI: 10.21533/pen.v5i1.73

2. Materials and Method

2.1. Material

In this study, it was used that export and import values of Bosnia and Herzegovina for wood and articles of wood, wood charcoal. The monthly data was used for examine the seasonal and trend components. This data covers the period of January 2007 and December 2015. Data were obtained from Trade statistics for international business development [20]. Data was taken as $1000. Minitab 16 was used for determine the best model while Eviews-8 was used for the analysis of stationary.

2.2. Method

2.2.1. Seasonal ARIMA model

The seasonal ARIMA (SARIMA) model is similar to the ARIMA model which known as a linear approximation for predicting future. This model consists of stages such as identification, estimation, diagnostic checking and forecasting. Accurate predictive models can improve with this model by removing the characteristics of seasonal variation through seasonal differences [21].

The SARIMA model consists of seasonal autoregressive term (P), seasonal integrated term (D), and seasonal moving average term (Q) as well as autoregressive term (p), integrated term (d), and moving average term (q). Generally, the SARIMA model represents as SARIMA (p, d, q)(P, D, Q) and is expressed by equations in follow

$$\varphi_p(B)\,\Phi_p(B^S)(1-B)^d(1-B^S)^D y_t=\delta+\theta_q(B)\Theta_Q(B^S)\alpha_t \quad (1)$$

$$\varphi_p(B)= 1-\varphi_1 B-\varphi_2 B^2-\ldots-\varphi_p B^p \quad (2)$$

$$\theta_q(B)= 1-\theta_1 B-\theta_2 B^2-\ldots-\theta_q B^q \quad (3)$$

$$\Phi_p(B^S)= 1-\Phi_S B^S-\Phi_{2S} B^{2S}-\ldots-\Phi_{PS} B^{PS} \quad (4)$$

$$\Theta_Q(B^S)= 1-\Theta_S B^S-\Theta_{2S} B^{2S}-\check{g}-\Theta_{QS} B^{QS} \quad (5)$$

Here, y_t is the observation value at time t, α_t is the lagged error at time t, B is the lag operator defined by $B_k y_t= y_{t-k}$; φ_p (p=1,2,…p), Φ_P (P=1,2,…,P), θ_q (q=1,2,..q) and Θ_Q (Q=1,2,…Q), p and q are the order of non-seasonal autoregressive and non-seasonal moving average, P and Q is the order of seasonal autoregressive and seasonal moving average, d is order of regular difference, D is order of seasonal difference and S is a seasonal length [21, 22].

2.2.2. Forecasting Accuracy Measurements

For the series, forecasting values are calculated and compared with the actual values of the series. There are several criteria for forecasting accuracy measurement. Forecasting accuracy measurements used in this study were given as follows:

Mean Absolute Percentage Error;

$$(\text{MAPE})=\sum\left|\frac{\check{y}_t-y_t}{y_t}\right|\frac{100}{n} \quad (6)$$

$$\text{Mean Square Error (MSE)}=\frac{\sum(\check{y}_t-y_t)^2}{n} \quad (7)$$

Here, $\check{y}_t$ is the forecasting value of model, y_t is the actual value of model and n is the number of observations [19, 23]. The criteria of MAPE for model evaluation were in Table 1.

Table 1. MAPE values for model evaluation [24]

MAPE (%)	Evaluation
MAPE ≤ 10%	High accuracy forecasting
10% < MAPE ≤ 20%	Good forecasting
20% < MAPE ≤ 50%	Reasonable forecasting
MAPE > 50%	Inaccurate forecasting

3. Results

Firstly, it must be provided to export and import series of stationary condition. For this, the stationary of export and import series were analyzed with Augmented Dickey-Fuller (ADF) unit root test and results shown in Table 2. It was seen that series is stationary in the 5% significance level according to ADF test when taken difference of the natural logarithm series. The 1stdifference of series was taken. Distribution graph of natural logarithm and differenced of export and import series were shown in Figure 1 and 2.

Table 2.Augmented Dickey-Fuller (ADF) test results

		Level	Natural logarithm	1st difference
Export series	Augmented Dickey-Fuller test statistic	-0,075962	0,245091	-2,867914
Import series	Augmented Dickey-Fuller test statistic	-0,376831	-0,108246	-2,645649
Test critical values	1% Level	-2,589531	-2,589531	-2,589531
	5% Level	-1,944248	-1,944248	-1,944248
	10% Level	-1,61451	-1,61451	-1,61451

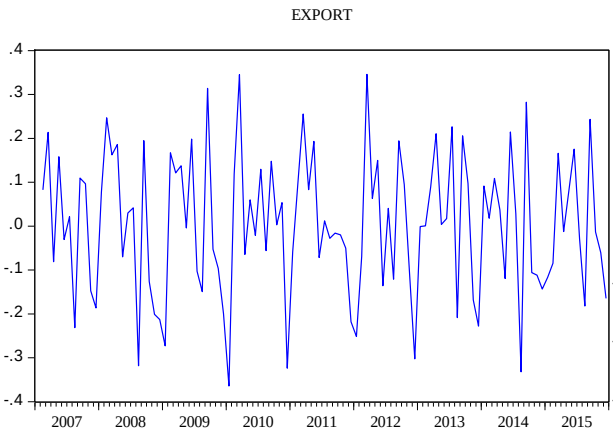

Figure 1.Stationarized export series of graphics

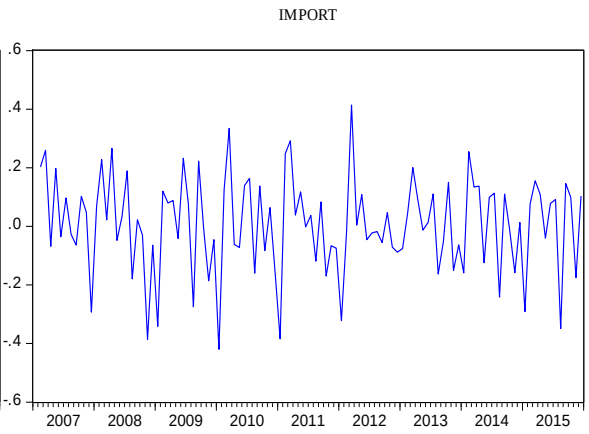

Figure 2.Stationarized import series of graphics

According to Figure 1 and 2, the mean and variance of export and import series are a constant. But, series comprise seasonality. For this, natural logarithm and differenced of export and import series were taken seasonal difference (12st difference). After obtaining these series of stationary conditions, a variety of ARIMA $(p,d,q)(P,D,Q)_{12}$ models has been tested by autocorrelation and partial autocorrelation graphics of the export and import series. Autocorrelation and partial autocorrelation graphics of stationarized these series were shown in Figure 3, 4, 5 and 6.

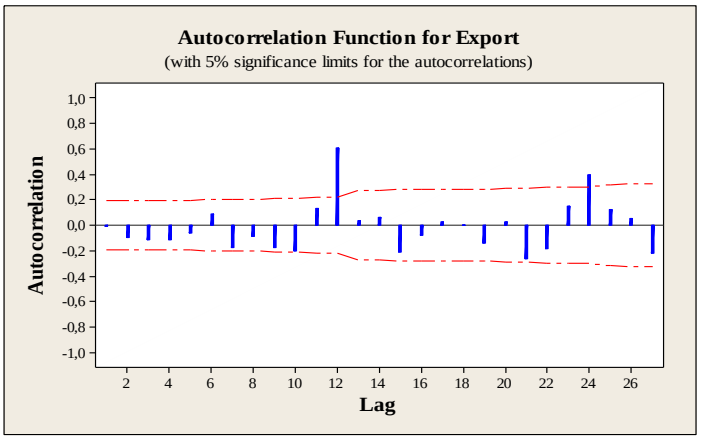

Figure 3. Autocorrelation graphic of stationarized export series

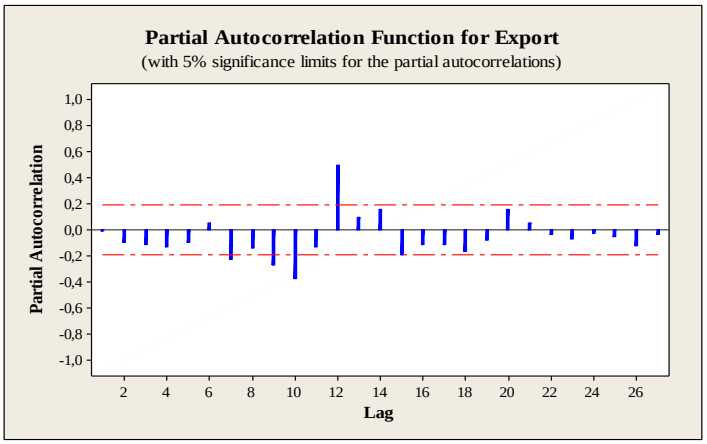

Figure 4. Partial autocorrelation graphic of stationarized export series

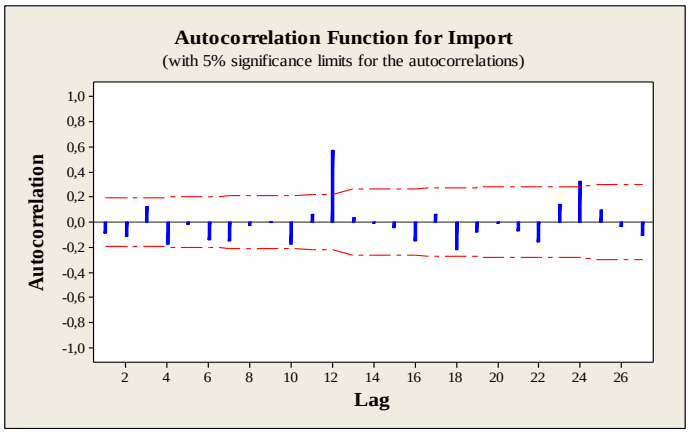

Figure 5. Autocorrelation graphic of stationarized import series

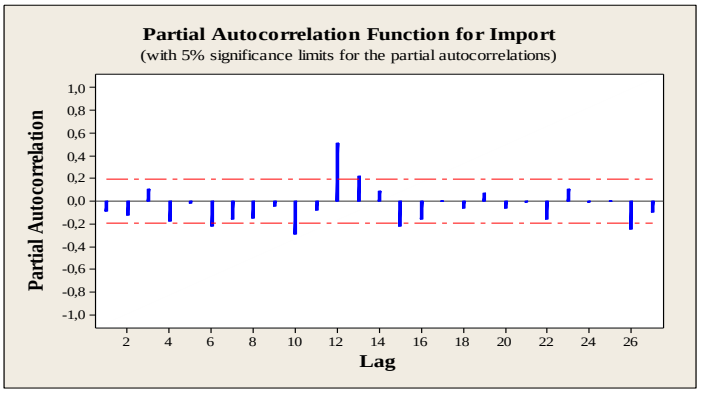

Figure 6. Partial autocorrelation graphic of stationarized import series

As a test results, ARIMA $(3,1,0)(0,1,2)_{12}$ model which have smallest values of the error sum of squares (SSE) and the mean square error (MSE) was determined as temporary model for both export and import values of Bosnia and Herzegovina for wood and articles of wood, wood charcoal. The results related to the model were given in Table 3 and 4. The suitability of models were tested with Ljung-Box Q statistic and results shown in Table 5 and 6.

Table 3.Analysis results of ARIMA $(3,1,0)(0,1,2)_{12}$ model for export

Variable	Coefficient	Std. Error	t-Statistic
AR(1)	-0,251	0,1023	-2,45
AR(2)	-0,074	0,107	-0,69
AR(3)	0,2464	0,1022	2,41
SMA(12)	0,5397	0,1066	5,06
SMA(24)	0,3528	0,1116	3,16
Number of observations		108	
After differencing		95	
The error sum of squares		0,945841	
The mean square error		0,010509	

Table 4.Analysis results of ARIMA$(3,1,0)(0,1,2)_{12}$ model for import

Variable	Coefficient	Std. Error	t-Statistic
AR(1)	-0,3234	0,1019	-3,17
AR(2)	-0,0659	0,1072	-0,61
AR(3)	0,2847	0,0998	2,85
SMA(12)	0,422	0,1098	3,84
SMA(24)	0,4456	0,1134	3,93
Number of observations		108	
After differencing		95	
The error sum of squares		0,845125	
The mean square error		0,00939	

Table 5.The Q_{LB} statistic and X^2 values of ARIMA $(3,1,0)(0,1,2)_{12}$ model residuals in different lags for export

Lags	$Q_{statistic}$	X^2_{table}(α=0.05)	Degree of freedom
12	13.9	14.07	7
24	27.6	30.14	19
36	36.9	43.77	31≈30
48	52.3	55.76	43≈40

Table 6.The Q_{LB} statistic and X^2 values of ARIMA $(3,1,0)(0,1,2)_{12}$ model residuals in different lags for import

Lags	$Q_{statistic}$	X^2_{table}(α=0.05)	Degree of freedom
12	12.8	14.07	7
24	19.9	30.14	19
36	28.6	43.77	31≈30
48	44.8	55.76	43≈40

While the actual and forecasting export values for wood and articles of wood, wood charcoal were shown in Figure 7, actual and forecasting export values in Figure8. In addition, the forecasting values for export and import were given in Table 7 and 8.

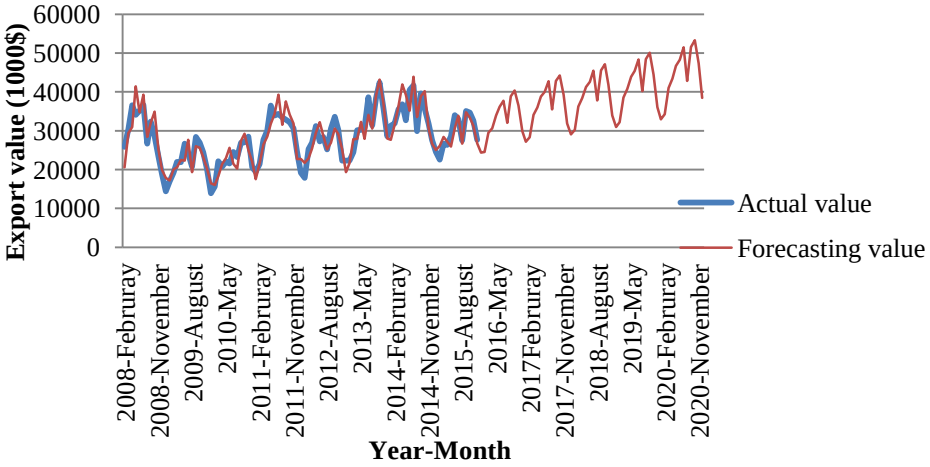

Figure 7. Actual and forecasting values for export (2008-2020)

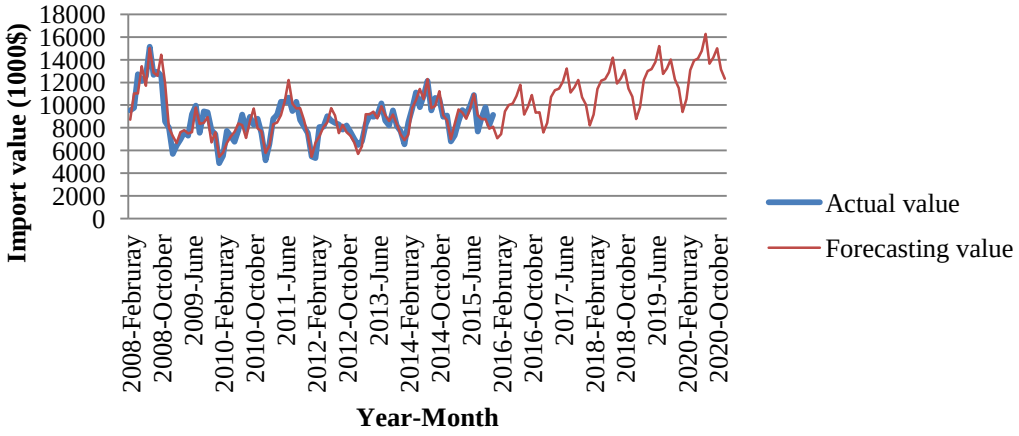

Figure 8. Actual and forecasting values for import (2008-2020)

Table 7.The forecasting values for export in 2016-2020 (1000$)

Months	**2016**	**2017**	**2018**	**2019**	**2020**
January	24404	27161	29070	30935	32919
Februray	24570	28367	30222	32160	34222
March	29440	34061	36248	38572	41046
April	30604	35988	38346	40805	43422

May	33925	38751	41234	43878	46691
June	36141	40055	42621	45354	48262
July	37683	42714	45469	48384	51487
August	32024	35528	37803	40227	42807
September	38846	42786	45529	48449	51555
October	40333	44238	47079	50098	53311
November	36483	39281	41798	44478	47331
December	29865	31885	33930	36106	38421

Table 8.The forecasting values for import in 2016-2020 (1000$)

Months	**2016**	**2017**	**2018**	**2019**	**2020**
January	7092	7587	8196	8779	9400
Februray	7442	8428	9171	9818	10513
March	9453	10716	11409	12215	13078
April	10007	11311	12151	13012	13932
May	10137	11441	12298	13167	14098
June	10802	12068	12882	13792	14768
July	11780	13237	14197	15202	16277
August	9177	11113	11908	12750	13652
September	9876	11559	12362	13236	14172
October	10875	12211	13085	14011	15002
November	9342	10695	11452	12262	13129
December	9365	10033	10738	11498	12311

4. Conclusions

The export and import values of Bosnia and Herzegovina for wood and articles of wood, wood charcoal with seasonal ARIMA model were estimated with seasonal ARIMA model. The natural logarithm, regular difference and seasonal difference of the series were taken. ACF and PACF graphics of the series for determine the appropriate models were examined. Q statistics were calculated for the appropriateness of the model. ARIMA $(3,1,0)(0,1,2)_{12}$ model was found as the best forecasting model for both export and import series. It was found that MAPE value of model for export is 8.12%, while MAPE value for import is 7.54%. It was estimated that export value of Bosnia and Herzegovina for wood and articles of wood, wood charcoal is approximately 531 million$, while import value is 160 million$ in 2020.

References

[1] Can M. "Forecasting with time series analysis in business", Phd Thesis, İstanbul University, Social Science Institute, Istanbul, Turkey, 2009.

[2] Hyndman, RJ, Athanasopoulos, G. "Forecasting: principles and practice", OTexts Publisher, 2014.

[3] Çevik O, Yürekli K. "Modeling of Yeşilırmak river's monthly flow series using seasonal ARIMA model",*Journal of Agricultural Science*, 9(3): 261-268, 2003.

[4] Ismail ZH, Mahpol KA."SARIMA model for forecasting Malaysian electricity generated", *MATEMATIKA*, 21(2): 143-152, 2005.

[5] Iqubal N, Bakhsh K, Maqbool A, Ahmad AS. "Use of the ARIMA model for forecasting wheat area and production in Pakistan", *Journal of Agriculture & Social Science,* 1(2): 120-122, 2005.

[6] Hsiao JM, Shieh CJ. "Evaluating the value of information sharing in a supply chain using an ARIMA model", *Int J AdvManufTechnol*, 27: 604-609, 2006.

[7] Altın A. "Modeling of water amount which goes into Dodurga dam by using Box-Jenkins technique", *Eng&Arch. Fac. Eskişehir Osmangazi University*, XX(1): 81-100, 2007.

[8] Akıncı M. "Stationary analysis in time series and an application on share in GNP of export", MSc. Thesis, Kafkas University Social Sciences Institute, Kars, Turkey, 2008.

[9] Nanthakumar L, Ibrahim Y. "Forecasting international tourism demand in Malaysia using Box-Jenkins SARIMA application", *South Asian Journal of Tourism and Heritage*, 3(2): 50-60, 2010.

[10] Emang D, Shitan M, Ghani ANA, Noor MK. "Forecasting with univariate time series models: a case of export demand for peninsular Malaysia's moulding and chipboard", *Journal of Sustainable Development*, 3(3): 157-161, 2010.

[11] Martinez EZ, da Silva EAS, Fabbro ALD. "A SARIMA forecasting model to predict the number of cases of dengue in campinas", *State of São Paulo, Brazil, Revista da Sociedade Brasileira de Medicina Tropical*, 44(4): 436-440, 2011.

[12] Polat Ö, Ersungur ŞM.“Forecasting foreign trade of Turkey”, *Journal of Business Economics and Political Science*, 1(1): 83-95, 2012.

[13] Karaman E, Fırat MZ. Modeling the test day milk yields via time series method. Journal of Kafkas University Veterinary Faculty 2013; 19(4): 659-664.

[14] Özer OO, İlkdoğan U. “The world cotton price forecasting by using Box-Jenkins model”, *Journal of Tekirdağ Agricultural Faculty*, 10(2): 13-20, 2013.

[15] Osarumwense OI. “Applicability of Box-Jenkins SARIMA model in rainfall forecasting: a case study of port-harcourt south south Nigeria*”, Canadian Journal on Computing in Mathematics, Natural Sciences, Engineering and Medicine*, 4(1): 1-4, 2013.

[16] Contreras J, Espinola R, Nogales FJ, Conejo AJ.“ARIMA models to predict next-day electricity prices”, *IEEE Transactions on Power System*, 18(3): 1014-1020, 2003.

[17] Demir A, Özmen Ö, Rashid A. “An estimation of Turkey’s export loss to Iraq”, *Procedia-Social and Behavioral Sciences*, 150: 1240-1247, 2014.

[18] Gikungu SW, Waititu AG, Kihoro JM. “Forecasting inflation rate in Kenya using SARIMA model”, *American Journal of Theoretical and Applied Statistics*, 4(1): 15-18, 2015.

[19] Chang YW, Liao MY.A “Seasonal ARIMA model of tourism forecasting: the case of Taiwan”,*Asia Pacific journal of Tourism Research*, 15(2): 215-221, 2015.

[20] TradeStatisticsfor International Business Development, List 2015 of ExportersandImportersfortheSelectedProducts 44.(http://www.trademap. org/Country_SelProductCountry_TS.aspx 20 Mayıs 2016).

[21] Jeong K, Koo C,Hong T. “An estimation model for determining the annual energy cost budget in educational facilities using SARIMA (seasonal autoregressive integrated moving average) and ANN (artificial neural network)”, *Energy*, 71: 71-79, 2014.

[22] Pao HT. “Forecast of electricity consumption and economic growth in Taiwan by state space modeling”, *Energy*, 34: 1779-1791, 2009.

[23] Göktaş Ö. “Theoretical and applied time series analysi”,. Beşir Publishing, İstanbul, Turkey, 2005.

[24] Lewis CD. “Industrial and business forecasting methods”, Published by Butterworths, London, 1982.

ISSN 2303-4521
PERIODICALS OF ENGINEERING AND NATURAL SCIENCES
Vol. 5 No. 1 (2017) – Special Issue (Recent Topics in Environmental Science)
Available online at: http://pen.ius.edu.ba

Usage of Fly Ash and Waste Slime Boron for Soil Stabilization

İsmail ZORLUER
Afyon Kocatepe University, Faculty of Engineering, Department of Civil Engineering, Afyonkarahisar, Turkey.

Süleyman GÜCEK
Afyon Kocatepe University, Dazkırı Vocational High School, Dazkırı, Afyonkarahisar, Turkey.

Abstract
Waste materials are hazardous and serious problem for environment. Because, they occur soil pollution, ground water pollution and also visual pollution. Especially, industrial wastes are composed in large quantities. Many scientists have made research to solve these problems. According to their results, they have suggested that usage of waste materials in many areas as a material or additive material. One of the areas is soil stabilization. Soil properties are improved with this additive wastes. In this study, laboratory tests were conducted on granular soil specimens amended with fly ash and slime waste boron. The specimens were prepared with granular soil and fly ash-waste boron at different ratios. They were compacted standard Proctor compaction energy and, than were cured 1, 7 and 28 days. After cure unconfined compressive tests were conducted to investigate the effect of fly ash-waste boron on granular soil strength. Addition of fly ash-waste boron increased soil strength. As a result, fly ash-waste boron can be used with granular soil for increasing strength. This is economical solution.

Keywords: Fly ash, Waste slime boron, Soil stabilization

1. Introduction

Waste materials are serious environmental problem because they have harmed to soil, ground water and also have formed visual pollution. Rapidly developing technology has increased production and consumption. This situation has increased energy needs too at the same way. The increasing of production and consumption results in the increase of amount of waste. Especially industrial wastes are formed serious problem due to very large quantities. In the developing countries, distinct rules of waste disposing are initiated to prevent the environment pollution. Also, many scientists research about usability of wastes in many areas. This case is positive effects on environment by means of recycling, regains to economy and reducing environmental pollution. Wastes materials were began to be used in soil stabilization like usage in many areas. Because these waste materials increases some parameters of soil like strength and decreases some parameters like settlement, permeability.

Borax is a highly soluble material and increases viscosity, toughness and strength in many materials and reduces the radiation, sound, thermal permeability. For this reason, boron products are used in many areas such as glass, drug, paint, airplane, ceramic industry, agriculture, metallurgy, nuclear applications, glaze and enameled coatings, steel and space industries, automotive industry, rocket fuel, capsule, radiation preventive sheaths, fire extinguishers, radio tube[1].

Turkey is a rich country with regards of boron reserve and has met 40-50% of World consumption. Total of annual raw material production is approximately 1.3 million tons in Turkey. With this production, a serious solid/liquid waste problem was revealed. Solid wastes are discarded in the open area, and liquid wastes are collected in dams [1].

Fly ash is the main by-products of coal combustion for electrical energy production. Fly ash is one of the waste materials that are generated by the coal industry in very large quantities. However, a small part (25% – 30%) of the fly ash can be used in many areas. Its utilization is not limited and it is added to cement and concrete products, construction materials as a light weight aggregate, infiltration barrier, underground, void filling, water and environmental improvement, and is used in geotechnical stabilization as an additive material, structural fill, cover material, unpaved roads,highway base structures, roadway and pavement etc. There are a lot of studies about fly ash used in the stabilization of soils. In the previous studies [2, 3, 4, 5, 6, 7] it was indicated that the engineering properties of fly ash amended soils have been improved. Generally, fly ash was used together with different additive materials like

DOI: 10.21533/pen.v5i1.74

cement, lime or industrial wastes like marble dust, cement kiln dust, etc.

On the other hand, boron compounds in this waste discharged to land dissolved by rain water, and pass to soil where they form some complexes with heavy metals such as Pb, Cu, Co, Ni, Cd, etc., so that the potential toxicity of these metals increases, and cause some serious health and environmental problems when the complexes pass to groundwater. Hence, there is a necessity of making use of this waste in large amount to avoid the environmental problems [1]. Fly ash is an important material for various applications. The utilization of fly ash in construction, removal of organic compounds, heavy metals, dyes, and zeolite synthesis can help a great deal in the reduction of environmental pollution. The unburned carbon in fly ash plays an important role for adsorption [8]. When fly ash is used together with waste materials, it is expected to reduce harmful effects of these waste materials.

In this study, laboratory tests will be conducted on granular soil specimens amended with fly ash and slime waste boron. The specimens will be prepared with granular soil and fly ash-waste slime boron at different ratios. They will be compacted standard Proctor compaction energy and, than will be cured 1, 7 and 28 days. After curing, unconfined compressive tests will be conducted to investigate the effect of fly ash-waste boron on granular soil strength.

2. Material and Method

The granular soil (SG) used in this study was obtained from Afyonkarahisar Municipality, Turkey. This material was used in road construction. It had 23 % particles passing the US No. 10 sieve (<2 mm), 5% passing US No. 200 sieve (<0.075 mm). Unit weight is 18.9 kN/m^3. It was classified as well graded gravel (GW) according to the Unified Soil Classification System (USCS) and A-1 according to the American Association of State Highway and Transportation Officials (AASHTO).

A-1 class material is a good subbase material in the ASSHTO standards. Some chemical compounds of the granular soil are shown in Table 1. The waste slime boron used in this study was obtained from Etibor Kırka Borax Company in Eskişehir, Turkey. Waste boron was dried and sieved from sieve #40, resulting in waste boron grains that are smaller than 425 μm. Some chemical compounds of the waste slime boron are shown in Table 1. The fly ash was obtained from Soma-B Power Plant in Manisa, Turkey. It is F class according to ASTM C 618 [9] and W class according to TS EN 197-1 standard [10]. Approximately, 80 % of the particles are finer than the U.S. No. 200 sieve size. Some chemical compounds of the waste fly ash are shown in Table 1.

Table 1. Chemical compounds of used materials (%).

	Waste boron	Fly ash	SG
SiO_2	21.64	48.28	0.24
Fe_2O_3	0.19	7.19	0.06
Al_2O_3	0.75	27.72	0.16
CaO	-	10.51	36.05
MgO	9.40	2.51	16.99
SO_3	-	3.16	-
P_2O_5	-	0.27	-
Ti_2O_2	16.77	1.28	0.01
Na_2O	7.88	-	-
B_2O_2	7.75	-	-
LOI	35.38	-	46.40

LOI: Loss of Ignition

Identification tests were performed according to TS 1900-1[11] standard. The distribution of the particle sizes was determined by sieving. For the sieve analysis, the granular soil was washed above the 0.075-mm sieve and dried in the drying oven. Then, it was sieved by a sieve set. For the standard and modified compaction tests, water was added to the dried granular soil material and mixed. The wet specimen was compacted in the compaction mold (diameter: 105 mm height: 115.5 mm). For the standard Proctor test, the compaction process was performed in three layers of approximately equal mass, each layer being given 25 blows from 2.5 kg rammer dropped from a height of 305 mm above the specimen. The maximum dry density and optimum water content were determined from the relationships between the dry density and the water content of these processes for every test separately. For the sample preparation, the granular soil was mixed with waste slime boron and fly ash at three different ratios and the dry weights of the materials were used for the mixtures. The percentage of additives was obtained from literature [5, 6, 8]. All of the specimens were compacted with standard Proctor compaction energies and optimum water contents. The compositions of the mixtures and the compaction characteristics are given in Table 2.

Table 2. Mixing Ratio and Compaction Characteristics of Specimens

	Mixing ratio	ρ_{dmax} (kN/m^2)	w_{opt} (%)
SG		2,19	7,5
5BR-10FA	SG+5% Boron + 10% Fly ash	2,09	8,1
10BR-20FA	SG+10% Boron + 20% Fly ash	2,00	9,9
15BR-30FA	SG+15% Boron + 30% Fly ash	1,92	10,1

pH and Electrical Conductivity (EC) values of specimens were measured. For this test, dried specimens were sieved with No:10$^{\#}$ sieve (2 mm). 10 g were weighed, then 50 mL distilled water were added and were mixed with specimens. After 1 hour,

measurements were performed. pH and Electrical Conductivity (EC) values of specimens are given in Table 3. After 24 hours and 96 hours, to see effects of additives and changes, measurements were performed again.

Table 3. pH and Electrical Conductivity (EC) values of specimens

	pH			EC (µS/cm)		
	1 h	**24 h**	**96 h**	**1h**	**24 h**	**96h**
SG	8,50	8,65	8,60	870	810	770
5BR-10FA	11,99	12,12	12,32	2443	2132	2142
10BR-20FA	12,16	12,14	12,39	2523	2154	2172
15BR-30FA	12,35	12,20	12,31	2616	2167	2136

2.1. Unconfined compressive strength test

The unconfined compressive strength (q_u) is a measure of the strength of the mixtures. It shows the effects of the additive materials to granular soil strength. The unconfined compressive strength test followed the procedures outlined in the TS 1900-2 standard [12]. A strain rate of 1 % / min was maintained during this test. The specimens that were mixed with the granular soil, waste slime boron and fly ash, were compacted in a standard Proctor mold. After compaction, the specimens were extruded with a hydraulic jack from the compaction mold. Two specimens were prepared from this mold separately for a mixture ratio. The specimens were sealed in a plastic wrap three times and covered with a wet cloth for controlling humidity. The cloth was wetted every day, and then, the specimens were cured 1, 7, and 28 days. Duplicated specimens were tested for the unconfined compressive test as quality control, and the averages of these two tests were reported as the results.

3. Results and discussion

The effects of the additive materials on the optimum water content and the maximum dry density are given in Table 2. The results show that the addition of additives causes an increase in the optimum water content and a decrease in max. dry density. The reason for the increase in the optimum water content is an increase in the particle surface area of samples due to the addition of finer materials. Similar trends have been obtained from some experimental works [3, 4, 5, 6, 7].

pH and EC test results indicate that additive materials increased values of pH and EC. This can be seen in Table 3. The pH increased from about 8,5 to about 12,0. EC values increased from 870 µS/cm to between 2443 µS/cm and 2616 µS/cm, depending on increase of additive. But, pH did not change much with increase additive material after from first additive. When time dependent effect of additive was observed, pH did not change much, EC decreased. At the end of 24 hours and 96 hours, EC values decreased to approximately 2130 - 2170 µS/cm. Furthermore, 15BR-30FA mixture was more effective than 5BR-10FA and 10BR-20FA for EC. Because EC value decreased from 2616 µS/cm (24 hours) to 2136 µS/cm at the end of 96 hours.

Unconfined compressive test results can be seen in figure 1, 2 and table 4. The strength increased in all specimens with the increase in additive amount. The highest strength values were obtained as 1438 kPa in 15BR-30FA mixture ratio. Similar situations were seen in the cure time increase. The strength values increase in the cure time in all the specimens. The increases were shown linear trend, but the strength of specimens with 15BR-30FA increased too much at the end of 28 day cure. Actually, in 1-day cure and 7-day cure, strength values of specimen with 15BR-30FA are less than strength values of specimen with 10BR-20FA. According to1-day cure and 7-day cure, optimum mixing ratio is 10BR-20FA because of higher strength values. Despite of the highest strength in the specimen with15BR-30FA after 28-day cure.

Table 4. Unconfined compression test results (kN/m^2)

	1 Day	**7 Day**	**28 Day**
SG	144,5	307,8	410,6
5BR-10FA	356,6	481,0	607,1
10BR-20FA	497,2	672,0	748,0
15BR-30FA	434,6	593,5	1438,0

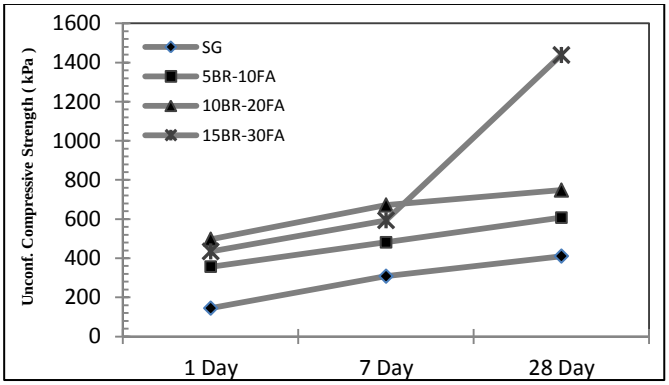

Figure 1. Unconfined compressive strength – cure time

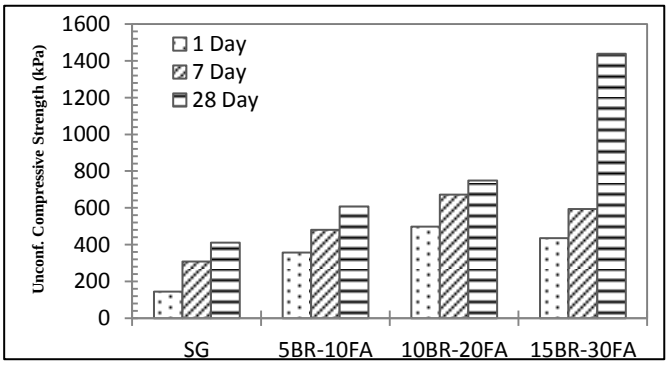

Figure 2. Unconfined compressive strength – additive ratio

Mostly these increases can be caused by fly ash, because there are a lot studies about fly ash in soil stabilization. And it is not also well known effect of boron to soil stabilization. But strength results are shown that boron is useable in soil stabilization. Boron waste should be used to reduce wastes in many areas.

Otherwise, heavy metals in the boron wastes are serious problem for ground water and soils [1]. When waste boron and fly ash are used together, fly ash can help to decrease this problem by absorption properties. The unburned carbon in fly ash plays an important role for adsorption [8]. Heavy metals are absorbed by fly ash, soil and ground water are protected from contaminant. However, it should be made chemical analyses to measure absorption capacity of fly ash.

4. Conclusions

Recycling of industrial waste is beneficial environmentally and economically. In economic terms, it is cheap, and in environmental terms, it decreases pollution. In this study, it is investigated the beneficial reuse of waste boron and fly ash in soil stabilization. Tests were performed on granular soil mixtures amended with waste boron and fly ash. pH and EC values measured in all mixtures. For unconfined compression tests, specimens were prepared with standard Proctor compaction energy and, than were cured 1, 7 and 28 days. Then, unconfined compressive strength tests were performed after cure time in these specimens. Waste boron and fly ash can be used as an additive material in soil stabilization. 10BR-20FA can be explained as a suitable mixing ratio. It should be made other chemical analyses on waste boron-fly ash mixtures and the impact of these wastes on soil and ground water should be investigated.

Acknowledgements

This study was supported from Commission of Scientific Research Projects (AKÜ-BAP) with the project, 16.KARIYER.47.

References

[1] Koyuncu H. Güney Y. Stabilization of borax wastes. First International Conference on Environmental Research and Assessment. Bucharest, Romania, March 23-27, 2003

[2] Arora S, Aydilek AH. Class F Fly-Ash-Amended Soils as Highway Base Materials Journal of Materials in Civil Engineering. 2005, 17, 640 – 649.

[3] Cetin B, Aydilek AH, Guney Y. Stabilization of recycled base materials with high carbon fly ash. Resources, Conservation and Recycling, 2010. 54,878 – 54,892.

[4] Vishwanathan R. Saylak D. Estakhri E. Stabilization of subgrade soils using fly ash. Ash Utilization Symposium. CAER. Kentucky. 1997. 204 211.

[5] Fauzi A, Nazmi WM, Fauzi UJ. Engineering Quality Improvement of Kuantan Clay Subgrade using Recycling and Reused Materials as Stabilizer. In The 3rd International Conference on Geotechnical Engineering for Disaster Mitigation and Rehabilitation (GEDMAR 2011). Semerang, Indonesia. 2011. 500–506.

[6] Zorluer I. Demirbas A. Use of marble dust and fly ash in stabilization of base material. Science and Engineering of Composite Materials. 2013. 20(1). 47–55

[7] Zorluer I. Gucek S. The effects of marble dust and fly ash on clay soil. Science and Engineering of Composite Materials. 2014. 21(1). 59–67.

[8] Ahmaruzzaman M. A review on the utilization of fly ash Progress in Energy and Combustion Science. 36. 2010. 327–363.

[9] ASTM C 618. Standard specification for coal fly ash and raw or calcined natural pozzolan for use in concrete. Annual Book of ASTM Standards. 2003.

[10] TS EN 197-1. (Turkish Standard) Cement – Part 1: Generally cements-compounds, properties and convenient criteria. 2002.

[11] TS 1900-1 (Turkish Standard). Methods of testing soils for civil engineering purposes in the laboratory – Part 1: Determination of physical properties. 2006.

[12] TS 1900-2. (Turkish Standard). Methods of testing soils for civil engineering purposes in the laboratory – Part 2: Determination of mechanical properties. 2006.

ISSN 2303-4521
PERIODICALS OF ENGINEERING AND NATURAL SCIENCES
Vol. 5 No. 1 (2017) – Special Issue (Recent Topics in Environmental Science)
Available online at: http://pen.ius.edu.ba

Assessment of the energy generation potential of photovoltaic systems in Caribbean region of Colombia

Manuel Fernando ARIZA TABA
Solar Energy Institute. Ege University.
Izmir, Turkey
mftaba@hotmail.com

Mavbuto MWANZA
Solar Energy Institute. Ege University.
Izmir, Turkey
mavbuto_mwanza@yahoo.com

Numan S. ÇETIN
Solar Energy Institute. Ege University,
Izmir, Turkey
ncetin@rocketmail.com

Koray ÜLGEN
Solar Energy Institute. Ege University,
Izmir, Turkey
Koray.ulgen@ege.edu.tr

Abstract
At present the use of solar energy for power generation has increased in recent years, this is due not only to climate change but also to reduce costs of solar technology materials and equipment. The paper assesses the energy generation potential of photovoltaic systems in the Caribbean region of Colombia based on data extracted from NASA Surface Meteorology and Solar Energy. The solar energy atlas for Caribbean region was generated using ArcGIS program. The analyzed results indicates that in the Caribbean region of Colombia there is a huge energy generation potential of photovoltaic systems with annual electricity generation of 1554.47kWh/kW$_p$ and performance ratio of 79.63% which is good for PV systems. This study is important as generated results are vital for the development of PV systems in the region and also the results can be used in the future social, economic and environmental impact study for deployment of these systems; and selecting the suitable area and appropriate technology that can adapt to the conditions of this region.

Keywords: Photovoltaic systems, Performance ratio, centralized grid connected (CGC), Capacity factor, Final yield.

1. Introduction

Today the awareness of the availability of solar energy is necessary for optimal utilization of the resources. Since this energy can be converted into useful energy through use of solar technologies. The case of photovoltaic or thermal systems the purpose is the generation of electricity. The photovoltaic technology has increased considerably year by year. In 2015 the capacity installed was at least 48,1 GW, as compared to 40 GW in 2014 [3]. The total photovoltaic capacity installed at the end of 2015 globally amounted to 227,1 GW [3]. The 24 International European Agency (IEA) photovoltaic power systems (PVPS) countries represented 197 GW of cumulative PV installations, the majority of these are grid connected. On the other hand, the non IEA PVPS countries represented 30 GW. However, countries with less than GW installed PV system were not included in the global installed capacity. Furthermore, some countries with more than a GW but whose total is difficult to quantify with accuracy were also excluded [3].

Colombia being close to the line of equator, it has regional geographic differences, which defines a number of factors that are specific to the characteristics of incidence of solar radiation. These vary depending on the area or geographical location (mountain or flat). The other factors include; distance from the sea, the average rainfall and conditions of the ground, which leads to a difference for radiation in each region of Colombia.

In the Caribbean region radiation and sunshine have a direct relationship with the values of precipitation (IDEAM) [1]; the lower radiation coincides with the period with more rain and less rain period with higher radiation. At the time when there is less rainfall, solar radiation level is high and represents an average temperature between 38 ° C and 40 ° C.

In the year 2015, The Institute of Hydrology, Meteorology and Environment Studies (IDEAM) for Colombia published the third map of solar radiation; this represents an aggregate of maps showing the spatial distribution of solar energy potential in Colombia. These maps show the average global solar radiation per day, average daily sunshine hours and solar ultraviolet radiation on flat surface.

However, despite of the Caribbean region having the highest annual solar radiation in range of 4-5 kWh/m^2-day as shown in figure 1 with La Guajira having the greatest solar potential compared with the other regions. However, solar energy for electricity

DOI: 10.21533/pen.v5i1.76

generation has not been exploited due to among the reasons few studies on the potential of photovoltaic systems for energy generation. Therefore, the aim of this paper is to study and assess the potential of the photovoltaic systems for energy generation in Caribbean region. Based on this information, it will be possible to quantify the solar energy potential for electricity generation for the Caribbean region. Furthermore, in the case of remote areas, for the national transport networks and energy distribution, this information is significant since it can be used in various projects. In addition, this information can be further be used in various requirement like communication, water pump systems, lighting, signing, heating, air conditioner and use in agriculture. At the same time, the information can also help to identify strategic regions, which are more appropriate for solar energy utilization and development to provide solutions necessary for the population.

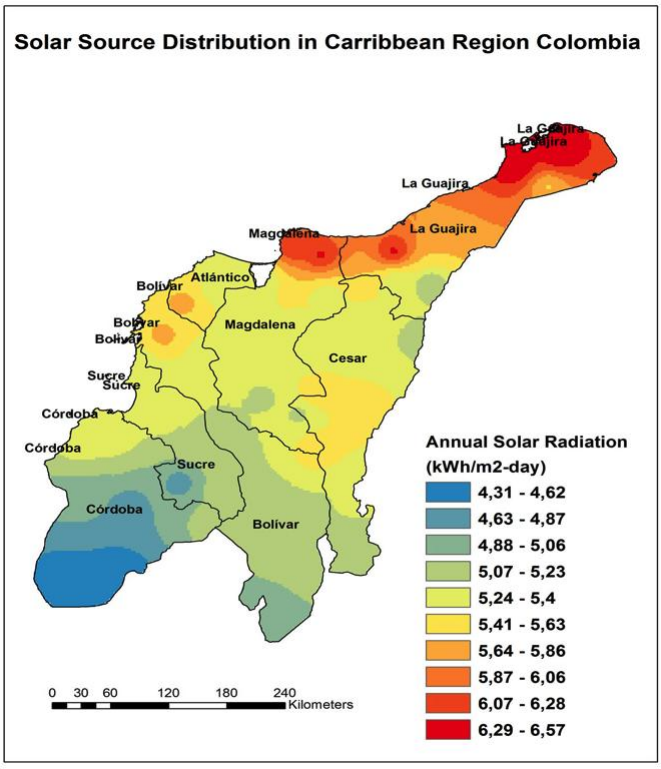

Figure 1. Solar source distribution in Caribbean region in Colombia

1.1. The status of electricity generation in Colombia

The main sources of electricity generation in Colombia are hydropower systems, gas, coal, fossil fuels, wind systems and biomass systems. In Colombia the capacity of energy generation by technologies are Hydropower 70.41%, Gas 10.86%, Coal 7.56%, liquids 8.81%, gas-liquids 1.78%, wind power 0.12% and biomass 0.74%. As shown in figure 2 and Table 1 [2].

Table 1. Technology Capacity of Colombia

Technology Capacity		
Technology	**Power (MW)**	**Participation (%)**
Hydropower	10.919,8	70,41
Thermal Gas	1.684,4	10,86
Thermal Coal	1.172,0	7,56
Liquids	1.366,0	8,81
Gas-Liquids	276,0	1,78
Wind	18,4	0,12
Biomass	72,3	0,47
Total	**15.508,8**	**100**

However, in month of January of 2015 the national interconnected system showed a decrease of the installed capacity due to the withdrawal of 46MW (Jet A1) from the system [2].

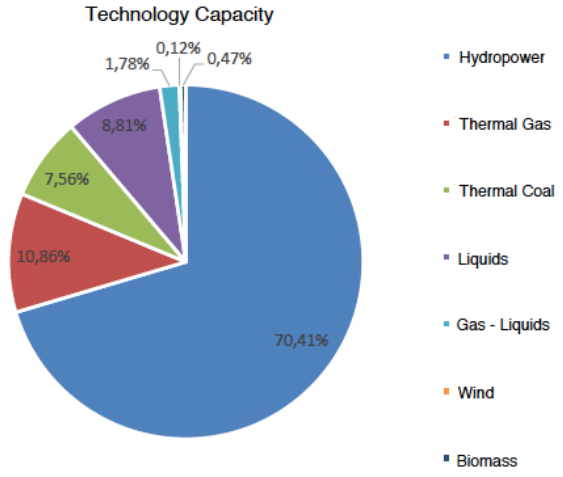

Figure 2. Energy technology Capacity in Colombia [2]

Table 2 shows the installed electric power capacity clustered by regions in terms of the technologies. Table 2 shows that the departments of Atlántico, Bolivar, Córdoba and La Guajira are the highest focal point of power production in the region [2].

Table 2. Technology capacity installed in the Caribbean region by resource type in MW [2]

	ACPM	WATER	BIOMASS	COAL	FUEL OIL	GAS	WIND	TOTAL
CARÍBBEAN	**462,0**	**338,0**		**296,0**	**297,0**	**1.331,0**	**18,4**	**2.742,4**
ATLÁNTİCO	153,0				110,0	1.241,0		1.504,0
BOLÍVAR	309,0				187,0	90,0		586,0
CÓRDOBA		338,0						338,0
GUAJIRA				296,0			18,4	314,4
CESAR								0,0
MAGDALENA								0,0
SUCRE								0,0

2. Material and methods

In Colombia the energy generation by PV systems are only used for household energy consumption (i.e. small household systems-SHS) and off-grid systems (mini grid) in remote areas where grid connection is not possible. Non-connected zones account for 52% of the country's area and diesel generators are commonly used to produce energy [4]. The use of diesel generators contribute to greenhouse gas emission and pollution of the environment[4].

In order to assess the energy generation potential of PV systems in Caribbean region of Colombia the following indicators has been used based on previous studies undertaken in other parts of the world [5-15]; performance ratio, capacity factor, final yield, suitable area, Theoretical, Geographical and technical energy potential. The data used in the study has been obtained from NASA Surface Meteorology and Solar Energy.

2.1 Estimation of PV Electricity Generation Potential

2.1.1 Energy Potential

Theoretical solar energy potential is defined by the radiation energy that reaches a specified area (e.g. 1 Km^2) within a defined time period (e.g. 1 year). [5]. The theoretical solar energy potential has been determined using the expression (1) [5]:

$$AEA_{th} = \mathrm{I} \times \mathrm{A} \times 365 \quad (1)$$

Where AEA_{th} is the available theoretical potential of annual solar energy (MJ/m^2-year), I is the global average solar radiation per day (MJ/m^2-day), A is the land area available (m^2) and 365 is the number of days in a year.

There are two types of grid connected PV system applications:

1) Centralized grid connected (CGC) PV system; perform the functions of centralized stations and generally are systems mounted on the ground and larger than 1MW [6].
2) Decentralized grid connected (DCGC) PV system; normally installed at roof-tops on the buildings or houses or close to houses but small in size [7, 8].

The geographical potential can be defined as the theoretical potential limited by suitable area for PV electricity energy generation and development. The geographical solar energy potential has been determined using the expression (2) [5]:

$$GP = I \times A_s \times 365 = AEA_{th} \times \left(\frac{A_s}{A}\right) \quad (2)$$

Where *GP* is the geographical potential of solar energy annual available (MJ/m^2-year), I is the global average solar radiation per day (MJ/m^2-day), A_s is the area considered accessible and suitable (m^2) for PV system development and 365 is the number of days in a year. The suitable area for land use are as shown in the table 3 [9,10]. The suitable area for CGC FV systems has been estimated as 66144km^2 which is 3,11% of the total surface area of Colombia.

Table 3. Total area and total suitable area for CGC PV

Department	Area (km^2)	Suitable Area (km^2)
LA GUAJIRA	20848	9446
CESAR	22905	12454
MAGDALENA	24188	9590
ATLÁNTICO	3388	1353
BOLÍVAR	25978	20303
SUCRE	10670	4001
CÓRDOBA	23980	9197
TOTAL	**132288**	**66144**[1]

The geographical and technical potential has been estimate by analyzing the available area, social factors and technical limitations.

Technical potential is defined as the part of the theoretical potential available by considering the fundamental restriction for the area utilization such as national parks, agriculture areas, forests, surface water bodies, and many other restricted or protected areas [5]. The technical potential of annual PV electricity generation has been determined using the expression (3)[5]:

$$EAP = \sum GP \times \eta_m \times PR \quad (3)$$

Where η_m is the module's conversion efficiency and PR is the PV system's performance ratio. The module's conversion efficiency depends on the type of solar cell and module temperature [5].

2.1.2 Performance ratio (PR)

The performance ratio, in some cases called "Quality factor" takes account total system losses such as inverter losses, cable losses, and thermal losses. It is appropriate to know the performance ratio from beginning up to end of the operation of the system, with the purpose of pinpoint causes of yield losses [11,12]. The performance ratio has been estimated using the expression (4), [11,12]:

$$PR = \frac{E_{AC}}{G_t \times \eta_{STC}} \quad (4)$$

The performance ratio can also be defined as the ratio between actual yield (i.e. annual production of electricity delivered at AC) and the target yield given by the expression (5), [13,14,15]:

$$PR = \frac{Y_f}{Y_r} = \frac{E_{real}}{E_{ideal}} = \eta_{deg}\eta_{tem}\eta_{soil}\eta_{inv} \quad (5)$$

[1] The data mentioned were approximate values but this does not ensure that the values correspond to actual data.

2.1.3 Capacity factor

The capacity factor can be defined as the ratio between average annual energy output and rated power of the considered module. For PV systems, the capacity factor is given by the expression (6) [16]:

$$CF = \frac{E_{AC}}{P_{PV,rated} \times 8760} \quad (6)$$

2.1.4 Cell temperature

The cell temperature can be defined as incoming irradiance and the others parameters, T_a the maximum ambient temperature, I is the in-plane irradiance and T_{NOCT} is the technology dependent nominal operating cell temperature, $T_{a,NOCT}$ is the ambient reference temperature (20°C) and I_{NOCT} the cell temperature at irradiance and the value is 1000 W/m^2 [17,18].

$$T_c = T_a + \frac{I}{I_{NOCT}} (T_{NOCT} - T_{a,NOCT}) \quad (7)$$

2.1.5 Module efficiency

The module efficiency can be estimated as the reference of PV panel efficiency $\eta_{PV,ref}$, the reference temperature T_{ref},(25°C), temperature coefficient of maximum power of the solar cells β and T_c cell/module temperature [19].

$$\eta_c = \eta_{PV,ref} (1 - \beta(T_C - T_{ref}) \quad (8)$$

3. Results and Discussion

In the study the potential of PV systems for energy generation in Caribbean region of Colombia has been carried out using analytical approach. The input technical data used for the assessment are summarized in table 4.

Table 4. Efficiency of the components

Components	Efficiency
PV efficiency ($\boldsymbol{\eta_{PV}}$)	13,8%
Inverter efficiency ($\boldsymbol{\eta_{CPU}}$)	95%
Others efficiencies[2] ($\boldsymbol{\eta_o}$)	90%
Cables ($\boldsymbol{\eta_{DC/AC}}$)	93%

Monitoring the solar radiation, temperature, and sunshine hours of the study area is very important, since these parameters have influence on the energy generation potential of the PV systems. The average monthly radiation on a horizontal plane to the Caribbean region is shown in Figure 4. The Caribbean region of Colombia has a substantial amount of solar radiation, with the annual average of daily solar radiation of 5.35kWh/m^2-day. The region has the maximum monthly average solar radiation in the month of March at 5.81kWh/m^2-day and the lowest in the month of November at 4.83kW/m^2-day. In short the monthly average solar radiation in Caribbean region varies between 4.83kWh/m^2-day and 5.81kWh/m^2-day. The region receives the total annual solar radiation of 1952.75kWh/m-year with total yearly peak sunshine hours of about 2190 hours, which is suitable for energy generation using PV systems. Thus, with these higher solar radiations being received in the region, makes it more suitable place for power generation from solar energy source. Furthermore, the average annual peak sunshine hour in the Caribbean region of Colombia is 6 hours per day and the maximum average air temperature is 34°C. [20].

The analyzed results show that, the efficiency of the multi-crystalline silicon module at maximum average air temperature is 11,96%, which correspond to a drop in the module efficiency by 1.84%. In other words, the performance of the PV system in this region is expected to drop due to high temperature. This drop in the module efficiency is as the result of higher temperatures. This drop in the module efficiency translates to loss of approximately 2000TWh of energy per year in the PV system.

The Caribbean region has a total surface area of approximately 132,288km^2 and receives annual average of daily solar radiation of 5.35kWh/m^2-day. Thus, considering the surface area and the average annual solar radiation and using equation 1, the theoretically solar energy potential for Caribbean region is found to be 258,3325TWh/year. Thus, the region receives about 258,332TWh/year of solar energy. Taking into consideration the restricted areas and land areas not suitable for PV system installation. The region have a total of about 66,144km^2 suitable area for PV systems installation. Using equation 2, the geographical solar energy potential for the region has been estimated at approximately 129,160TWh/year.

The multi-crystalline silicon with the following specification; nominal output power Pmax of 200Wp, voltage at Pmax of 26.4V, Current at Pmax of 7.6A, module efficiency of 13.8% and surface area of 1.45m2 was used to evaluate the technical solar energy potential of the Caribbean region. The capacity factor for a multi-crystalline silicon module under the Caribbean region weather condition is found to be 17.75% and due to temperature effect, the efficiency of the module is found to reduce to 11.96%. Furthermore, the multi-crystalline silicon module is found to have 79.63% performance ratio and the 1554.47kWh/kWp yearly final yield. The total amount of solar energy technical potential for Caribbean region is about 12,301TWh/year.

[2] This refers to the temperatures and other losses generated on the photovoltaic panel

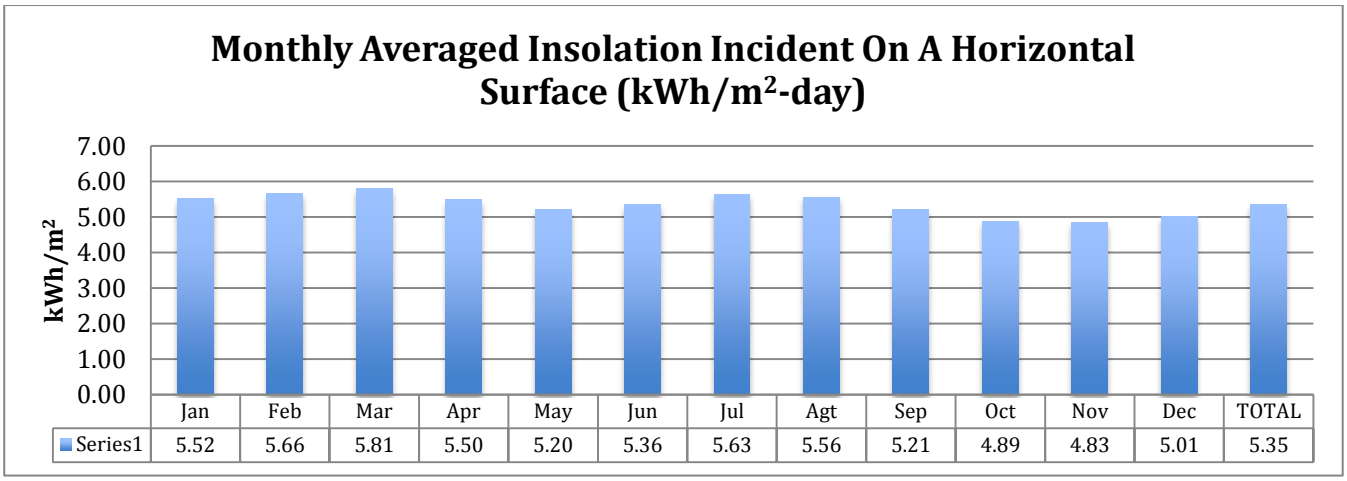

Figure 4. Monthly averaged insolation incident on a horizontal surface [21].

Table 5 below summarizes the results of the study corresponding to solar energy potential in terms of theoretical, geographical and technical potential, and performance indices for the PV system that is performance ratio, capacity factor and the efficiency of the module.

Table 5. Theoretical, geographical and technical potential of CGC PV solar.

	Theoretical potential (TWh/yr)	Module efficiency (%)	Geographical potential (TWh/yr)	Performance ratio (PR) (%)	Capacity factor (%)	Final yield (kWh/kW$_P$)	Technical potential (TWh/yr)
CGC PV	258,300	11.96	129,16 0	79.63	17,75	1554.47	12,300.87

4. Conclusion

The paper has presented the energy generation potential of PV systems in Caribbean region. The region has considerable energy potential and would contribute to power generation that can be used to replace the fossil fuel power plants. As it can be noticed from table 2, more than 50% of energy generation in the region is from the fossil power plants. The use of solar energy technologies would reduce the environmental, social and cultural impacts that result from the use of fossil fuel for energy generation.

In this paper, the energy output, capacity factor and performance ratio of the photovoltaic systems in the Caribbean region in Colombia has been evaluated using monthly average daily global solar irradiation data available at NASA Surface Meteorology and Solar Energy. Multi-crystalline silicon photovoltaic module had been considered in this study to estimate the solar energy generation potential for Caribbean region. The analyzed results of the study indicates that the multi-crystalline silicon module have performance ratio of 79.63% and capacity factor of 17.75% under weather condition of Caribbean region. Therefore, the study concludes that 1554.47kWh electricity can be generated annually from a 1kW$_P$ CGC PV system in Caribbean region of Colombia at a performance ratio of 79.63%. Thus, with ever increasing fossil fuel price, air pollution due to use of fossil fuels and droughts affecting the hydropower system in Colombia, Solar energy generation of PV systems offers the best alternative solution for the Caribbean region and Colombia.

References

[1] The institute of hydrology, meteorology and environment studies [IDEAM]. (2015). Forecasts and Alerts. Available: <http://www.ideam.gov.co/ >. Accessed: April 2016.

[2] Mining and Power Planning Unit [UPME]. (2015). İnforme mensual de variables de generación y del Mercado Eléctrico Colombiano. Available: <http://www.upme.gov.co/ >. Accessed: March 2016.

[3] IEA-PVS Reporting Countries, Becquerel Institute (BE), RTS Corporation (JP) SolarPower Europe (EU).(2016). Snapshot of Global Photovoltaic Markets - IEA PVPS. Available: <http://www.iea-pvps.org/index.php?id=trends0>. Accessed: May 2016.

[4] Procolombia. (2015). Electric power in Colombia - Investment opportunities - Power Generation. Available: <http://www.procolombia.co>. Accessed: March 2016.

[5] Nicolai Herrmann. Regional energy 2050 : a sustainability-oriented strategic backcasting methodology for local utilities / Nicolai Herrmann. Mering, Germany: München ; Mering : Hampp, 2011.

[6] Ottmar Edenhofer, Ramón Pichs Madruga, Youba Sokoba. Renewable Energy Soruces and Climate Change Mitigation Special Report of the Intergovernmental Panel on Climate Change. 2012, pp 354. Available

<http://www.cambridge.org/9781107607101>. Accessed: May 2016.

[7] Ram Joshi, Maharshi Pathak, Decentralized Grid-connected Power Generation Potential in India: From Perspective of Energy Efficiency Buildings. (2013). Availabe: <http://www.sciencedirect.com>. Accessed: March 2016.

[8] Hanumath Prasad Ikkurti, Suman Saha. A comprehensive techno-economic review of microinverters for Building Integrated Photovoltaics (BIPV). CSIR-Network Institute for Solar Energy, Drives & Control System Technology Group, CSIR-Central Mechanical Engineering Research Institute, Mahatma Gandhi Avenue, Durgapur 713209, India. Available: <http://www.sciencedirect.com/science/article/pii/S1364032115002348>.

[9] National Geographic Portal, (2016). Colombia. Geographic Institute Agustín Codazzi [IGAC]. Available: <http://www.igac.gov.co/igac>.

[10] DaftLogic. Google Maps Area Calculator Tool. Available: < https://www.daftlogic.com/projects-google-maps-area-calculator-tool.htm>.

[11] Eicker U. Solar technologies for buildings. John Wiley and Sons; 2003.

[12] Nakagami H, Ishihar O, Sakai K, Tanaka A. Performance of residential PV system under actual field conditions in western part of Japan. In: International solar energy conference, solar engineering, American Society of Mechanical Engineers; 2003. p. 491–498.

[13] Kymakis E, Kalykakis S, Papazoglou TM. Performance analysis of a grid connected photovoltaic park on the island of Crete. Energy Convers Manage 2009;50(3):433.

[14] Photovoltaic power systems programme. Cost and performance trends in grid connected photovoltaic systems and case studies. IEA-PVPS T2-06; 2007

[15] The German solar energy society. Planning and installing photovoltaic systems: a guide for installers, architects and engineers. UK: James and James; 2006.

[16] Kymakis E, Kalykakis S, Papazoglou TM. Performance analysis of a grid connected photovoltaic park on the Island of Crete. Energy Convers Manage 2009;50(3):433–8.

[17] Markvart T (editor). Solar electricity. 2nd edition. Chichester: Wiley; 2000.

[18] Skoplaki E, Boudouvis AG, Palyvos JA. A simple correlation for the operating temperature of photovoltaic modules of arbitrary mounting. Sol Energ Mat Sol C 2008; 92: p. 1393-1402.

[19]Evans DL, Florschuetz LW. Cost studies on terrestrial photovoltaic power systems with sunlight concentration. Solar Energy 1977;19:255-62.

[20] The institute of hydrology, meteorology and environment studies [IDEAM]. (2015). Forecasts and Alerts.
Available:<http://atlas.ideam.gov.co/visorAtlasClimatologico.html>. Accessed: May 2016.

[21] NASA Surface Meteorology and Solar Energy. <https://eosweb.larc.nasa.gov/cgi-bin/sse/grid.cgi?email=skip@larc.nasa.gov>.

ISSN 2303-4521
PERIODICALS OF ENGINEERING AND NATURAL SCIENCES
Vol. 5 No. 1 (2017) – Special Issue (Recent Topics in Environmental Science)
Available online at: http://pen.ius.edu.ba

Adsorption of Copper Metal Ion from Aqueous Solution by Nanoscale Zero Valent Iron (nZVI) Supported on Activated Carbon

Kubra ALTUNTAS
Yildiz Technical University, Environmental Engineering Department, Istanbul, Turkey

Eyup DEBIK
Yildiz Technical University, Environmental Engineering Department, Istanbul, Turkey

Duyguhan Kozal
Yildiz Technical University, Environmental Engineering Department, Istanbul, Turkey

Ilkız Irem YORUK
Yildiz Technical University, Environmental Engineering Department, Istanbul, Turkey

Abstract
Copper is from one of the most important heavy metals, which adheres to the ecological system by harmful human activities. It is toxic, persistent, and non-biodegradable metal, which causes environmental pollution in both the atmosphere and aquatic environment. Copper pollution found in undesirable concentrations in industrial wastewaters especially from electronics industries, cooling systems and plating industry. Physical methods are mostly applied to remove Cu(II) including adsorption and membrane processes. Nanoparticles (e.g. nano zero valent iron (nZVI), carbon nanotubes, titanium dioxide nanoparticle) have been considered to be promising alternatives to conventional adsorbents. They have advantages by having more surface area and nano-sized pores, which helps to adsorb more molecules. In this study, in order to enhance adsorption by activated carbon and lower the cost of nanoparticle synthesis, nZVI is synthesized on activated carbon(AC-nZVI). It was investigated for its effectiveness in copper removal from aqueous solution. The effect of AC-nZVI dosage, pH and the initial concentration of Cu were investigated. Adsorption capacities are obtained for nZVI and AC-nZVI as 414 mg/g and 510 mg/g, respectively. 200mg/L AC-nZVI concentration was determined as sufficient for %96 removal rate. Langmuir isotherm gave the best fit and the maximum adsorption capacity according to Langmuir isotherm is calculated as 588,24 mg/g.

Keywords: Adsorption; Nano-Zero Valent Iron (nZVI); Activated Carbon; Copper Removal

1. Introduction

Nanotechnology became a popular topic in environmental engineering practices with increasing number of studies on soil remediation and also water and wastewater pollution applications. Conducted studies on nano zero valent iron, especially on heavy metal removal, demonstrated that it is effective by means of its high adsorption capacity [1-4].

Copper is a material used in the electronics industries, cooling systems by having the characteristic feature of high electrical and thermal conductivity. Also it is used as plating material due to its rustproof specification. Heavy metals enter to the ecological system by human activities and bioaccumulate through food chains and lead carcinogenic effects on human [4-6]. They have persistent and non-biodegradable characteristics, which cause environmental pollution in both atmospheric and aquatic environment [4-7]. Several techniques have been applied for heavy metal removal including adsorption by activated carbon, natural low-cost adsorbents and gamma alumina, ion-exchange system, membrane processes, electrochemical applications [5-6,8-12]. Many studies have demonstrated that nano zero valent iron (nZVI) can effectively be used to remove chrome and arsenic as heavy metals [13-16].

The purpose of this study is to enhance adsorption by supporting nano zero valent iron on activated carbon. For this aim, nZVI is synthesized on activated carbon and it is investigated for its effectiveness in copper removal. The effect of AC-nZVI dosage, reaction time and initial copper concentration is also investigated.

2. Materials and Method

2.1. Synthesis of AC-nZVI

In order to clean powdered activated carbon before synthesis of nZVI-coated activated carbon (AC-nZVI), powder activated carbon was kept in 5% nitric acid solution for 1 day. Then, it was washed with ultra-pure water and ethanol to remove acid and ethanol content was lost by keeping in oven over night. AC-nZVI was synthesized in 50% ratio with nZVI. For this, the predicted amount of nZVI is calculated with reaction occurred in borohydride method.

$$Fe^{2+} + 2BH^{4-} + 6H_2O \rightarrow 2Fe^0 + 2B(OH)_3 + 7H_2\uparrow$$

$FeSO_4.7H_2O$ solution was dissolved in water:ethanol (30:70, v:v) mixture. AC was added in the same

DOI: 10.21533/pen.v5i1.77

predicted amount of synthesized nZVI into this solution. To prevent aggregation PEG 2000 was also used. NaBH4 was added dropwise with the rate of 20 mL/min to iron sulfate solution to occur above reaction. The obtained mixture is containing nZVI coated activated carbon particles and it was washed with ethanol and pure water to inhibit sulfate and boron ions' negative effects. In order to demonstrate activated carbon effect, nZVI is synthesized by the same method.

2.2. Experimental Method

$CuSO_4$ (MERCK) was used to prepare the synthetic samples. The experiment sets were conducted with 100 mL of copper containing synthetic samples with different amount of AC-nZVI particles and shaked at 150 rpm and 20ºC constant temperature. Prepared samples were centrifuged at 6000 rpm for 5 minutes for separation of AC-nZVI particles. The initial and effluent copper analysis was executed in Perkin Elmer Atomic AdsorptionSpectrometer C-400.

2.3. Isoterm

Adsorption isotherms are the most common calculations to describe adsorption process. Isotherms give the relationship between pollutant concentration adsorbed on known amount of adsorbent and equilibrium solution concentration. The equations, commonly used to assess the experimental isotherm data, were developed by Freundlich and Langmuir.
The Freundlich isotherm is expressed as follows [17]:

$$q_e = K_f C_e^{1/n}$$

where,

q_e: unit mass substance adsorbed by unit mass adsorbent (mg/g),

K_f: Freundlich capacity factor (mg/g),

C_e: Effulent concentration,

1/n: Freundlich density parameter.

The Langmuir isotherm, in turn, is expressed as follows [17]:

$$q_e = \frac{q_{max} \cdot K_L \cdot C_e}{1 + K_L \cdot C_e}$$

where,

q_e: unit mass substance adsorbed by unit mass adsorbent (mg/g),

C_e: effluent pollutant concentration (mg/L),

q_{max}: maximum adsorption capacity (mg/g), and

K_L; empirical coefficients.

3. Results and Discussion

3.1. Effect of Initial Copper Concentration on Removal

In order to demonstrate the effect of copper concentration on removal rate, the research was established in 100 ml of sample volume with 10, 25, 50, 100 and 150 mg/L copper ion concentration and 400 mg/L concentration of AC-nZVI as adsorbent. After determined contact time, the samples were centrifuged at 6000 rpm for 5 minutes to remove particles from water. In Figure 1, removal rates and adsorption capacity is stated in terms of obtained data.

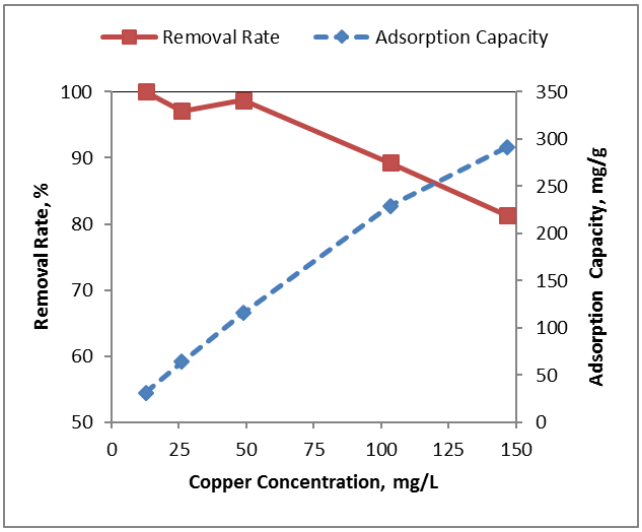

Figure 1. Effect of Initial Copper Concentration

It can be seen in Figure 1 that removal rate was decreased after 50 mg/L concentration of copper ion. The removal rate with 10, 25 and 50 mg/L initial concentration was obtained in higher rate of 98%. In addition to this removal rate was still higher than 80% in the highest selected copper concentration of 150 mg/L. Adsorption capacity was increased with the increment of initial copper concentration as expected. The slope of adsorption capacity plot was almost linear.

It can be concluded that the maximum adsorption capacity is not achieved with 150 mg/L copper ion concentration.

3.2. Effect of Contact Time and AC-nZVI Concentration on Removal

Experiments were conducted to determine the effect of contact time and AC-nZVI concentration on removal rate by using 2-120 minutes of contact time and 50-400 mg/L AC-nZVI concentration at 150 rpm at 20ºC. The concentration of copper was selected as 50 mg/L. Different samples was taken in 2, 5, 10, 20, 30, 60 and 120 minutes and centrifuged immediately at 6000 rpm for 5 minutes to remove AC-nZVI particles from water for copper analysis. Figure 2 and Figure 3 are demonstrating the effect of contact time and adsorbent concentration.

It is shown in Figure 2 that the large portion of removal was captured in the first 5 minutes and removal was almost stable for each experiment after 10 minutes of contact time. This can be due to reach of maximum

adsorption capacity. It is also observed that the removal efficiency increased with the increase of adsorbent concentration as expected. After 200 mg/L of adsorbent concentration the increase trend was reduced. The highest removal rate of 99.50% was achieved with 400 mg/L after 20 minutes of contact time. 200 mg/L AC-nZVI concentration can be selected as optimum concentration in according with low increase in higher adsorbent concentration.

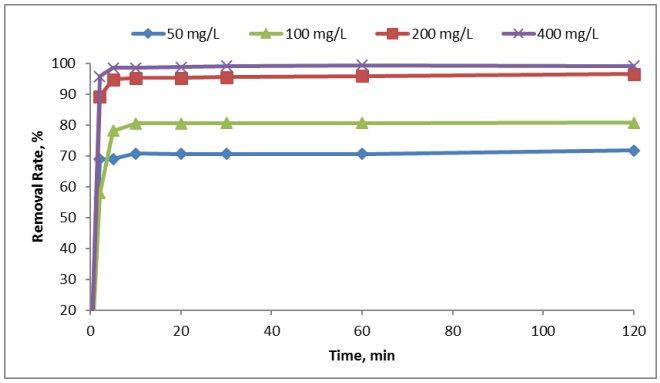

Figure 1. Effect of Contact Time and Adsorbent Concentration on Removal Rate

In Figure 3 the adsorption capacity variance according to adsorbent concentration is shown. As the adsorption capacity was 790 mg/g for 50 mg/L adsorbent concentration, it is decreased with adsorbent concentration as expected. Activated carbon was supported with nZVI in order to enhance removal rate.

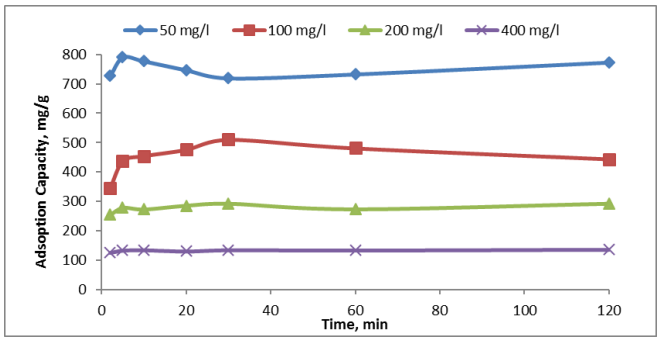

Figure 2. Change in Adsorption Capacity by Contact Time and Adsorbent Concentration

As the maximum adsorption capacity of activated carbon was changing between 6 – 39 mg/g for copper ion removal [18-19], the maximum adsorption capacity of AC-nZVI was obtained at 790 mg/g. In Figure 4, adsorption capacity in the effect of adsorbent concentration can be seen for nZVI and AC-nZVI. The experiments were conducted for 30 minutes at same adsorbent concentration and 50 mg/L copper ion concentration. While adsorption capacity of nZVI for 100 mg/L adsorbent concentration is 414 mg/g, it was 510 mg/g for AC-nZVI. Adsorption capacity is increase by supporting activated carbon with nZVI.

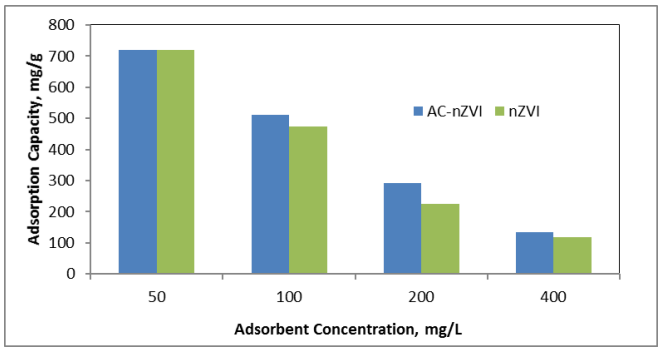

Figure 3. Difference of Adsorption Capacities of nZVI and AC-nZVI

3.3. Adsorption Isoterm

R^2 (Determination Coefficient) is a positive value between 0 and 1; and the closer the value 1 shows that the distribution is consistent. Isotherm plots belong to Freundlich and Langmuir Isotherm can be seen in Figure 5 and the calculated coefficient is given in Table 1. By considering determination coefficients of isotherm plots, Langmuir isotherm shows the most suitable isotherm. According to Langmuir isotherm, maximum adsorption capacity is calculated as 588,24 mg/g.

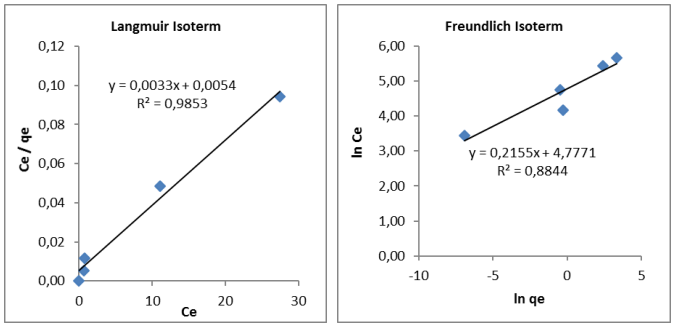

Figure 4. Langmuir and Freundlich Isotherm Plots

Table 1. Coefficient of Isotherms

Langmuir Isotherm		Freundlich Isotherm	
q_{max}	588,24	K_f	237,508
K_L	0,630	n	4,640
R^2	0,985	R^2	0,884

4. Conclusions

In this study, it is aimed to enhance nZVI adsorption capacity by supporting activated carbon in copper ion removal. Effect of initial copper concentration, contact time and adsorbent concentration was investigated and thereafter the adsorption capacity variance of activated carbon, nZVI and AC-nZVI was disclosed. Even the initial concentration of copper was as high as 150 mg/L, removal rate was obtained at 81% with 400 mg/L AC-nZVI concentration in 30 minutes of contact time. 50 mg/L of the selected lowest initial copper concentration was almost totally removed by AC-nZVI. The large portion of removal was achieved at 5 minutes

of contact time. The removal rate was increased with the concentration of AC-nZVI, however the difference on removal rate belong to 200 mg/L and 400mg/L AC-nZVI concentration was negligible. 200mg/L AC-nZVI concentration was determined to be sufficient for %96 removal rate. While the copper ion adsorption capacity of activated carbon was 6-39 mg/g according to literature, the adsorption capacities belong to nZVI and AC-nZVI is 414 mg/g and 510 mg/g, respectively. This shows the effect of nZVI supported on activated carbon to remove copper from the solution. Adsorption capacity of activated carbon is increased by supporting nZVI on activated carbon. This gives an advantage of lower adsorbent concentration and higher removal rate in the removal of copper metal ions. Langmuir isotherm give the best fit and the maximum adsorption capacity according to Langmuir isotherm is calculated as 588,24 mg/g.

References

[1] Kurniawana T. A., Sillanpääa M. E., Sillanpää M., "Nano–Adsorbents For Remediation of Aquatic Environment: Local and Practical Solutions For Global Water Pollution Problems" *Crit. Rev. Env. Sci. Technol.,* 42(2011) 1233-1295.

[2] Pradeep T., Anshup, "Nobel Metal Nanoparticles For Water Purification: A Critical Review" *Thin Solid Films*, 517 (2009) 6441-6478.

[3] Ulucan, K., Noberi, C., Coşkun, T., Üstündağ, C. B., Debik, E., & Kaya, C. "Disinfection By-Products Removal by Nanoparticles Sintered in Zeolite" *Journal of Clean Energy Technologies*, 2013; 1(2): 120-123.

[4] Lin L., Xu X., CharalambosPapelis, Tzahi Y. Cath, Pei Xu. "Sorption of metals and metalloids from reverse osmosis concentrate on drinking water treatment solids" *Sep. Purif. Technol.* 2014; 134:37–45

[5] Demiral H., Güngör C. "Adsorption of copper(II) from aqueous solutions on activated carbon prepared from grape bagasse" *J. Clean. Prod.* 2016. 124:103–113

[6] Kabuk H.A., Avsar Y., Ilhan F., Ulucan K. "Comparison of pH Adjustment and Electrocoagulation Processes on Treatability of Metal Plating Wastewater" *Separ. Sci. and Technol.* 2014. 49:613-618

[7] Kuzu S. L., Saral A., Demir S., Summak G., Demir G. "A detailed investigation of ambient aerosol composition and size distribution in an urban atmosphere" *Environ. Sci. Pollut. Res*. 2013. 20:2556–2568

[8] Papas B. N., Whitten J. L. "Adsorption of copper on a γ-alumina support" *Surface Science*. 2016; 651:22–27

[9] Eom, T.H.; Lee, C.H.; Kim, J.H.; Lee, C-H. "Development of an ion exchange system for plating wastewater treatment" *Desalin*. 2005. 180: 163–172.

[10] Elcik H., Celik S. O., Cakmakci M., Ozkaya B. "Performance of nanofiltration and reverseosmosis membranes for arsenic removal from drinking water" *Desalin. Water. Treat.* 2016; DOI: 10.1080/19443994.2015.1111812

[11] Varank, G., Demir, A., Bilgili, M., Top, S., Sekman, E., Yazıcı, S., Erkan, H. S. "Equilibrium and kinetic studies on the removal of heavy metal ions by natural low-cost adsorbents" *Environ. Prot. Eng.* 2014; 40(3): 43-61.

[12] Beyazit N. "Copper(II), Chromium(VI) and Nickel(II) Removal from Metal Plating Effluent by Electrocoagulation" *Int. J. Electrochem. Sci.* 2014; 9:4315 – 4330

[13] Zhu H.J.., Jia Y.F., Wu X., Wang H. "Removal of arsenic from water by supported nano zero-valent iron on activated carbon" *J. Hazard. Mater.* 2009, 172:1591-1596.

[14] Shi L.N., Zhang X., Zhen Z.L.. "Removal of Chromium (VI) from wastewater using bentonite-supported nanoscale zero-valent iron" *Water Res.* 2011, 45: 886-892.

[15] Geng B., Jin Z., Li T., Qi X. "Kinetics of hexavalent chromium removal from water by chitosan-Fe-0 nanoparticles" *Chemosphere*, 2009, 75: 825-830.

[16] Kakavandi, B, Kalantary RR, Farzadkia M., Mahvi A.H., Esrafili A., Azari A., Yari A.R., Javid A.B. "Enhanced chromium (VI) removal using activated carbon modified by zero valent iron and silver bimetallic nanoparticles" *J. Environ. Health Sci. Eng.* 12:115, 2014

[17] Fouladgar M., Beheshti M., Sabzyan H. "Single and binary adsorption of nickel and copper from aqueous solutions by γ-alumina nanoparticles: Equilibrium and kinetic modeling" *J. Mol. Liq.* 2015. 211:1060-1073

[18] Kobya M., Demirbas E., Senturk E. , Ince M. "Adsorption of heavy metal ions from aqueous solutions by activated carbon prepared from apricot stone" *Biosource Technol.* 2005. 36(13):1518-1521

[19] Imamoglu M., Tekir O. "Removal of copper (II) and lead (II) ions from aqueous solutions by adsorption on activated carbon from a new precursor hazelnut husks" *Desalin*. 2008; 228:1-3:108-113

ISSN 2303-4521

PERIODICALS OF ENGINEERING AND NATURAL SCIENCES
Vol. 5 No. 1 (2017) – Special Issue (Recent Topics in Environmental Science)
Available online at: http://pen.ius.edu.ba

A comparative study on Soil Properties and Applications Review with EERA and NERA in İstanbul-MARMARAY Project between Kazlıçeşme to Sirkeci

Günay Beyhan
Sakarya University, Engineering Faculty -Sakarya Turkey
gbeyhan@sakarya.edu.tr

Ayhan Keskinsezer
Sakarya University, Engineering Faculty-Sakarya Turkey

Sunay Beyhan
DumlupınarUniversity, Engineering Faculty-Kütahya Turkey

Abstract
Over the course of history Marmara region in North-western Turkey has been the site of numerous destructive earthquakes. Based on historical and instrumental earthquake records, the Marmara sea region is one of the most seismically active regions of the Eastern Mediterranean. The Marmara region is under the influence of the western part of the North Anatolian Fault Zone (NAFZ) and the N-S extensional regime of Western Turkey. Therefore, the earthquake risk analysis is very important for the MARMARAY Project. 76 km-long MARMARAY Project is an important project not only for Turkey but also for the world because it joins the two continents through railway. It will also serve for a comfortable and healthy way of environment, providing a contemporary solution for urban transportation.

Geotechnical and geological parameters of the region were obtained from analyses of seven boreholes. In this paper, using average wave velocities in layers, thickness, density and formation data based on the PS logs, 43 m and 65.5 m depths ranging from 7 different boring logs in a ground-wise different geological regions in İstanbul, ground response functions were obtained. Based on the soil profiles transferred to EERA (Equivalent - Linear Earthquake Site Response Analyses of Layered Soil Deposits) and NERA (Nonlinear Earthquake Site Response Analyses of Layered Soil Deposits) softwares, the rock soil record of August 17, 1999 Kocaeli earthquake in İstanbul – Beşiktaş Ministry of Public Works and Settlement (IBMPWS), response and design spectrums that may be considered crucial in case of an earthquake were obtained. The acceleration record was used as an input motion having PGA value of 0,04287 g (east-west component) which was applied on sublayers (i.e. sand, gravel, clay) using EERA and NERA programs. The analysis is done by keeping constant damping ratio of 5%.

Also nonlinear analysis was compared with the linear method of analysis. Stages involved in ground response analyses to develop site-specific response spectra at a soil site are summarized. Some of the known site response analysis methods are summarized and similarities and differences between linear and nonlinear methods.

Keywords: PS logging; MARMARAY; EERA; NERA; Earthquake Site Response Analysis; Seismic Excitation

1. Introduction

Because a major earthquake is expected in the off-shore south of İstanbul along the North Anatolian Fault Zone in the upcoming decades, the Bosporus and its vicinity with historical monuments and big engineering structures including suspended bridges and high-rise buildings either completed or under construction have a very high probability to expose destructive strong-ground motion. One of the big and complicated engineering structure in the Bosporus is the newly-completed MARMARAY including an immersed tunnel structure over the bottom with many public stations and tens of kilometers of railway connections onshore.

Site response analysis is usually the first step of any seismic soil-structure study. Geotechnical earthquake engineers and engineering geologist have been trying to find both practical and most appropriate solution techniques for ground response analysis under earthquake loadings. Site response of a two layered soil deposit with the assumption of linear and rigid base bedrock (or viscoelastic half-space) was analyzed by using linear approach. The amplification spectrum of the soil column is computed between the top and the bottom of this soil deposit. The change in the intensity and the frequency content of the motion due to the propagation of seismic waves in soil deposits and the existence of topographic features, commonly referred to as site effects, have a direct impact on the response of

DOI: 10.21533/pen.v5i1.78

structures during each of these earthquake events [1]. Geotechnical earthquake engineering deals with the effects of earthquakes on people and environments. Thus, engineering geologist and geotechnical earthquake engineers try to find most appropriate methods to reduce the magnitude of earthquake related hazards.

Evaluation of ground response is one of the most crucial problems encountered in geotechnical earthquake analysis. Ground response analyses are used to predict surface ground motions for development of design response spectra, to evaluate dynamic stresses and strains for evaluation of liquefaction hazards, and to determine the earthquake-induced forces that can lead to instability of earth and earth-retaining structures [2].

In this regard first quantitative studies have been conducted using strong-motion data after 1970s. Several methods have been proposed for evaluating site effects by using ground motion data, such as soil-to-rock spectral ratios [3], a generalized inversion [4, 5], and horizontal-to-vertical spectral ratios [6, 7, 8, 9, 10, 11, 12, 13].

The acceleration response spectra are mainly used to predict the effects of earthquake magnitudes on the relative frequency content of ground-bedrock motions. Even though seismic waves generally travel tens of kilometers of rock and less than 100 m of soil, the soil plays a very important role in determining the characteristics of ground motion [2]. Due to the complexity of the nonlinearity mechanism, dynamic behavior of soil during strong ground shaking has not been evaluated quantitatively based on the observed ground-motion records. Among the various aspects of the local site effects, nonlinear soil response in sedimentary layers during strong ground shaking has been a controversial issue for a long time [14]. A number of experimental works have been done to establish the stress – strain behavior of various types of soil [15, 16]

In theory, the term of site amplification refers to the increase in the amplitudes of seismic waves as they pass through the soft soil layers near the earth's surface. The increase is due to the low impedance of soil layers near the surface, where impedance is defined as the product of the mass density of soil and the wave propagation velocity. One of the basic problems to be solved by geotechnical engineers in regions, where earthquake hazards exist, is to estimate the site-specific dynamic response of the soil deposit under a level ground motion. The solution of this problem allows the geotechnical engineers to evaluate the potential for liquefaction, to conduct the first analytical phase of seismic stability evaluations for slopes and embankments, to calculate site natural periods, to assess ground motion amplification, and to provide structural engineers with various parameters, primarily response spectra, for design and safety evaluations of structures [17].

The acceleration time histories thus obtained together with the complete description of the dynamic properties of the soils determined from geophysical seismic studies are used to understand the responses of the soil columns to earthquake waves. Understanding of site response of geological materials under seismic loading is an important element in developing a well-established constitutive model.

Analytical methods for site response analysis include many parameters. The effects of these parameters are important to investigate on site response analysis in order to make confident evaluations of earthquake ground motions at the site. [13, 15, 18] investigated the effects of site parameters such as secant shear modulus, low-strain damping ratio, types of sand and clay, location of water table, and depth of bedrock. These studies have shown that the secant shear modulus, depth of bedrock, and types of sand and clay have a significant effect on the results of site response analysis. However, the low-strain damping ratio and variations of water tables have only a minor influence on site response analysis [19]. There are two approaches methods in site response analysis. These approaches have commonly been employed for representing soil stress–strain behavior during cyclic loading, for application in site response analysis. The first, in which the soil is modeled by a series of springs and frictional elements (Iwan model), uses Masing's rules to establish the shape of the cyclic, hysteresis curves [20].

This model does not normally simulate cyclic loading of soils, observed strain dependence of the shear modulus and damping ratio. On the other hand, Masing's rule does not provide an adequate approximation simultaneously for shear modulus and damping ratio. In the second approach, damping is modeled as a viscous. This approach is adopted, which uses a pseudo-linear treatment, and applies an iterative procedure in order to account for the strain dependence of modulus and damping [21].

The linear model is one of the most widely used approaches to model soil nonlinearity. To approximate the actual nonlinear, inelastic response of soil, an equivalent linear approach was proposed by [21]. In the equivalent linear approach, linear analyses are performed with soil properties that are iteratively adjusted to be consistent with an effective level of shear strain induced in the soil. [22, 23, 24] showed that equivalent linear analysis shows larger peak

acceleration because the method calculates acceleration in high frequency range large.

The main shortcoming of the linear method is its inability to take account of the strong strain dependence observed experimentally for shear modulus and damping ratio. The best that can be done with the linear model is to apply the method of iterations, and to set values of shear. Site response analysis can be of two kinds. These methods are linear and nonlinear site response analysis. Here are two basic approaches is made. Previous earthquakes, the ground motions on soft soil sites were found to be generally larger than those of nearby rock outcrops, depending on local soil conditions. Therefore, the linear response assay was developed. In order to conduct one-dimensional site response analyses, EERA [10] and NERA [11] softwares are used. The dynamic site response analyses led to results including spectral amplifications, velocities and accelerations. These methods are a modern implementation of the well-known concepts of site response analysis. [25] studied the effect of nonlinearity on site response analysis and evaluated ground surface response, taking into account the local soil and subsurface soil properties for the proposed bridge over the river at Sirdjan Boulevard road subjected to earthquake vibration with the assumption of rigid viscoelasticity. They showed that based on one-dimensional site response analysis, the effect of nonlinear soil behavior is one of the key factors for response spectra. They showed that based on one-dimensional site response analysis, the effect of nonlinear soil behavior is one of the key factors for response spectra. In another study, the ground response functions at the free surface in different geological locations in the metropolitan area of İstanbul have been obtained using average wave velocities, thicknesses, and densities of the geological layers based on the PS logs from seven different boring logs with depth ranging from 43 to 60 m during the MARMARAY Project. The E–W component of the acceleration record of the August 17, 1999 Kocaeli earthquake at Beşiktaş, district on the rock has been transferred to NERA software to obtain response and design spectrums that are considered to be crucial during earthquake strong ground motion [26].

A similar study, [27] studied in LNG port project in Assaluyeh, situated south of Iran. In their paper, the one-dimensional ground response of a near-fault earthquake is compared by two methods. An equivalent linear method based on total stress modeling in frequency domain and a nonlinear method based on effective stress modeling in time domain.

The main objective of this paper is to compare the linear (EERA) and nonlinear (NERA) site response analysis techniques with the numerically approach and to show their similarities and differences.

Linear and nonlinear site response analyses methods

To seismic soil response, two approaches are considered: the equivalent linear approach and a nonlinear elastoplastic modeling. In the following, theory and background of these two methods are reviewed.

The equivalent linear site response analysis (EERA)

The nonlinearity of soil behavior is known very well thus most reasonable approaches to provide reasonable estimates of site response is very challenging area in geoscience. The theory of approximation of real nonlinear dynamic soil behavior by equivalent linear approach was proposed firstly by [21]. Equivalent-linear modeling of dynamic soil behavior utilizes relationships that describe the variation of shear strain of material shear modulus (G) and hysteretic damping ratio (ζ) (Fig. 1a).

Previous earthquakes, the ground motions on soft soil sites were found to be generally larger than those of nearby rock outcrops, depending on local soil conditions. In order to conduct one-dimensional site response analyses, EERA software is used [10]. The dynamic site response analyses led to results including spectral amplifications, velocities and accelerations. Twelve different material properties are used in analyses conducted via EERA software. EERA is a modern implementation of the well-known concepts of equivalent linear earthquake site response analysis.

$$\rho \frac{\partial^2 u}{\partial t^2} = \frac{\partial \tau_{hv}}{\partial v} + \frac{\partial \sigma_h}{\partial h} + \frac{\partial \tau_{hn}}{\partial n} \qquad (1)$$

Where ρ is unit soil mass density, u is horizontal displacement, t is time, τ_{hv} is shear stress in the vertical plane within which horizontal displacement occurs, σ_h is axial stress (positive when tensile) in direction of displacement u, τ_{hv} is shear stress in the plane perpendicular to the plane within which horizontal displacement occurs, v, h, n are the vertical, horizontal and normal direction respectively (Eq.1).

If one-dimensional wave propagation is considered instead of three-dimensional propagation then the stress gradients $\partial\sigma_h/\partial h$ and $\partial\tau_{hn}/\partial n$ are zero and only the stress gradient $\partial\tau_{hv}/\partial v$ exists. Using zero stress gradients $\partial\sigma_h/\partial h$ and $\partial\tau_{hn}/\partial n$ in one-dimensional analysis causes inevitably under prediction of the horizontal acceleration $\partial^2 u/\partial t^2$ near basin edges. An apparent increase in $\partial\tau_{hv}/\partial v$ is necessary in one-dimensional analysis to compensate for the ignored stress gradients $\partial\sigma_h/\partial h \; and \; \partial\tau_{hn}/\partial n$ near basin edges.

Equation (1) is valid for any stress-strain relationship but cannot be solved directly because it mixes stresses with displacements [2]. In real materials, part of the elastic energy of a traveling wave is always converted to heat. Viscous damping is often used to represent this dissipation of elastic energy because of its mathematical convenience. For the purpose of visco elastic wave propagation analysis, soil is usually represented as Kelvin-Voigt model [2].

One way to address the issues of basin edge effects in to define and use modification factors for one-dimensional analyses near basin edges. The factors would be used in conjunction with one-dimensional analyses, to determine site specific seismic hazards caused by local ground layers.

The equation of motion in the horizontal direction for a three-dimensional elastic soil is developed in many textbooks [2].

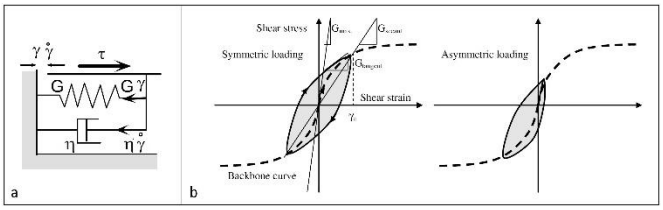

Figure 1. One-dimensional layered soil deposit system [21].

$$\tau_{hv} = G \cdot \gamma_{hv} + \eta \cdot \frac{\partial \gamma_{hv}}{\partial t} \quad (2)$$

Where G is shear modulus, shear strain $\gamma_{hv} = \partial u / \partial v$ and η is the viscosity of soil $G = \xi(\pi f)^{-1}$, ξ is damping ratio, f is the frequency of shear stress reversal and t is time. The equation for one-dimensional wave propagation becomes [21] (Eq.2).

In this part, equivalent linear approximation of nonlinear stress – strain response in EERA is described

$$\rho \cdot \frac{\partial^2 u}{\partial t^2} = G \cdot \frac{\partial^2 u}{\partial v^2} + \eta \cdot \frac{\partial^3 u}{\partial v^2 \partial t} \quad (3)$$

The analysis is usually performed in frequency domain because of its high speed in comparison with time domain analysis (Eq.3). Ground motion is represented by a Fourier series for a number of frequencies f. Soil viscosity η is related to the damping ratio ξ as $\eta = G \cdot \xi(\pi \cdot f)^{-1}$. Because of the modulus and damping ratio non-linear dependence on shear strain magnitude, an equivalent linear approach is used in the computation in frequency domain [21].

An increase in $\partial^2 u / \partial t^2$ in equivalent one-dimensional analyses is considered by factoring actual transversal wave velocities of soil layers in one-dimensional analyses.

These relationships are commonly referred to as modulus reduction and damping curves. One of the first computer programs developed for this purpose was SHAKE [21]. SHAKE computes the response in a horizontally layered soil-rock system subjected to transient and vertical traveling shear waves. SHAKE assumes that the cyclic soil behavior can be simulated using an equivalent linear model, which is extensively described in the geotechnical earthquake engineering literatures [2].

The width of the hysteretic loop is related to the area, which is a measure of internal energy dissipation. The dissipation involves the transformation of energy or work into heat, by particles friction due to their movements. A damping ratio ξ is frequently used as a measure of the energy dissipation [2].

$$\xi = \frac{W_D}{4 \cdot \pi \cdot W_s} = \frac{1}{2 \cdot \pi} \cdot \frac{A_{loop}}{G_{secant} \cdot \gamma_c^2} \quad (4)$$

Where W_D is the dissipated energy, W_s is the maximum strain energy, i.e. the area of the triangle in Fig. 1b. bordered by G_{secant} line, the vertical at γ_c and shear strain axis; and A_{loop} is the area of the hysteretic loop (Eq.4). Soil parameters G_{secant} and ξ are often referred to as equivalent linear soil parameters.

In the equivalent linear approach, as previously described in Fig. 1b, the shear modulus and damping ration are taken as functions of shear strain amplitude by iterations so that they become consistent with the level of the strain induced in each layer. The effective shear strain of the equivalent linear analysis is calculated as:

$$\gamma_{sff} = R_y \gamma_{max} \quad (5)$$

(γ_{max} is the maximum shear strain in the layer and R_y is a strain reduction factor).

Nonlinear and Hysteretic Model (NERA)

As illustrated in Fig. 2a, [28] and [29] proposed to model nonlinear stress-strain curves using a series of n mechanical elements, having different stiffness k_i and sliding resistance R_i. Her after, their model is referred to as the IM model. The sliders have increasing resistance (i.e., $R_1 < R_2 < ... < R_n$). Initially the residual stresses in all sliders are equal to zero. During a monotonic loading, slider i yields when the shear stress τ reaches R_i. After having yielded, slider i retains a positive residual stress equal to R_i. As shown in Fig. 2b, the stress-strain curve generated by the IM model for two sliders (i.e, n = 2) is piecewise linear, whereas the corresponding slope and tangential modulus H varies in steps. In the case of an IM model with n sliders, the stress increment $d\tau$ and strain increment $d\gamma$ are related through:

$$d\tau/d\gamma = H \quad (6)$$

Where the tangential modulus H is:

$$H = \begin{cases} H_1 = k_1 & if\ 0 \le \tau < R_1 \\ H_2 = (k_1^{-1} + k_2^{-1})^{-1} & if\ R_1 \le \tau < R_2 \\ H_{n-1} = (k_1^{-1} + k_2^{-1} + \cdots + k_{n-1}^{-1})^{-1}\ if\ R_{n-2} \le \tau < R_{n-1} \\ H_n = (k_1^{-1} + k_2^{-1} + \cdots + k_{n-1}^{-1} + k_n^{-1})^{-1}\ if\ R_{n-1} \le \tau < R_n \\ 0 \qquad if\ \tau = R_n \end{cases} \quad (7)$$

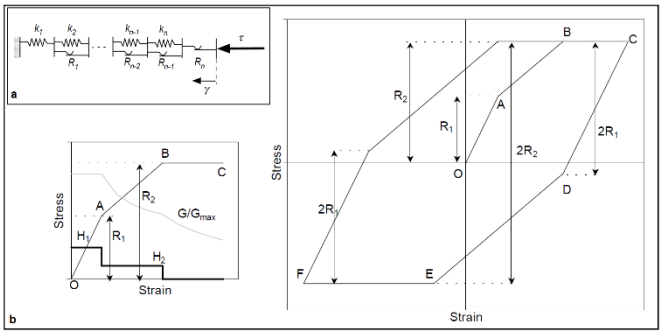

Figure 2. Backbone curve (left) during loading and hysteretic stress-strain loop (right) of IM model during loading-unloading cycle [11].

As shown in Fig. 2b, the stress-strain curve during a loading is referred to a backbone curve. When the loading changes direction (i.e., unloading), the residual stress in slider *i* decreases; slider *i* yields in unloading when its residual stress reaches - R_i , i.e., after the stress τ decreases -2 R_i. Instead of yield stress, it is convenient to introduce the back stress α_I: slider *i* yields in loading and unloading when τ becomes equal to $\alpha_I + R_i$ and $\alpha_I - R_i$, respectively. The IM model assumes that parameters R_i are constant whereas the back stress α_I varies during loading processes. As shown in Fig. 2b, the cyclic stress-strain curves are hysteretic, and follows Masing similitude rule [30]. Curve CDEF is obtained from curve OABC by a simitude with a factor of 2.

The stress-strain curves of the IM model can be calculated using the algorithm. This algorithm returns an exact value of stress τ independently of the strain increment amplitude Δγ. At first, the algorithm attempts to calculate the stress increment Δτ using the strain increment Δγ and modulus H_1. If $\tau+\Delta\tau \le \alpha_1 + R_1$ (loading), then τ+Δτ is accepted; the stress is smaller than the yield stress of slider 1. If $\tau+\Delta\tau > \alpha_1 + R_1$, the strain increment Δγ was too large, and the stress τ+Δτ exceeded the yield stress of slider 1; the tangential modulus of the stress-strain response was H_1 only for the stress increment $\Delta\tau = \alpha_1 + R_i - \tau$ and strain increment $\Delta\tau/H_1$. The algorithm is reapplied to slider 2, instead of slider 1, using the remaining strain increment $\Delta\gamma - \Delta\tau/H_1$. The algorithm is repeated for other sliders until τ+Δτ becomes smaller than the yield stress of slider *j*. Each time, the remaining strain increment referred to as Δ*x* becomes smaller. At this time, the back stresses of sliders 1 to *j-1* are updated. The algorithm works for loading and unloading through the use of variable x, which is set to 1 for loading and -1 for unloading respectively.

The nonlinear backbone curve of Fig. 2b can be described in terms a variation of secant shear modulus G with shear strain γ, especially by n data points, i.e., G_i-γ_I, i = 1,…, n. In this case, the tangential shear modulus H_i, is related to the secant modulus G_i, as follows:

$$H_i = \frac{G_{i+1}\gamma_{i+1} - G_i\gamma_i}{\gamma_{i+1} - \gamma_i} \quad i = 2, \ldots\ldots, n-1 \ and\ H_n = 0 \quad (8)$$

Assuming that the back stress α_i is initially equal to zero, R_i is:

$$R_i = G_i\gamma_i \quad i = 1, \ldots., n \quad (9)$$

Equations 8 and 9 imply that the maximum shear resistance is $R_n = G_n\gamma_n$ i.e., is specified by the last point of the $G-\gamma$ curve. When the $G/G_{max}-\gamma$ are specified, then Eqs. 8 and 9 become:

$$H_i = G_{max}\frac{G_{i+1}\gamma_{i+1} - G_i\gamma_i}{\gamma_{i+1} - \gamma_i} \quad i = 2, \ldots\ldots, n-1$$

$$and\ R_i = G_{max}G_i'\gamma_i \quad i = 1, \ldots., n \quad (10)$$

Where $G_i' = G_i/G_{max}$.

Geological and Tectonic Setting

The geology of the area consists of Paleozoic and Cenozoic-age formations (Fig. 3). The Trakya formation of the Paleozoic-age is represented by sandstone, siltstone, and claystone alternations and forms the basement in the study area. Unconformable overlying Miocene age deposits are differentiated as the Çukurçeşme, Güngören, and Bakırköy formations and constitute clastics, fine-grained and precipitated sediments, respectively, denoting a fluvial-to-lacustrine depositional environment. Alluvial deposits are limited to roughly north–south trending creek or stream valleys. Based on drill holes by the MARMARAY Tube Tunnel Project-2005 in the vicinity of the excavation site, a simplified geological section is produced (Fig. 4). Artificial filling and part of the Quaternary deposits are located above the present sea level. At the boundary of the Quaternary and Miocene deposits, a dark gray-black clay deposit is found in a small depression-like paleotopographical setting.

We considered it a small swamp, formed on the floodplain of Lykos Stream along an abandoned distributary channel, as indicated by tree roots and abundant plant material.

Based on surface geology investigations and evaluation of the findings of 107 borings carried out in the area and its vicinity for various purposes, the local

geological sequence and soil profile are established. These studies indicate that Neogene deposits outcrop in the region which comprises a sequence of strata unconformable overlying the Lower Carboniferous greywacke (Trakya fm.) and Eocene limestones (Kırklareli fm.). The Neogene sequence, deposition of which started transgressively in Late Oligocene, is composed of from bottom to top, basal gravel and conglomerate, interbedded green over consolidated clay and sand, and in the upper zone, due to a lacustrine environment getting shallower at the end of the Miocene, gray-green sand, organic clay, white/cream marl and fossiliferous limestone interbedded with clay (Bakırköy fm.) as an uninterrupted sequence. Fig. 3 shows the location of the site in the geological map of İstanbul [32], [33], and Fig. 4 displays the geographical positions of the borings and the grid overlay used in the area. The geological map of the study area is given in Fig. 3.

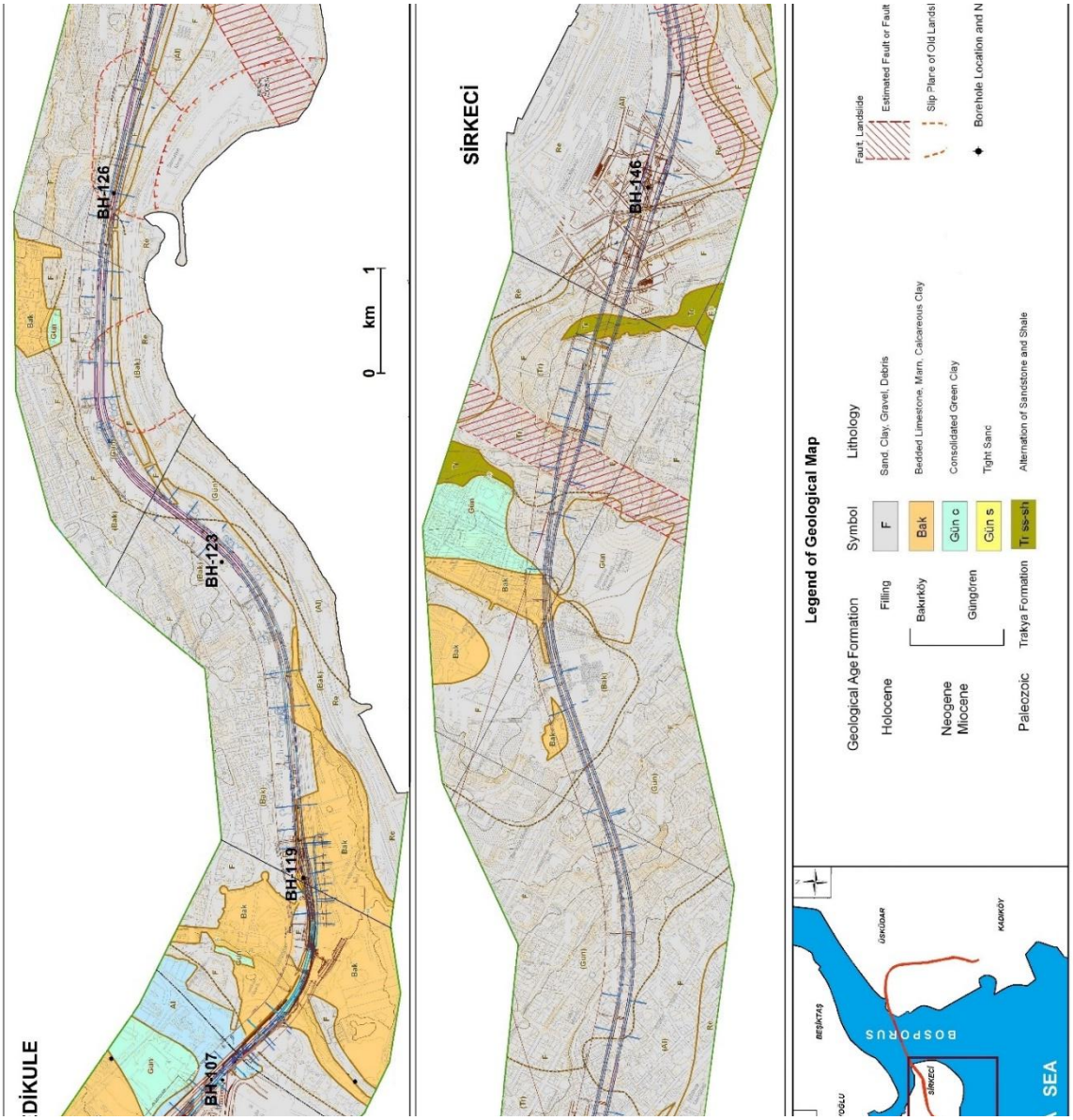

Figure 3. The geological Map of Study Area [31].

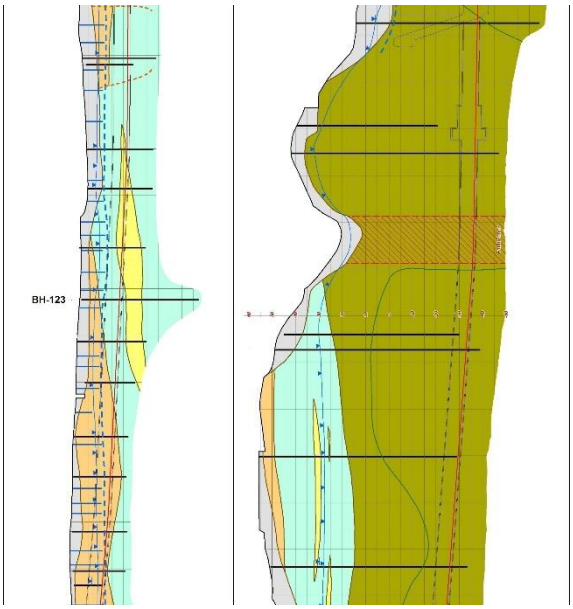

Figure 4. MARMARAY structure cross section and boreholes locations [31].

The site has widespread outcrops of limestone/marl inter bedded and transitional with limy clay, belonging to the Bakırköy formation, which is 20–30 m thick. The lithologies forming the Bakırköy formation are not only marls and low-strength limestone. It is, in fact, a sequence of inter bedded sand, clay, marl and limestone. The underlying Gürpınar formation is composed of green, fissured, over consolidated clays occasionally inter bedded with sand layers, only outcrops in a small area near the northeast end of the site, as a result of faulting. While the Gürpınar formation is 40 – 60 m thick towards the north end of the site, data from water wells up to 250 m deep confirm that the formation gets thicker towards the south and southwest and reaches to a thickness of 200 m in the coastal zone. The formation is unconformable on the Trakya formation in the north and, as shown in cross-section A–A′ (Fig. 4), unconformable on the Middle Eocene–Lower Oligocene Kırklareli formation in the southern half of Zeytinburnu province [34].

The second stage excavations of İstanbul Metro are carried out generally in Trakya and Güngören formation. Trakya formation (TF) consists of sandstone–siltstone–claystone–shale sequences. Limestone and conglomerates layers are also rarely observed. There are diabase and andesite dykes having some 10 m thickness. In the south of tunnel alignment, middle-upper age Miocene sediments consists of Çukurçeşme formation containing loose gravel–sand–silt, Güngören formation with clay–marn layer and Bakırkoy formation having limestone with shale and marl [35]. Many faults and geologic discontinuities exist in the area due to Alpine Orogenies. The overburden thickness above the tunnels varies between 11 and 42 m, and the distance between going–coming tunnels varies between 30 and 32 m.

The Marmara region is tectonically very active. The North Anatolian Transform Fault Zone (NAFZ) cuts across the region in an E–W direction, following the major axis of the Sea of Marmara. In the region the rate of right-lateral offset along the NAFZ has been measured to be about 18 mm/yr [36], [37]. The NAFZ is widely known to have generated large earthquakes (M>7) at 125– 150 yr intervals. In the Düzce and Kocaeli (İzmit) earthquakes of 1999, the lateral offset along the fault locally exceeded 5 m [38], [39]. The İstanbul area is a fault block bounded on the south by the NAFZ and on the north by the South Boundary Fault of the Black Sea Basin [40], [41]. This fault-bounded block is forced to rotate anticlockwise due to the sinistral shear. This rotation is expressed clearly in the geomorphology; major hills and the valleys trend obliquely to the two faults, following a long way before reaching the surrounding seas. Simultaneously with the anticlockwise rotation, the fault block has been elevated at a rather slow rate of about 0.2 mm/yr. However, these tectonically induced slow vertical motions have not caused radical changes in the study area during the recent 8000–10,000 yr period. But, some more remarkable local vertical movements caused by the activities of the NAFZ cannot be ruled out.

Geotechnical Properties of the Study Area

The dynamic properties of the soils in the area were evaluated by use of the data obtained from seven boreholes. The soil classes in the upper 30 m are dominantly silty sand and clays of high/low plasticity. These evaluations underline poor engineering conditions of soils beyond Southern Coasts of İstanbul.

A basic statistical evaluation of the soil property database will be utilized to better characterize the soils in the area. From the Fig. 4 it can be reliably expounded that the dominant characteristic of the soils are silty/clayey sand, sandy/gravel, gravel and clays of high/low plasticity.

MARMARAY line, from BH-119 borehole to until BH-130A boreholes are located in Güngören formation also to The Marmara Sea from BH-130A borehole is located in the Thrace formation. On the fault zone in the Thrace formation is clearly observed the intensity of tectonic deformation in the region. Accordingly, BH-107, BH-119 and BH-123 boreholes are comprised from sand, clay and gravel mixtures. BH-126, BH-130-A, BH-134 and BH-146 boreholes after deep the 30 m are composed of mudstone, claystone and sandstone.

The Linear and Nonlinear Site Response Analyses of the Study Area

İstanbul is the largest city in Turkey and the area has experienced high levels of earthquake ground motion. Four earthquakes of M 7.6 (1509, 1719, and 1766) and M 7.0 (1894) situated in the Marmara Sea have generated intensities up to X–XI in the city Following the 1999 Kocaeli earthquake, the high probability of a large event affecting İstanbul in the near future has been put forward by various researchers [42], [43]. There are two main hypotheses about the rupture characteristics of this event. [44] argue that a large magnitude earthquake (Mw 7.6–7.7) caused by a 175 km through going rupture of the so-called Main Marmara Fault (northern strand of the North Anatolian Fault in the Marmara Sea) will take place in the near future. On the other hand, based on their observations on submarine fault scarps in the Marmara Sea, [45] argue that the 1912 Ganos earthquake on the westernmost on-land segment of the Main Marmara Fault crossed the Ganos restraining bend into the Sea of Marmara for 60 km with a right-lateral slip of 5m, ending in the Central Basin step-over. These findings result in a total rupture length of 140 km for the 1912 event, contradicting the 50 km on-land rupture, previously suggested by [46].

[47] made a comprehensive deterministic approach to the earthquake hazard in İstanbul city. Therefore, the scenario earthquakes were computed by deterministic seismic hazard analysis integrated with time-dependent probabilistic hazard assessments by [48] and [49].

Obtain the site response results, analyses are conducted by use of EERA and NERA softwares in this study. The EERA and NERA softwares are in spreadsheets format and has the ability to include unlimited dynamic soil models in soil response calculations by one dimensional linear and nonlinear methods. A damped linear elastic model and nonlinear analyses are used to demonstrate the nonlinear behavior of the soil layers. The stress–strain properties of the soils are instructed by use of the relationships expressing the change of shear modulus and damping with the shear strain level. Thus, the soil profiles were prepared from the database for the calculation of average shear wave velocities.

Selection of Ground Motion Records

The studied sites are subjected to ground motion caused by events originated in the plate inshore seismic zones. One acceleration record from in plate zones were selected for the site response analysis of the soil deposit. The earthquake Kocaeli 1999, with PGA (magnitude = 7.4 Mb) value of 0,04287 g, at Prime Ministry Disaster & Emergency Management Presidency İstanbul Station (PMDEMPIS) for site, the Fourier spectra is shown in Fig. 5.

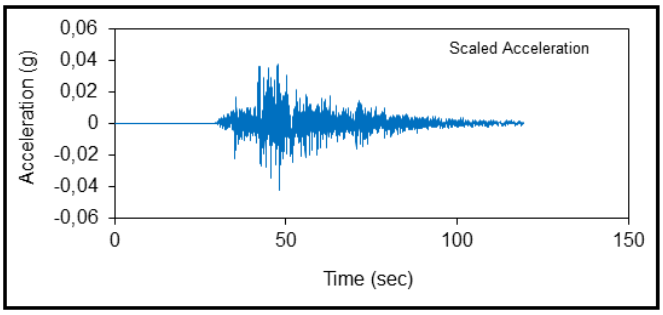

Figure 5. Record of accelerograph of horizontal component of The earthquake Kocaeli 1999 at IBMPWS station obtained from PMDEMPIS online virtual data center.

Local soil is mainly sandy clay and clays of high/low plasticity poorly graded but usually very dense. It can be seen that these time histories present relatively high frequencies, high accelerations and long durations as it is common in this region.

Input time history are applied on each of the soil profiles by the EERA and NERA softwares to obtain the site responses, and the resulting database consisted of dynamic soil behavior, including spectral acceleration-time variation as well as its maximum.

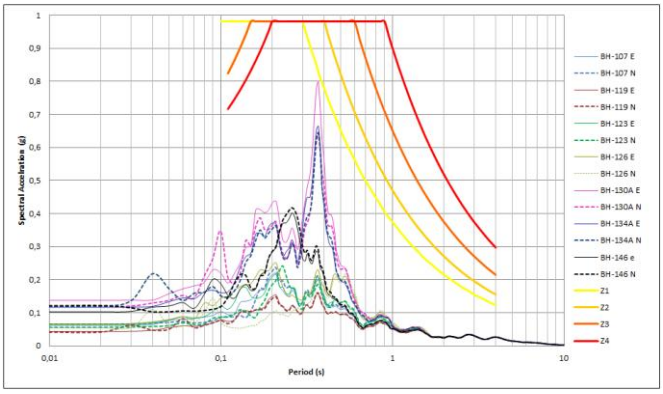

Figure 6. Exemplary surface spectral acceleration–period relationships belonging to various boreholes of the investigation area and comparison of the earthquake Kocaeli 1999 elastic behavior acceleration spectrums with Turkish Earthquake Regulation Spectrums (2007 elastic medium, EERA and NERA).

Seven exemplary surface spectral acceleration–period variations from different boreholes are given in Fig. 6. Borings in separate grids were evaluated under the given input time history and the maximum spectral acceleration against period variation is determined in each boring location. During past earthquakes, the ground motions on soft soil sites were found to be generally larger than those of nearby rock outcrops, depending on local soil conditions.

[50] made a comprehensive deterministic approach to the earthquake hazard in İstanbul city. By İstanbul Metropolitan Municipality (IMM) for İstanbul city earthquake scenario was constructed by the method of Kobayashi-Midorikawa. The study included a comparison of fifteen different earthquake scenarios. Comparison of these scenarios led to the conclusion that an earthquake which is probable to occur on NAFZ will generate ground motions having a magnitude of approximate Mw = 7.5, radiating an energy level greater than those of the rest of the scenarios [51]. In order to obtain the site response results, analyses are conducted by use of EERA [10] and NERA [11] softwares.

Modeling of Profile Geometry and Soil Properties

Generalized soil profiles were established from the borehole drilled at BH-107, BH-119, BH-123 BH-126, BH-130A, BH-134 and BH-146 boreholes. The wells are located along the MARMARAY line. All boreholes are located in alluvial soil. Because of the lower shear-wave zone and the lower shear strengths values were measured in boreholes. Modulus of rigidity or shear modulus can be explained using elastic properties of soil layers. Shear modulus of soils for the site analysis is determined by [16].

EERA and NERA programs obtained change of max shear stress with depth are shown in Fig. 7. Accordingly, the max shear stress-depth change in BH-126, BH-130A, BH-134 and BH-146 boreholes are seen in the range of 25 kPA-50 kPA in EERA method. If the method of NERA, the max shear stress-depth change in BH-123, BH-126, BH-130A, BH-134 and BH-146 boreholes are seen in the range of 20 kPA-40 kPA. Moreover, BH-107, BH-119 and BH-123 boreholes are in low acceleration category in EERA. If the method of NERA, BH-107 and BH-119 boreholes are in low acceleration category. According to Fig.8, change max shear stress-depth of these boreholes are monitored in the range of 16 kPA-20 kPA in EERA method, 10 kPA-15 kPA in NERA method.

Focusing on Fig. 8, it can be stressed that the alluvial region near The Marmara Sea, soils especially under Kazlıçeşme, Yenikapı and Zeytinburnu district the lowest shear wave velocities, ranging between 0–100 m/s. The shear wave velocity (V_{S30}) variation of the soils given in Fig. 8 enlightens the reason of the low strength of the soils in the area, which is dominancy of these soil classes. Shear wave velocities of upper 65 m are between 194–518 m/s at BH-107, BH-119 and BH-123 boreholes. Shear wave velocities for layers deeper than 20 meters are between 782–2173 m/s at BH-126, BH-130A, BH-134 and BH-146 boreholes. Furthermore, outcropping bedrock in the BH-134 and BH-146 boreholes are probably the reason of the V values between greater than 950 m/s. MARMARAY route constitutes the basis of the Thrace formation. Some boreholes into this formation extend.

The shear modulus increases drastically from 140 MPa to 240 MPa at depth of 35 meters and decreases drastically from 240 MPa to 140 MPa at depth of 20 m at BH-130A borehole, and shear modulus decreases from 200 MPa to 160 MPa at depth of 17 meters at BH-107 borehole. Furthermore, the shear modulus increases dramatically from 480 MPa to 1300 MPa at depth of 54 meters at BH-126 borehole. Accordingly, the shear modulus increases dramatically from 50 MPa to 6500 MPa at depth of 34 meters at BH-134 borehole and from 400 MPa to 1800 MPa at depth of 22 meters at BH-146 borehole (Fig. 8).

According to the results of the EERA method solution; The amplitude ratios (1.3-8 ratio) values of acceleration are seen to be different in boreholes. The amplitude ratios of the BH-107, BH-119 and BH-123 are low. However, other boreholes, the amplitude ratios are high (3-8 ratio) (Fig.9). Frequency of maximum amplification (Hz) and maximum amplification values are given in Table-1. Frequency of maximum amplification (Hz) in BH-123 borehole is high (7.4 Hz), BH-126 borehole is low (2.0 Hz). Similarly, maximum amplification in BH-130A borehole is high (7.83), BH-119 borehole is low (1.23).

According to the results of the NERA method solution; The amplitude ratios (1.4-8.5 ratio) values of acceleration are seen to be different in boreholes. The amplitude ratios of the BH-107, BH-119, BH-130A and BH-134 are low. However, other boreholes, the amplitude ratios are high (5.5-8 ratio) (Fig. 9). Frequency of maximum amplification (Hz) and maximum amplification values are given in Table-1. Frequency of maximum amplification (Hz) in BH-126 borehole is high (49.7 Hz), BH-126 borehole is low

(8.05 Hz). Similarly, maximum amplification in BH-123 borehole is high (36.27), BH-119 borehole is low (2.0).

The Fourier response in the form of spectra indicates the ideal situation of variation in amplitudes at different frequencies. BH-146 borehole away from these two wells is over and marine sediments.

Therefore, the spectral acceleration values are high. In addition, Fig. 10 demonstrates the variation of peak spectral acceleration values in the investigation area. Calculated surface spectral accelerations in the area ascend to 0.80 g, and the observed lowest value is 0.15 g. with EERA method. If the method of NERA, calculated surface spectral accelerations in the area ascend to 0.65 g, and the observed lowest value is 0.16 g. Because, these wells are located in the area of marine sediments. Analyzing the Table-1, it is seen that majority of BH-130A and BH-134 boreholes are in high acceleration category.

According to the EERA and NERA methods, they are understood that majority of BH-130A, BH-134 and BH-146 boreholes are under high ground shaking risk (Table 2). Additionally, individual areas in the shoreline to Marmara Sea and creek beds are under the threat of relatively medium to low ground shaking risk. Small areas of relatively low ground shaking risk are observed in BH-107, BH-119, BH-123 and BH-126 boreholes.

Conclusions

MARMARAY is a very large project for İstanbul. A million people carrying capacity per day is a railway project. The construction of such a major project, could be planned the largest earthquake in the region. The study area due to NAFZ has a very high seismic risk. To obtain response spectra for design of structures the spectral acceleration values for layers deposited at the sites were defined using computer programs EERA and NERA. MARMARAY project is many boreholes drilled. However, the seven boreholes were examined in this study.

Hence, PS logging and V_S measured in seven boreholes were transferred to EERA and NERA softwares. Then, calculated by the EERA and NERA softwares soil

Boreholes	BH-107		BH-119		BH-123		BH-126		BH-130A		BH-134		BH-146	
	EERA	NERA	EERA	NERA	EERA	NERA	EERA	NERA	EERA	NERA	EERA	NERA	EERA	NERA
Maximum Amp.	1.58	2.88	1.23	2.00	1.73	**36.27**	2.87	11.01	**7.83**	2.96	6.05	2.58	5.16	5.26
Freq. of Max. Amp. (Hz)	2.8	8.05	2.4	18.92	**7.4**	**48.68**	2.0	**49.70**	2.6	28.62	2.8	17.15	3.8	12.33

Table 1. Maximum amplification and frequency of maximum amplification (Hz) of boreholes

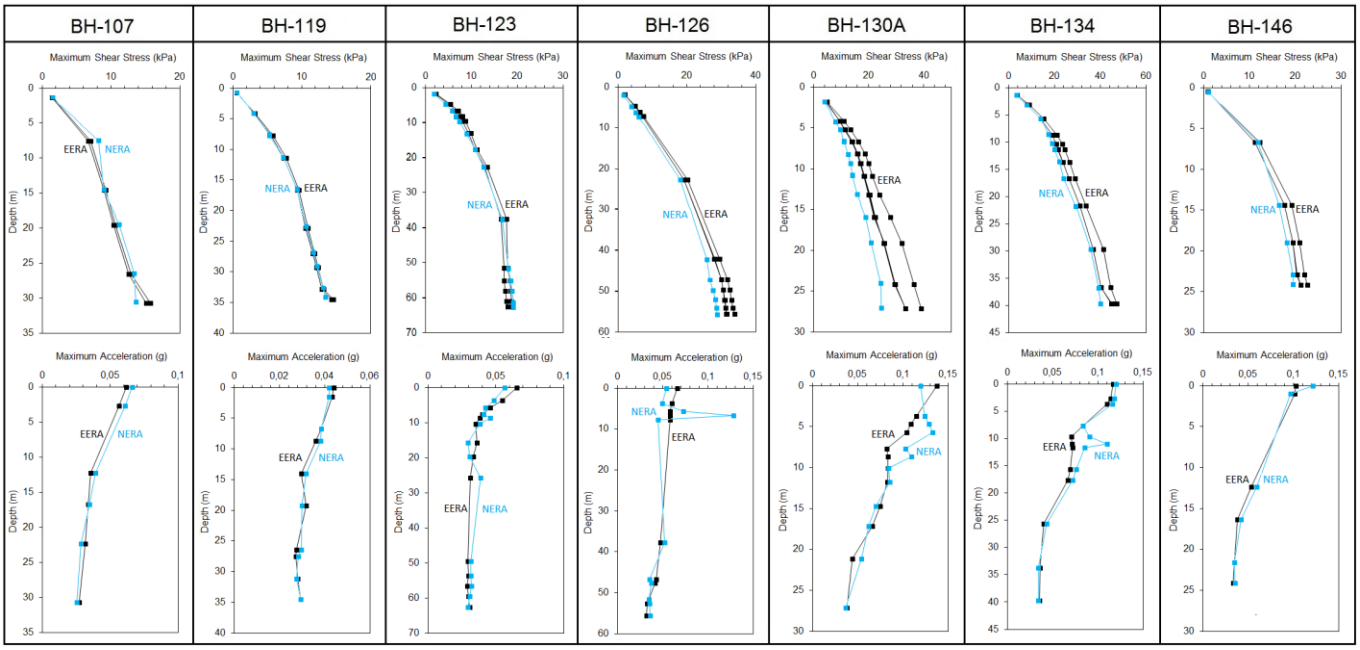

Figure 7. Max shear stress variation with depth of the boreholes (Results of the 1D ground response analysis performed with EERA and NERA)

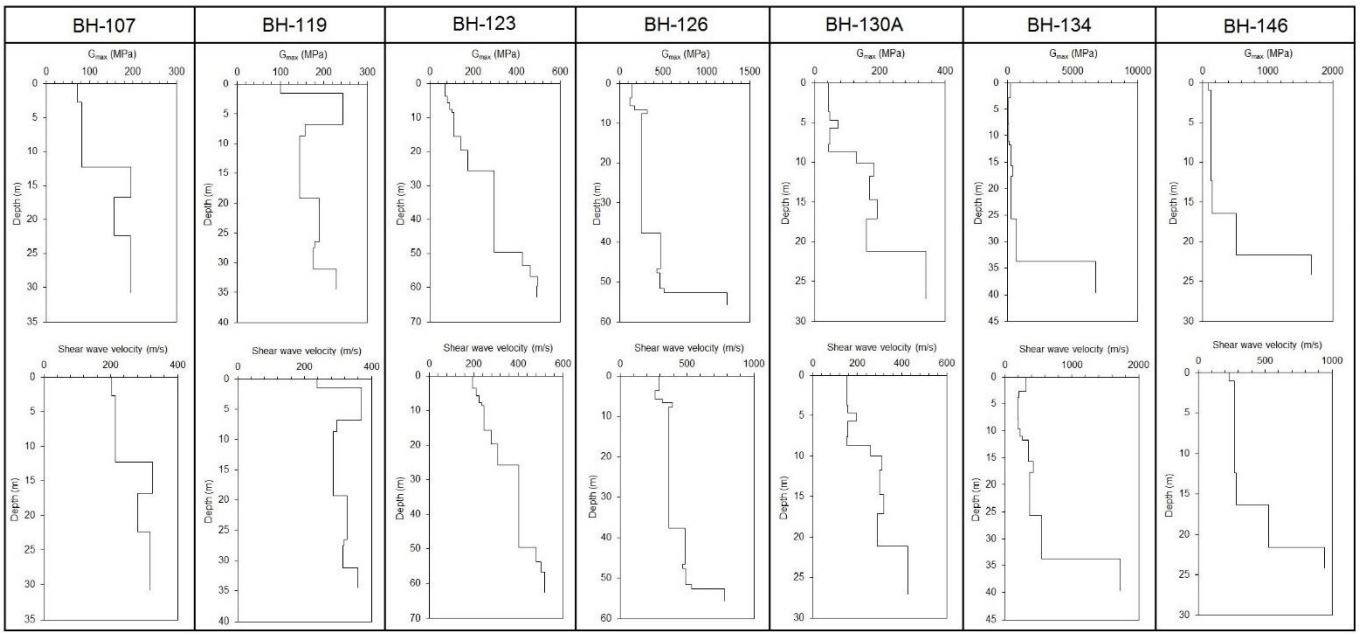

Figure 8. G_{max}- depth and shear stress - depth variation graphics of the boreholes (from EERA and NERA)

Table 2. Max Period (s) and max spectral acceleration (g) of boreholes

Boreholes	BH-107		BH-119		BH-123		BH-126		BH-130A		BH-134		BH-146	
	EERA	NERA	EERA	NERA	EERA	NERA	EERA	NERA	EERA	NERA	EERA	NERA	EERA	NERA
Max Period (s)	0.21	0.21	0.36	0.37	0.21	0.23	0.21	0.53	0.37	0.37	0.37	0.37	0.23	0.25
Max Spectral acceleration (g)	0.22	0.24	0.15	0.16	0.21	0.24	0.25	0.22	0.80	0.65	0.66	0.64	0.44	0.45

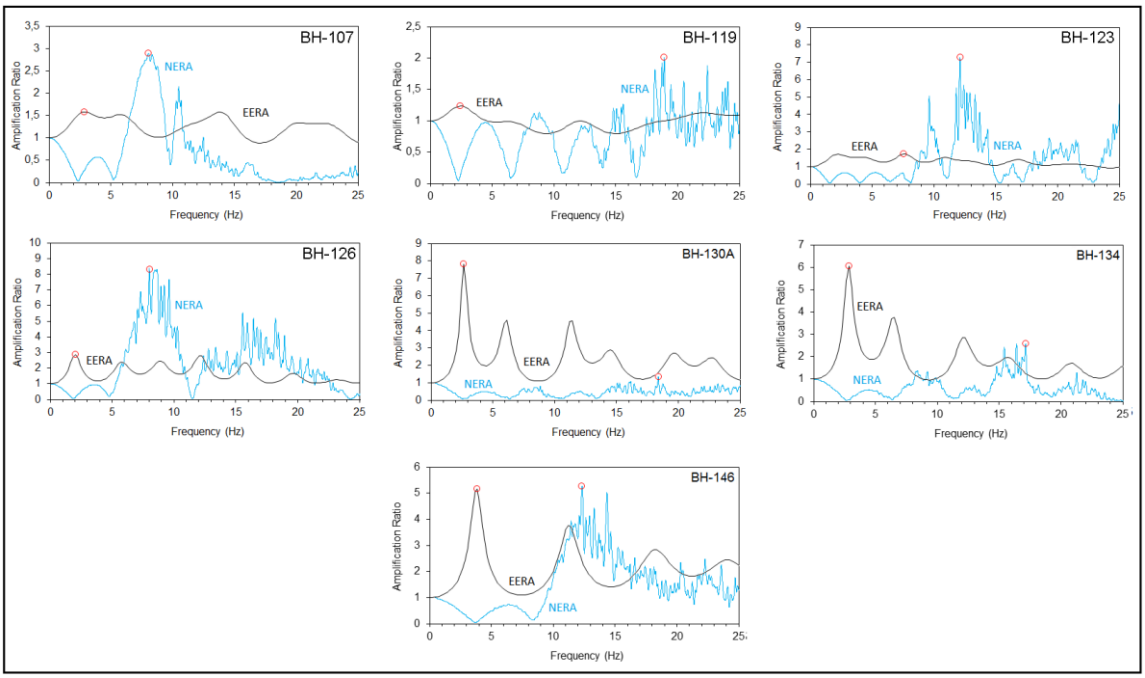

Figure 9. Amplitude ratio values of acceleration in boreholes (comparative EERA and NERA).

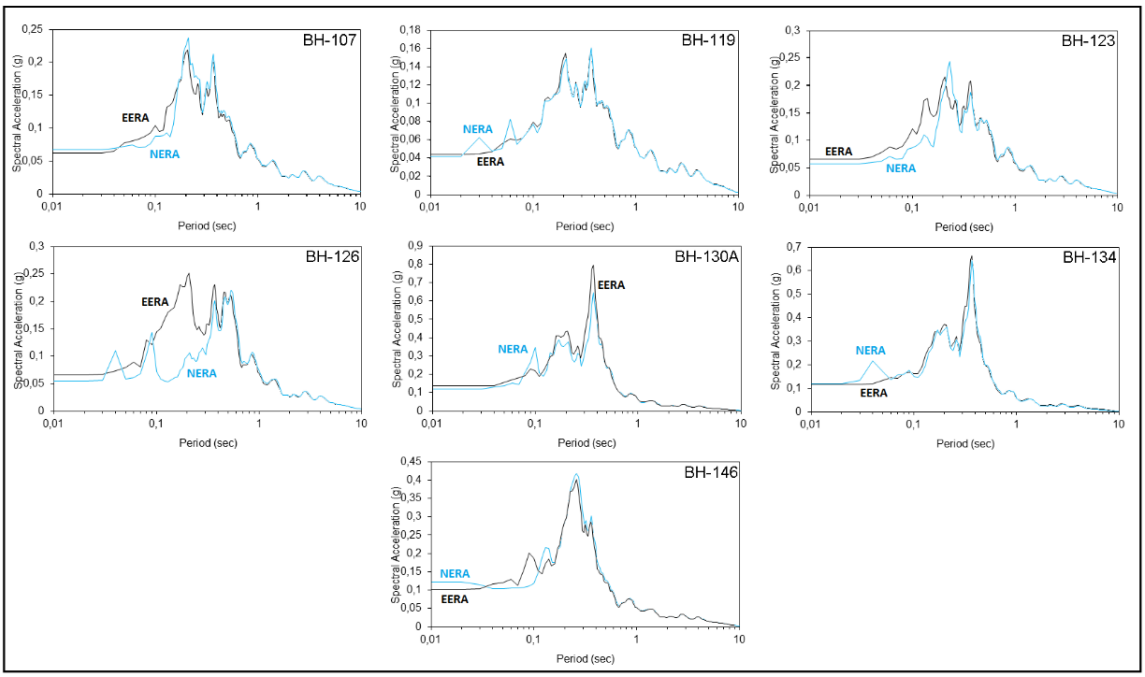

Figure 10. Spectral acceleration and Period relationship of the boreholes (comparative EERA and NERA)

Table 3. The calculated maximum values of boreholes.

Time Domain				Frequency Domain	
Borehole Number	Acceleration (g)	Particular Velocity (m/s)	Displacement (m)	Spectral Acceleration (g)	Dominant Period (s)
17 Aug Kocaeli earthquake acceleration record of 0.04287 g was measured at the IBMPWS					
BH-107	0.062	0.002	0.031	0.22	0.21

BH-119	0.044	0.001	0.026	0.15	**0.36**
BH-123	0.065	0.003	0.037	0.22	0.21
BH-126	0.066	0.003	0.043	0.25	0.21
BH-130A	**0.138**	0.004	0.073	0.80	**0.37**
BH-134	**0.117**	0.003	0.064	0.66	**0.37**
BH-146	**0.103**	0.001	0.038	0.40	0.26

parameters and behavior acceleration spectrums are compared with Turkish Earthquake Regulation.

The results obtained from the geological and engineering investigations have provided useful information regarding the physical and engineering properties of the surface soil samples as well as alluvium and land-slide materials at dam site and reservoir area. EERA and NERA calculations have produced plenty of data describing the response of the boreholes under 17 August Kocaeli earthquake, where the results can be processed in several boreholes. Therefore, the joints between stations are important but weaker parts of the earthquake-resistant design of the MARMARAY tunnel. Not only must they have superior anti-deformation properties, but they are also observed to prevent unacceptable deformation under seismic loading. Hence, more attention should be paid to seismic response analysis of the flexible joints.

According to spectral acceleration-period graphics, there is a difference 300 m/s velocity between down layer and top layer in BH-130A borehole in EERA methods. Similarly, there is a difference 700 m/s velocity between down layer and top layer in BH-134 borehole, there is a difference 1900 m/s velocity between down layer and top layer BH-146 borehole. Spectrums of BH-126, BH-130A, BH-134 and BH-146 boreholes show similar features (Fig. 10).

With regard to NERA method there is a difference ~100 m/s velocity between down layer and top layer in BH-107 borehole. Similarly, there is a difference ~1400 m/s velocity between down layer and top layer in BH-134 borehole. Also, spectrums of BH-119, BH-130A and BH-134 boreholes show similar features; on the other hand BH-107, BH-126 and BH-146 boreholes show similar features (Fig. 10).

At the location of stations connections where there are joint points, Fig.8 illustrates the lower shear strengths values of tunnel build when the seismic waves are propagating along all over directions, lower shear-wave zone when the seismic waves are propagating along all over directions. Due to the alteration of the soil, surface layer thickness is 3-5 m. The impact of the building on the soil has been ratio of 5 %.

According to EERA method, dominant period from 0.36 s to 0.37 s are increasing in BH-119, BH-130A and BH-134 boreholes. If the method of NERA, dominant period from 0.37 s to 0.53 s are increasing in BH-119, BH-126, BH-130A and BH-134 boreholes. Therefore, this area is expected to become more dominant low frequency S waves. The largest maximum accelerations were measured in the BH-130A borehole to EERA method, in the BH-119 borehole to NERA method. Similary the lowest maximum acceleration was measured in the BH-119 borehole to EERA method, in the BH-119 borehole to NERA method.

Accelerations of the BH-130A, BH-134 and BH-146 boreholes at the time domain same results were scaled in both EERA and NERA methods. In both methods, maximum accelerations are input acceleration (0,0426 g) increase (1-2 storey). In acceleration the largest amplification (0.138 g) is in BH-130A borehole to EERA method (Table 3). Similary in acceleration the largest amplification (0.120 g) are in BH-130A, BH-134 and BH-146 boreholes to NERA method (Table 3).

On the other hand amplification ratio-frequency graphics for each borehole in Figure 9 reflect approximate vibration frequency values of the soil layers from the free surface to the deep end of the borehole, as apparent from the comparison of Figures 4 and 9. Maximum amplification ratios for BH-126 and BH-123 boreholes increase to 8 as compared to BH-119 and BH-130A boreholes having value of 2 in NERA method, because the former boreholes were drilled within the consolidated green clay layers. Similarly, maximum amplification ratios for BH-130A and BH-134 boreholes increase (within the fault zone) to 6-8 as compared to BH-107, BH119 and BH-123 boreholes having value of 2 in EERA method, because the former boreholes were drilled within the consolidated green clay and tight sand layers.

Therefore, this area is of low frequency S wave. The largest maximum acceleration was measured in the BH-

130A (in EERA) borehole. Large spectral amplitudes shift larger periods because EERA and NERA analysis has been carried out using a relatively far seismic source, namely the 17 August 1999 İzmit earthquake (Mw=7.4). The effective peak acceleration is 0.3 g; the fundamental period is about 0.15-0.53 s for the long distance scenario earthquakes. These period intervals are characteristic for the Z3 type of soil (T_A = 0.15 s and T_B = 0.60 s) given in the Earthquake Design Code of Turkey [51]. The width of the spectrum is dominated by the local soil type and the effective ground acceleration determines the peak value of the spectral acceleration between the short and long characteristic periods. Based on these plots a slightly modified design spectrum of Z3 type of soils is proposed as shown in Fig. 6 with colored lines.

The lowest maximum acceleration was measured in the BH-119 borehole. For an input acceleration value of 0.0426 g, maximum accelerations of the BH-130A, BH-134 and BH-146 boreholes in the time domain are obtained to be between 0.42-0.65, indicating amplifications in the order of ten folds. These boreholes are considered to be located within the fault zone (Table 3).

Since fundamental periods of boreholes labelled as BH-119, BH-130A and BH-134 are 0.37 s, sites of these boreholes are in Z3 soil class. On the other hand BH-130A and BH-134 boreholes are within the fault zone and their accelerations values are obtained to be high such as 0.64-065 g. Within the boreholes under investigation, the maximum fundamental period value (0.53 s) is estimated for BH-126 and the site of this borehole, therefore, is deemed suitable as Z4 soil class. The periods of the other boreholes (e.g. BH-107, BH-123 and BH-146) are in the range 0.21-0.25 s and their sites are classified as Z2 soil class.

Acknowledgements

The authors would like to thanks MSc. Sercan ÖZTÜRK and TAISEI Corporation.

References

[1] Y. M. A. Hashash, D. R. Grohalski, C. A. Philips, "Recent advances in nonlinear site response analysis", *5th International Conference on Recent Advances in Geotechnical Earthquake Engineering and Soil Dynamics* No.4. Sandiego California, 2010.

[2] S. L. Kramer, "Geotechnical Earthquake Engineering", 1st edn. Prentice-Hall, New Jersey, 1996.

[3] R. D. Borcherdt, "Effects of local geology on ground notion near San Francisco Bay", *Bull. Seismol. Soc. Am.* 60: 29–81, 1970.

[4] T. Iwata, K. Irikura, "Source parameters of the 1983 Japan Sea earthquake sequence", *J. Phys. Earth*. 36:155–184, 1988

[5] J. Boatwright, J. B. Fletcher and T. E. Fumal, "A general inversion scheme for source, site and propagation characteristics using multiply recorded sets of moderate-sized earthquakes", *Bull. Seism. Soc. Am.,* 81, 1754-1782, 1991.

[6] Y. Nakamura, "On the urgent earthquake detection and alarm system (UrEDAS)", In: Proceedings of World. Conference in Earthquake Engineering, 1988.

[7] J. Lermo, F. J. Chavez-Garcia, "Site effects evaluation using spectral ratios with only one station", *Bull Seismol. Soc. Am.* 83: 1574–1594, 1993.

[8] E. H. Field, K. H. Jacob, "A comparison and test of various site-response estimation techniques, including three that are not reference-site dependent", *Bull. Seism. Soc. Am.* 85: 1127–1143,1995.

[9] F. Yamazaki, M. A. Ansary, "Horizontal-to-vertical spectrum ratio of earthquake ground motion for site characterization", *Earthquake Eng. Struct. Dyn.* 26: 671–689, 1997. JSSMFE: 14–31

[10] J. P. Bardet, K. Ichii, C. H. Lin, "EERA, A Computer Program for Equivalent Linear Earthquake Site Response Analysis of Layered Soils Deposits", University of Southern California, Los Angeles, 2000.

[11] J. P. Bardet, T. Tobita, "NERA: A computer program for nonlinear earthquake site response analyses of layered soil deposits", Department of Civil Engineering, University of Southern California, Los Angeles, CA, 43 pp, 2001.

[12] I. Lam, C. F. Tsai, G. R. Martin, "Determination of site dependent spectra using nonlinear analysis", In: *2nd international conference on microzonation*, San Francisco, CA, 1978.

[13] W. B. Joyner, A. T. F. Chen, "Calculation of nonlinear ground response in earthquakes", *Bull. Seismol. Soc. Am.* 65: 1315–1336, 1975.

[14] S. M. M. M. Hosseini and M. A. Pajouh, "Comparative study on the equivalent linear and the fully nonlinear site response analysis approaches", *Arab. J. Geosci.* 5:587–597, 2012. DOI 10.1007/s12517-010-0228-9

[15] H. B. Seed, I. M. Idriss, "Soil moduli and damping factors for dynamic response analysis", Report EERC 70-10, 1970. University of California, Berkeley, Earthquake Engineering Research Center.

[16] B. O. Hardin, V. P. Dmevich, "Shear modulus and damping in soil: measurement and parameter effects" *J. Soil Mech. Found Div*. 98: 603–624, 1972.

[17] E. Şafak "Local site effects and dynamic soil behavior", *Soil Dynamics and Earthquake Engineering* 21, 453-458, 2001.

[18] H. H. M. Hwang, C. S. Lee, "Parametric study of site response analysis", *Soil Dyn. Earthq. Eng*. 10 (6): 282–290, 1991.

[19] H. Arslan and B. Siyahi, "A comparative study on linear and nonlinear site response analysis", *Environ Geol*. 50: 1193–1200, 2006. DOI 10.1007/s00254-006-0291-4

[20] H. B. Seed, R. V. Whitman, H. Dezfulian, R. Dobry, I. M. Idriss, "Soil conditions and building damage in the 1967 Caracas earthquake", *J. Soil Mech Found Div*. ASCE 98:787–806, 1972.

[21] P. B. Schnabel, J. Lysmer, H. B. Seed, "SHAKE: a computer program for earthquake response analysis of horizontally layered sites", 1972. Report No. EERC72-12, University of California, Berkeley.

[22] N. Yoshida, "Applicability of conventional computer code SHAKE to nonlinear problem", *Proc. Symposium on Amplification of Ground Shaking in Soft Ground*, JSSMFE, pp14-31, 1994. (in Japanese)

[23] H. C. Huang, C S. Shieh, H. C. Chiu, "Linear and nonlinear behaviors of soft soil layers using Lotung downhole array in Taiwan" *Terr. Atmos. Ocean Sci*. 12: 503–524, 2001.

[24] N. Yoshida, S. Iai, "Nonlinear site response analysis and its evaluation and prediction", In: *2nd International symposium on the effect of surface geology on seismic motion*, Yokosuka, Japan, pp 71–90, 1998.

[25] A. A. Shahri, B. Esfandiyari, H. Hamzeloo, "Evaluation of a nonlinear seismic geotechnical site response analysis method subjected to earthquake vibrations (case study: Kerman Province, Iran)". *Arab J Geosci* 4:1103–1116, 2011.

[26] G. Beyhan, A. Keskinsezer and S. Öztürk, "Soil properties and applications review with NERA (nonlinear earthquake site response analyses) in İstanbul-MARMARAY Project between Kazlıçeşme to Sirkeci", *Environmental Earth Science* January, 75:93, 2016. DOI 10.1007/s12665-015-4783-y

[27] M. Adampira, H. Alielahi, M. Panji and H. Koohsari, "Comparison of equivalent linear and nonlinearmethods in seismic analysis of liquefiable site response due to near-fault incident waves: a case study", *Arab J Geosci* 8:3103–3118, 2015.

[28] W. D. Iwan, "On a class of models for the yielding behavior of continuous and composite systems, Journal of Applied Mechanics", *ASME*, Vol. 34, pp.612-617, 1967.

[29] Z. Mróz, "On the description of anisotropic workhardening", *Journal of Mechanics and Physics of Solids*, Vol.15, pp.163-175, 1967.

[30] G. Masing "Eigenspannungen und Verfestigung beim Messing", *Proceedings of the Second International Congress of Applied Mechanics*, pp.332-335, 1926.

[31] TAISEI, Marmaray project map, 2011 (unpublished).

[32] M. Yıldırım, "Engineering Geological evaluation of solid waste landfill sites: two examples from İstanbul, Turkey", *Bulletin of Engineering Geology* 55, 151–158, 1997.

[33] M. Yıldırım, E. Savaşkan, "İstanbul Tersiyer Çökellerinin Stratigrafisi ve Mühendislik Özellikleri", *Uluslararası Mühendislik Jeolojisi Türk Milli Komitesi Bülteni*, 18, pp. 48–62, 2002. İstanbul (in Turkish)

[34] K. Özaydın, A. Ansal, M. Erdik, M. Yıldırım, H. Kılıç, Ş. Adatepe, P. T. Özener, M. Tonoroğlu, K. Şeşetyan, M. Demircioğlu, "Earthquake Master Plan For İstanbul, Zeytinburnu Pilot Project", "Report on Geological and Geotechnical Evaluation for Seismic Microzonation and Seismic Microzonation for Ground Shaking" Yıldız Tecknical University, Fac. of Civil Eng. Geotechnical Department., Boğaziçi University, Kandilli Observatory and Earthquake Research Inst. (in Turkish), 2004.

[35] E. Usta, "İstanbul Metro Yenikapi–Unkapani engineering geology", Master Thesis, İstanbul Technical University, İstanbul, Turkey, 2004.

[36] F. Flerit, R. Armijo, G. C. P King, B. Meyer, A. Barka, "Slip partitioning in the Sea of Marmara pull-apart determined from GPS velocity vectors", *Geophysical Journal International* 154, 1–7, 2003.

[37] N. Pondard, R. Armijo, G. C. P. King, B. Meyer, F. Flerit, "Fault interactions in the Sea of Marmara pull-apart (North Anatolian Fault): earthquake clustering and propagating earthquake sequences", Geophysical Journal International 171, 1185–1197, 2007.

[38] M. N. Toksöz, R. E. Reilinger, C. G. Doll, A. Barka, N. Yalçın, "Izmit (Turkey) Earthquake of 17 August 1999: first report", *Seismological Research Letters* 70 (6), 669–679 November/December, 1999.

[39] R. E. Reilinger, S. Ergintav, R. Bürgmann, S. McClusky, O. Lenk, A. Barka, O. Gürkan, L. Hearn, K. L. Feigl, R. Çakmak, B. Aktuğ, H. Özener, M. N. Töksoz, "Coseismic and Postseismic Fault Slip for the 17 August 1999, M=7.5, Izmit, Turkey Earthquake", *Science* 289, 1519–1524, 2000.

[40] Y. Yılmaz, "Morphotectonic development of the southern Black Sea Region and the Bosphorus Channel", In: Yanko-Hombach V, Gilbert A, Panin N, Dolukhanov P (Eds.) The Black Sea Flood Question: Changes in Coastline, Climate, and Human Settlement. NATO Science Series IV-Earth and Environmental Sciences. Kluwer Academic Press, Springer, Dordrecht, The Netherlands, pp. 537–569, 2007.

[41] Y. Yılmaz, G. Gökaşan, A. Y. Erbay, "Morphotectonic development of the Marmara Region", Tectonophysics 488, 51–70, 2010.

[42] X. Le Pichon, A. M. C. Sengor, T. Taymaz, "The Marmara fault and the future İstanbul earthquake", In: Karaca M, Ural DN, editors. *ITU-IAHS international conference on the Kocaeli earthquake, 17 August 1999*, İstanbul Technical University, Turkey, p. 41–54, 1999.

[43] T. Parsons, "Recalculated probability of M47 earthquakes beneath the Sea of Marmara, Turkey", Journal of Geophysical Research; 109:B05304, 2004. doi:10.1029/2003JB002667

[44] X. Le Pichon, N. Chamot-Rooke, C. Rangin, A. M. C. Şengör, "The North Anatolian Fault in the Sea of Marmara", *Journal of Geophysical Research* 108 (B4): 2179, 2003. doi:10.1029/ 2002JB001862

[45] R. Armijo, N. Pondard, B. Meyer, G. Uçarkuş, B. M. De Lepinay, J. Malavieille, S. Dominguez, M A. Gustcher, S. Schmidt, C. Beck, N. Çağatay, Z. Cakir, C. Imren, K. Eris, B. Natalin, S. Özalaybey, L. Tolun, I. Lefevre, L. Seeber, L. Gasperini, C. Rangin, Ö. Emre and K. Sarıkavak. "Submarine fault scarps in the Sea of Marmara pull-apart (North Anatolian Fault): Implications for seismic hazard in İstanbul", *Geochemistry, Geophysics, and Geosystems:* 6 (6) 1–29, 2005. doi:10.1029/2004GC000896

[46] N. N. Ambraseys, C. Finkel, "The Saros-Marmara earthquake of 9 August 1912", *Journal of Earthquake Engineering and Structural Dynamics*, 15/1: 189–212, 1987.

[47] A. Ansal, A. Akinci, G. Cultrera, M. Erdik, V. Pessina, G. Tönük, G. Ameri, "Loss estimation in İstanbul based on deterministic earthquake scenarios of the Marmara Sea region (Turkey)", *Soil Dynamics and Earthquake Engineering* 29, 699–709, 2009.

[48] M. Erdik, M. Demircioğlu, K. Sesetyan, E. Durukal, "Assessment of earthquake hazard for Bakirköy, Gemlik, Bandırma, Tekirdağ and Körfez", WB MEER project-A3 component, microzonation and hazard vulnerability studies for disaster mitigation in pilot municipalities, Boğaziçi University, Kandilli Observatory and Earthquake Engineering Research Institute, 2005.

[49] R. Spence, E. So, G. Ameri, A. Akinci, M. Cocco, G. Cultrera, G. Franceschina, F. Pacor, V. Pessina, A. M. Lombardi, G. Zonno, A. Carvalho, A. Campos Costa, E. Coelho, K. Pitilakis, A. Anastasiadis, K. Kakderi, M. Alexoudi, "Technical report on the scenario earthquake definitions for three cities", Deliverable 83, Project lessloss on risk mitigation for earthquakes and landslides, Sub-Project 10 - earthquake disaster scenario predictions and loss modelling for urban areas. Sixth Framework Programme, 2005.

[50] M. Erdik, Z. Cagnan, C. Zulfikar, K. Sesetyan, M. B. Demircioğlu, E. Durukal, C. Kariptas, "Development of Rapid Earthquake Loss Assessment Methodologies for Euro-MED Region", *Proc. 14. World Conference on Earthquake Engrg*. Paper ID: S04-004, 2008.

[51] IMM – OYO – Boğaziçi University, Kandilli Observatory and Earthquake Research Institute, 2009, Earthquake scenario of İstanbul city.

ISSN 2303-4521
PERIODICALS OF ENGINEERING AND NATURAL SCIENCES
Vol. 5 No. 1 (2017) – Special Issue (Recent Topics in Environmental Science)
Available online at: http://pen.ius.edu.ba

The Production of Polyurethane from Waste Vegetable Oil-Based Polyols and Modelling of Rheological Properties

Ercan Aydoğmuş
Department of Chemical Engineering, Faculty of Engineering,
Fırat University, 23119, Elazığ, Turkey

Fethi Kamışlı
Department of Chemical Engineering, Faculty of Engineering,
Fırat University, 23119, Elazığ, Turkey

Abstract
Polyols in polyurethane production is of great importance. The future will increase the production of polyols from renewable sources. The result of the reduction of fossil fuels will be important in the use of renewable resources. Especially important alternative which will expand polyols production from vegetable oils. Polyols derived from vegetable oil will be produced by epoxidation, hydroxylation and purification.
In this study, some vegetable-oil based polyols were produced from the different wastes vegetables oils with the catalysts. The produced polyols compared with commercial polyols with rheological properties as viscosity, temperature, shear stress, shear rate. The rheological properties of the polyols were modelling with general equations based on experimental data.
Polyurethane produced from waste vegetable oil-based polyols and investigated density and effective thermal conductivity.

Keywords: Waste Vegetable Oil-Based Polyols; Polyurethane; Rheological Properties; Modelling

1. Introduction

Polyurethane, low thermal conductivity, easy to use, flexibility, high mechanical strength, it is preferred in many fields. Polyols are the most important raw materials in the polyurethane industry. But the world's oil supply is decreasing rapidly with each passing day. Therefore, an inquiry from renewable sources that can replace the petroleum-based polyol. The common view is that the natural plant and animal oils of alternative raw materials.

Studies in the literature have epoxidized oil-based polyether polyol instead of soy-based polyols were produced using the vegetable oil.

Compared to petroleum-based polyols in polyurethane production from vegetable oil polyol produced with a smaller amount of isocyanate used. The polyurethane produced with the polyol produced from vegetable oil decreased compression resistance [8].

The polyurethane material in the work they added crystallized calcium carbonate and silica particles. It has been shown to become smaller the size of filler by adding the closed spherical cells. Mechanical properties of polyurethane materials were modeled. Moreover, the effect of the particle size of the filler was investigated [11].

Wood powder was added as filler to the polyurethane derived from castor oil-based polyol. The polyurethane of the swelling time was compared with commercial polyols, and castor oil-based polyols. Increasing the filler had negative impact on the effective thermal conductivity. Effective thermal conductivity compared to commercial polyurethane material of the castor oil-based polyurethane material has been found to be lower. Increasing the filler has negative impact on the effective heat transfer coefficient. Density polyurethane material has been found to be between 36 and 39 kg/m^3. TGA value of the thermal stability of the castor oil-based polyurethane material has been found to be more commercially polyol product [12].

Boron organic compounds were used as filler in polyurethane production. Boron organic based - polyurethane compounds were observed that decrease with the increase friability. Boron organic compounds rates were seen to increase with the increase of compressive strength. The softening temperature has been found that increasing the content of boron organic compounds fell from 230 ° C to 180 ° C [16].

The goal of this study is to determine the rheological properties and modeling for polyols and the viscosity to each waste vegetable oil based-polyols are measured at different temperatures (25, 30, 35, 40, 45 and 50 °C) by using a rotary viscometer (Brookfield DV-II). Samples were sheared with several different rotational speeds at

DOI: 10.21533/pen.v5i1.79

an increasing order. One of the most important parameters required in the design of technological processes in polyurethane industries the viscosity of raw materials. Data obtained for apparent viscosity and rotational speed were used to describe the flow behavior by the model equations both in the forward (increasing shear rate) and backward (decreasing shear rate) - measurement.

2. Material and Methods

The polyols are produced from the waste vegetable oils in three consecutive steps which are epoxidation, hydroxylation and purification. The temperature of the system is kept under the control in order to keep temperature at certain value. When it is reached to the desired reaction temperature, the peroxides are added into the vegetable oils in acidic medium by the aid of dropping funnel in the certain time.

After the reaction is completed, the mixture is taken into separatory funnel and after for a while the mixture separates in two phases with the upper phase of the epoxidized vegetable oil. After the epoxidation step, neutralization with water and the hydroxylation starts. Especially hydroxylation with alcoholysis is frequently preferred in the production of polyols. The purification process is being carried with rotary evaporator to get rid of impurities such as water, heptane and etc. The polyols produced from the vegetable oil are being used in the production of polyurethane by checking the number of hydroxyl. The structures of the hydroxyl compounds were investigated with the FTIR spectrometer. The polyurethane was produced from the different vegetable oil-based polyols and commercial polyols. The characteristic properties of the polyurethane such as thermal conductivity, the structures of porosity, density were determined. The polyurethane produced from the different vegetable oils is being compared one another in terms of thermal properties.

The improvement in the thermal properties of polyurethane is quite important in terms of energy efficiency since polyurethane is used for insulation in the building. Therefore, the thermal properties of the polyurethane produced from the vegetable oils have tried to improve by using different type of catalyst. Polyurethane catalysts help to improve the mechanical and thermal properties and are asked to contribute to the economy by reducing dependence on foreign raw materials towards polyol synthesized from vegetable oil. It also created to compare the actual results with theoretical models and the damage to the environment of raw materials used in production are intended to minimize.

In this study the viscosities of the polyols produced from different the vegetable oils were measured by using a rotary viscometer (Brookfield DV-II) at different temperatures (25, 30, 35, 40, 45 and 50 °C). Samples were sheared with several different rotational speeds (2.5, 5, 10, 20, 30 and 50 rpm) at an increasing order. Data obtained for apparent viscosity and rotational speed were used to describe the flow behavior by the model equations.

3. Mathematical Models

Brookfield rotational viscometer (Model DV-II, Brookfield Engineering Laboratories) equipped with spindle 21 was used. Enough samples nearly 8 mL in the beaker were used to immerse the groove on the spindle with guard leg. Temperature was kept constant using thermostatically controlled electrical system. Shear rate (γ) and shear stress (τ) were read from viscometer directly. Shear stress and shear rate can also be calculated by using Eq. (1), (2) and (3).

$$\gamma = \beta.N \quad (1)$$

$$\tau = \mu.\gamma \quad (2)$$

$$\tau = k.(\gamma)^n \quad (3)$$

Where; N is rotational speed (rpm), τ is shear stress (Pa), μ is the apparent viscosity (mPa. s), k is the consistency coefficient (mPa.s), n is flow behavior index and β is coefficient (dimensionless).

$$\mu_{linear} = A.T + B \quad (4)$$

$$\mu_{exponential} = C.\exp(D.T) \quad (5)$$

$$\mu_{power} = E.T^F \quad (6)$$

$$\mu_{logarithmic} = G.\ln(T) + H \quad (7)$$

$$\mu_{polynomial} = I.T^2 + J.T + K \quad (8)$$

$$\mu_{new} = \exp(-T) + a.T + b \quad (9)$$

4. Figures and Tables

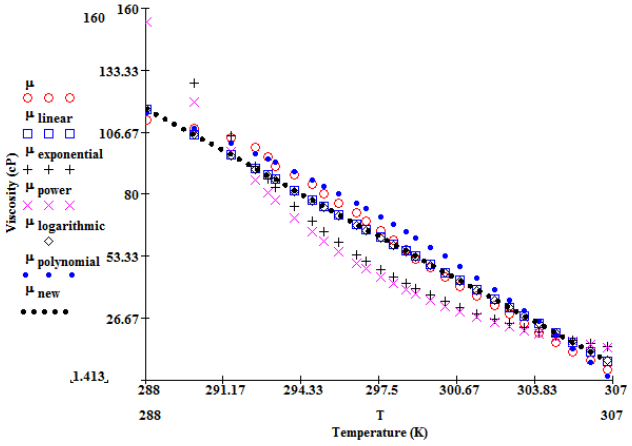

Figure 1. The effect of temperature on viscosity, hazelnut oil-based polyols (H), comparison with model equations.

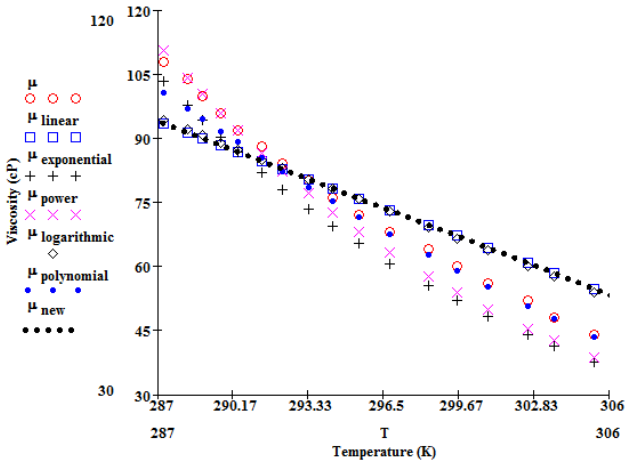

Figure 2. The effect of temperature on viscosity, canola oil-based polyols (Ca), comparison with model equations.

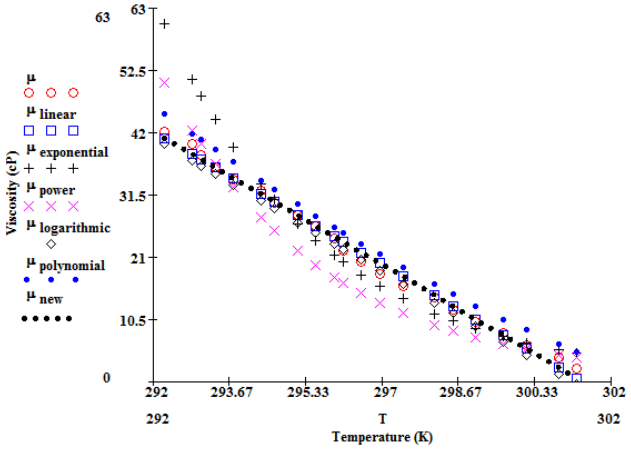

Figure 3. The effect of temperature on viscosity, linseed oil-based polyols (L), comparison with model equations.

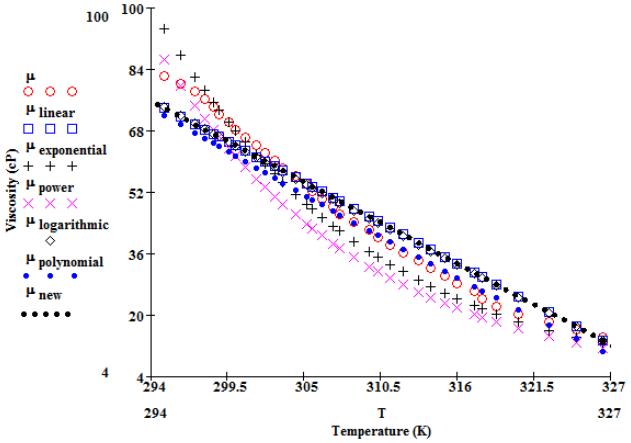

Figure 4. The effect of temperature on viscosity, corn oil-based polyols (Co), comparison with model equations.

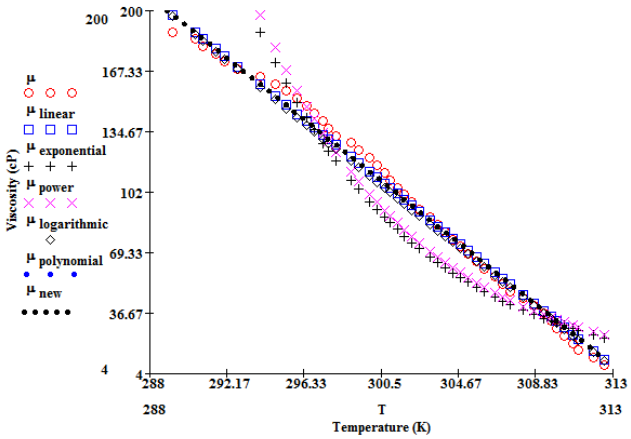

Figure 5. The effect of temperature on viscosity, cottonseed oil-based polyols (Cs), comparison with model equations.

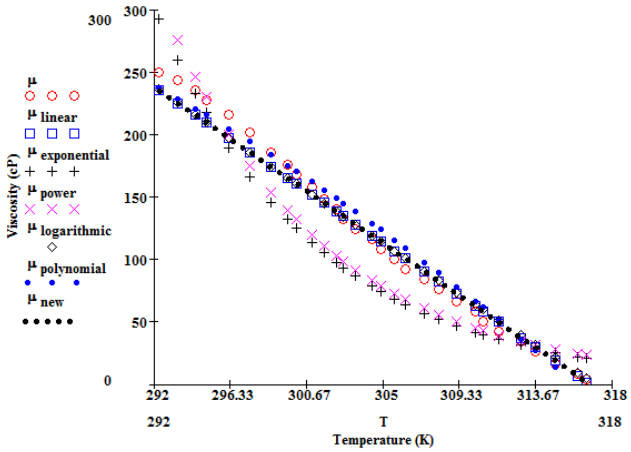

Figure 6. The effect of temperature on viscosity, soybean oil-based polyols (S), comparison with model equations.

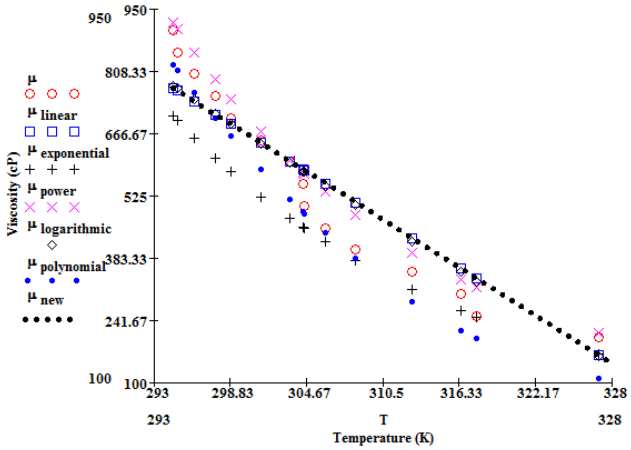

Figure 7. The effect of temperature on viscosity, commercial polyols (C), comparison with model equations.

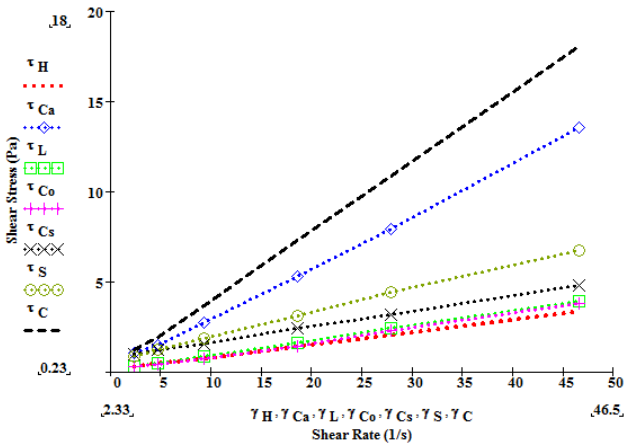

Figure 8. Shear stress vs shear rate for different vegetable oil-based polyols

Table 1. Correlation coefficients for linear model

Polyols	A	B	R^2
Soybean	-9.6579	3058.5	0.9702
Cotton	-7.9912	2508.7	0.9855
Corn	-1.9308	643.23	0.9588
Hazelnut	-5.8209	1793.2	0.9567
Canola	-2.1367	707.18	0.9296
Linseed	-4.4974	1355.3	0.9929

Table 2. Correlation coefficients for exponential model

Polyols	C	D	R^2
Soybean	2.10^{6}	-0.109	0.7668
Cotton	5.10^{16}	-0.113	0.7897
Corn	2.10^{10}	-0.065	0.8920
Hazelnut	4.10^{18}	-0.131	0.7809
Canola	1.10^{9}	-0.056	0.9653
Linseed	5.10^{37}	-0.283	0.9066

Table 3. Correlation coefficients for power law model

Polyols	E	F	R^2
Soybean	6.10^{82}	-32.56	0.7542
Cotton	7.10^{85}	-33.85	0.7809
Corn	4.10^{51}	-20.11	0.8773
Hazelnut	1.10^{97}	-38.55	0.7717
Canola	2.10^{44}	-17.19	0.9593
Linseed	4.10^{208}	-83.91	0.9044

Table 4. Correlation coefficients for logarithmic model

Polyols	G	H	R^2
Soybean	-2906	16736	0.9667
Cotton	-2400	13798	0.9830
Corn	-601.1	3492.4	0.9600
Hazelnut	-1721	9862.8	0.9524
Canola	-663.2	3848.3	0.9404
Linseed	-1335	7619.5	0.9935

Table 5. Correlation coefficients for polynomial model

Polyols	I	J	K	R^2
Soybean	-0.095	47.629	-5576.5	0.979
Cotton	-0.105	55.433	7025.3	0.995
Corn	0.006	-5.377	1179.4	0.961
Hazelnut	-0.144	79.46	-10842	0.987
Canola	0.039	-26.51	4465.6	0.994
Linseed	0.132	-82.93	12991	0.998

Table 6. Correlation coefficients for new model

Polyols	a	b	R^2
Soybean	-9.65795	3058.480	0.9996
Cotton	-7.97888	2505.030	0.9997
Corn	-1.93083	643.2298	0.9998
Hazelnut	-5.82090	1793.152	0.9998
Canola	-2.13662	707.1342	0.9997
Linseed	-4.49741	1355.300	1.0000

5. Results and Discussion

In this study, the temperature dependence of the viscosity of the vegetable oil-based polyol; model equations compared with experimental data. In Figures: 1, 2, 3, 4, 5, 6 and 7; the variation of apparent viscosities of polyols as a function of temperature were compared with model equations and experimental results. Operating temperatures of the assay were measured by raising temperature stepwise in a water bath. Waste vegetable oil-based polyols were measured by different rotational speeds (2.5, 5, 10, 20, 30 and 50 rpm) at an increasing order. According to the experimental results regression coefficients of model equations (4), (5), (6), (7), (8) and (9) were determined.

In this study, variations of viscosities of soybean oil, cottonseed oil, corn oil, hazelnut oil, canola oil, linseed oil-based polyols and commercial polyols were determined a function of temperature. It is known that the viscosity of the fluid decreases as temperature increases. The tested polyols showed Newtonian and non- Newtonian fluids behavior at certain temperature range.

As can be seen in Figures (1), (2), (3), (4), (5), (6) and (7) the viscosities of all types polyols irrespective of their production sources decrease substantially with increasing temperature. Heating may rapture molecular entanglement and bonds may stabilize the molecular structure and reduce the effect molecular volume in the polyols. In other words, as temperature increases, thermal energy of

molecules increases and molecular distance develop due to reduction of intermolecular force and hence viscosity of fluid decreases. When thermal energy of molecules increases, molecular entanglement aligns easily and molecular structure stabilizes quickly since the molecules with high thermal energy move over one another easily.

As can be seen in Figure 8 the highest viscosity belongs to the commercial polyols while the lowest viscosity belongs to the polyol obtained from the raw hazelnut oil. The viscosities of polyols from high to low can be put in order as $\mu_c > \mu_{ca} > \mu_s > \mu_{cs} > \mu_c > \mu_L > \mu_{co} > \mu_h$, here μ_c, μ_{ca}, μ_s, μ_{cs}, μ_c, μ_L, μ_{c0} and μ_h denote the viscosities of commercial polyol and polyols obtained from raw canola oil, soybean oil, cottonseed oil, linseed oil, corn (maize) oil and raw hazelnut oil, respectively. Furthermore it can been seen that all types of polyols show almost Newtonian behavior.

The regression coefficients and correlation coefficients of each model equation for each polyol obtained from different vegetable oils are given Tables 1, 2, 3, 4 and 5. As can be figured out from comparison of Tables, high values of R-squared were obtained for polynomial model irrespective of polyols obtained sources. Moreover, the developed new model has the highest values for R-squared.

Several types of polyurethane structures were produced with the waste vegetable oil based polyols. The effective thermal conductivities of these structures were measured. The influences of the thermal conductivity of polyurethane, the porosity, the size and spatial distribution of pores on the effective thermal conductivity of these structures were analyzed. The results indicated that the effective thermal conductivity of the polyurethane varied between 0.020 W/m K and 0.030 W/m K. Effective thermal conductivity was measured with TLS 100 instrument according to method of ASTM D5334.

In addition, density of polyurethane samples produced from vegetable base-polyols were measured to be 18 and 55 kg/m^3. Density is inversely proportional with effective thermal conductivity.

The petroleum-based polyols and vegetable-based polyols have different hydroxyl numbers, which were used to produce polyurethane. Waste vegetable oil based polyol in different ratios were added into the petroleum-based polyols. The mechanical properties of the polyurethane produced in the present study decreased with increasing waste vegetable oil based polyol ratios. In the experimental study, the hydroxyl numbers of vegetable-based polyols were optimized by varying temperature, reaction time and catalyst.

Waste vegetable oil-based polyols increases the number of hydroxyl groups and thus polyurethane bonding becomes stronger.

The temperature dependent-apparent viscosity of vegetable oil-based polyol; model equations and experimental data were compared with one another.

The operating temperature of the assay was measured by raising temperature stepwise in a water bath. According to the experimental data; the linear and non-linear regression were made to determine coefficients of regression in the model equations.

Abbreviations

H: Hazelnut oil-based polyols
Ca: Canola oil-based polyols
L: Linseed oil-based polyols
Co: Corn oil-based polyols
Cs: Cottonseed oil-based polyols
S: Soybean oil-based polyols
C: Commercial polyols
μ: Apparent viscosity (cP)
γ: Shear rate (1/s)
τ: Shear stress
N: Rotational speed (rpm)
k: Consistency coefficient (mPa.s)
n: Flow behavior index
β: Coefficient (dimensionless)

References

[1] A. Andersson, S. Lundmark, A. Magnusson and F. H. J. Maurer, "Vibration and Acoustic Damping of Flexible Polyurethane Foams Modified with a Hyper branched Polymer," *Journal of Cellular Plastics*, vol. 01, pp. 01-21, 2009.

[2] J. L. R. Armenta, T. Heinze and A. M. M. Martinez, "New Polyurethane Foams Modified with Cellulose Derivatives," *European Polymer Journal*, vol. 40, pp. 2803-2812, 2004.

[3] R. Bashirzadeh and A. Gharehbaghi, "An investigation on reactivity, mechanical and fire properties of PU flexible foam," *Journal of Cellular Plastics*, vol. 01, pp. 01-30, 2009.

[4] X. C. Bian, J. H. Tang and Z. M. Li, "Flame retardancy of whisker silicon oxide/rigid polyurethane

foam composites with expandable graphite," *Journal of Applied Polymer Science,* vol. 110, pp. 3871-3879, 2008.

[5] X. C. Bian, J. H. Tang and Z. M. Li, "Flame retardancy of hollow glass microsphere/rigid polyurethane foams in the presence of expandable graphite," *Journal of Applied Polymer Science,* vol. 110, pp. 3871-3879, 2008.

[6] D. S. Han, I. B. Park, M. H. Kimi, B. J. Noh, W. S. Kim and J. M. Lee, "The effects of glass fiber reinforcement on the mechanical behavior of polyurethane foam," *Journal of Mechanical Science and Technology,* vol. 24, pp. 263-266, 2010.

[7] L. Indennidate, D. Cannoletta, F. Lionetto, A. Greco and A. Maffezzoli, "Nanofilled polyols for viscoelastic polyurethane foams," *Society of Chemical Industry,* vol. 59, pp. 486-491, 2009.

[8] A. A. Lubguban, Y. C. Tu, Z. R. Lozada, F. H. Hsieh and G. J. Suppes, 2009, "Noncatalytic polymerization of ethylene glycol and epoxy molecules for rigid polyurethane foam applications," *Journal of Applied Polymer Science,* vol. 112, pp. 2185-2194, 2009.

[9] X. Y. Meng, L. Ye, X. G. Zhang, P. M. Tang, J. H. Tang, X. Ji, and Z. M. Li, "Effects of expandable graphite and ammonium polyphosphate on the flame-retardant and mechanical properties of rigid polyurethane foams," *Journal of Applied Polymer Science,* vol. 114, pp. 853-863, 2009.

[10] D. Mello, S. H. Pezzin and S. C. Amico, "The effect of post-consumer pet particles on the performance of flexible polyurethane foams", *Polymer Testing,* vol. 28, pp. 702-708, 2009.

[11] F. S. Michel, L. Chazeau and J. Y. Cavaillé, "Mechanical properties of high density polyurethane foams: II effect of the filler size," *Composites Science and Technology,* vol. 66, pp. 2709-2718, 2006.

[12] M. A. Mosiewicki, G. A. Dell'Arciprete, M. I. Aranguren and N. E. Marcovich, "Polyurethane foams obtained from castor oil-based polyol and filled with wood flour," *Journal of Composite Materials,* vol. 01, pp. 1-16, 2009.

[13] M. M. A. Nikje and Z. M. Tehrani, "Thermal and mechanical properties of polyurethane rigid foam/modified nanosilica composite," *Polymer Engineering and Science,* vol. 50, pp. 468-473, 2010.

[14] M. M. A. Nikje and Z. M. Tehrani, "Polyurethane rigid foams reinforced by doubly modified nanosilica," *Journal of Cellular Plastics,* vol. 01, pp. 01-14, 2010.

[15] I. Racz, E. Andersen, M. I. Aranguren and N. E. Marcovich, "Wood flour-recycled polyol based polyurethane lightweight composites," *Journal of Composite Materials,* vol. 43, pp. 2871-2884, 2009.

[16] J. P. Sadowska and B. Czupryński, "New compounds for production of polyurethane foams," *Journal of Applied Polymer Science,* vol. 102, pp. 5918-5926, 2006.

[17] M. Thirumal, K. Dipak, N. K. Singha, B. S. Manjunath and Y. P. Naik, "Effect of a nanoclay on the mechanical, thermal and flame retardant properties of rigid polyurethane foam," *Journal of Macromolecular Science,* vol. 46, pp. 704-712, 2009.

[18] M. Thirumal, N. K. Singha, K. Dipak, B. S. Manjunath and Y.P. Naik, "Halogen-free flame-retardant rigid polyurethane foams: effect of alumina trihydrate and triphenylphosphate on the properties of polyurethane foams," *Journal of Applied Polymer Science,* vol. 116, pp. 2260-2268, 2010.

ISSN 2303-4521
PERIODICALS OF ENGINEERING AND NATURAL SCIENCES
Vol. 5 No. 1 (2017) – Special Issue (Recent Topics in Environmental Science)
Available online at: http://pen.ius.edu.ba

Pyrolysis Kinetics of Pine Sawdust in a Fixed Bed

Melek Yılgın
Department of Chemical Engineering, Faculty of Engineering, Fırat University, 23119, Elazığ, Turkey

Dursun Pehlivan,
Department of Chemical Engineering, Faculty of Engineering, Fırat University, 23119, Elazığ, Turkey

Ercan Aydoğmuş
Department of Chemical Engineering, Faculty of Engineering, Fırat University, 23119, Elazığ, Turkey

Neslihan Duranay
Department of Chemical Engineering, Faculty of Engineering, Fırat University, 23119, Elazığ, Turkey

Abstract
Currently worldwide studies are being done on the utilisation of lignocellulosic materials or biomasses as substitutes of fossil fuels to afford energy needs of today's world. Pyrolysis is one of the most promising techniques for apprising biomass into economically viable renewable fuels. In this work, pyrolysis behaviour of pine sawdust was investigated experimentally in a fixed bed system with mass measurements under nitrogen as sweeping gas. The main objective was to interpret mass loss of pine sawdust during pyrolysis at varied heating rates and to estimate kinetic constants using the best mathematical model among the popular solid phase decomposition models. Regression tests are separately applied to conversion data for 473 – 593 K and 593 – 773 K temperature ranges, corresponding respectively decomposition of hemicelluloses and cellulose, and cellulose and lignin. The quality of fit increased with heating rate and none of the proposed models had any superiority to others. The results implied that volatiles evolution during pyrolysis was increasingly controlled chemically with heating rate.

Keywords: Pine wood, pyrolysis, kinetics, fixed bed

1. Introduction

Depletion in the fossil fuel reserves, considerations about global warming and environmental pollution caused by fossil fuel usage has persuaded the efforts to seek renewable energy options worldwide. Biomass can be looked upon environmentally-friendly and sustainable energy source to reduce net carbon emissions [1,2]. Some benefits on the environment can be acquired from the ease of use of agricultural and forest residues and the raw materials involving them. If the bio-wastes are not handled properly, they may create major environmental problems [3].

Thermochemical conversion processes such as combustion, gasification and pyrolysis of lignocellulosic biomasses have received very much attention as methods for renewable energy and fuel production during the last decades [4]. These technologies, which come usually into mind in environmental issues, furnish perfect ways in the utilisation of agricultural and forest wastes for supplying energy. Lignocellulosic biomasses are usually heterogeneous materials of complex chemical structure. Because their physical and chemical compositions vary over a wide range depending on the source, the applicability of thermo-chemical process technologies has become more complicated. For example, wood is composed of hemicelluloses, cellulose and lignin which decompose respectively 225-325 ℃, 305-375 ℃ and 250-500 ℃ temperature ranges [5].

Among the processes, pyrolysis has received major consideration because it is not only a one-step process but also first stage of combustion or gasification processes. During pyrolysis, the macromolecules of biomass are decomposed to form a bio char while concurrently evolving condensable vapours (liquids) and gas of lighter molecular mass than the parent molecules. The liquids and gases obtained can be used as fuels where their composition and heating value are appropriate [6]. Thermal decomposition kinetics of biomass is of prime importance in conversions for energy and secondary renewable products to design effectively any thermo-chemical process [7].

Thermal decomposition reactions during pyrolysis of wood can be tracked by measuring continuously its mass loss as in a traditional Thermal Gravimetric Analysis (TGA) and quantitative methods developed for reaction chemistry can be applied to obtain kinetic parameters of reaction order, activation energy and pre-exponential factor [8]. These parameters are functions of heating rate, material size, moisture content and heating medium. Thermal analysis results are

DOI: 10.21533/pen.v5i1.80

dominantly used factors to form the reactivity equations. Although the magnitude of pre-exponential factor depends on the nature of decomposing material, activation energy is affected considerably by heating rate. For this reason, reactivity of wood is usually expressed by its own activation energy [9]. With the growing concern given on biomass pyrolysis for conversions into renewable fuels, immense literature on the wood decomposition kinetics has accumulated during the past decades. Although TGA instruments are sophisticated devices for decomposition kinetics of samples as few amounts of solid powder, which may in some instances not be representative of whole material, valuable results could be obtained with larger amounts than those used in TGA. It is therefore, the objective of this work to track the mass of decomposing biomass during pyrolysis and use the data to elucidate the suitability of the mathematical models given in literature until now.

2. Material and Methods

Pine wood chips for this study were supplied from a local wood workshop in Elazig. After grinding, they were sieved and 16 + 35 mesh size is retained for the experiments. Mass data during pyrolysis of sample was obtained using the system shown in Figure 1. The heating chamber consists of an electrically heated 35mmIDx90mmOD 120 mm length vertical chamber of refractory block holding heating elements. A 20mmIDx22mmOD 250mm length quartz tube was situated into the chamber. At the inlet, the tube has a circular refractory lid with 10 mm diameter hole which held a bended glass tube for entrance of nitrogen as sweeping gas. Quartz tube has a 14 mm diameter stainless steel wire mesh basket inside, fitted to top end of a 1.4 mm diameter and 250 mm length vertical stainless steel rod. The bottom end of the rod is fitted to a square stainless steel plate standing on a top balance of 0.001 g accuracy. To prevent condensation of the pyrolysis vapours on the balance, bottom end of the quartz tube has a glass adapter whose diameter decrease smoothly to 6mm towards the rod.

Before the experiments, refractory lid of quartz tube was removed and 1.00 g pine wood sample was dropped on the basket using a glass funnel. After reassembling the lid, nitrogen flow (100 ml.min^{-1}.) was allowed to pass through the quartz tube for 5 min. After that, heating of the chamber was started and first mass reading was taken. The mass recordings during pyrolysis were made at 2 min. intervals. Heating and temperature control of the chamber were accomplished by using a variable output voltage transformer which powers a PID programmable temperature controller with a NiCr thermocouple positioned at the same level with the basket in the quartz tube. Nitrogen flow was maintained throughout the run. Heating rates of 5, 10 and 15 ℃ /min. were applied in the separate runs.

Pyrolysis was continued 15 min. after heating the chamber to the final 500 ℃ temperature. After that heating was stopped and the system was left to cool under nitrogen flow. The basket was removed and mass of pyrolysis residue on the basket was weighted to compare to the last mass readings.

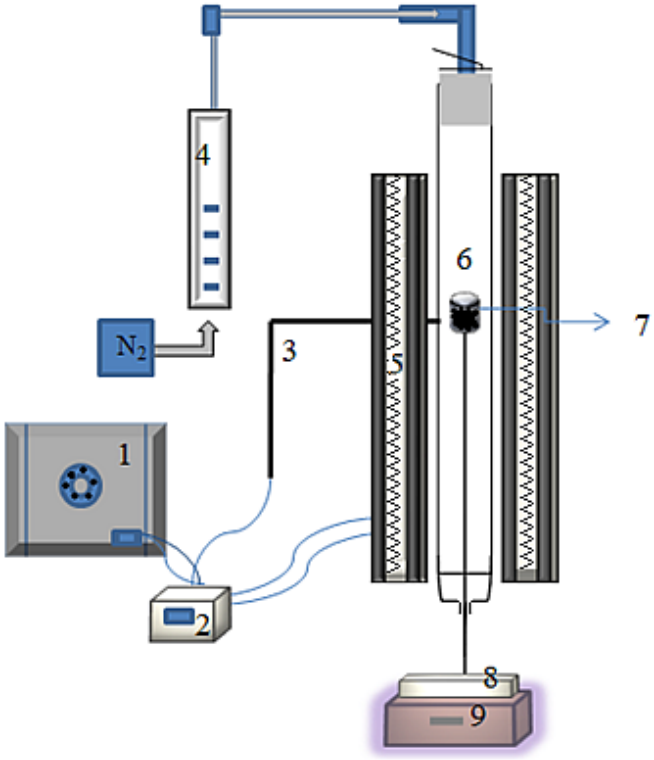

Figure 1. Experimental system; 1, variable output transformer; 2, temperature controller; 3, thermocouple; 4, flow meter; 5, vertical furnace; 6, quartz tube; 7, basket; 8, supporting plate; 9, top balance

3. Mathematical Model

Pyrolysis rate of a solid depends on the temperature and the amount of material. If it is assumed that only a single reaction is involved, the following equations for α conversion ratio and its changing rate can be used to describe the progress of reaction:

$$\alpha = \frac{W_0 - W}{W_0 - W_\infty} \quad (1)$$

$$\frac{d\alpha}{dt} = k(T)f(\alpha) \quad (2)$$

where t and T are time and absolute temperature respectively. Subscripts 0 and ∞ stand for the initial and final mass of decomposing material respectively while w denotes the mass at any time. f(α) is the kinetic function related to the reaction mechanism. Many different equations for f(α) each has certain reasonable theoretical grounds are given in literature for the solid phase decomposition reactions [10,11]. Some of them,

which are tested by the experimentally obtained mass change data, are listed in Table 1.

Normally Arrhenius expression is used for the rate constant:

$$k = A\exp\left(-\frac{E}{RT}\right) \quad (3)$$

Here E, A and R are the activation energy, pre-exponential factor and gas constants respectively. Then, Eq. (2) becomes.

$$\frac{d\propto}{dt} = A\exp\left(-\frac{E}{RT}\right) f(\propto) \quad (4)$$

Reaction time and temperature can be used interchangeably when the sample temperature increases linearly with time during reaction. If linear heating rate is b, Eq. (4) can be written as.

$$\frac{d\propto}{dT} = \frac{A}{b}\exp\left(-\frac{E}{RT}\right) f(\alpha) \quad (5)$$

Integration gives g(α)

$$g(\alpha) = \int_0^{\alpha} \frac{d\alpha}{f(\alpha)} = \frac{A}{b}\int_0^{T\propto} \exp\left(-\frac{E}{RT}\right) dT \quad (6)$$

The expressions of g(α) corresponding to each kinetic function are also shown in Table 1. It is possible to determine kinetic parameters by using either kinetic function or its integral. In the integral method, the integral on the right side of Eq. (6) should be solved. Unfortunately, it has no exact analytical solution and some approximations are generally used. If u= E/RT is defined, Eq. (6) can be written in the following form.

$$g(\propto) = \frac{AE}{bR}\int_u^{\infty} \frac{\exp(-u)}{u^2} du = \frac{AE}{bR} p(u) \quad (7)$$

where p(u) represent the rightmost term known as the temperature integral in Eq. (6). In the Coats and Redfern method, p(u) in Eq. (7) is approximated by using a Taylor series expansion to yield the following expression (12):

$$\ln\frac{g(\alpha)}{T^2 Q(E/RT)} = \ln\frac{AR}{bE} - \frac{E}{RT} \quad (8)$$

Table 1. Algebraic expressions for f(α) and g(α) considered in this work

Kinetic Models	f(α)	g(α)
Parabolic Law (**D1**)	$\frac{1}{\alpha}$	$\frac{\alpha^2}{2}$
Holt-Cutler-Wadsword (**D2**)	$1/-ln(1-\alpha)$	(1-α)ln(1- α)+α
Jander (**D3**)	$\frac{(1-\alpha)^{2/3}}{1-(1-\alpha)^{1/3}}$	$\frac{3}{2}(1-(1-\alpha)^{1/3})^2$
Ginstling-Brounshtein (**D4**)	$\frac{(1-\alpha)^{1/3}}{1-(1-\alpha)^{1/3}}$	$\frac{3}{2}(1-\frac{2\alpha}{3}-(1-\alpha)^{2/3})$
Zhuravlev-Lesokhin-Tempelmen (**D5**)	$\frac{(1-\alpha)^{5/2}}{1-(1-\alpha)^{1/3}}$	$\frac{3}{2}((1-\alpha)^{-\frac{1}{3}}-1)^2$
Komatsu-Uemuro (anti Jander) (**D6**)	$\frac{(1+\alpha)^{2/3}}{(1+\alpha)^{1/3}-1}$	$\frac{3}{2}((1+\alpha)^{\frac{1}{3}}-1)^2$

Table 2. Proximate analyse results of the pine wood sample (%w)

Moisture	5.12
Volatile matter	80.73
Ash	1.10
Fixed carbon*	13.05

*: By difference

4. Results and Discussion

Proximate analysis results of pinewood are given in Table 2. The amount of volatile matter implies that more than 80% of pinewood could be volatilized under thermal decomposition conditions. Figs. 2, 3, 4 show mass recording results of pine sawdust during pyrolysis at three heating rates from room temperature to 500 ℃. It is clearly seen that thermal decomposition curves look like traditional TGA curves and can be divided into three regions according to their changing pattern. The first region of small slope may be attributed to evaporation of physically adsorbed water, smaller molecular weights volatiles and partial decomposition of hemicelluloses. The second region of higher slope than the first represents predominantly decomposition of major wood components of hemicelluloses, cellulose and lignin. In the third region of small slope secondary decomposition reactions of major wood components take place [5]. In order to get better fit of the data for the selected models, two temperature regions, over which certain wood components predominantly decompose, were assumed. Mass loss over 473 – 593 K range is contributed by decomposition of mainly hemicelluloses, lesser extent cellulose and weakly lignin, whereas mass loss over 593 – 773 K range is contributed moderately by decomposition of cellulose and mainly lignin. For this reason, regression tests are separately applied for conversion ratio data corresponding to these regions. The results obtained with these models are given in Table 3. It can be seen that quality of fit or regression coefficients are not high for 5 K/min. and increase with heating rate, reaching to 0.968 for Zhurovlev–Lesokhin–Tempelman model. However, none of the models seem to have any appearent superiority to others for the two temperature ranges and at three heating rates. Thus, only kinetic parameters are seen to be comparable with the results obtained for similar biomasses. Activation energies change between 18.0-20.1, 24.4-32.8 and 44.5-47.8 kJ/mole for heating rates of 5, 10 and 15 K/min. respectively, which imply effect of chemical control on the volatiles evolution during pyrolysis increase with

heating rate. For a single heating rate, the differences between magnitudes of activation energies are not considerable. However, values of activation energies are higher at higher heating rates.

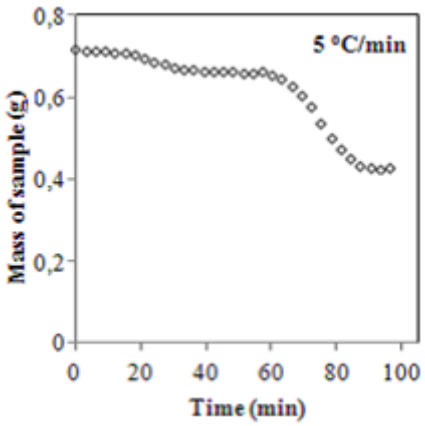

Figure 2. Changes in mass of pine wood during pyrolysis at 5 ℃/min heating rates to 500 ℃

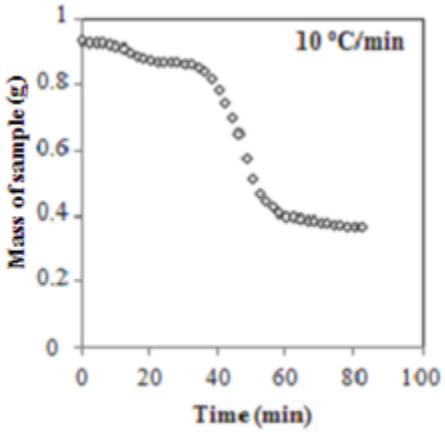

Figure 3. Changes in mass of pine wood during pyrolysis at 10 ℃/min heating rates to 500 ℃

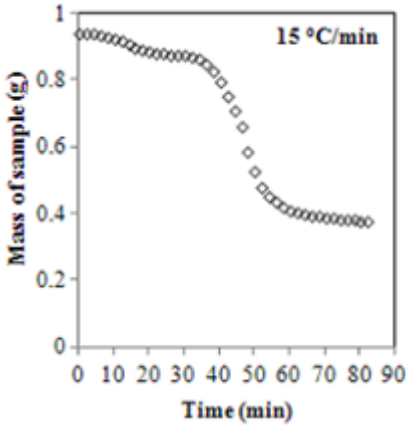

Figure 4. Changes in mass of pine wood during pyrolysis at 15 ℃/min heating rates to 500 ℃

Table 3. Kinetic parameters from regression analysis of conversion ratios for final temperature of 773 K

Heating rate (K/min)	Mathematical Model	Components	Temperature range (K)	Ea (KJ/mol)	A (min^{-1})	R^2
5	Parabolic Law	Hemicel.+ Cellulose	473 – 593	18.7	0.007	0.842
		Lignin	593 – 773	19.0	0.002	0.818
	Holt – Cutler – Wadsworth	Hemicel.+ Cellulose	473 – 593	19.1	0.008	0.844
		Lignin	593 – 773	19.5	0.002	0.819
	Jander	Hemicel.+ Cellulose	473 – 593	19.4	0.003	0.847
		Lignin	593 – 773	20.0	0.001	0.821
	Ginstling – Brounshtein.	Hemicel.+ Cellulose	473 – 593	19.2	0.003	0.845
		Lignin	593 – 773	19.7	0.001	0.820
	Zhurovlev–Lesokhin - Tempelman	Hemicel.+ Cellulose	473 – 593	20.1	0.004	0.851
		Lignin	593 – 773	21.1	0.001	0.824
	Komatsu – Uemura	Hemicel.+ Cellulose	473 – 593	18.1	0.002	0.837
		Lignin	593 – 773	18.0	0.001	0.814
10	Parabolic Law	Hemicel.+ Cellulose	473 – 593	31.4	0.065	0.909
		Lignin	593 – 773	25.6	0.005	0.892
	Holt – Cutler – Wadsworth	Hemicel.+ Cellulose	473 – 593	31.7	0.072	0.910
		Lignin	593 – 773	26.3	0.006	0.892
	Jander	Hemicel.+ Cellulose	473 – 593	32.1	0.027	0.912
		Lignin	593 – 773	26.9	0.002	0.893
	Ginstling – Brounshtein	Hemicel.+ Cellulose	473 – 593	31.9	0.025	0.911
		Lignin	593 – 773	26.5	0.003	0.893
	Zhurovlev – Lesokhin -	Hemicel.+ Cellulose	473 – 593	32.8	0.034	0.914

	Tempelman	Lignin	593 – 773	28.3	0.004	0.894
	Komatsu – Uemura	Hemicel.+ Cellulose	473 – 593	30.7	0.018	0.907
		Lignin	593 – 773	24.4	0.002	0.890
15	Parabolic Law	Hemicel.+ Cellulose	473 – 593	46.7	3.365	0.965
		Lignin	593 – 773	45.3	1.198	0.956
	Holt – Cutler – Wadsworth	Hemicel.+ Cellulose	473 – 593	47.0	3.684	0.966
		Lignin	593 – 773	44.5	1.247	0.954
	Jander	Hemicel.+ Cellulose	473 – 593	47.2	1.346	0.966
		Lignin	593 – 773	45.1	1.258	0.958
	Ginstling – Brounshtein.	Hemicel.+ Cellulose	473 – 593	47.1	1.266	0.966
		Lignin	593 – 773	44.8	1.207	0.956
	Zhurovlev – Lesokhin - Tempelman	Hemicel.+ Cellulose	473 – 593	47.8	1.618	0.968
		Lignin	593 – 773	46.1	1.358	0.959
	Komatsu – Uemura	Hemicel.+ Cellulose	473 – 593	46.1	0.945	0.964
		Lignin	593 – 773	44.6	1.124	0.953

5. Conclusions

Regression coefficients for the tested models are not high for 5 K/min. However, they tend to increase with heating rate.

None of the models seems to have any appearent superiority to others for the two temperature ranges and at three heating rates.

For a single heating rate, the differences between magnitudes of activation energies for the proposed models are not considerable.

The level of activation energies for volatiles evolution during pyrolysis imply contribution of diffusion control for lower heating rates and increasing effect of chemical control with increasing heating rate.

References

[1] L. J. R. Nunes, J.C.O. Matias, J. P. S. Catalão, "Mixed biomass pellets for thermal energy production: a review of combustion models," *Apply Energy*, vol.127, pp. 135–40, 2014.

[2] S. W. Du, W. H. Chen, J. A. Lucas, "Pre-treatment of biomass by torrefaction and carbonization for coal blend used in pulverized coal injection," *Bio-resource Technology*, vol. 09, pp. 161-333, 2014.

[3] L. Li, N. Zhao, X. Fu, M. Shao, S. Qin, "Thermo-gravimetric and kinetic analysis of spirulina wastes under nitrogen and air atmospheres," *Bio-resource Technology*, vol. 140, pp. 152–157, 2003.

[4] P. McKendry, "Energy production from biomass conversion technologies," *Bio-resource Technology*, vol. 83, pp. 47–54, 2002.

[5] J. M. Prins, J. K. Ptasinski, F. J. J. G. Janssen, J. Krzysztof, "Torrefaction of wood weight loss kinetics," *JAnalApplPyrolysis*, vol. 34, pp. 77-28, 2006.

[6] C. Di Blasi, "Modeling chemical and physical processes of wood and biomass pyrolysis," *Prog. Energy Combustion*, vol. 34, pp.47–90, 2008.

[7] T. H. Damartzis, D. Vamvuka, S. Sfakiotakis, A. Zabaniotou, "Thermal degradation studies and kinetic modeling of cardoon pyrolysis using thermogravimetric analysis," *Bio-resource Technology*, vol. 102, pp. 6230–6238, 2011.

[8] S. Y. Yorulmaz, A. T. Atimtay, "Investigation of combustion kinetics of treated and untreated waste wood samples with thermo-gravimetric analysis," *Fuel Process Technology*, vol. 90, pp. 939–946, 2009.

[9] E. S. Ella, G. Yuan, T. A. Mays, Simple kinetic analysis to determine the intrinsic reactivity of coal chars, *Fuel Process Technology*, vol. 84, pp.1920–1925, 2005.

[10] J. J. M. O´rfao, F. G. Martins, "Kinetic analysis of thermo-gravimetric data obtained under linear temperature programming-a method based on calculations of the temperature integral by interpolation," *Thermochimica Acta*, vol. 390, pp. 195–211, 2002.

[11] J. E. White, W. J. Catallo, B. L. Legendre, "Biomass pyrolysis kinetics: A comparative critical review with relevant agricultural residue case studies," *JAnalApplPyrolysis*, vol. 91, pp. 1–33, 2011

ISSN 2303-4521
PERIODICALS OF ENGINEERING AND NATURAL SCIENCES
Vol. 5 No. 1 (2017) – Special Issue (Recent Topics in Environmental Science)
Available online at: http://pen.ius.edu.ba

Evaluation of Soil Quality in Sapanca Lake Basin

Asude Ateş
Faculty of Engineering, Department of Environmental Engineering Sakarya University, 54187, Sakarya TURKEY

Nihan Calişkan
Faculty of Engineering, Department of Environmental Engineering Sakarya University, 54187, Sakarya TURKEY

Hülya Demirel
Sakarya University, Sakarya Vocational School, Environmental Protection and Control Department, Sakarya TURKEY

Abstract
The aim of the study is determination of the physical and chemical properties of the soil, which is taken around the Sapanca Lake. For this purpose, a total of 30 soil samples has been collected in order to represent the basin from 10 plots where 0-40 cm depth. Sapanca Lake is an important drinking water source for the Marmara region; it is supplied in both underground and side creeks. The content and the quality of water are affected by the soil structure in the basin. Therefore, soil structure has been evaluated with regard to color, organic matter, organic carbon, conductivity, pH, oxidation-reduction potential (ORP), salinity parameters. Munsell soil color chart is used for determining soil color. In terms of determination, half of the soil samples has been found to be dark brown in color. And the according to the results has been found just as pH 7-9, conductivity 150-500 µS/cm, salinity 81-300 mg/l, ORP 81-115 mg/l, organic matter 1% -10% in the range of, respectively. Determination of soil quality parameters of the study area is very important in terms of protection of ecology and living health, controlling environmental pollution and improvement of water quality.

Keywords: Soil pollution; soil quality; Sapanca; organic compounds

1. Introduction

Living life, protection and development of ecological balance has become increasingly important due to environmental pollution in recent years. The pollution which resulting of rapid population growth, unplanned urbanization, industrialization, not using agricultural lands efficiently and occurring negative changes in wetlands is adversely affect the life. Reducing negative effects on natural resources policy should be developed by making the planning for improvement of soil and water resources. Wetlands have to live several changes over time as a part of nature and natural phenomena. These changes, not only occur through natural events but also they can occur with human intervention. Besides, changes occurring in the soil become impractical using wetlands and especially drinking water supplies. It is also one of the most important stage that land planning and management according to the evaluation of soil quality criteria. Also soil form part of the environmental quality. Researches have showed that environmental quality criteria bases to determine the quality of soil such as water quality, soil erosion and air quality values. For this purpose various studies have been made;

Ozkan, K. et al., (2007), have been identified relationship among soil color and structure, and soil type, organic matter content, total lime content and soil acidity (pH) in Beysehir Lake Basin. According to the statistical analysis results, important relationships have been identified among especially soil color groups and structure types, and soil organic matter content and total lime content of the class. Dindaroglu, T. et al., (2013), forest soil health have been pursued according to the new soil quality index value in the Kuzgun Basin. On forests and grasslands, the northern slope views and the low height, it have been identified that, health of the soil in the area is very good, on the contrary especially on the high-altitude pastures, and the extreme views of the slopes and in the southern area, health of the soil is damaged.

Cimrin, K. et al., (2006), have been conducted a study to identify some macro and micro nutrient content of agricultural soil and to determine the relationship between some soil properties in Van. From the area where wheat cultivation made, has taken a total of 52 soil samples from 26 points for represent the region including two different depth, 0-20 and 20-40 cm. Ozbek, A. K. (2004), were evaluated in terms of soil quality index parameters in the soil located 6103 ha which is part of the Asagi Pasinler Plain would be irrigated. It have been identified that on Asagi Pasinler Plain, the region is degrade in terms of pH, organic matter; on the contrary in terms of the soil quality parameters such as soil texture, drainage and

DOI: 10.21533/pen.v5i1.90

groundwater quality the region have the quality soil resources.

Cao, S. K. at al., (2011), combined actual field sampling data with geostatistical to study the characteristic and spatial variability of soil organic matter and organic carbon content around Qinghai Lake. The results showed that the mean content of soil organic carbon is 5.95 ± 3.40%, and organic matter is 3.45 ± 1.97%, both are low.

Purpose of this study is to evaluate in terms of soil quality on the Sapanca Lake Basin and to shed light on the choice of the most appropriate management practices for water and soil resources in the region.

2. Material and methods

2.1 Working area

Sapanca Lake is the freshwater lake where located in the eastern part of the Marmara Region. It has occurred result from tectonic formations in Sakarya. Sapanca Lake coordinates is 400 43 'north-300 15' East, and its altitude is 36 m. Sapanca Lake acreage is 42 km2, east-west direction length is 16 km and a width is 5, 5 km. The perimeter of the lake is 39 km and 26 km of this belongs to the province of Sakarya and 13 km the province of Kocaeli [1].

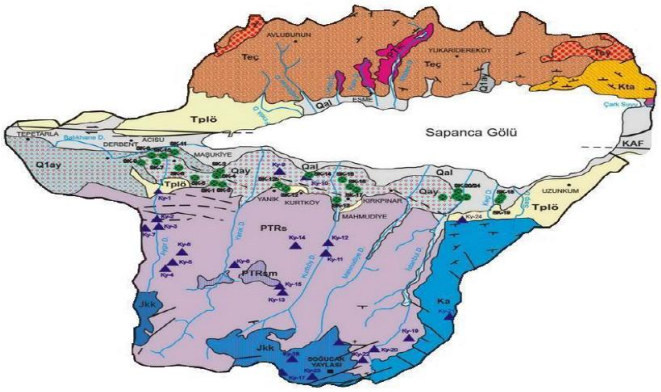

Figure 1. Sapanca Lake and Environment [2]

In lake basin Arifiye, Sapanca, Mahmudiye, Memnuniye, Esentepe, Aşagıdere, Serdivan, Adapazari, Kirkpinar Municipalities and Yanıkköy, Kurtköy, Uzunkum, Yukarıdere and other village settlements located in Sakarya province border; Maşukiye, Esme, Derbent, Acısu and other villages settlements located in Kocaeli province border. In these village settlements is made generally agricultural production.

2.2 Factors Affecting the Soil Structure in the Study Area

2.2.1 Agricultural Operations

It disrupts the nutrient during production, consumption and storage of foodstuffs and destroying harmful pathogens, chemicals used to destroy weeds and microorganisms are often the agrochemicals and "pesticides" we say. None of the drugs, which applied to soil and the field, is stay in application areas. They wafting elsewhere by natural factors such as wind, rain adhering to substance physical - chemical properties. In addition, they create environmental problems. In this way, the possibility of contamination is very high in Sapanca Lake.

2.2.2 Highway and Railroads

D-100 highway passes from north of the Sapanca Lake and TEM Anatolian Highway passes from the south very closely. This situation adversely affect nearby vegetation due to exhaust gases. This will affect the ecological balance of the lake in the long term negatively. Contamination occurs with reaching tires and oil residue from highway both the soil and the lake through rain. Wastewater reached in evacuation channel from TEM Anatolia highway, 300-400 m. intervals throughout Sapanca Lake. And the point in the shore which wastewater reached, pollution is observed on the soil. Releasing emissions into the atmosphere from motor vehicles also has a negative impact on the quality of water and soil.

2.3 Determination of Soil Quality

A total of 30 soil samples from 10 points have been taken from 0-40 cm depth for represent the Sapanca basin. Taken soil samples have been waited until they lost completely their wetness on 1050C. Then, soil sieved to 10 mm were prepared for physical and chemical analysis. Soil structure has been evaluated in terms of organic matter, organic carbon, conductivity, pH, oxidation-reduction potential (ORP), salinity and color parameters. When determining parameter values, the standard method have been used. Soil color is determined by matching the color of taken sample with color swatch in the Munsell Color Scale [8].

3. Results

Color groups of basins have grouped benefiting from in Munsell color scale and their codes have written (Table 1).

Table 1. According to the Munsell color scale color groups and codes of Beysehir lake basin soil

Soil Color Groups	Soil Color Group Codes
Dark Reddish Brown	2,5 YR 3/4, 5 YR 3/4 ve 5 YR 3/3
Reddish Brown	2,5 YR 4/4, 5 YR 4/3, 5 YR 4/4, 5YR 5/3 ve 5YR 5/4
Brownish Dark Brown	10 YR 4/3, 7,5 YR 4/8 ve 7.5 YR 4/2
Brown 1	10 YR 5/3, 7,5 YR 5/4 ve 7,5 YR 5/2

Brown 2	7.5 YR 5/4 ve 7,5 YR 5/2

Samples taken from 10 stations where we determined before in the basin have assayed in terms of organic matter, organic carbon, conductivity, pH, oxidation-reduction potential (ORP), salinity and color parameters, and the obtained results have given in Table 2.

Table 2. Some Quality Parameters of Sapanca Lake Basin Soil

	Conductivity (µS/cm)	SAL (mg/L)	pH	ORP (mV)	Organic Matter %	Organic Carbon %
1. St.	316,27	0,17	8,39	146,1	6,15	3,57
2. St.	177,03	0,09	8,39	144,33	2,88	1,67
3. St.	347,1	0,17	8,31	156,53	4,27	2,47
4. St.	316,03	0,16	8	148,86	5,68	3,29
5. St.	260,5	0,14	8,09	145,3	4,81	2,78
6. St.	346,5	0,18	8,22	141,63	7,08	4,1
7. St.	407	0,22	8,24	148,63	10,03	5,82
8. St.	358,43	0,19	8,31	143,4	6,59	3,82
9. St.	196,13	0,1	8,33	147,5	5,39	3,12
10. St.	297,93	0,16	8,31	154,17	8,32	4,82

4. Discussion

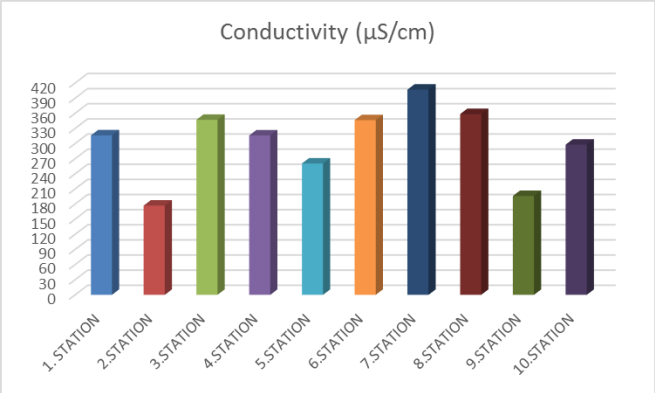

Figure 2. Distribution of Conductivity Parameters in Soil

According to the Figure 2, when we examined conductivity values of 10 stations, the lowest conductivity values in 2. station where located in Sapanca Uzunkum and the highest conductivity values in 7. station where is Balıkhane stream position. These values are 177.03 and 407 µS/cm, respectively.

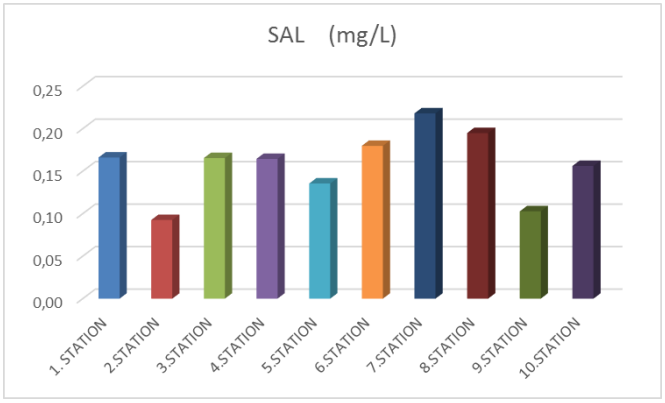

Figure 3. Distribution of Salinity Parameters in Soil

When Figure 3 examined some stations' salinity values indicate proximity according to the salinity of the samples. The lowest salinity values in 2. station where located in Sapanca Uzunkum and the highest salinity values in 7. station where is Balıkhane stream is position. The average salinity in each examples 0.09 to 0.22 mg / L.

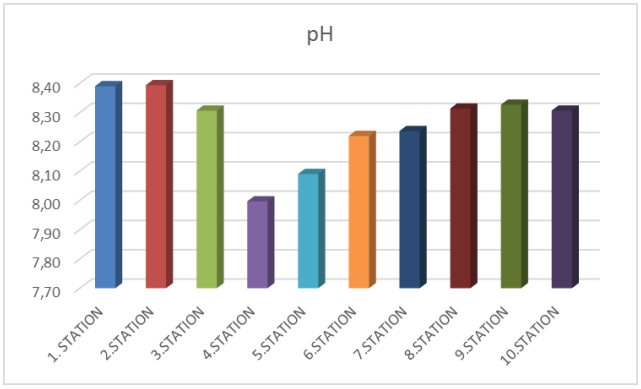

Figure 4. Distribution of pH Parameters in Soil

As it can be seen in Figure 4, according to the pH of soil samples the minimum value in 4. Station is located in Kurtköy. The highest pH values in 1. station is located in Golbasi and in 2. station is located in Uzunkum. Both values are equal. pH values are 8,00 and 8,39 respectively.

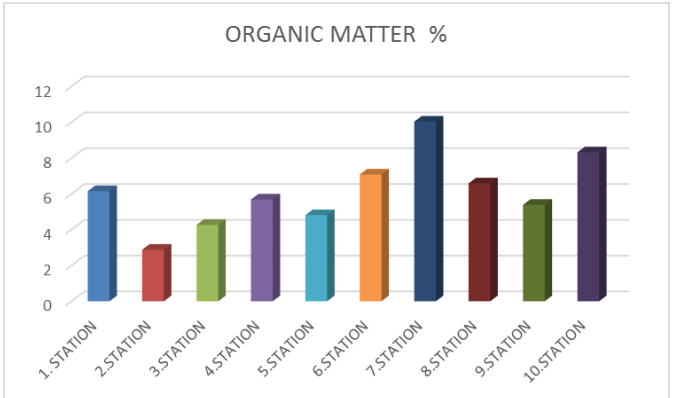

Figure 5. Distribution of Organic Matter Parameters in Soil

As it can be seen in Figure 5, organic matter contents in all soil samples are different. The lowest organic matter content of soil sample were taken from station 2. Moreover, the highest organic matter content of soil sample were taken from station 7.

5. Conclusions

Soil reaction has a special significance due to give information about soil properties easily. pH values are considered neutral between 6,6-7,3 in field work [9]. The average pH of each 30 samples is between 8,00 – 8,39 and it is classified as slightly alkaline. Salinity in the soil is divided into four levels according to the severity as it is seen in Table 3. The average salinity of each samples is between 0,09 – 0,22 mg/L and it is classified as slightly salty.

Organic matter is partially decomposed, partly disintegrated the accumulation of plant and animal residues. This matter are disintegrated continuously by soil microorganisms and continue to decay. Therefore, matter is not a permanent in soil [9]. Grouping of organic matter in the soil is as in Table 3. Organic matter range of taken 30 samples from 0-40 cm depth is between % 2,88 – 10,03 and they are rich especially in terms of organic matter. In the standard soil, %50 to %60 of the amount of organic matter is organic carbon. Organic carbon determination can be found with Walkley-Black method; also, it can be calculate with stoichiometric ratios. In this study, Organic carbon determination is made with stoichiometric ratios and it is between % 1,67 – 5,82. Analyzed soil samples are rich in terms of organic carbon, because of they are rich in terms of organic matter. The high agricultural activities in Sapanca are results from both the high amount of organic matter in the soil and the soil suitability for agricultural activities. The most important elements for agricultural activities are nitrogen, phosphorus and carbon. Results of examinations are shown that carbon content is sufficient for the growth of plants.

Electrical conductivity is the result of electrical resistance. Unit of measurement is decisiemens per meter or milliohms per centimeter. While increased ionic concentration, electrical conductivity is increased. The soil which 40000 µS/m and over conductivity in 25 ºC is considered as salty.

The presence of salt reduces water-holding capacity of the soil [10]. Conductivities of the study areas are lower than 40000 µS/m, thus they are sodic and their conductivity is well.

The color of the soil affects the temperature of the soil surface. Black and dark-colored soils absorbs more heat from the sun. Black and brown soil is indicate the presence of organic matter. Light-colored soils are not hot. Red soils include a good level of oxidized iron minerals [10]. Sapanca lake basin soils are usually in brown tones.

Table 3. Provisions in Standards for Soil Parameter Values

ANALYSIS TYPE	STANDARD SIZE	MEANING
Soil Reaction	<4,5 4,6-5,5 5,6-6,5 6,6-7,5 7,5-8,5 8,5+	Strong Acid Medium Degree Acid Mild Degree Acid Neutral Mild Alkaline Strong Alkaline
Soil Salinity	0,0-0,15 0,15-0,35 0,35-0,65 0,65+	Without salt Mild Salted Medium Salted Multi Salted
Organic Matter	0-1 1-2 2-3 3-4 4+	Too Few Less Medium Good High
Conductivity (µS/cm)	>80000 40000-80000 <40000	Bad Medium Good

Sapanca Lake is one of the most important drinking water source for the in particular Marmara Region. While it supplies drinking water requirement of Sakarya, it supplies requirement of a major industrial company, which is very important for both Kocaeli and Turkey. Sapanca Lake fed from streams as well as groundwater. Many factors affect the quality of water. One of them is the soil structure and content. Examination of drinking water sources at regular intervals shed light on improvement studies. However, for the protection of drinking water sources the water quality parameters will not be enough to examine alone. Besides, the soil structure and quality of the drinking water basins should determine and should be examined at regular intervals. Finally, this study contribute to creation of a comprehensive database by public authorities.

References

[1] Kocaeli Provincial Directorate of Environment and Forestry, Kocaeli Provincial Environmental Status Report, 2006.

[2] Uzun, A., Keleş, R., Bal, İ., Environmental pollution from vehicles on highway and their effects on the Sapanca Lake.

[3] Özkan, K., Mert, A., Gülsoy, S. (2007). Relationships between soil colour, soil structure and some soil properties in Beyşehir Watershed. Turkish

Journal of Forestry Türkiye Ormancılık Dergisi, 2, 9-22.

[4] Dindaroğlu, T., Canbolat, M. Y. (2013). Forest Soil Health Monitoring Using New Soil Quality Index Values: The Case of Kuzgun Basin. Kahramanmaras Sutcu Imam University Journal Of Natural Sciences, 16(4), 1-7.

[5] Çimrin, K. M., Boysan, S. (2006). Nutrient status of Van agricultural soils and their relationships with some soil properties. Yüzüncü Yıl University Journal of Agricultural Sciences, 16(2), 105-111.

[6] Özbek, A. K. (2004). Evaluating soil quality index parameters for Asagi Pasinler Plain soils. Ecology, 13(51), 39-44.

[7] Cao, S. K., Chen, K. L., Cao, G. C., Zhang, L., Ma, J., Yang, L., Lu, H. (2011). The Analysis of Characteristic and Spatial Variability or Soil Organic Matter and Organic Carbon around Qinghai Lake. Procedia Environmental Sciences, 10, 678-684.

[8] Günal, H., Erşahin, S. (2006). Use of Quantified Color Parameters in Estimation of Soil Properties. Journal of Agricultural Sciences, 12(1), 85-92.

[9] Ministry of Agriculture and Rural Affairs. Soil and Land Classification Standards Technical Instructions and Related Legislation.

[10] http://www.orfeteknik.com.tr/orta-kutuphane3.htm Date of Access: 30.05.2016

ISSN 2303-4521

PERIODICALS OF ENGINEERING AND NATURAL SCIENCES
Vol. 5 No. 1 (2017) – Special Issue (Recent Topics in Environmental Science)
Available online at: http://pen.ius.edu.ba

CONSTRUCTION OF BIOPARKS ON DEVASTATED LAND IN URBAN AREAS

Zehrudin Osmanović
University of Tuzla, Faculty of Technology, Department of Chemical engineering Univerzitetska 8, Tuzla, Bosnia and Herzegovina

Samira Huseinović
University of Tuzla, Faculty of Sciences and Mathematics, Department of Biology Univerzitetska 4, Tuzla, Bosnia and Herzegovina

Sanida Bektić
University of Tuzla, Faculty of Sciences and Mathematics, Department of Biology Univerzitetska 4, Tuzla, Bosnia and Herzegovina

Semir Ahmetbegović
University of Tuzla, Faculty of Sciences and Mathematics, Department of Geography Univerzitetska 4, Tuzla, Bosnia and Herzegovina

Abstract
Lukavac, as many other Bosnian and Herzegovinian industrial cities, especially in the winter period, has deteriorated air quality and the greatest polluters are industry, individual heating and transportation. Considering that Lukavac is situated in the valley in which numerous industrial facilities are installed, in the periods of unfavorable weather conditions the town and its surroundings are naturally predisposed for additional air pollution. In this paper we analyze the possibility to form bioparks, which would have positive impacts on the ecological and economic conditions in Lukavac and similar environments. To establish the bioparks, the degraded and abandoned land surfaces, caused by soil erosion or the surface exploitation of mineral resources, could be used. These are located at numerous locations and cover large areas, both in Lukavac and in other industrial areas in Bosnia and Herzegovina.
This paper presents the basic biological characteristics of paulownia and possibilities of planting this tree in areas that are now unused, in the space which is characterized by extreme pollution of atmospheric complex. The selected method is bioremediation, and in this case it is the planting of biological material or woody plant species Paulownija elongata. In this way the degraded surfaces would get the function of biological parks, that is, they would become "oxygen producer" surfaces, and absorbers of CO_2 which is emitted from industrial plants. This species has rapid growth and development of biomass, so the bioparks could be used to serve as the surfaces for alternative fuel with minimal amounts of sulfur, and also as eco - educational parks.

Keywords: air quality, air pollution, Biopark, bioremediation, paulownia, Lukavac.

1. Introduction

With the rise in energy production and consumption, economic recovery, an increasing number of cars on the roads and a larger number of households and business facilities in need of heating and electricity, there is an increasing adverse impact on the environment. In the area of Lukavac town in Bosnia and Herzegovina, in addition to a series of geoecological problems, of which the most emphasized are the degradation of agricultural land, water pollution, many landslides, there is also a pronounced air pollution.

The subject of this research is the analysis and evaluation of air quality in the city area of Lukavac that was made in the period 2005-2014. The task of the research is to determine the level of air pollution by individual pollutants, their comparison with the permissible concentrations and limit values as well as providing guidelines on remedial of the quality of atmospheric complex.

The hypothesis of this paper is: The state of air quality that has been deteriorated by industrial production in the industrial zone of Lukavac can be significantly improved by biological methods, that is, by establishing bioparks with selected plant species. From the above are derived six sub-hypotheses, which are:

1. The state of air quality in Lukavac is not at satisfying level;
2. Paulownia is a plant that with its biological cycle has a positive impact on the atmospheric complex;
3. There is a wide usage value of Paulownia in industry;

DOI: 10.21533/pen.v5i1.10

4. Paulownia is the type of wood that can be used as an alternative fuel to industrial production, thus reducing emissions of harmful gases;
5. Paulownia has a large consumption of CO_2;
6. The area of Lukavac has known considerable surfaces of unused land and a favorable climate for planting out Paulownia.

Given the complexity of the studied subject here we applied more scientific methods and procedures, which are the statistical method that is used to process the data obtained by the established monitoring of air quality, the comparative method used for comparing the air quality data measured at measuring stations, also used for data comparison between earlier periods and new values and for comparing the value with the legal limits. We carried out experiments and laboratory studies in the evaluation of the calorific value of paulownia and conducted field observations, that is, we directly observed the terrain and visited nursery garden which grows paulownia.

2. Material and Methods

This work consists of theoretical and practical parts. In the theoretical part, defined are biological and physiological characteristics of *Paulownia elongata* S.Y. Hu. The practical part of the work includes several scientific methods and procedures. A statistic method is used to process data obtained from the established monitoring of air quality, then a comparative method is used for comparing the air quality data measured at measuring stations, also used for data comparison between earlier periods and new values and for comparing the value with the legal limits. The method of field research is applied when considering pedogeographic traits and seeing the use of certain soils. In addition to the above, the paper used a cartographic method to obtain the data about the area.

We carried out experiments and laboratory studies in the evaluation of the calorific value of *Paulownia*. Also, we implemented field observations, that is, made direct observation of the terrain and visited the nursery that grows the mentioned species.

3. Research results

3.1. The state of air quality in Lukavac

The state of air quality of Lukavac and other bosnian-herzegovinian industrial cities are not at a satisfactory level. In the analyzed period (2005-2014), SO_2 concentrations were elevated significantly during the cold period of the year. The increased concentration of sulfur dioxide (SO_2), in the winter, is the result of - in addition to industrial production - combustion of fossil fuels, especially coal (brown coal and lignite) due to the large number of boiler rooms in the city and its surroundings as well as the impact of industry in the city, or in its immediate vicinity. During this period the warning thresholds of hourly values were exceeded eight times, and the alert threshold values exceeded 20 times. The concentrations of NO_2 in the area of Lukavac are, similarly to the values of SO_2, increased during the cold period of the year, but in the analyzed period there were not recorded hourly exceedings of the threshold of warning and alarm of this pollutant. The concentration of carbon monoxide (CO) reached high values during the entire monitoring period. The content of CO is increased during the fall and winter [1].

The concentration of deposited dust ($PM_{2.5}$) was increased during the cold period of the year, ie. during the heating season, which indicates that the main reason for the high content of deposited dust is its emission from individual furnaces and boiler rooms. It was noted that it exceeded the alert threshold 3 times, and the value of $PM_{2.5}$ reached the threshold of alarm 2 times. It is estimated that 1,337 households have individual boiler rooms and spend ten tons of lignite and six m^3 of wood in one heating season, warming the total residential area [19].

The main problem in the field of air pollution by industry is the use of geoecologically unacceptable production technologies that are not in accordance with best available technologies (BAT). Pollutants emitted from agriculture to the environment are ammonia (NH_3), methane (CH_4) and nitrous oxide (N_2O) [9].

Anticyclonic weather situation in the colder times of the year also adversely affects the air quality. Then there are frequent occurrences of fog, mist and temperature inversions, which contributes to the retention of pollutants in the ground layer of air. Smog rises to the height of the inversion layer and forms a smoke screen or "cap" over Lukavac.

3.2. Recommendation for growing the woody species *Paulownia elongata* SY Hu

The tree *Paulownia elongata SY Hu* reaches a height of over 10 meters, with a wide conical crown. The leaves are large, green, their lower surface pubescent. Paulownia wood has the color of honey. It produces small seed, 1.4 mm to 3 mm, located in pods. The pod has oval shape and it is woody, with a size from 2.5 to 5 cm. It is a noninvasive type that thrives also in very sparse soil.

Paulownia elongata is a hard wood, but at the same time it is the lightest known wood weighing 272 to 336 kg/m^3 (average 304 kg/m^3). The wood is light in color and almost without knots, with resistance to bending and twisting making it perfect for carving. Fire-resistant point - the point of lighting is twice the size of pine's, which is especially interesting for coastal areas which are in summer exposed to increased risk of fire [13,14].

Paulownia can not survive on poorly drained soils. The most favorable are lands toward the south (sunny side). The soil should be drained, or may not accumulate or hold water. Underground water flows should not be closer than 1.5m to the ground. In heavy clay soils paulownia grows more slowly. Paulownia does not tolerate acidic soils. The pH should be between 5 and 8. If it is possible, the autumn plowing is suggested, but it will be enough to have early spring deep plowing only. When plowing, it is good to additionally fertilizethe land in order to accelerate the growth of paulownia. Before setting up the foil with pipes for drip irrigation to drop, it is necessary to chop the ground. The role of the foil is multiple: it ensures a higher temperature of the soil, retains moisture, prevents weed growth ... Rows of foil are placed at every 4 meters [2].

Planting begins by wetting the soil beneath the foil and drilling holes in the ground through the foil. It is necessary to dig a hole with a diameter of 60 cm and depth of 80 cm. In this excavated hole a part of excavated soil that is mixed with manure and fertilizers should be returned back in the hole until it is deep 30-40 cm. The tree should be cut to 2-3 cm above the ground and buried with the rest of the soil. Distance between seedlings of paulownia under the foil is 4 meters. Planting of paulownia is made only in the spring!

Year Zero - There is no need for major interventions in the plants because they will be anyway cut to ground level next spring. If they occur, possible excess shoots from the same root (more stems) can be disposed of.It is necessary to control the grass and weeds between the foil, so as not to escalate and choke seedlings. If there is no rain in the spring it requires watering 1-2 times a week. In summer, if it is dry, 2-3 times.

The first year - at the beginning of April it is necessary to cut down the tree / stem of paulownia at a height of 1 cm above ground level and cover the cut part with a thin layer of soil (1-2 cm) to reduce drying out the roots. From each root will appear a few shoots. When they grow up to 10 cm is necessary to keep the strongest, and have the rest removed. In this year, watering is as important as in the zero year. It is also important to mow the grass and weeds so that would not initially be higher than seedlings. Before falling leaves, the stems will have already become woody [5].

The second year - in the spring the stems/tree of paulownia which became woody will begin to leaf through. From below we should rip off all the leaves except for the last half a meter at the top. By this we achieve that a tree in the early years grows as much in height. In the following years, we are waiting for the tree to reach a diameter of 35-40 cm when it is ready for harvesting. This should be after 7-10 years (depending on conditions). After cutting, from the existing root, in the fall, a few new shoots of paulownia will spring up. The cultivation is then continued as instructed for the first year. Since now the root is very strong (even 10 m deep), the growth of paulownia will be even faster.

One hectare of land with 625 trees of Paulownia elongata for three years brings a staggering 57 tons of timber, and for 8-10 years even 190 tons are possible. At about the eighth-tenth year the tree has an average of 1 m^3 of timber and it is possible to be exploited 3 times because after each cutting it will drive a new seedling which in 8-10 years again reaches the same amount of wood in ideal conditions. By comparison, a poplar tree usually takes 15-20 years to maturity, oak 30-40 years, and pine 70-75 years. Every two years one can expect up to 100 tons of wood biomass per 1 hectare [8,20]. A cubic meter in the industrial mode of planting, on the world market reaches the price of up to 1100 USD (Paulownia is at the world's stock markets mostly sold under its Japanese name: Kiri.)

3.3. The use of Paulownia

Because of the resistance to humidity, paulownia tree is used for the production of furniture which is resistant to deformation. Because of its low resin content, wooden material of paulownia has a low level of risk of fire, because it is difficult to initiate it to burn. In addition to the mentioned characteristics, an essential feature of paulownia wood in furniture production is being resistant to attacks of wood-eaters. Because of its softness, paulownia wood is possible to be decorated with most complex carvings. Another characteristic of paulownia is its decorative use. Namely, because of the beautiful flowers that adorn the wide treetop of this tree it is often used for landscaping parks. The flowers are rich in nectar and antioxidants. The leaves absorb up to 10 times more carbon emissions than other types of trees. Abundant blooms and size of leaves also help in successful reforestation and recovery of burned forests, and for its branched root the tree is used against soil erosion. Extremely important and valuable use of paulownia comes out from its honey-bearing properties. Its importance as honey-bearing type, in addition to the quality of honey, lies in the fact that the bees do not need to visit a lot of flowers to be 'filled', since the flowers are extremely rich in nectar. From one hectare bees can collect between 900 and 1000 kilograms of nectar that is by the quality in the rank of acacia and sage honey. It has bright colors and is quite light in weight, with a strong odor. It also serves as a healing agent [4,3].

KYOTO program of environmental protection ranks *Paulownia* in the first place among the plants, like a mine of oxygen and air cleaner. Given that it is harder

and harder to follow the prices of energy sources we use every day and that are in constant increase due to reduced reserves, *Paulownia* as a wood biomass presents an energy source that renews itself, because after cutting it grows back from the stump.

Additionally, Paulownia gives high calorific value of 4,700 kcal / kg with negligible sulfur content during combustion. The whole planet seek to reduce greenhouse gas emissions, and *Paulownia* absorbs significantly more CO_2 than other tree species (eg. 4 acres of *Paulownia* absorbs in one year up to 13 tons of CO_2 from the atmosphere and it affects climatic changes).

Figure 1. Paulownija elongata, d.o.o Voćni rasadnik, Srebrenik, July 2016

Paulownia turns untreated land into green fields. It is environmentally acceptable solution for cultivating manure and restoring land destroyed by human activities. Paulownia is ideal for reinforcement of river banks and in the fight against erosion. Cities and municipalities could implement, with the support of the public, environmental projects using paulownia, while for forestry purposes could be used programs for rural development.

Paulownia tree is a "small manufacturer" of heat taking into account a cubic meter of wood biomass. By comparison, 1 m^3 of paulownia with the humidity of 15% gives about 1069 kWhs of thermal energy, while the same amount of oak in combustion produce almost twice the energy - 2,363 kWh. These results are a consequence of lower density paulownia, but also the fact that 1 kg of any tree of the same moisture content gives about the same amount of heat energy because the chemical composition of all kinds are about the same. The possibility of using Paulowniain industry is wide. It can be used as technical wood, but also as an alternative fuel with significantly lower emissions of SO_2 [12], Table 2.

Table 1. Binding of CO_2

Tree species	**kg CO_2/ha**
Alpine pine	48000
Paulownia	8181,73
Cork oak	4500
Eucalipto	491,21

Table 2. Paulownia as alternative fuel

Type of energy source	SO_2 (t/day)			CO_2 (t/day)		
Coal	1,73			206,34		
70 % coal +30 % alternative fuel	Coal	Alternative fuel		Coal	Alternative fuel	
	1,21	0,66		144,44	65,23	
	1,87			209,67		
70 % coal +30 % (15 % alt. fuel +15 % paulownia)	Coal	Alternative fuel	Paulownia	Coal	Alternative fuel	Paulownia
	1,21	0,33	0,02	144,44	32,65	32,61
		0,35			65,27	
	1,56			209,71		
70 % coal +30 % paulownia)	1,21	Paulownia		144,44	Paulownia	
		0,03			65,31	
	1,24			209,75		

4. Discussion

Usable areas for planting paulownia in the area of Lukavac are: free farmlands, conditionally stable and unstable slopes that have got developed (standard) lands, lands in industrial zones that are unoccupied by infrastructure facilities, as well as areas where is present surface exploitation of mineral resources and landfills of tailings with prior pedological reclamation.

Thanks to the large leaf surface and the fact that the underside of the leaf has dense hair, this species can absorb significant amounts of sulfur dioxide and dust particles. Results of the analysis of heavy metals (Zn, Fe, Pb, Cu, Ni, Cr, Mn, Cd, As, Hg) in the leaves of woody species *Paulownia elongata* SY Hu growing in urban areas clearly show that *Paulownia elongata* SY Hu is a tolerant species, and can be recommended for forming tree lines along urban and regional roads as well as for the formation of wind protection zones along the main roads [6,18]. *Paulownia* can absorb heavy metals from the soil and from the air.

Heavy metals in the soil may be the result of natural pedogenetic processes [22], as well as of anthropogenic factors that lead to environmental pollution. A very important source of heavy metals and other polluters of soil and plants is traffic [10,17]. Plants bring in heavy metals constantly during the vegetation period. The highest values are reached at the end of the growing season [7,16]. Also, there are many literature references that point to the impact of heavy metals on morphological, anatomical and physiological characteristic of woody species among others [11]. Species of the genus Paulownia, according to many

literature data, indicate the possibility of adopting heavy metals [15,21]. The level of tolerance of this species to pollution of air, is the basis for its development and survival in the urban environment.

Paulownia species are very suitable for decoration and enriching environment, and the need of reforestation. They are also equally suitable for landscaping of urban and industrial areas [23].

Paulownia is a tree that has the capabilities of very high intake of nitrates, heavy metals and other elements from shallow and deep layers of the earth. It has a unique root system where the roots grow at a depth of over 2m. Due to, even several meters deep rooting system, it is used for the rehabilitation of landslides. Such a root system, in combination with the rapid growth of paulownia enables interchange of much more nutrients as opposed to other species, thus giving a great potential in bio-remediation of contaminated soil.

Paulownia also has a significant role in the rehabilitation and protection of soil from erosion.

Usable surfaces for planting paulownia, in the area of Lukavac, are: free farmlands, conditionally stable and unstable slopes that have got developed (standard) soil, lands of industrial zones that are not occupied by infrastructure facilities, as well as areas with present surface mining of mineral raw materials, and tailings dumps with prior soil reclamation. By surface mining of coal and other mineral resources, vast areas were degraded. An example is the Tuzla and Zenica coal basin. In accordance with legislation that treats the exploitation of mineral resources and environmental protection, mines are required to recultivate degraded areas, however, it is not the practice in our country.

5. Conclusions

Based on the conducted analyzes, it was concluded that in Lukavac, as well as in other industrial cities in Bosnia and Herzegovina, air quality is not at a satisfactory level. It is particularly expressed in increased concentration of SO_2 due to extensive use of fossil fuels.

Paulownia is a plant that with its biological cycle has a positive effect on the atmospheric complex. With biological methods, that is, by planting the selected plant species status of air quality in the industrial zone of Lukavac can be significantly improved. This type of wood can be used as an alternative fuel in industrial production, thus reducing emissions of harmful gases, and at the same time it is a major consumer of CO_2.

The area of Lukavac has considerable areas of unused land and favorable climatic conditions for planting Paulownia, or establishment of Bioparks which would have economic, environmental and educational function (Paulownia elongata S. Y. Hu).

References

[1] Ahmetbegović, S. i Gutić, S. (2015): Stanje kvaliteta zraka u Lukavcu, Naučna konferencija "Kulturno-historijsko i prirodno naslijeđe općine Lukavac", Javna ustanova biblioteka Lukavac i Zavod za zaštitu i korištenje kulturno-historijskog i prirodnog naslijeđa Tuzlanskog kantona, Lukavac, pp. 644-658;

[2] Ates, S., Ni, Y., Akgul, M., Tozluoglu, A. (2008): Characterization and evaluation of Paulownia elongota as a raw material for paper production, African Journal of Biotechnology Vol. 7 (22), pp. 4153-4158, 19 November;

[3] Barton, I, Nicholas , I., Eckroyd, C. (2007): Paulownia. Forest research bulletin No 231. New Zealand forest research institute. Rotorua. P. 71.;

[4] Cvjetičanin, R. Perović, M. (2009): Pregled vrsta roda paulovnija (*Paulownija* sieb.et zucc.) i njihove bioekološke. Šumarstvo. 3-4 conference „Forestry in achieving millenium goals“. Novi Sad, Serbia. P. 88.;

[5] Jovanović – Dunjić, P. (1974): Rod Paulownija. In: Flora Srbije VI. Srpska akademija nauka i umetnosti,Odeljenje prirodno- matematičkih nauka. Beograd. 161-162.;

[6] Knežević et al (2009): Concentrations of heavy metals in soil and leaves of plant species Paulownia elongata S.Y.Hu and Paulownia fortunei Hemsl African Journal of Biotechnology Vol. 8 (20), pp. 5422-5429.

[7] Krstić B., Stanković D., Igić R., Nikolić N. (2007) Biotechnol. & Biotechnol. Eq., 21(4), 431-436.

[8] Krussmann, G. (1986): Manual of cultivated broad-leaved trees and shrubs, Vol. II. Batsford ltd. London. 445.;

[9] LEAP, Akcioni plan zaštite okoliša općine Lukavac, Lukavac, 2011.

[10] Memmon, A., Aktoprakligil, D., Özdemir, A., Vertii, A. (2001): Heavy metal accumulation and detoxifikation mechanisms in plants. Turk. J. Bot. 25: 111-121.

[11] Nikolić, N. (2009): Effects of heavy metals on morpho-anatomical and physiological characteristics of poplar clones (Populus sp.) Doctor thesis. Faculty of Sciences, Novi Sad, Serbia.

[12] Osmanović, Z., Haračić, N., Zelić, J.(2016): Analiza mogućnosti upotrebe paulownije (Paulownia elongata) kao alternativnog goriva u cementnoj industriji u cilju smanjenja emisije polutanata. XI Naučno-stručni simpzij sa međunarodnim učešćem, Zenica 21.-22. april 2016. godine;

[13] Perović , M, Cvjetićanin , R. (2008): Paulownia elongata Sh.-Z.. Hu and Paulownia;

[14] Popović, J., Radošević, G. (2008): Anatomsko-hemijske karakteristike drvnih vlakana vrste Paulownia fortunei seem. Hemsl. Šumarstvo 4. Beograd. 71-77.

[15] Shaw, A.J. (1990): Heavy Metal Tolerance in Plants: Evolutionary Aspects. In: CRC Press (Ed.), pp. 39-53.

[16] Stanković, D., Krstić, B., Igić, R. (2005): Sadržaj mangana u zemljištu i lišću nekih vrsta drveća u NP ‘’Fruška gora’’. Glasnik šumarskog fakulteta, 91, 207-217.

[17] Stanković, D. (2008b): Biljke i saobraćaj. Monography, p. 1-98. Zadužbina Andrejević., Beograd

[18] Stanković, D., Nikolić, M.S., Krstić, B., Vilotić, D. (2009): Heavy Metals in the Leaves of Tree Species Paulownia Elongata S.Y.Hu in the Region of the City of Belgrade. Biotechnology & Biotechnological Equipment, 23:3, 1330-1336.

[19] State of the Environment of Lukavac report 2012;

[20] Vasiljević , S. (1983): Paulownia. In: Šumarska enciklopedija 2. Jugoslavenski leksikografski zavod. Str. 607.

[21] Wang, J., Zhang, CB., Jin, ZX. (2009): The distribution and phytoavailability of heavy metal fractions in rhizosphere soils of Paulowniu fortunei (seem) Hems near a Pb/Zn smelter in Guangdong, PR China. Geoderma, 148(3-4): 299-306.

[22] Woolhouse, HW. (1983): Toxicity and tolerance in the response of plants to metals. In: Encyclopedia of Plant Phisiol., New Series, Vol. 12 C, Springer-Verlag, New York, Heidelberg, Berlin, pp. 246-289.

[23] Zhao-Hu, Z. et al. (1986): Paulownia in China: Cultivation and utilization by Chinese academy of forestry staff; Asian network for biological sciences and international development research centre.